The Effects of Environmental Factors on the Toxicity of Nanomaterials in Fish

By

Yueyang Zhang

A thesis submitted in partial fulfillment of the requirements for the degree of

Doctor of Philosophy

in

Physiology, Cell and Developmental Biology

Department of Biological Sciences

University of Alberta

© Yueyang Zhang, 2021

Abstract

Nanomaterials (NMs) are materials that are between 1 and 100 nm at least one dimension. While natural processes (volcanos, lightning, erosion, etc.) have been producing NMs for the entirety of the earth's existence, recent advances in material sciences have produced novel engineered NMs developed and manufactured for specific purposes in consumer goods and industrial applications. Due to the widespread use and rapidly increasing production of NMs, more engineered NMs will inevitably be released into the environment through indirect or direct release and thus will interact with environmental factors and organisms. This has raised concern with regulators and the public alike regarding the potential hazard of these engineered NMs. Another recent source of NMs results from the production, release, and subsequent environmental breakdown of plastics, leading to the presence of nanoplastics (NPLs) now ubiquitously found in aquatic environments. My thesis examines the potential for adverse effects of both engineered NMs and NPLs, with a specific focus on the interactive effects of these materials in the presence of modulating environmental factors such as ultraviolet (UV) light and natural organic matter on the toxicity/hazard o fishes. First, the effects of cerium oxides nanoparticles (CeO_2 NPs) were examined using the Amazonian fish, the cardinal tetra (*Paracheirodon axelrodi*) as a model organism. Toxicity was examined either under laboratory light or UV light conditions with or without the addition of natural organic matter (NOM) from Rio Negro Amazon River water. Sub-lethal effects such as lipid peroxidation and gill malformations were evaluated and potentiation of toxicity by UV light and mitigation of these effects by NOM was demonstrated. In the second series of investigations, zebrafish (*Danio rerio*) embryos were exposed to novel nano-enabled

pesticide formulations azoxystrobin (nAz) or conventional azoxystrobin (Az) either under laboratory light or UV light. Evaluation of multiple endpoints including lethality, oxygen consumption, yolk consumption, changes in antioxidant enzyme activity, alternations in gene expression and lipid peroxidation demonstrated significant potentiation of toxicity by UV light and a mechanism for the generation of reactive oxygen species under UV light as the potentiating factor was proposed. Similar to engineered nanomaterials, the potential hazard of NPLs as carriers of organic materials (the so-called "Trojan Horse" hypothesis) was then investigated using both zebrafish embryos and rainbow trout fingerlings (Oncorhynchus mykiss) as model species. Specifically, embryos or fingerlings exposed to NPLs either alone or coated with a model polycyclic aromatic hydrocarbon (PAH) phenanthrene were used to demonstrate the carrier function of NPLs for organic pollutants. Also investigated were the modulating effects of NOM on the noted potentiation of PAH uptake in rainbow trout fingerlings by NPLs. The results presented in this thesis represent 1) the first study to demonstrate the UV-induced sub-lethal effects of CeO_2 NPs on fish at low environmental pH (~4.5), including the protective properties of NOM to reduce the noted UV-induced toxicity, 2) the first comprehensive and systematic report on the UV-induced lethal and sub-lethal effects of pesticide on zebrafish embryos, including demonstration of much higher toxicity associated with exposure to nano-enabled formulations when compared to conventionally applied pesticides, 3) the first comprehensive research to show both sorptions of phenanthrene onto the surface of NPLs and the carrier function of NPLs for facilitating the uptake of phenanthrene by zebrafish embryos and rainbow trout fingerlings. As part of this study, I also demonstrated mitigating effects of NOM on the co-contaminant carrier function of NPLs. My thesis improves our

understanding of the effects of environmental factors on the toxicity of various NMs and

NPLs, including the potentiation of hydrophobic organic pollutant uptake by NPs by the

"Trojan Horse" effect. This thesis will provide much-needed data for regulators, risk

assessors and the public to evaluate the potential impact of NMs and NPLs in the

environment.

Preface

      This thesis is an original work by Yueyang Zhang. This research is approved by the University of Alberta Animal Care and Use Committee and governed by the protocol AUP00000001 (2015-2020): Effects of nanoparticle exposure on zebrafish, trout and cardinal tetras development and physiology.

      Some of the experiments conducted for this thesis are part of an international and national research collaboration, which was led by Dr. Greg G. Goss at the University of Alberta. I (Yueyang Zhang) performed the majority of the work presented in this original thesis. I was invited to submit Chapter 1 as chapter 3 in the book titled "*Nanotoxicology*" by Doak, S., Clift, M., & Lead, J. Chapters 2 and 4 have been published in Environmental Science: Nano. Chapter 3 has been published in Nanotoxicology. Chapter 5 will be submitted for possible publication in Environmental Science: Nano. The bibliographical details for each data chapter are listed below and included at the beginning of each corresponding chapter. The roles of all authors for each data chapter with experimental contributions of certain authors are described below:

Chapter 2

Y. Zhang, T. A. Blewett, A. L. Val and G. G. Goss. UV-induced toxicity of cerium oxide nanoparticles (CeO_2 NPs) and the protective properties of natural organic matter (NOM) from the Rio Negro Amazon River, *Environmental Science: Nano*, 2018, **5**, 476-486 DOI: 10.1039/C7EN00842B.

YYZ, TAB, ALV and GGG conceived and designed the experiments. YYZ, TAB, GGG and ALV performed the experiments. YYZ, TAB and GGG analyzed the data. ALV and GGG contributed to reagents, materials, and analysis tools. YYZ, TAB, ALV and GGG wrote, drafted and revised the manuscript.

Chapter 3

Y. Zhang, C. Sheedy, D. Nilsson and G. G. Goss. Evaluation of interactive effects of UV light and nano encapsulation on the toxicity of azoxystrobin on zebrafish, Nanotoxicology, 2019, 1-18 DOI: 10.1080/17435390.2019.1690064.

YYZ and GGG conceived and designed the experiments. YYZ, CS, and DN performed the experiments. YYZ, CS, DN and GGG analyzed the data. CS, DN and GGG contributed reagents, materials, and analysis tools. YYZ, CS, DN and GGG wrote, drafted and revised the manuscript

Chapter 4

Y. Zhang and G. G. Goss. Potentiation of polycyclic aromatic hydrocarbon uptake in zebrafish embryos by nanoplastics, *Environmental Science: Nano*, 2020, DOI: 10.1039/D0EN00163E DOI: 10.1039/D0EN00163E

YYZ and GGG conceived and designed the experiments. YYZ performed the experiments. GGG contributed reagents, materials, and analysis tools. YYZ and GGG analyzed the data. YYZ and GGG drafted and revised the manuscript.

Chapter 5

Y. Zhang and G. G. Goss. The "Trojan Horse" Effect of Nanoplastics: Potentiation of Polycyclic Aromatic Hydrocarbon Uptake in Rainbow trout (*Oncorhynchus mykiss*) and the Mitigating Effects of Natural Organic Matter. *Environmental Science: Nano.* To be submitted.

YYZ and GGG conceived and designed the experiments. YYZ performed the experiments. GGG contributed reagents, materials, and analysis tools. YYZ and GGG analyzed the data. YYZ and GGG drafted and revised the manuscript.

Acknowledgments

First and foremost, I express my deepest gratitude to my supervisor, Dr. Greg Goss, for his immeasurable amount of support and guidance through my program. I would like to acknowledge my committee members, Dr. Keith Tierney and Dr. James Stafford, for providing support and advice for my research. I would also like to thank my internal examiner, Dr. Michael Serpe, and my external examiner. Dr. Rebecca Klaper, for taking the time to read this thesis, attending my Ph.D. defense and providing feedback.

I am grateful to the University of Alberta and Alberta Innovates for awarding me the Alberta Graduate Excellence Scholarship and Alberta Innovates Graduate Student Scholarship (Nano) respectively. Their financial support provides much-needed help to allow me to spend more time on my research and relieve some financial burden.

I would like to recognize and thank my colleagues and collaborators who helped my research and contributed to the work. Many thanks to Dr. Scott Smith from Wilfrid Laurier University for his analysis of the FEEM plots and PARAFAC for natural organic matter content, Arlene Oatway for helping obtain TEM images of CeO_2 NPs and teaching hematoxylin and eosin staining, Dr. Hosnay Mobarok for performing XPS and analyze XPS data, Shannon Flynn for analyzing ICP-MS. Many thanks to Dr. Yuhe He for providing zebrafish primers and teaching quantitative polymerase chain reaction, Dr. Lindsey Felix for DLS analysis and Dr. Van Ortega for teaching TBARS assay, Western Blot and improving dissection skill. Thanks to Vive Crop Protection for providing nano-enabled azoxystrobin, conventional azoxystrobin, input polymer and Allosperse, and the Biological Sciences Animal Services for cardinal tetra and zebrafish care.

Table of Contents

Chapter 5

The "Trojan Horse" Effect of Nanoplastics: Potentiation of Polycyclic Aromatic Hydrocarbon Uptake in Rainbow trout and the Mitigating Effects of Natural Organic Matter

List of Tables

List of Figures

List of Abbreviations

* Terms are abbreviated after first use within each chapter.

2-DR	2-deoxy-D-ribose
4-HNE	4-hydroxy-2-nonenal
7-ER	7-ethoxyresorufin
Ag NPs	silver NPs
ATP	adenosine triphosphate
Au NPs	gold NPs
Az	conventional azoxystrobin
BHT	butylated hydroxytoluene
cat	*catalase*
CavME	caveolae-mediated endocytosis
CEM	clathrin-mediated endocytosis
CeO_2	cerium oxide
-COOH	carboxyl group
cpm	Counts per minute
Cu NPs	copper NPs
CuO NPs	copper oxide NPs
ddH_2O	double-distilled water
DLS	dynamic light scattering
DLVO	Derjaguin Landau Verwey Overbeek
DMSO	dimethyl sulfoxide
EDL	electrical double layer
ef1α	*elongation factor 1 alpha*
ETC	electron transport chain
EROD	ethoxyresorufin-o-deethylase
FA	fulvic acid
Fe	iron
FEEMs	fluorescence excitation-emission matrices
gst	*glutathione S-transferase*
GPX	glutathione peroxidase
gpx1a	*glutathione peroxidase 1a*
gpx1b	*glutathione peroxidase 1b*
HA	humic acid
HDD	hydrodynamic diameter
H_2O_2	hydrogen peroxide
HOMO	highest occupied molecular orbital
hpf	hours post-fertilization
HR	heart rate
hsp70	*heat shock protein 70*
ICP-MS	inductively coupled plasma-mass spectroscopy
ILCM	interlamellar cell mass
IS	ionic strength
LC_{50}	median lethal concentration
LOAEC	lowest observed adverse effect concentratio

LogK$_{ow}$	octanol/water partition coefficient
LUMO	lowest unoccupied molecular orbital
MDA	malondialdehyde
MP	macropinocytosis
MPs	microplastics
Nanomaterials	NMs
nAz	nano-enabled azoxystrobin formulation
NCBI	National Center for Biotechnology Information
Ni NPs	nickel NPs
NOM	natural organic matter
POPs	persistent organic pollutants
PS-NPLs	polystyrene nanoplastics
NPs	nanoparticles
NPLs	nanoplastics
O$_2^{\cdot-}$	superoxide radical
•OH	hydroxyl radicals
PAA	polyacrylic acid
PAHs	polycyclic aromatic hydrocarbons
PARAFAC	parallel factor analysis
PBS	phosphate-buffered saline
PDI	polydispersity index
PVP	polyvinylpyrrolidone
PZC	point of zero charge
qPCR	quantitative polymerase chain reaction
RNS	reactive nitrogen species
RO	reverse osmosis
ROS	reactive oxygen species
RTgill-W1	rainbow trout gill epithelial cell line
SA	specific activity
SOD	superoxide dismutase
sod 1	*superoxide dismutase 1*
sod 2	*superoxide dismutase 2*
SSA	specific surface area
TBA	thiobarbituric acid
TBARS	thiobarbituric acid reactive substances
TCA	trichloroacetic acid
TEM	transmission electron microscopy
TEP	1, 1, 3, 3-tetraethoxypropane
TiO$_2$	titanium dioxide
TMS	tricaine methanesulfonate
USD	United States dollars
UV	ultraviolet
W	wet weight
XPS	X-ray photoelectron spectroscopy
ZnO NPs	zinc oxide NPs

Chapter 1

Introduction

1.1 Introduction

Nanomaterials (NMs) have been present in the environment since before the existence of humans.[1, 2] The natural events on the earth, including volcanic eruptions, forest fires, and dust storms, have been contributing non-engineered NMs to the environment for many years.[1, 2] These NMs include particulate materials in the atmosphere, colloid and natural organic matter (NOM) in aquatic systems, and minerals and NOM in the soils.[1] On the other hand, engineered NMs are intentionally designed and manufactured for specific purposes.[2] Moreover, the weathering of large plastics has been generating a large number of microplastics and nanoplastics, which has become a new emerging environmental concern.[3-5] The modern field of nanoscience and nanotechnology has been rapidly advancing, and the industry has been proliferating since the first introduction of the concept by Richard Feynman, in 1959.[6] Nanotechnology is now a multi-billion dollar industry and has been growing rapidly every year.[7, 8] The worldwide market of nanotechnology-based products was estimated to be approximately 15 billion United States dollars (USD)[8] in 2015 (the latest year with publicly available data) and the field is expected to have more than 15% annual growth in the next 5 years.[9] According to StatNano, more than 8,000 nanotechnology-based products are commercially available worldwide in 2018.[10] These include not only high-end applications, including quantum dots in imaging and nano-enabled medical products,[7] but also daily consumer goods, such as titanium dioxide (TiO_2) nanoparticles (NPs) in sunscreen, cerium oxide (CeO_2) NPs as diesel fuel additives and nano-enabled pesticides.[11] Although the use of NMs provides many benefits in various applications, much of these NMs will undoubtedly end up in the environment either through the direct application (e.g., nano-enabled pesticides), via direct release from

wastewater treatment plants or indirect release due to the end life cycle of various

nanotechnology-based products.[12] In each case, the NMs (pristine or transformed during

the life cycle), will interact with numerous environmental factors and organisms.[13, 14] As

such, it is evident that it is necessary to evaluate the environmental risk of NMs in

ecologically relevant conditions to accurately assess risk.[2, 13, 14]

NMs are materials with a length of 1-100 nm in at least one dimension and often

have unique properties comparing to their bulk and dissolved form counterparts.[7] The

specific surface area (SSA) of NMs increases exponentially with decreasing diameter,

which can act to significantly increase the ability to move through the environment, interact

with environmental factors, affect cellular uptake rate, and move between compartments

inside an animal.[7, 11] As size decreases, there is a significantly increased potential of NMs

to interact with the surrounding environment and living organisms.[7, 11, 15] Over the last

decade, abiotic factors, including pH, ionic strength (IS), NOM and ultraviolet (UV) light,

have been shown to affect aggregation, bioavailability and toxicity of NMs in many

studies.[7, 16-19] The purpose of this chapter is to summarize some intrinsic properties affecting

the environmental toxicity of NMs and highlight some of the results from recent research

on the effects of environmental factors on the toxicity of nanomaterials.

1.2 Characteristics of Nanomaterials Modulating Their Toxicity

The characterization of NMs themselves in both pristine and more importantly,

environmentally relevant conditions is crucial in determining their potential for harm.[20]

Since the early 2000s, nanotoxicologists have worked to identify some of the more

important intrinsic properties including size, surface charge, shape and crystal structure, which play a critical role in determining the toxicity of NMs while more recently, recognition of environmental factors as modulators of toxicity (extrinsic properties), interacting with the intrinsic properties have become more studied.[20-23] An understanding and integration of all these factors are necessary when assigning hazards and risks to a particular material.

1.2.1 Size

The size of an NM modulates its interaction with living organisms, including an NM's internalization, mechanism and toxicity.[20, 24] Endocytosis is an energy-dependent process used by cells to internalize molecules, and communicate with the biological environment and other cells.[24-26] Endocytosis is divided into four pathways including phagocytosis, macropinocytosis, clathrin-mediated endocytosis and caveolae-mediated endocytosis.[25] Effects of the primary size of NMs have been extensively studied in mammalian cell lines and while caution should be exercised when cross-reading to environmental receptors, we can use these findings as surrogates to inform our understanding of the effects of nanomaterials on non-mammalian biota. In a recent review of mammalian cell line nanoparticle uptake, results suggest that each NM has its optimal size for cellular uptake.[24] For example, the 100 nm polystyrene nanoparticles have higher cellular uptake efficiency than 50, 200, 500 and 1000 nm while 50 nm has the lowest uptake rate of all the sizes tested.[25] However, only a few studies have examined the effects of particle size on cellular uptake in fish cells.[26] A recent study demonstrated that smaller

polyvinylpyrrolidone (PVP) coated silver (Ag) NPs had lower cellular accumulation in rainbow trout (*Oncorhynchus mykiss*) gill epithelial cell line (RTgill-W1), but a higher rate of being transported through the multilayers of cells when compared to larger citrate coated Ag NPs.[27] Another paper from our laboratory revealed that clathrin-mediated endocytosis (CME), caveolae-mediated endocytosis (CavME) and macropinocytosis (MP) were all involved in the uptake of 10 nm Nile-red-loaded NPs (< 100 nm hydrodynamic diameter in L-15 medium) into RTgill cells, with CME being the dominant pathway.[26] This finding is consistent with the results from mammalian cell line studies which suggest that CME is the major uptake pathway for smaller NPs and cellular uptake shifted towards CavME and MP as NMs' size increases, and the uptake efficiency decreases when size is above a certain threshold.[24, 28] However, given that only one size of NM was tested in RTgill cells, the independent effects of primary size on the pathway for uptake of NMs into fish cell lines has not been investigated.

With regard to testing particle size in *in vivo* environmental models, there are only a few studies specifically and accurately address the issue of particle size. One study showed that *Daphnia magna* exposed to TiO_2 NPs with the primary size of 25 nm had the highest rate of immobilization when compared to animals exposed to smaller (10 nm) and larger (220 nm) sized particles. In that study, the varying toxicity was attributed to higher hydroxyl radicals generation in the intermediately sized materials.[29] Another study designed to examine the effect of the size of Ag NPs demonstrated a size-dependent distribution and toxicity in rainbow trout.[30] Ag NPs with a primary size of 10 nm had greater accumulation on the gills when compared to 35 nm and 600 nm Ag NPs. Furthermore, 10 nm Ag NPs significantly increased the gene expression of *cyp1a2* in the

gills which may indicate up-regulation of oxidative metabolism due to external or internal oxidative stress.[30] Similar trends were observed in adult zebrafish (*Danio rerio*) where citrate-coated Ag NPs with a primary size of 20 nm had significantly higher uptake through the gill and intestine, was associated with higher damage on the gills including fusion of secondary lamellae, hyperplasia and inflammation, and reduced Na^+/K^+ ATPase activity by 57% in the gill, significantly greater compared to the 21% reduction found in fish exposed to citrate-coated Ag NPs with a primary size of 100 nm.[31]

1.2.2 Surface charge

   Cell membranes on water contact surfaces such as gills or skin are negatively charged due to the presence of sialic acid-based glycosylation of membrane proteins.[32, 33] As a result, positively charged NMs have a much higher affinity to the outer epithelial membrane and can be taken up more efficiently than negatively charged and neutral NMs due to the electrostatic interaction between cells and these positively charged NMs.[32, 34, 35] For example, a study by Ganguly and colleagues suggested that the cellular uptake of positively charged Au NPs is approximately five times higher than the uptake rate of negatively charge Au NPs.[32] Similarly, in an *in vivo* study in *D. magna*, researchers demonstrated that enterocytes of the gut had significantly higher reactive oxygen species (ROS) production when exposed to positively charged Au NPs than negatively charged NPs at all three concentrations (1, 10 and 50 µg L^{-1}) tested.[36] Their results also suggested that the levels of *glutathione S-transferase* (*gst*) and *heat shock protein 70* (*hsp70*) expression were significantly upregulated by positively charged particles at a concentration

of 50 μg L^{-1} while negatively charged NPs did not cause any significant change in gene expression.[36] Silva and colleagues reported that Ag NPs with negatively charged coating had lower median lethal concentration (LC$_{50}$) values on *D. magna* than positively charged and neutral Ag NPs.[37] Altogether, this demonstrates that surface charge is a significant mediator of exposure and dose for aquatic organisms.

1.2.3 Shape

The shape of the NMs can affect zeta-potential, SSA and stability of given NMs, each of which has been demonstrated to alter NM toxicity.[20, 22, 38, 39] Studies suggested that the shape of the NM can alter SSA which may bring out significant changes in SSA and dissolution behavior.[22, 40] For example, Misra et al. characterized copper oxide (CuO) NPs in two different shapes including spheres (7 nm) and rods (7 nm x 40 nm) with the same length at one dimension. The point of zero charge (PZC, see section 1.3.1 for details) of the sphere was higher than the rod, and this may be due to the higher SSA of the sphere. These authors also found that the dissolution of spherical CuO NPs (2.5%) was higher than the rod-shaped NPs (0.8%) over 7 days, which also can be explained by the higher SSA of the sphere.[22] The shape-dependent characteristic of NMs has been shown to alter their toxicity directly. In *in vivo* study in adult zebrafish, the LC$_{50}$ value of spherical nickel (Ni) NPs with 60 nm diameter was 361 mg L^{-1}, three times higher than the LC$_{50}$ value of dendritic Ni NPs with a similar 60nm aggregated size. However, spherical Ni NPs had a much higher rate of uptake (~3 times greater) than dendritic NPs.[41] Similar studies on *D. magna* have also supported that differences in toxicity of NMs result from different shapes.[42, 43] In one study,

long rod gold (Au) NPs (25nm x 146 nm) caused a significantly higher mortality rate in *D. magna* neonates than both short rod Au NPs (25nm x 60 nm) and spherical Au NPs (25 nm). The results also showed that both positively charged rods and spheres induced significant ROS generation in *D. magna*, but the ROS level returned to normal level 24 h after being exposed to spherical NPs while ROS level remained high in *D. magna* exposed to short rod NPs after 24 h.[43] Therefore, it is worth to consider and report the shape of NMs when investigating their toxicity.

1.2.4 Crystal structure

The crystal structure has been reported to have an impact on both solubility/dissolution of NM and interaction of NMs with UV light, each of which has the potential to alter the toxicity of given NMs.[44, 45] The solubility and dissolution behavior of NMs play an essential role in the bioavailability, rate of uptake and toxicity of each type of NM.[7, 21, 45] With regard to crystallinity, TiO_2 NPs have three described crystal structure forms (anatase, rutile and brookite) but only anatase and rutile are natural forms, and each is widely used in various applications.[44, 46] Anatase TiO_2 NPs are more toxic to a variety of organisms, including mammalian cell lines, green algae and *D magna*.[23, 44, 47] A study on green algae *Chlorella* sp. showed that anatase TiO_2 NPs reduced the growth of algae by 75% at an arguably non-ecologically relevant nominal concentration of 1000 mg L^{-1} at pH 6.5 while rutile TiO_2 NPs did not have any significant impact on the growth at the same concentration.[48] The median effective concentration (EC_{50}) value of immobility of *D. magna* exposed to 99.5% anatase TiO_2 with a primary size of 20 nm was 35.3 mg L^{-1}, and

the EC_{50} value increased to over 100 mg L^{-1} when rutile TiO_2 NPs were added and the purity of anatase reduced to 70%.[47] While these studies suggested that the higher toxicity of anatase TiO_2 NPs was due to its higher solubility[44, 45], we suggest that the differences in toxicity may be more attributable to differences in crystallinity. Both anatase and rutile TiO_2 NPs are practically insoluble (less than 0.000066% dissolution rate) at or close to neutral pH (7) where these tests were conducted. While the study did show that anatase TiO_2 NPs had a higher dissolution (0.022% over 2 h) than that rutile form (0.00016% over 2 h), this was conducted in a solution with a very low pH (1.5) which is not ecologically or biologically relevant.[45] We believe that a better explanation is that anatase form produces more ROS than rutile form, even under non-UV conditions, and that uptake of particles likely induced ROS-mediated toxicity.[44, 48] Other studies have confirmed a role for crystallinity in superoxide radical ($O_2^{\bullet-}$) formation under both laboratory (non-UV) and UV condition. In each case, rutile TiO_2 NPs (30 nm x 70 nm) have been shown to demonstrate lower photoactivity when compared to the crystalline anatase form (30-50 nm), resulting in substantially higher $O_2^{\bullet-}$ generation by the anatase form under UV light conditions.[49] Kakuma et al. proposed a mechanism for the lower production of ROS in rutile TiO_2 NPs. Their study demonstrated that the smaller distance between Ti atoms in rutile (296 pm 379 pm in anatase TiO_2) leads to the formation of Ti-OO-Ti on the surface, which causes rapid formation of O_2 by oxidation.[50] Therefore, it is essential to report crystal structure when studying the toxicity of NMs with more than one crystal structure.

1.2.5 Dissolution

9

Many studies have demonstrated that dissolution of metallic NMs and release of free metal ions either acted as the primary mechanism of toxicity to aquatic organisms or contributed to part of the toxicity, especially in an aqueous medium.[7, 21] There is a substantial amount of literature on the mechanisms and mediation of various metals toxicity in aquatic animals.[51-53] This chapter will not cover the specific aspects of metal toxicity *per se* but instead focus on the environmental properties affecting dissolution and subsequent toxicity. Dissolution depends on the intrinsic characteristics of the NMs including particle size, particle type, concentration and also specific environmental factors including pH, temperature and NOM.[7, 54] Dissolution of many metallic NPs has been shown to increase as concentration decreases due to lower aggregation/increased dispersion at lower concentrations.[55, 56] As particle size decreases, the SSA increases exponentially, which results in a higher percentage of atoms exposed to the environment and therefore a higher dissolution rate.[7, 54] In a study on the size-dependent dissolution of zinc oxide (ZnO) NPs, a particle with the smallest primary size (4 nm) had the highest dissolution rate (5.7%) comparing to 15 nm (2.2%) and 241 nm (1.0%) at pH 7.5.[57] Environmental pH has almost no impact on the dissolution of TiO_2 NPs while that of ZnO NPs is highly dependent on the environmental pH.[16, 57, 58] CeO_2 NPs are relatively insoluble in the water at pH >5, but their dissolution become pH-dependent when environmental pH is lower than 4.5.[59] Studies have shown that increasing temperature and low pH tend to enhance the dissolution rate of metallic NMs[7, 21] while NOM can increase dissolution by donating chelating agents for metal ions or reduce dissolution by preventing interaction between particles and water molecules when adsorption onto the surface of the particles.[9, 54] Two studies on ZnO NPs dissolution and toxicity demonstrated that iron (Fe) doped ZnO NPs

had significantly lower dissolution rate as Fe percentage increasing. They also concluded that ZnO NPs reduced the hatching success of zebrafish embryos to approximately 40% while 1%, 4% and 10% Fe-doped ZnO NPs with a similar particle size as ZnO NPs increased hatching success to over 65%.[60, 61] Therefore, it is necessary to definitively address, in each study, potential confounding issues of the presence of separate toxicity of dissolved ions compared with the toxicity of NP in the presence of dissolved ions and by subtraction, address the toxicity of the NP itself. Authors of papers are highly encouraged to report dissolution rates when describing the exposure toxicity of any given NMs.

1.3 Environmental Factors Affecting the Toxicity of Nanomaterials

Once released into the environment, NMs and their subsequent biological effects are known to be modulated by various environmental factors including IS, pH, NOM and UV light, each of which can cause distinct physicochemical changes (e.g., agglomeration/aggregation, change in surface charge and electronic excitation) that have the potential to alter bioavailability and the toxicity of NMs. [7, 20, 62]
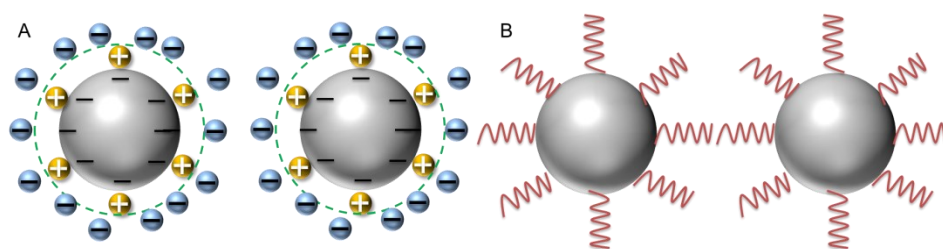
Figure 1-1. Electrostatic stabilization (A) and steric stabilization (B) of NMs.

1.3.1 Ionic strength and pH

While the pristine sizes of NMs (as discussed above) play distinct roles in diffusivity and transport, the actual size as demonstrated in the environment during the exposure period also plays an integral role in determining their distribution and bioavailability to aquatic organisms.[7] The stability of NMs can be achieved mainly by two mechanisms, electrostatic stabilization and steric stabilization (Figure 1-1).[7, 20, 62, 63] However, sterically stabilized uncharged polymer-coated NMs are relatively insensitive to ionic strength and pH.[62, 63] A study published in 2010 demonstrated that the zeta-potential and hydrodynamic diameter (HDD) of PVP coated Ag NPs did not significantly change over the pH range from 3 to 9 and ionic strength of 10 and 100 mM.[62] Therefore, electrostatically stabilized NMs are the focus of this section. Derjaguin Landau Verwey Overbeek (DLVO) theory states that the size and stability of NMs in suspension are affected by the sum of van der Waals forces (attractive forces) and electrostatic forces (repulsive forces).[7, 13, 20, 64] Aggregation occurs when the attractive forces dominate repulsive forces and the opposite is true for disaggregation.[9, 15, 16] Electrostatic repulsive forces are generated by the electrical double layers (Figure 1-2) of particles interacting with each other.[20] IS and pH are two important abiotic factors that have effects on NM agglomeration by affecting their electrical double layer (EDL).[18, 20, 58] The repulsive energy generated by the EDL is a function of surface charge (zeta potential) and the thickness of EDL.[20] Studies have shown that high IS in solution results in a reduction of the thickness of EDL and subsequent greater interaction between particles.[7, 20, 62, 64] The higher IS reduces the electrostatic repulsive forces by shielding or neutralization which will increase agglomeration.[7, 20, 62, 64] In general, the toxicity of an NM is usually reduced when there is a significant aggregation of the NM into larger agglomerates.[29, 65-67] A few papers have linked increasing ionic

strengths to both increase agglomeration with direct resulting lower relative toxicity.[29, 65] For example, the EC_{50} value of TiO_2 NPs on the immobility of *D. magna* was increased from 1.28 mg L^{-1} (10 nm) and 0.53 mg L^{-1} (25nm) in a medium with IS of 865 µM to 2.9 mg L^{-1} and 1.1 mg L^{-1} in a medium with IS of 8653 µM respectively.[29] Similar trends were also found in Ag NPs. The lowest observed adverse effect concentration (LOAEC) of immobility was estimated to be 11.25 µg L^{-1} when *D. magna* were exposed to Ag NPs (7 nm) while the LOAEC decreased to 2.5 µg L^{-1} when *D. magna* exposed to the same NPs at the same concentration but in the ten-fold diluted media.[67] A study on the effects of Ag NPs on zebrafish embryos demonstrated that Ag NPs suspension with both primary sizes of 20 nm and 100 nm had significantly lower LC_{50} values in ultrapure water and the media with IS of approximately 187.5µM than the media with IS of about 22.9 mM. The EC_{50} of mortality and malformation for citrate-stabilized Ag NPs suspension was also significantly lower in the media with IS of 22.9 mM.[65]
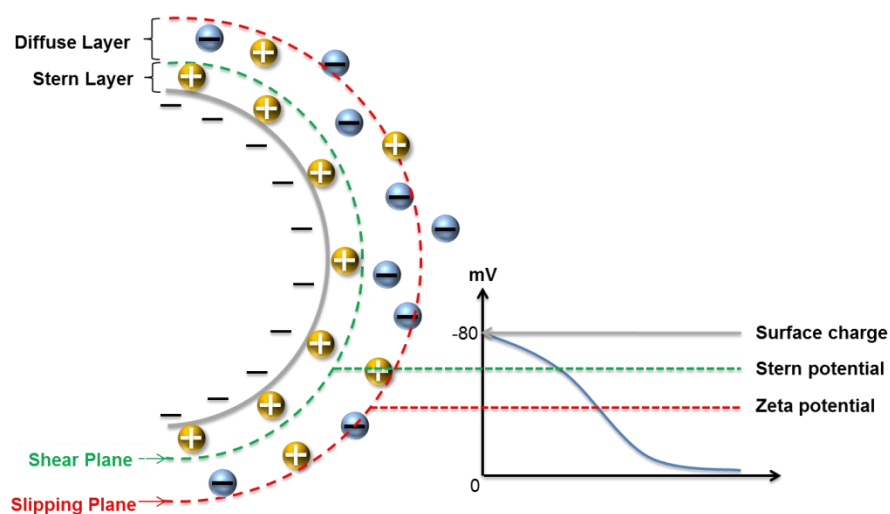
Figure 1-2. The simplified model of the electrical double layer at a negatively charged NM's surface in an aqueous medium.

Environmental pH also plays an important role in controlling the zeta potential, resulting in aggregation/agglomeration, and therefore toxicity of given NMs.[20, 62] Zeta potential measures the electric potential at a certain distance from the plane of shear[62] and it is not the same as surface charge (Figure 1-2).[20] For a constant medium ionic strength, the zeta potential, surface charge and HDD of a given NM are significantly affected by the pH of the aqueous medium.[19, 20, 62] The PZC is the pH of a given medium when NM has zero net surface charge. Therefore, the absence of electrostatic repulsive force prevents disagglomeration and NMs will settle out of suspension eventually.[20, 58, 62] As pH becomes progressively lower than PZC, NMs have a more positively charged surface. On the other hand, NMs are more negatively charged as pH is progressively higher than the specific PZC.[18, 20, 58] In general, an NM with the zeta potential higher than +20 mV or lower than -20 mV is considered stable and its agglomeration rate is low or even close to zero.[18, 62] In an aquatic environment where ionic strength is low and pH is far away from the NM's PZC, NMs will have generally low agglomeration rate and are more likely to remain suspended as individual particles or small agglomerates in the medium.[18, 20] As discussed above (see section 1.2.2), cell membranes are negatively charged.[32, 33] The alterations of environmental pH below PZC will result in positively charged NMs which leads to a higher binding potential to respiratory surfaces including gills and skin. Accumulation of NMs on the surface of gills can result in simply irritation and mucus hypersecretion which have a negative impact on gas transport, osmoregulation and alter the uptake of molecules across the biological membrane through normal endocytotic processes.[68] Therefore, pH affects the toxicity of NMs through both altering their aggregation/agglomeration and altering the interaction of the individual and agglomerated materials with respiratory surfaces. For

example, an *in vitro* study reported that 24-hour aged ZnO NPs with lower aggregation size had a significantly higher negative impact on the mitochondrial activity of RAW 264.7 cell line at concentrations of 10, 15 and 20 μg mL^{-1}, and induced higher generation of ROS at a concentration of 10 μg mL^{-1} than ZnO NPs with higher aggregation size.[69] An *in vivo* study reported that 48h- EC$_{50}$ value of immobility of *D. magna* exposed to citrate-coated Ag NPs was significantly higher (1.5 times) in the environment with pH of 8 than that in pH of 6.5 when there was no significant difference in the Ag$^+$ concentration. It also demonstrated that lower pH significantly reduced the number of offspring produced during the exposure, and increased mortality from 30% at pH of 8 to 90% without the presence of NOM and from 20% at pH of 8 to 40% with the presence of NOM after exposed to 78 μg L^{-1} NPs for 21 days.[70] In whole animal studies examining the effects of IS and pH on aggregation and the toxicity of NMs, researchers have often used NMs with different concentrations and/or they compared NMs to their bulk form counterparts to achieve different aggregation size/rate.[71-73] However, in many studies, researchers have failed to characterize NMs in the environmental test conditions, using the characterization of their bulk/pristine forms as a guide. This has perhaps led to simplistic interpretations of the principle toxicological drivers. In media with biological organisms, NMs can assume different/new physiochemical properties which should be considered to properly interpret these ecotoxicity studies. In many cases, the aggregation/agglomerations and resulting changes in concentration, and/or significant changes in ion concentration were not accounted for, inevitably acting as confounding factors.[7, 71, 73] In general, NMs with lower aggregation size/rate are considered to have more toxic potential largely due to the greater surface area available for biological interactions and increased potential for transport into the animal.[7,

[11, 71, 73] The combination of low agglomeration rate, small size and high SSA will increase the bioavailability of the NMs to interact with living organisms in the water column.[7] An aquatic environment with higher ionic strength and/or pHs close to PZC will enhance the agglomeration of NMs resulting NMs settling out and concentrating at the bottom of the test vessel or in the sediment. In this case, the risk is transferred from pelagic to benthic organisms and negatively buoyant embryos.[7, 14, 19] As mentioned in section 1.2.3, pH can also have significant effects on the dissolution of specific metallic NMs resulting in changes in dissolved ion concentration which potentially can mediate some of the toxicity of metallic NMs (e.g. ZnO NPs and Ag NPs).[30, 54] In summary, environmental ionic strength and environmental pH can have a significant impact on the aggregation, dissolution, distribution, bioavailability and the potential target organisms of NMs.

1.3.2 Ultraviolet light

Solar radiation has important effects on every life on Earth.[74] Its UV component is divided into three groups based on wavelength, including UVA (315-400 nm), UVB (280-315 nm) and UVC (100-280 nm).[74, 75] The shorter wavelength UVC and UVB are the most damaging, but all the UVC is blocked and the majority of UVB is absorbed by the stratospheric ozone layer. Large amounts of UVA can pass through the stratospheric ozone layer and reach the surface and therefore this type of UV light has more environmental relevance.[74] The majority of nanotoxicity studies are performed in laboratory conditions,[7, 12] where fluorescent lamps used emit negligible amounts of UVA and UVB radiation.[75] However, many NMs released into the environment either are wide band-gap

semiconductors or have semiconductor properties.[38] Studies have shown that these NMs can absorb energy including photon energy (light) and phonon energy (heat). When the energy input is at or above the band gap between the valence band and conduction band, electron on valence electrons will absorb enough energy to jump to the conduction band becoming a free electron and leave a positively charged hole (Figure 1-3).[17, 38] This results in an electron-hole pair, which can react with oxygen and water molecules in the environment to produce ROS.[17, 38] ROS are highly reactive due to their unpaired electron and can cause cellular damage when overwhelming a cells/organisms antioxidant defense system.[71, 76-78] ROS and reactive nitrogen species (RNS) are naturally derived substances in normal metabolism. For example, NO• and H_2O_2 play an important role in cellular signaling and regulating apoptosis.[79] They are also involved in the recognition process by macrophages and neutrophils in the innate immune system and combating bacterial infections by immune cells.[78, 80, 81] Similarly, superoxide radical ($O_2^{•-}$) is generated due to incomplete reduction in the mitochondria during oxidative phosphorylation.[38, 79] Therefore, an antioxidant defense system has evolved to both regulate endogenous ROS/RNS production and also mitigate ROS/RNS caused by external stress.[78] Antioxidant enzymes such as catalase, glutathione peroxidase (GPx) and superoxide dismutase (SOD), and antioxidants like glutathione are all part of this process.[78-80] Nevertheless, when band gap semiconductor NMs are exposed to UV light, many studies have shown they generate ROS causing excess oxidative stress. When the systemic manifestation of ROS overwhelms an organisms' antioxidant defense capacity, the negative effects of ROS and NOS include excess lipid peroxidation and protein carbonylation which can be used as a marker of excess ROS/NOS exposure.[21, 29, 38]
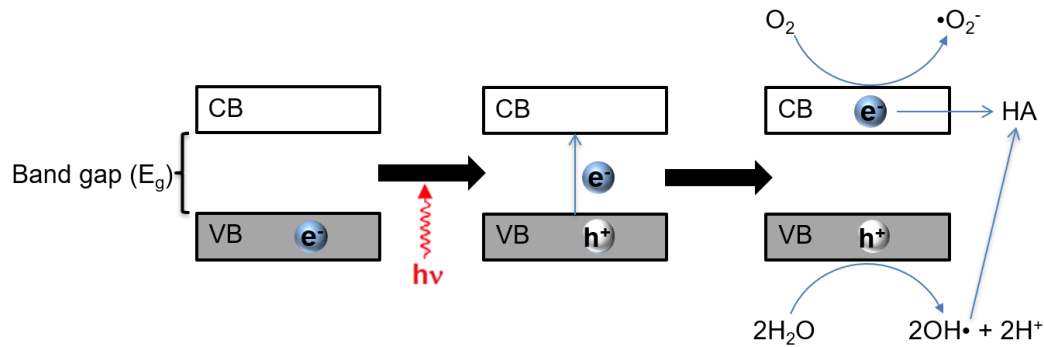
Figure 1-3. The generation of reactive oxygen species (ROS) on the surface of semiconductor NMs under UV radiation exposure and the scavenging activity of humic acid (HA). Valence band (VB), conduction band (CB).

Most studies on phototoxicity of semiconductor NMs have focused on metal oxide nanoparticles, especially TiO_2 NPs, in a variety of species.[17, 29, 38, 82] Phytoplankton are the foundation of the food web in the aquatic environment where they contribute to over 100 million tons of carbon cycle every day as the dominant primary producers.[83, 84] Phytoplankton rely on solar energy for photosynthesis so they may be vulnerable to photo-inducible NMs.[29, 83, 84] A study reported that TiO_2 NPs at concentrations of 1 to 3 mg L^{-1} significantly suppressed the population growth rate from 50% to almost 100% in three marine phytoplankton species under UV.[83] Locomotion is important to the aqueous organism for feeding and avoiding predation so the decreased mobility will reduce their ability to survive in nature. Wyrwoll et al. reported that TiO_2 NPs with 25 nm primary size had higher phototoxicity on *D. magna* under UV exposure than laboratory light. The EC_{50} of immobility was 0.53 mg L^{-1} (nominal concentration) under UV exposure while *D. magna* did not show any immobility at the concentration of 100 mg L^{-1} under laboratory light at 48-hour exposure.[29] This study also suggested a significant increase in the

production of •OH and $O_2^{\bullet-}$ by UV light may be the cause of the phototoxicity of TiO_2

NPs.[29] Studies also showed UV light increased the mortality of *D. magna* during 48-hour

exposure (LC_{50}=29.8 µg L^{-1} under UV stimulation vs. $LC_{50} > 500$ mg L^{-1} under laboratory

light) and reduced growth rate in other marine phytoplankton species exposed to TiO_2 NPs

at a concentration of 1 mg L^{-1} and above under UV exposure.[17, 83] Therefore, any change in

abundance and biomass of phytoplankton and primary consumer in food chain caused by

co-exposure of semiconductor NMs and UV light may have a significant impact on the

stability of the ecosystem.

The early development stage of organisms is a complex process and very vulnerable to

chemical disturbance (Figure 1-4).[82] A study done by Bar-Ilan et al. demonstrated that UV

illumination significantly reduced survival rate and increased the incidence of

malformation, including yolk sac edema, pericardial edema, spine stunting and tail

abnormality, of zebrafish embryo exposed to TiO_2 NPs for 92 h starting from 4 hours post-

fertilization (hpf). This may be explained by the dramatic increase in •OH production in the

water by TiO_2 NPs under UV illumination.[82] Phototoxicity of NMs has been reported in

other species at different life stages. The LC_{50} of juvenile Japanese Medaka exposed to

TiO_2 NPs for 96 h was significantly decreased from the nominal concentration of 155 mg

L^{-1} under laboratory light to 2.19 mg L^{-1} under UV light.[17] Similar results were reported by

Ma et al. in *D. magna*. The 48-hour LC_{50} value decreased from over 500 µg L^{-1} under

laboratory light to 29.8 µg L^{-1} under UV light.[17]

For less well-studied semiconductor NMs, Zhang et al. examined the effects of CeO_2

NPs on the lipid peroxidation and morphological alternations in gills of cardinal tetra. CeO_2

NPs under the stimulation of UV light significantly induced lipid peroxidation in gills at

medium (2 mg L^{-1}) and high (5 mg L^{-1}) nominal concentrations.[85] Moreover, co-exposure of CeO$_2$ NPs and UV light caused the medium to serve damage on gills including an increase in interlamellar cell mass, fusion of lamellae, hyperplasia of primary lamellae and lifting of respiratory epithelium (Figure 2-8).[85] Authors concluded that observed photo-toxicity of CeO$_2$ can be explained by the increase in the generation of hydroxyl radical under UV light.[85] Therefore, toxicity studies on NMs, especially band gap NMs, should include UV stimulation to enhance the understanding of the potential phototoxic effects in an environmentally realistic condition.
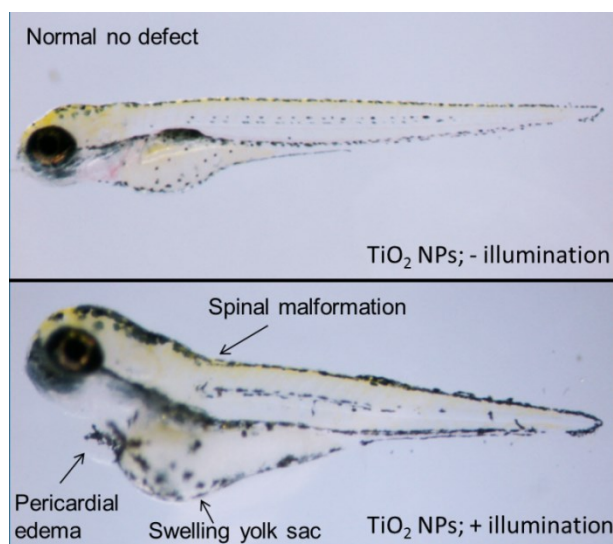
Figure 1-4. Morphology of zebrafish embryo at 120 hpf after exposed to 1 mg L^{-1} TiO$_2$ NPs (25 nm) under UV light (+ illumination) and laboratory light (- illumination).

1.3.3 Natural organic matter

Natural organic matter is an anionic heterogeneous matrix of carbon-based compounds formed from the microbial decomposition of plants, algae and animals, and their waste

products.[2] The composition of degraded products varies between different origins and shows temporal changes[2, 76] and therefore, in this review, NOM is referred to as a bulk constituent primarily dominated by humic and fluvic acids. For a more complete understanding of the role(s) or different constituents of NOM on the interaction with NMs, the reader is referred to some excellent papers by Nason et al.[86] and Gallego-Urrea et al.[87] NOM is present in both terrestrial and aquatic environments, and humic acid (HA) and fulvic acid (FA) are two of the most abundant compositions in many origins of NOM.[2] NOM is divided into a hydrophobic portion which contains aliphatic carbon and a hydrophilic portion which is composed of humic-like substances.[2, 88] The carboxyl group (-COOH) in the hydrophobic portion and phenolic group hydrophilic portion make NOM negatively charged at the pH value of natural water.[2, 88] Aggregation/disaggregation mainly depends on the environmental pH, environmental divalent ion concentration, concentration ratio of NOM to NMs and PZC of NMs.[58] The adsorption of low molecular mass NOM onto NMs' surface forms an ecocorona, which will increase the electrostatic repulsion between NMs due to more negative zeta potential or increase steric repulsion caused by adsorption of NOM on the surface[20, 71] to reduce the aggregation and increase the stability of NMs in the water column[13, 89, 90] when the concentration of divalent ions (i.e. Ca^{2+} and Mg^{2+}) is lower than the critical coagulation concentration (Figure 1-5).[20, 58] However, NOM can also cause bridging effects to enhance the aggregation in the environment with high ionic strength and the presence of (Figure 1-5).[18, 19] Studies have shown that the formation of an ecocorona can modulate the toxicity of NMs in a variety of aquatic species.[2, 7, 54, 91] The EC_{50} on the growth rate of unicellular green algae *P. subcapitata* was determined to be 1.24 mg L^{-1} in CeO_2 NPs and 0.27 mg L^{-1} in TiO_2 NPs. The presence of Suwannee River

NOM at a concentration of 8 mg L^{-1} increased EC$_{50}$ values (> 30 mg L^{-1}) of both NPs way above ecologically relevant concentration.[92] The presence of NOM from three different origins has been reported to significantly increase LC$_{50}$ values of Ag NPs, especially copper nanoparticles (Cu NPs), on *Ceriodaphnia dubia*.[91] This reduction in toxicity may be explained through three mechanisms 1) the adsorption of NOM onto NMs' surface can reduce the direct interaction between NMs' surface and organisms, decrease the cellular uptake of NMs, and reduce the bioavailability of NMs to lower the toxicity of NMs;[76, 90, 93] 2) the adsorption of NOM can decrease the interaction between metallic NMs' surface and water molecules to reduce the dissolution which will decrease the toxicity caused by metallic ions;[9, 54, 94] 3) free ions released from NPs can be complexed by the presence of NOM and therefore the bioavailability of free ions is reduced.[54] On the other hand, the adsorption of high molecular mass NOM and increased aggregation due to charge neutralization and bridging effects will favor the removal of NMs from the water column and increase the bioavailability to the organisms in the sediments.[19, 58, 94] Therefore, the presence of NOM not only affects the distribution and bioavailability of NMs in the environment but also play an important role in determining the toxicity of NMs in organisms.
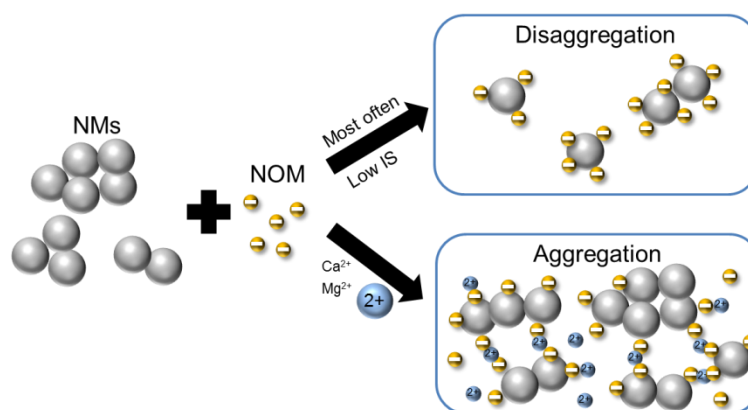
Figure 1-5. Modified schematic particle stability diagram of nanomaterials interacting with natural organic matter and divalent ions.[2, 18, 58]

As discussed in section 1.3.2, UV light can induce the toxicity of NMs, especially semiconductor NPs. In recent years, NOM has been found to have protective property against phototoxicity of NMs.[7, 9, 95] NOM is able to attenuate UV light to reduce the amount and the intensity of UV light received by NMs.[16] Humic acid present in many NOM are considered to be an electron acceptor pool.[2, 9, 96, 97] Studies have shown that NOM containing humic acid can accept electrons excited by UV light and quench the production of ROS which can reduce the photo-toxicity of NMs (Figure 1-3).[2, 7, 9, 16] For example, Wormington et al. demonstrated that NOM at the concentration of 4 mg L^{-1} reduced the morality of *D. magna* from over 90% (0 mg L^{-1} NOM) to less than 10% when exposed to 1.5 mg L^{-1} TiO$_2$ NPs under UV light for 48 h. Such a significant decrease in toxicity can be partially explained by the reduced production of H$_2$O$_2$ equivalents measured in the media at the presence of NOM due to its ROS quenching ability.[16] These results showed the protective property of NOM against photo-toxicity of NMs.

1.4 Thesis Goals

The main objectives of my research were to 1) determine if environmental factors, including UV light and NOM, can modulate the lethal and sub-lethal effects of NM on aquatic organisms, 2) evaluate the toxicological effects of metal oxide nanoparticles, nano-enabled pesticides and nanoplastics on various aquatic organisms at multiple biological levels of organization. 3) investigate the mechanisms of toxicity. The thesis objectives mentioned above are not chapter-specific.

Chapter 2

UV induced toxicity of cerium oxide nanoparticles (CeO₂ NPs) and the protective properties of natural organic matter (NOM) from the Rio Negro Amazon River
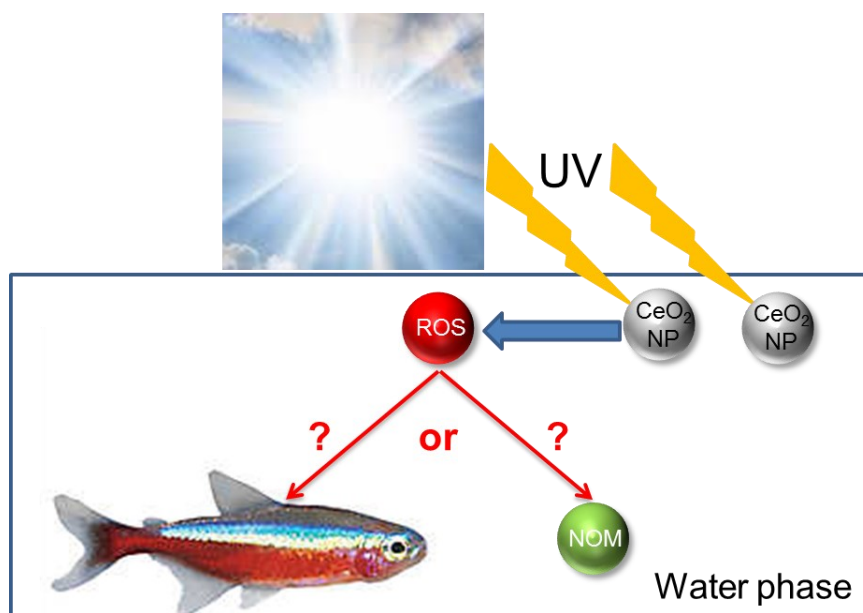
Y. Zhang, T. A. Blewett, A. L. Val and G. G. Goss, UV-induced toxicity of cerium oxide nanoparticles (CeO₂ NPs) and the protective properties of natural organic matter (NOM) from the Rio Negro Amazon River, *Environmental Science: Nano*, 2018, **5**, 476-486 DOI: 10.1039/C7EN00842B.

2.1. Introduction

The main industry of the Amazon basin region has switched from the traditional rubber industry to petroleum refining, automotive and mobile phone manufacturing since the late 20th century.[98] Ships/boats are still the major route of transportation in this region due to underdeveloped ground transportation infrastructure.[98] Similarly, electric power to remote villages is almost entirely derived from the use of diesel generators.[99] CeO_2 particles are widely used as a diesel fuel additive to increase the efficiency of diesel fuel burning and the combustion of soot to reduce the emissions, thereby providing a direct route of entry into the environment.[76, 100] Increasing use of cerium oxide nanoparticles (CeO_2 NPs) in a variety of products has raised the potential for release into this very sensitive environment and has attracted concerns about their impact on aquatic organisms.[100, 101] Amongst the most commonly produced NPs, CeO_2 NPs have a global production estimated to be over 10,000 tons in 2014 alone.[102] As catalysts they have a significant oxidative capacity, surface reactive properties and are known to absorb ultraviolet (UV) radiation in $\sim$ 400 nm range, amongst the strongest of any oxide metal.[100, 103] Approximately 4,400 tons CeO_2 NPs were used as a diesel fuel additive in 2014 and of these, an estimated, 15% would be present as NPs.[102]

CeO_2 NPs are commonly considered to be insoluble and poorly dispersive in most natural water systems where the pH > 6 and ionic concentrations are high,[76, 100, 104] and thus, potential environmental impacts of CeO_2 on aquatic animals have attracted little attention.[100, 101] However, the waters of the Rio Negro are especially unique in their chemical properties and likely represent a "worst-case scenario" for the potential toxicity of CeO_2 NPs. The waters of the Rio Negro have very low ion concentrations, nearing those of distilled water (Na^+, 16.5 ± 5.3 $\mu mol\ L^{-1}$; K^+, 8.2 ± 2.7 $\mu mol\ L^{-1}$; Ca^{2+}, 5.3 ± 1.6 $\mu mol\ L^{-1}$; Mg^{2+}, 4.7 ± 1.4

μmol L^{-1}; and Cl$^-$, 47.9 ± 19.7 μmol L^{-1}),[105] low pH (reaching values below pH 4.5),[106] high concentrations of natural organic matter (NOM, 10.65 ± 0.53 mg L^{-1})[107] and experience high UV intensity (> 2.4 W m^{-2} UVA intensity) during the day,[108] each of which may exacerbate CeO$_2$ toxicity. The bioavailability and toxicity of CeO$_2$ NPs may vary considerably depending on a number of these abiotic factors.[109] Studies have shown that CeO$_2$ NPs display increasing and substantial solubility (i.e. release of Ce^{3+}/Ce^{4+} ions) in soft water with a pH less than 4[90, 104] and under low ionic strength.[14, 90] Similarly, UV light has been reported to induce toxicity of various metal oxide NPs, including CeO$_2$, due to their photocatalytic properties allowing them to generate reactive oxygen species (ROS) under UV light.[7, 110-112] Finally, the presence of NOM can either increase or decrease aggregation/agglomeration of NPs depending on the composition[14, 89, 90, 109, 113, 114] and studies have also shown that NOM can attenuate the ROS mediated effects.[16, 89]

One species of note, that is native to the Rio Negro Amazon Basin is the cardinal tetra (*Paracheirodon axelrodi* Géry, 1960).[24] The tetra is a common aquarium trade species originating from the Rio Negro Amazon Basin.[115] They are adapted to living in these unique waters and are an appropriate species for the study of CeO$_2$ toxicity.[115] In the current study, we sought to assess the potential effects of UV light and NOM on the toxicity of CeO$_2$ NPs.

2.2 Methods and Materials

2.2.1 Isolation of NOM from Rio Negro water

Rio Negro water samples were collected near Novo Airão city, 180 km upstream from Manaus Brazil, following the method used by Duarte et al.[116] Briefly, water samples were pumped through 1μm wound filter to a reverse-osmosis unit (Vontron® ULP21-4021 polyamide membrane, Permution, model PEOS-0001, Curitiba, Brazil) and then were treated with cation exchange resin (Amberlite IR-118 (H), Sigma-Aldrich, St. Louis, USA) to remove Na^+ and Ca^{2+} from concentrate to allow for independent reconstitution of Rio Negro humic acids (HA) in experimental treatments. Concentrated water was pumped through 0.45μm filters (AcrodiscTM, Pall, Ann Arbour, USA) and stored at 4 °C for further analysis and used in live fish experiments.

2.2.2 Animals and maintenance

Adult cardinal tetras (approximately 300 mg) aged 4 to 8 months were housed in four 60-L glass tanks filled with home-made soft water (double-distilled H_2O, ddH_2O, with 11.6 mg L^{-1} NaCl, 11 mg L^{-1} $CaCl_2$). The water was kept at a temperature of $22 \pm 1°C$ and treated with 0.1 M HCl twice daily to maintain pH at 4.5 (measured by an electrode connected to a pH meter; Accumet Basic, AB15, Fisher Scientific). Fish were fed daily (1% body weight per day) a diet with ground tropical fish flakes (Nutrafin Max) to satiation and were kept on a 16 h light: 8 h dark photoperiod throughout the study. All animal research was approved under the University of Alberta which was approved by the Canadian Council for Animal Care Committee under protocol AUP 00000001 to Dr. Goss.

2.2.3 Preparation of the cerium oxide nanoparticle suspensions

Cerium oxide nanopowder (CeO$_2$, 99.97%, 10-30 nm; Stock#: US3036, CAS#: 1306-38-3) was purchased from US Research Nanomaterials, Inc. (Houston, Texas, USA) and stored in the dark at room temperature. Nanopowder was suspended in either autoclaved double-distilled water (ddH$_2$O) or Rio Negro Amazon waters (Brazil; NOM water) at nominal concentrations of 0, 0.5, 2 and 5 mg L^{-1}, treated with 0.1 M HCl to adjust pH to 4.5, and NaCl and CaCl$_2$•2H$_2$O were added to adjust concentration of Na$^+$ to 10 µmol L^{-1} and concentration of Ca^{2+} to 5 µmol L^{-1}. The suspensions were sonicated in a water bath (50/60 Hz, 117 V, 1 A, Branson 2200, Branson Ultrasonics Corporation, CT, USA) for 5 min at room temperature and then mixed with vortex (Fisher Vortex Genie 2, Fisher Scientific) for 10 s before taking aliquots for further analysis or addition to exposure tanks.

2.2.4 Characterization of cerium oxide nanoparticles

Samples of cerium oxide NPs suspension at 5 mg L^{-1} were pipetted onto a carbon-coated copper grid and dried for 3 h. Transmission electron microscopy (TEM, FEI Tecnai-20) was used to confirm the shape and size of nanoparticles. Dynamic light scattering (DLS; Zetasizer Nano Series, Malvern Instruments Ltd.) in 173° backscatter mode (Zetasizer software, v. 7.01) was used to characterize the size, surface potential and aggregation of NPs in 0.5, 2 and 5 mg L^{-1} test suspensions at 28.5°C over time. Mean z-average hydrodynamic diameter (HDD), polydispersity index (PDI) and zeta (ζ) potential were measured by DLS at 0, 2, 4, 6, 12, 24, 48, 72 and 96 h. The cell (ZEN 1002) was inserted into a cuvette and then any remaining air bubbles were removed by gently flicking

the cuvette to avoid interference with the measurements of zeta potential. Samples were covered by parafilm and kept static between measurements.

X-ray photoelectron spectroscopy (XPS) was performed by a Kratos Axis Ultra instrument operating in energy spectrum mode at 210 W following the procedure described by Kumar et al. to determine the ratio of Ce^{3+} and Ce^{4+} in CeO_2 NPs suspended in ddH_2O (see Supplementary Text A2-1).[117]

2.2.5 Dissolution experiments

Dissolution experiments were performed to calculate the concentration of free metal ions present in the nanoparticle test suspensions over a 96 h period (see Supplementary Text A2-2).

2.2.6 Hydroxyl radical generation

Hydroxyl radical (•OH) generation in the water was determined by using a modified method described by Felix et al.[110] Briefly, 1 mL of a 2-deoxy-D-ribose (2-DR) stock solution (400 mM) was made by adding 53.6 mg 2-DR powder (Sigma; 31170) into ddH_2O. The stock solution was vortexed for 1 min and sonicated in a water bath for 5 min before use. 4.95 mL of 0, 0.5, 2 and 5 mg L^{-1} CeO_2 NPs in either ddH_2O or Rio Negro Amazon water were added into individual wells of four polystyrene 12-well plates, followed by 50 μL of 2-DR stock solution in each well. A handheld UVX digital radiometer was used to measure the spectral irradiance from UV lamp with UVA (UVX-

36; calibrated at 365 nm) or UVB (UVX-31; calibrated at 310 nm) sensor (Ultra-Violet Products Ltd., CA, USA). Two 12-well plates were incubated 5 cm under UV light (UVA: 3.1 ± 0.29 W m^{-2}, UVB: 1.7 ± 0.21 W m^{-2}) for 30 min while the other two plates were incubated under laboratory light. After incubation, TBARS assay (see below) was used to analyze the amount of •OH generated by the CeO_2 in the presence/absence of UV light (see 1.2.7).

2.2.7 Co-exposure of cardinal tetras to nanoparticles and simulated UV light

Fish were randomly selected and placed into a 5-L (28cm x 14cm x 13 cm) tanks filled with 1-L of either autoclaved double-distilled water or Rio Negro waters (Amazonas, Brazil), titrated to pH 4.5, and at 22 °C with the concentration of CeO_2 NPs at 0.5, 2 or 5 mg L^{-1}. Fish in Rio Negro waters alone served as control. Preliminary experiments in Brazil were conducted outside in the presence of natural sunlight and UV profile was measured and reported (see Figures S2-1 & S2-2). For sunlight exposure in the laboratory at the University of Alberta, half of the tanks were placed in a container of water regulated by a digital refrigerated bath (Isotemp 3016D, Fisher Scientific) 17 cm under a UV lamp (UVA: 0.67 ± 0.14 W m^{-2}, UVB: 0.33 ± 0.10 W m^{-2}) and illuminated for 12 h per day for 2 or 4 consecutive days. During the exposure, fish were fed once per day (1% body weight per day) with ground tropical fish flakes, but were fasted 24 h before the end of each exposure period (48 h and 96 h). The water surface in the tanks was 17 cm below the UV lamp. The other half was placed under regular lighting. 50% of the NP suspensions were renewed daily during the experiment. 50 mL water sample was collected before the

exposure started. At the end of each exposure period, 50 mL water samples were collected and then fish anesthetized with MS-222 (0.1g L^{-1} buffered with NaHCO$_3^-$), and the first left gill arch of each fish was removed and fixed in 10% formalin in 1.5 mL microcentrifuge tube at room temperature overnight. The rest of the gill and liver were collected and stored at -80 °C until further analyses.

2.2.8 Concentration and composition of NOM

The water samples at a concentration of 0 mg L^{-1} NPs were used to determine the dissolved organic carbon (DOC) concentrations and compositions (see Supplementary Text A2-3). Two-dimensional fluorescence excitation-emission matrices (FEEMs) were generated by MATLAB (MathWorks, Natick, MA, USA) and in-house scripts. Parallel factor analysis (PARAFAC) modeling was performed using the PLS Toolbox (Eigenvectors Inc, WA, USA) in Matlab as described by DePalma et al. 2010 to quantify the four fluorescent components of NOM, humic-like, fulvic-like, tyrosine-like and tryptophan-like substances.[118] The scans of pure tyrosine and tryptophan were used as weighting factors to recover the relative fractions of each of the four fluorophores contributing to the measured total fluorescence of each sample.

2.2.9 Inductively Coupled Plasma-Mass Spectroscopy

Water samples from the exposure experiments and dialysis were analyzed by an Agilent 8800 Triple Quadrupole ICP-MS (ICP-MS/MS) to determine the concentration of Cerium (see Supplementary Text A2-4).

2.2.10 Determination of lipid peroxidation

A modified thiobarbituric acid reactive substances (TBARS) assay was used to assess lipid peroxidation in gill and liver tissues.[119] Frozen tissue was homogenized in 250 µL phosphate buffer (pH 7.5) using a hand-held tissue pestle homogenizer on ice for 15s and then centrifuged at 1000g for 90 s at 4 °C. One hundred and thirty microliter supernatant and 0- 6.25 µmol L^{-1} 1, 1, 3, 3-tetraethoxypropane (TEP) standard (Sigma) were transferred to 1.5 mL Eppendorf tube on ice, and diluted with 455 µl phosphate buffer and treated with 32.5 µl butylated hydroxytoluene (BHT) and 162.5 µL 50% trichloroacetic acid (TCA). Samples were vortexed and centrifuged at 13,000 g for 2 minutes. One hundred and twenty microliter supernatant was transferred in triplicate to each of 3 wells of a black-walled 96-well plate (Greiner Cellstar, Frickenhausen, Germany) and 75 µL 1.3% thiobarbituric acid (TBA) dissolved in 0.3% NaOH was added into each well. The plate was then covered with a film and incubated for 90 minutes at 90 °C. A microplate reader (1420 Multilabel Counter, VICTOR 3 V, PerkinElmer, MA, USA) was used to measure the fluorescence excitation at 531 nm and emission at 572 nm. Protein concentration was determined using the Pierce BCA Protein Assay Kit (Thermo Scientific; 23227). The values of TBARS were expressed as nmol TEP equivalents/µg protein.

2.2.11 Histological examination of gills

Tissue slides were prepared and processed for histology examination following the standard techniques with hematoxylin and eosin staining (see Supplementary Text A2-5). Slides were examined using ZEISS Axio Scope A1 which connected to an Optronics

Digital Camera linked to a computer. The images of tissue were processed, and the length and width of lamellae were measured by PictureFrame Software Ver 2.3. ImageJ (Ver 1.5i) was used to determine the interlamellar cell mass.

2.2.12 Statistical analysis

GraphPad Prism (Version. 6.0, GraphPad Software Inc.) was used to run statistical analysis and create graphs. The normality and homoscedasticity were evaluated by Shapiro-Wilk and Breusch-Pagan (α=0.05) tests, respectively. Two-way analysis of variance (ANOVA, α=0.05) with Tukey's multiple comparison tests (α=0.05) was used to compare between no UV and UV stimulated treatment groups, and ddH$_2$O and Rio Negro water across different NOM concentrations. If the data did not meet the assumptions of ANOVA, then a generalized linear model was used (α=0.05). Two-way repeated-measures ANOVA (α=0.05) was used to compare the hydrodynamic diameters and zeta-potentials of CeO$_2$ NPs in ddH$_2$O and Rio Negro water over 96 h. All data are presented as mean ± standard error of the mean (SEM) of 3 to 6 fish/procedures as independent experimental replicates.

2.3 Results

2.3.1 Physicochemical characteristics of CeO$_2$ NPs

TEM images of CeO$_2$ NPs in the ddH$_2$O determined the size of individual NPs ranged from 20.00 to 30.15 nm with an average size of 24.41 ± 4.13 nm (Figure 2-1). Figure 2-1B also demonstrates the aggregation of CeO$_2$ NPs in ddH$_2$O, even at a nominal concentration of 0.5 mg L^{-1}.

The hydrodynamic diameters of CeO$_2$ NPs in the ddH$_2$O at the nominal concentration

of 0.5, 2 and 5 mg L^{-1} were all significantly affected by time and/or the presence of NOM (Figure 2-2). More specifically, NOM significantly reduced the average measured diameter (more dispersed, lower aggregation size) of NPs at 0.5 and 2 mg L^{-1} from 0 up to 4 h (Figure 2-2A & 2-2B), while the same phenomenon was only observed at 0 h in 5 mg L^{-1} (Figure 2-2C). The influence of NOM on zeta-potential was less pronounced with only a decreased zeta-potential of CeO$_2$ NPs at 96 h in 0.5 mg L^{-1} ($p= 0.001$), and at 12 h ($p<0.001$) and 72 h ($p= 0.037$) in 5 mg L^{-1} (Figure 3A & 3C). No significant difference was found in the 2 mg L^{-1} group (Figure 2-3B).

The narrow scan XPS survey spectra of CeO$_2$ NPs samples were shown in Figure S2-3. The XPS spectra were corrected with the C (1s) peak at 284.6 eV. The letters "u$_0$ (v$_0$), u$_2$ (v$_2$) and u$_4$ (v$_4$)" in the spectra indicated three final states of Ce^{4+} for Ce3d$_{3/2}$ (Ce3d$_{5/2}$) and the letters "u$_1$ (v$_1$) and u$_3$ (v$_3$)" indicated two final states of Ce^{3+} for Ce3d$_{3/2}$ (Ce3d$_{5/2}$). The spin orbit doublets for CeO$_2$ NPs samples (Ce3d$_{3/2}$ and Ce3d$_{5/2}$) suggested that both 3+ and 4+ valence states were present in the samples. The percentage of Ce^{4+} was found to be 79% while Ce^{3+} was 21%.

2.3.2 Dissolution

The dissolution experiments were conducted to determine the concentration of cerium ions released from the CeO$_2$ NPs in the suspensions over 96 h dialysis period. The ion concentrations in all the suspensions tested were below the detection limit (0.000176 mg L^{-1}) of ICP-MS from 0 to 96 h suggesting the minimal dissolution of particles.

2.3.3 Water chemistry

The concentrations of dissolved organic carbon did not change during the exposures (Table S2-1). Water sources were generally similar in terms of sharing similar optical components (FEEM), but the relative importance of each component did vary (Figure S2-4). Fluorescence spectrophotometry data indicated measurable fluorescence for all NOM samples. Figure S4A&C displayed fluorophores that contained more humic- and fulvic acid-like fluorescence, as exhibited by the emissions observed in the range of 400-450 nm. Low fluorophore peaks for tyrosine-like and tryptophan-like substances (emissions in the 300 nm range) were also displayed after UV exposure (Fig S2-4B&D). Absolute fractions were also changed with the addition of UV regardless of time. From FEEM plots, PARAFAC analysis determined the concentrations of humic-, fulvic-, tryptophan- and tyrosine-like components of each NOM. Humic acid (HA) like fluorophores from PARAFAC analysis dropped from 2.9 to 2.3 under UV light exposure (Table S2-2). This trend was observed at both 48 and 96 hour time points with regards to UV exposure.

ICP-MS analysis of total cerium concentrations from the water samples collected during the exposure of CeO_2 NPs at 0, 12, 48 and 96 h showed that the actual concentrations detected were all below the nominal concentrations (Table S2-3), likely due to rapid sedimentation. The concentration of CeO_2 NP in the water with a nominal concentration of 0.5 mg L^{-1} collected at the end of the fish exposure experiment was below the detection limit (0.048 mg L^{-1}) while it was still detectable at higher nominal CeO_2 concentrations.

2.3.4 Hydroxyl radical generation by CeO_2 NPs

The generation of hydroxyl radicals in ddH_2O and Rio Negro water was both concentration and UV-light dependent (Figure 2-4). Thirty minutes incubation under UV

light significantly induced the production of •OH (6.84 ± 2.04 nmol TEP Equivalent mL^{-1}) in ddH$_2$O at a concentration of 5 mg L^{-1} CeO$_2$ NPs ($p < 0.001$). UV light also increased the •OH generation (3.40 ± 0.41 nmol TEP Equivalent mL^{-1}) in NOM water at concentration of 5 mg L^{-1} CeO$_2$ NPs ($p < 0.001$). The presence of natural organic matter significantly decreased the production of •OH in both UV exposed ($p < 0.001$) and non-UV exposed (1.60 ± 0.58 nmol TEP Equivalent mL^{-1}; $p = 0.005$) groups at 5 mg L^{-1}.

2.3.5 Tissue effects of nanoparticle and UV co-exposure

Lipid peroxidation was displayed in gill tissue as measured by TBARS (Figure 2-5). UV light significantly induced the lipid peroxidation in ddH$_2$O at concentration of 2 (2.57 ± 0.97 nmol TEP Equivalent/µg protein; $p < 0.001$) and 5 mg L^{-1} (2.01 ± 0.56 nmol TEP Equivalent/µg protein; $p = 0.001$) CeO$_2$ NPs over 48 h. The presence of NOM significantly reduced the lipid peroxidation caused by UV and CeO$_2$ NPs co-exposure at nominal concentrations of 2 (0.97 ± 0.72 nmol TEP Equivalent/µg protein; $p = 0.003$) and 5 mg L^{-1} (0.26 ± 0.25 nmol TEP Equivalent/µg protein; $p = 0.001$). No effect was observed in the liver tissue (Figure 2-6).

2.3.6 Morphological effects on gills

Histological examination of the gills of cardinal tetras at the end of 48-hour exposure showed normal morphology in NOM water without UV light (control; Figure 2-8A). The length and width of the secondary lamellae were not significantly affected by UV light or nanoparticles in the gill tissues of the exposed fish (Figure S2-8-S2-11). However, UV light with the presence of CeO$_2$ NPs caused higher proliferation or hypertrophy of epithelial cells

in the interlamellar region in gills of cardinal tetras in ddH_2O at concentration of 0.5 (p= 0.024), 2 (p= 0.002) and 5 (p= 0.049) mg L^{-1} after 48 h (Figure 2-7). The presence of NOM significantly reduced the occurrence of interlamellar cell mass (ILCM) proliferation under co-exposure of UV and CeO_2 NPs (p < 0.001 for 0.5 mg L^{-1}; p= 0.002 for 2 mg L^{-1}; p < 0.001 for 5 mg L^{-1}), and at 0.5 mg L^{-1} (p= 0.027) without UV light (Figure 2-7). Co-exposure of NPs and UV light in ddH_2O caused some minor to severe gill alterations (Figure 2-8). A high degree of hyperplasia of the lamellar epithelium occurred in all ddH_2O, UV exposed groups (Figure 2-8B, 2-8D, 2-8F & 2-8H). The complete fusion of lamellae (①) was only observed in 0.5 mg L^{-1} in ddH2O under UV light (Figure 2-8D). Hyperplasia of primary lamellae (②) and lifting of the respiratory epithelium (③) were also observed in all ddH_2O groups under UV light (Figure 2-8B, 2-8D, 2-8F & 2-8H).

2.4. Discussion

Overall, this study demonstrates CeO_2 NP exposure can induce a myriad of biological indicators of toxicity (lipid peroxidation, ILCM formation, alterations in gill morphology) when exposed to UV but not under laboratory light conditions. UV light was demonstrated to significantly increase the •OH generated by CeO_2 NPs and is thought to be the cause of the lipid peroxidation and other histological responses (e.g ILCM formation) in the fish gill. While NOM was shown to increase the dispersibility and hence increase the potential for biological interaction, overall, NOM reduced the noted biological effects. This study confirms and extends the concern that toxicity tests conducted in regular laboratory lighting settings could underestimate the risk of NPs in the aquatic environment and supports previous research findings that solar radiation must be considered in econanotoxicological

studies where catalytic NPs are being tested.[110] Despite the potential for significant dissolution of CeO_2 NP at low pH and low ion concentrations, we were unable to observe any significant release of free metal ions ($Ce3^+/Ce4^+$) from CeO_2 NPs (below detection limit: 0.000176 mg L^{-1}) suggesting that effects were indeed mediated solely by the CeO_2 NP themselves.

2.4.1 Ecological relevance of studying CeO_2 NPs in Amazonian waters

Titanium oxide nanoparticles (TiO_2 NPs) are one of the most studied nanoparticles, including numerous studies on their aggregation and deposition, interaction with NOM and photo-toxicity on various aquatic species.[16-18, 82, 120] However, studies on the toxicity of CeO_2 NPs, especially in the aquatic environment, are extremely limited.[100, 101] Since CeO_2 NPs share some similarities with TiO_2 NPs, researchers attempt to extend results from TiO_2 NPs studies to predict CeO_2 NPs and have tended to use moderate environmental conditions (e.g pH 6-8, moderately hard water) to test both TiO_2 and CeO_2 NPs.[100, 103] CeO_2 NPs (like TiO_2) are insoluble and poorly dispersive in these media, would aggregate quickly and have very low bioavailability to aquatic species.[76, 100, 104, 121] However, the unique chemical properties of Rio Negro Amazon River water can significantly increase bioavailability and photocatalytic activity of CeO_2 NPs and thus has the potential to affect aquatic organisms.[105-108] The increasing use of CeO_2 NPs as a catalyst for petroleum-based combustion refining and diesel fuel burning in the region increases the chance of exposure to CeO_2 NPs.[76, 100, 103] Furthermore, unlike TiO_2 NPs, Ce has two valence states, Ce^{4+} and Ce^{3+} (Figure S2-3) and this may alter toxicity as well.[76, 103, 112] Ce^{3+} has known to have antioxidant properties and its abundance increases as pH of aqueous solution decreases while Ce^{4+} acts as prooxidant.[103,

[112, 122] Finally, current literature surrounding the toxicity of CeO_2 NPs have shown mixed results with a few studies demonstrating antioxidant activity while others have suggested CeO_2 NPs can cause oxidative stress.[76, 100, 103, 112, 123]

2.4.2 Characterization and water chemistry

The DLS results showed that the presence of NOM reduced the hydrodynamic diameter of CeO_2 NPs. In most literature, NOM has often been reported to adsorb onto the NPs surface to stabilize NPs and prevent aggregation by increasing the electrostatic repulsion between NPs.[13, 16, 89, 90, 122, 124] This mechanism was usually involved in the increased absolute value of zeta-potential of NPs, which resulted in higher electrostatic repulsion between NPs.[89, 109, 124] However, the zeta potential of CeO_2 NPs without NOM was already negative which repelled the negatively charged NOM and decreased the adsorption of NOM onto NPs.[18] Therefore, the presence of NOM did not change the zeta potential in the current study. Few studies have shown that the bridging effect between humic acid and NPs could form large particles depending on the NPs to humic acid ratio.[58, 124] Therefore, the other explanation for decreasing hydrodynamic diameters could be that NOM enhanced the aggregation of NPs and NPs became large enough to precipitate out of the suspension,[58, 124] so that the size of NPs remained in the suspensions was decreasing over 96 h.

Ce atoms can exist as both Ce^{3+} or Ce^{4+} in CeO_2 NPs[76, 103, 112] whereby Ce^{4+} is associated with oxidative stress while Ce^{3+} has been reported to have free radical scavenging ability.[103, 112, 125, 126] Even though not statistically significant, adding CeO_2 NPs to the water tended to reduce lipid peroxidation in gills without UV exposure, likely due to removal from the water column by increased complexation and precipitation. XPS analysis showed that

21% Ce was presented as Ce^{3+} in the NPs (Figure S2-3). Since Ce^{4+} requires solar energy to generate ROS (see below),[82, 111] Ce^{3+} had the predominant activity over Ce^{4+} without UV light. Therefore, in laboratory conditions, Ce^{3+} can competitively react with hydroxyl radicals to reduce oxidative stress on the organisms.[103]

The concentrations of DOC were not significantly affected by the UV light or the duration of the exposure (Table S2-1). However, exposure to UV can change the composition of NOM.[16, 127] The humic substances were partially broken down into products including fulvic-, tyrosine- and tryotophan- like substances (Table S2-2).

2.4.3 UV-induced toxicity of CeO_2 NPs

This study demonstrated the phototoxic effect of CeO_2 NPs through the generation of ROS. The production of hydroxyl radicals was significantly increased by UV light at 5 mg L^{-1} in ddH_2O. The UV light-induced toxicity of metal oxide NPs to aquatic animals has been well documented in many studies on fish cell lines,[111, 128] zebrafish and embryos,[7, 82, 110, 111] and other aquatic organisms.[16, 17] Since CeO_2 NPs is photocatalytic like other metal oxides NPs, they share similarities in the mechanism of their phototoxicity.[76, 100] Under the UV light, CeO_2 NPs absorb the solar energy, excite an electron, and transfer the electron to the conduction band, which will create an electron-hole pair.[76, 82, 111] The electron-hole pair can react with water molecules and oxygen on the particle surface to produce ROS.[82, 111] ROS is very reactive and can cause oxidative stress.[7, 110, 111, 129] The high surface area to volume ratio is an important physicochemical property of NPs.[7, 130, 131] This leads to higher numbers of CeO_2 molecules with electron-hole pair available on the surface of the particles to be interacted with.[129, 131] Therefore, more ROS may be generated and lead to more significant

oxidative stress damage.[82]

The adverse effects caused by oxidative stress have been well documented, these include, damage to cellular constituents such as RNA, DNA, protein structure, and cell membranes.[110, 112, 132, 133] In the current study, the exposure to UV light for 48 h significantly induced the lipid peroxidation in the gills of cardinal tetra at 2 and 5 mg L^{-1} in ddH_2O. Since •OH has been well documented to frequently attack lipid molecules in several studies,[112, 134, 135] the increased lipid peroxidation at 5 mg L^{-1} can be caused by oxidative stress from the increased production of •OH under UV light. However, the results at 2 mg L^{-1} between TBARS and •OH were not consistent. This suggests that the amount of •OH induced by UV at 2 mg L^{-1} may be below the detection limit of our 2-DR assay.[110] Also, the 2-DR assay can only capture the presence of •OH[136] while CeO_2 NPs may have also produced other types of ROS (superoxide and peroxynitrite) causing lipid peroxidation even at 2 mg L^{-1}.[112] These results show that both NP concentration and UV light affect lipid peroxidation in the gills. However, no effect was found in liver tissue. The lack of change in lipid peroxidation (TBARS) in the liver may reflect 1) there was not sufficient amount of •OH diffused through gills and distributed to the liver to cause adverse effect due to the low stability of •OH[137], 2) oxidative stress caused protein oxidation instead of lipid peroxidation or 3) Liver tissue has a higher antioxidant enzymatic activity to cope with increased oxidative stress.[138] Therefore, more sensitive biomarkers may be more appropriate to detect potential oxidative stress in the liver, such as the formation of protein carbonyls, antioxidant enzyme activity including catalase and superoxide dismutase activity, the elevation of glutathione, and/or genes expression related to antioxidants.[77] No significant changes in lipid peroxidation were detected in gills at 96 h (Figure S2-5). This may be due to increased total antioxidant

enzyme activities in the gills after 96 h of exposure, which reduced TBARS results.

Fish gills play important roles in maintaining physiological homeostasis and are ideally suited for respiration, ion exchange, acid-base regulation and excretion.[120, 139] Gills are exposed to the external milieu and are ideally suited to sub-lethal detection of toxicant exposure like NPs.[120, 139] Previous studies have shown gill damage caused by NP exposure including hyperplasia, swollen mucus and chloride cells, oedema, epithelial lifting and fusion of lamellae.[120, 137, 139-142] In the present study, no alternations were observed in gills of fish that were not exposed to UV light while 100% of the UV exposed fish present at least one of the 3 noted morphological effects. The most pronounced morphological change was the increase in the ILCM in UV exposed ddH$_2$O groups. This can be explained by hyperplasia of primary lamellae epithelial cells,[137, 139] and swelling of the mucus cells and chloride cells at basal secondary lamellae.[137, 142] The increasing secretion of mucus and enlargement of mucus cells in gills are defense mechanisms against metal pollutants.[137, 140] Other NPs like TiO$_2$ NPs have been reported to induce the mucus secretion.[120, 137] The increased ILCM reduces the surface area of lamellae, which results in diffusion distance and thus decreased oxygen uptake.[143] Therefore, NP exposure under UV exposure may reduce aerobic respiration and cause hypoxemia in fish.[140, 143] In the current study mucus did not fully protect the gills from the UV-induced toxicity of CeO$_2$ NPs as more severe pathologies were observed. Epithelial lifting was observed in the presence of CeO$_2$ NPs in ddH$_2$O under UV light. Epithelial lifting is the separation of the outer layer of epithelial cells from secondary lamellae [144] and usually caused by oedema.[144, 145] It indicates the degeneration and necrosis of epithelium from the lamellae,[145] which may be caused by the produced oxidative damage from •OH production. Therefore, reduced oxygen uptake ability caused by damages in the

gills due to the co-exposure of UV and CeO$_2$ NPs have the potential to affect cardinal tetras' swimming ability and their survival in nature.

2.4.4 The protective properties of natural organic matter

Many studies have shown that NOM affects the aggregation of NPs and thus stabilize NPs.[7, 13, 19, 89, 113, 146] However, only a few studies have focused on the potential interactive effects of NOM and NPs.[16, 90] Our results have demonstrated that the presence of NOM significantly decreased the toxicity of CeO$_2$, especially under UV light, including reduced •OH generation, decreased lipid peroxidation in gills, lower ILCM and decreased gill damage. NOM protects aquatic organisms from the UV-induced toxicity of NPs through two potential mechanisms. First, quinone in humic acid-like substance has been shown to be an electron acceptor, thus it can capture the electrons excited by UV light to prevent ROS from generating in the water.[96, 97] Second, NOM likely reduces the percentage of UV light that penetrates the water column (UV attenuation) and in turn reduces the generation of ROS.[16, 147] The range of concentration of NOM in Rio Negro water was between 13 and 15 mg of C L^{-1} of DOC (Table S2-1). Previous studies by Wormington et al. determined the relationship between NOM concentration and UV attenuation[16] and found that approximately 20% UV attenuation occurs by 13 to 15 mg L^{-1} NOM.[16] This decreases the amount of solar energy that can be absorbed by NPs to create an electron-hole pair; therefore, decreasing the potential for ROS generation in the water.

2.5. Conclusion

This study is the first to demonstrate the reduction of phototoxicity of CeO$_2$ NPs in an

aquatic organism by NOM. Acting like other metal oxides NPs, acute co-exposure to CeO_2 NPs and UV light increases the generation of hydroxyl radicals in the water, which results in lipid peroxidation and gill damage. The presence of NOM reduces the adverse effects caused by CeO_2 NPs, especially under UV light, across all concentrations. However, it is important to note that the UV intensity is less than the natural UV observed in the Rio Negro region (Figure S2-1 and S2-2), and thus the phototoxicity of CeO_2 NPs may be higher in Rio Negro water. Therefore, it is difficult to tell if the NOM can fully protect aquatic organisms in the Rio Negro River from co-exposure. Further studies examining physiologically relevant endpoints such as swim performance and the behavior of fish co-exposed to CeO_2 NPs and UV light will increase our understanding of the potential combined effects of NP, NOM and sunlight.
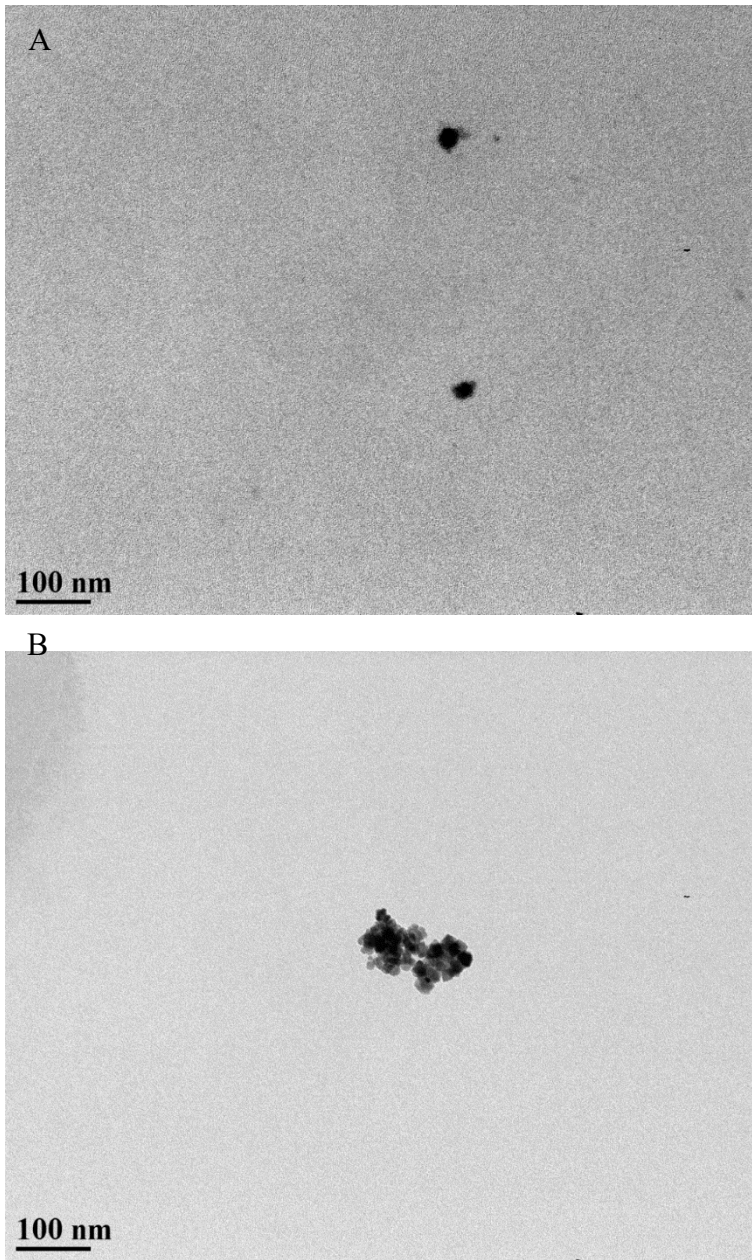
Figure 2-1. TEM images of CeO_2 NPs in ddH_2O at pH 4.5, scale bar = 100nm. (A) individual NPs at nominal concentration of 0.5 mg L^{-1}; (B) aggregated NPs at concentration of 0.5 mg L^{-1}. Values are mean ± SEM.
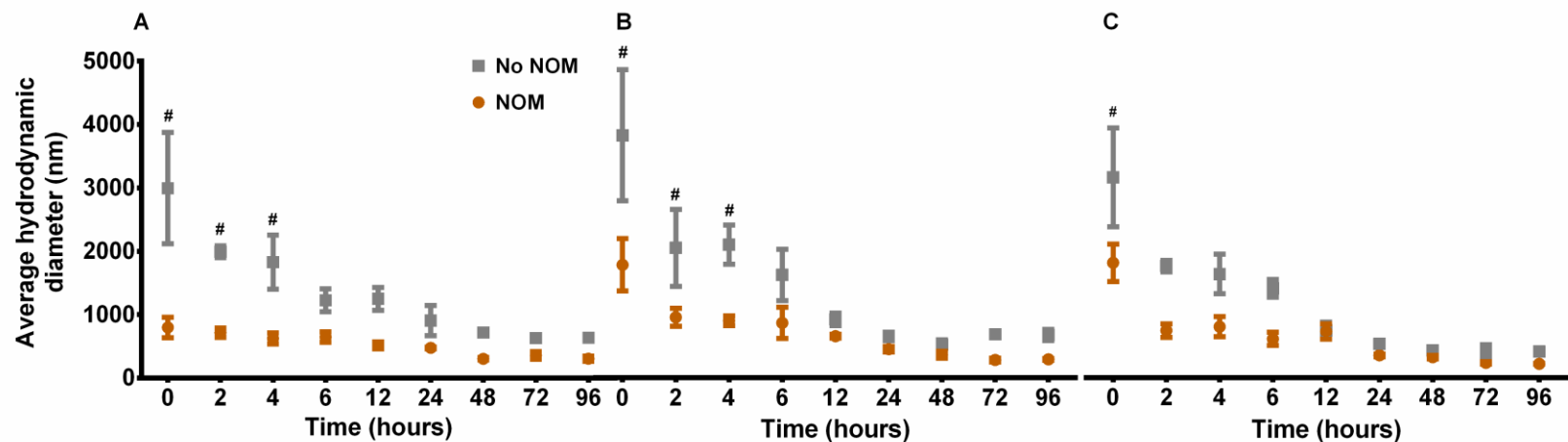
Figure 2-2. The average hydrodynamic diameter of CeO$_2$ NPs in ddH$_2$O (NOM-) and Rio Negro water (NOM+) measured by DLS at 0, 2, 4, 6, 12, 24, 48, 72 and 96 h. (A) at nominal concentration of 0.5 mg L^{-1}; (B) at nominal concentration of 2 mg L^{-1}; (C) at nominal concentration of 5 mg L^{-1}. # indicates NOM significantly decreases the hydrodynamic diameter of NPs. Values are mean ± SEM.
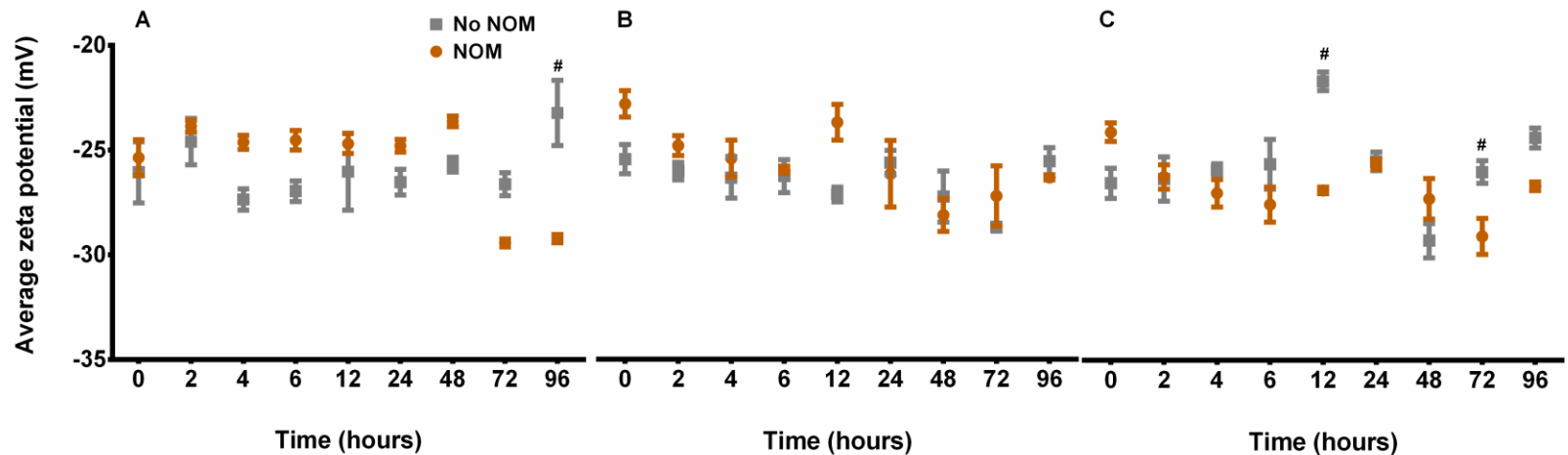
Figure 2-3. The average zeta-potential of CeO_2 NPs in ddH_2O (NOM-) and Rio Negro water (NOM+) measured by DLS at 0, 2, 4, 6, 12, 24, 48, 72 and 96 h. (A) at nominal concentration of 0.5 mg L^{-1}; (B) at nominal concentration of 2 mg L^{-1}; (C) at nominal concentration of 5 mg L^{-1}. # indicates NOM significantly decreases the zeta-potential of NPs. Values are mean ± SEM.
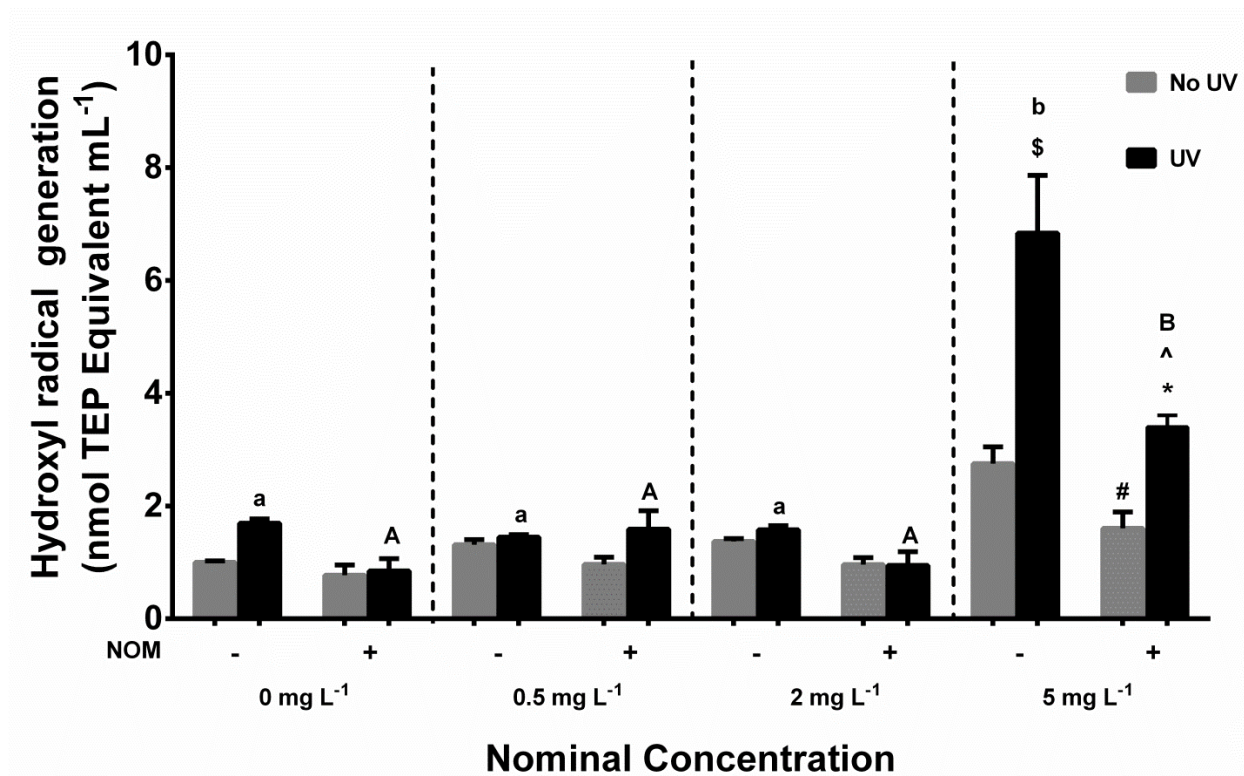
Figure 2-4. Generation of •OH of CeO_2 NPs suspension at nominal concentrations of 0 (control), 0.5, 2 and 5 mg L^{-1} in ddH_2O (NOM-) and Rio Negro water (NOM+) with or without UV light (n=4). * indicates NOM significantly reduces •OH production under UV light. # indicates NOM significantly reduces •OH production without UV light. $ indicates UV light significantly increases •OH production in ddH_2O. ^ indicates UV light significantly increases •OH production in NOM water. Lower case letters indicate significant difference within ddH_2O group over difference concentrations. Upper case letters indicate significant difference within NOM water group over difference concentrations. Values are mean ± SEM.
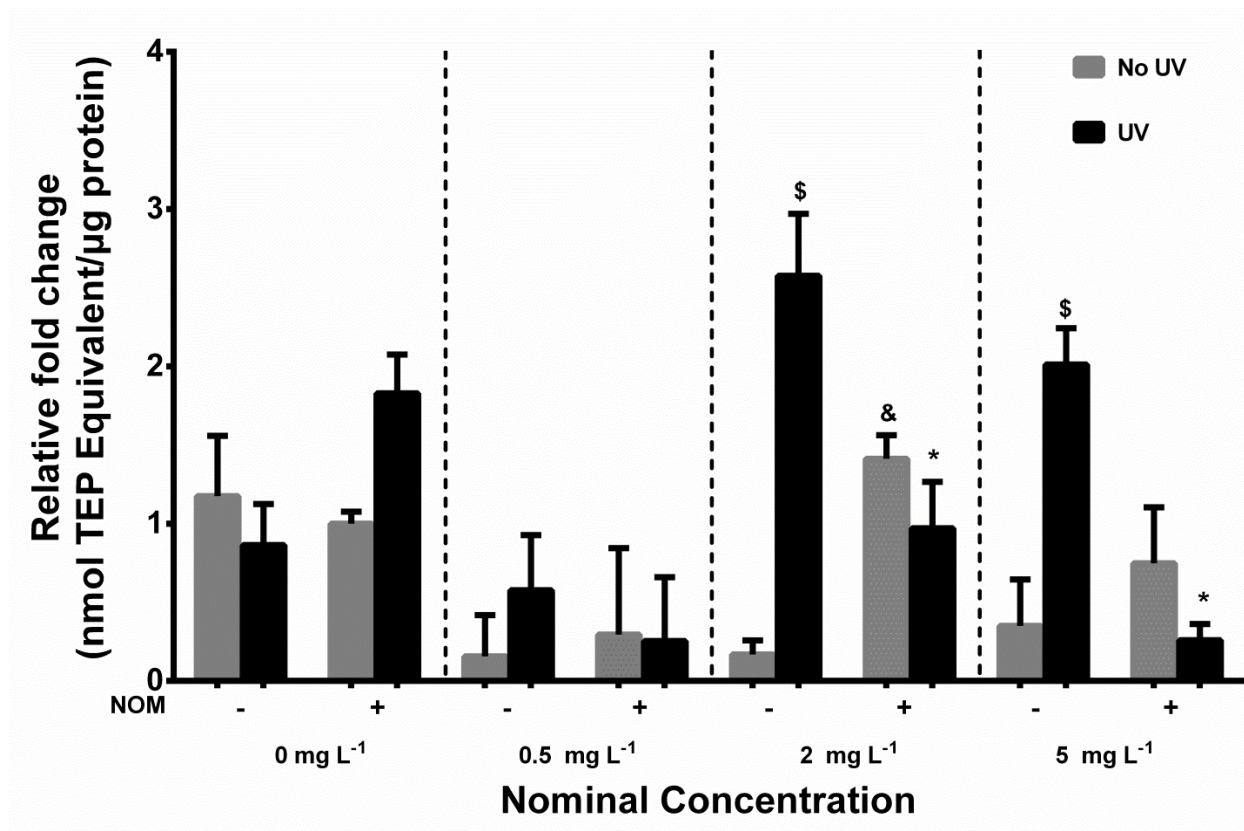
Figure 2-5. Lipid peroxidation in gills of cardinal tetra exposed to CeO_2 NPs suspension at nominal concentrations of 0, 0.5, 2 and 5 mg L^{-1} in ddH_2O (NOM-) and Rio Negro water (NOM+) with or without UV light for 48 h (n=6). Relative fold change (NOM without UV at 0 mg L^{-1} were used as reference) of TBARS expressed as nmol TEP Equivalent/μg protein. * indicates NOM significantly reduces TBARS under UV light. # indicates NOM significantly reduces TBARS without UV light. & indicates NOM significantly increases TBARS without UV light. Values are mean ± SEM.
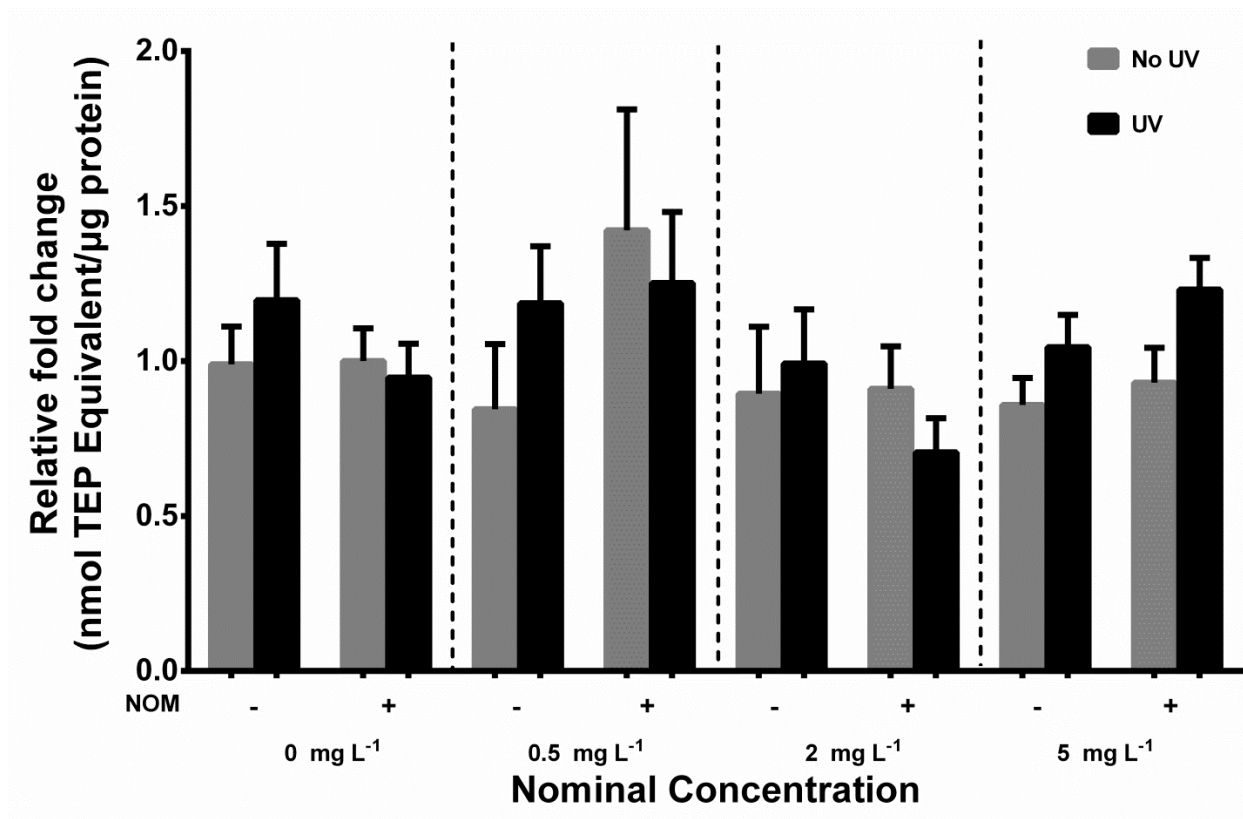
Figure 2-6. Lipid peroxidation in livers of cardinal tetra exposed to CeO_2 NPs suspension at nominal concentrations of 0, 0.5, 2 and 5 mg L^{-1} in ddH_2O (NOM-) and Rio Negro water (NOM+) with or without UV light for 48 h (n=6). Relative fold change (NOM without UV at 0 mg L^{-1} were used as reference) of TBARS expressed as nmol TEP Equivalent/μg protein. Values are mean ± SEM.
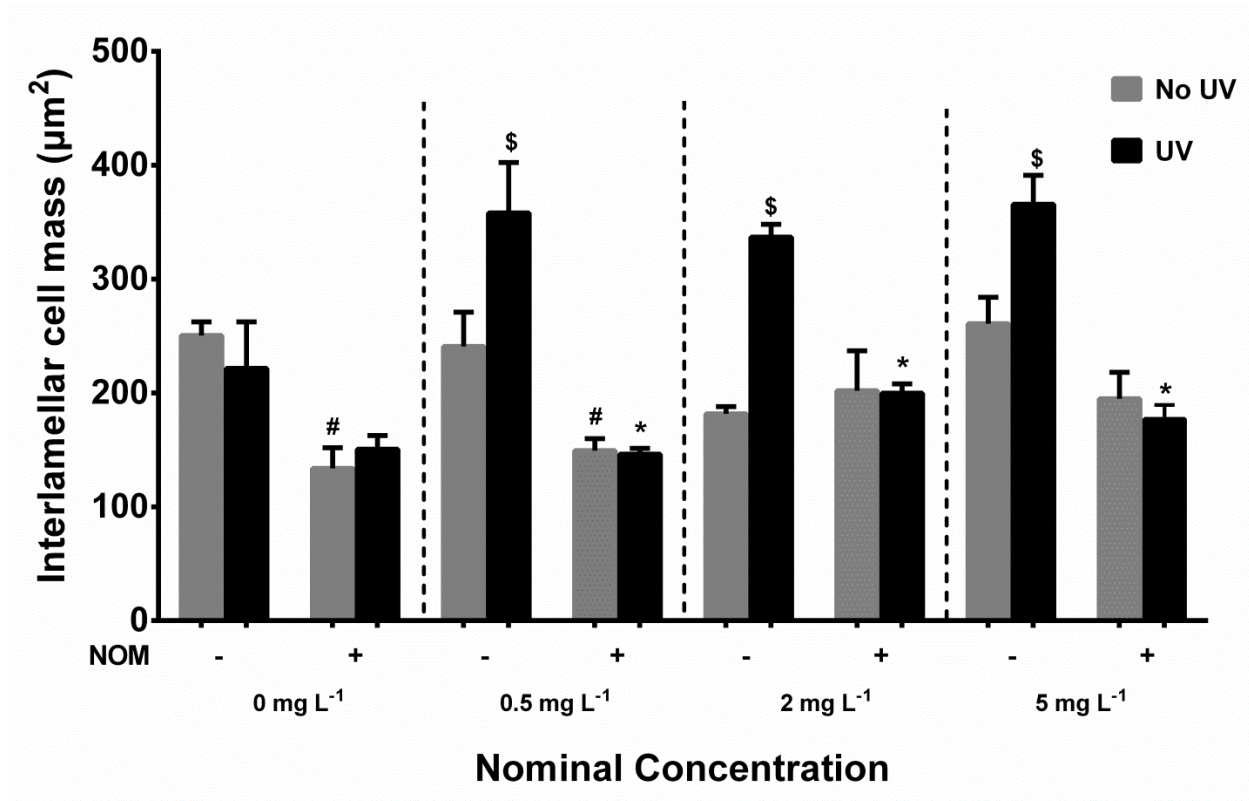
Figure 2-7. The interlamellar cell mass (μm^2) of gills of cardinal tetra exposed to CeO_2 NPs suspension at nominal concentrations of 0, 0.5, 2 and 5 mg L^{-1} in ddH_2O (NOM-) and Rio Negro water (NOM+) with or without UV light for 48 h (n=4). Values are mean ± SEM. * indicates NOM significantly reduces ILCM under UV light. Values are mean ± SEM. # indicates NOM significantly reduces ILCM without UV light. $ indicates UV light significantly increases ILCM in ddH_2O.
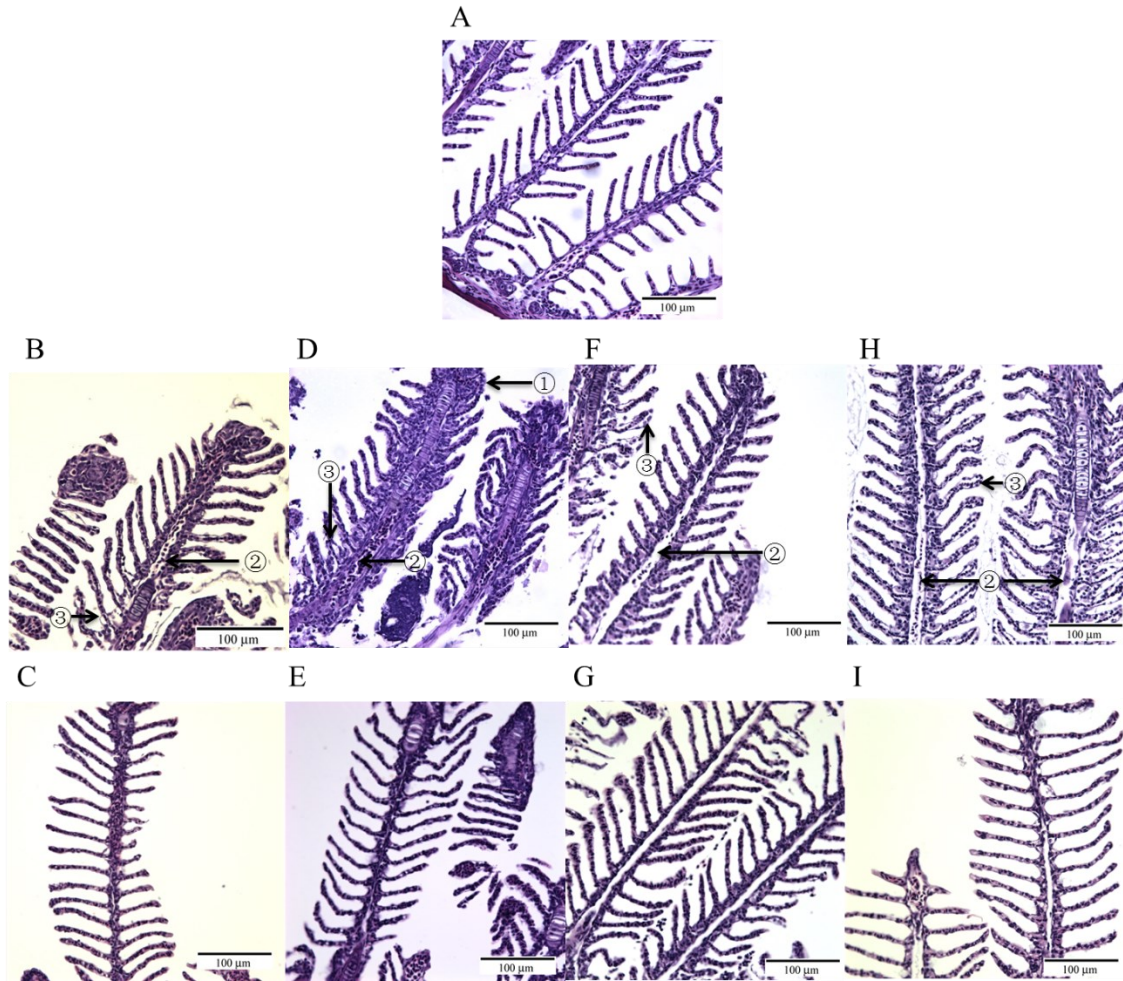
Figure 2-8. Gill morphology visualized through light microscopy in cardinal tetra 48 h after co-exposure to CeO_2 NPs and UV light (Haematoxylin and Eosin stain, x400) at various nominal concentrations. (A) Control (0 mg L^{-1} NPs in Rio Negro water, no UV); (B) 0 mg L^{-1} NPs in ddH_2O under UV light; (C) 0 mg L^{-1} in in Rio Negro water under UV light; (D) 0.5 mg L^{-1} NPs in ddH_2O under UV light; (E) 0.5 mg L^{-1} in in Rio Negro water under UV light; (F) 2 mg L^{-1} NPs in ddH_2O under UV light; (G) 2 mg L^{-1} in in Rio Negro water under UV light; (H) 5 mg L^{-1} NPs in ddH_2O under UV light; (I) 5 mg L^{-1} in in Rio Negro water under UV light. The fusion of several lamellae (①). Hyperplasia of primary lamellae (②). Lifting of the respiratory epithelium and oedema (③).

Chapter 3

Evaluation of interactive effects of UV light and nano encapsulation on the toxicity of
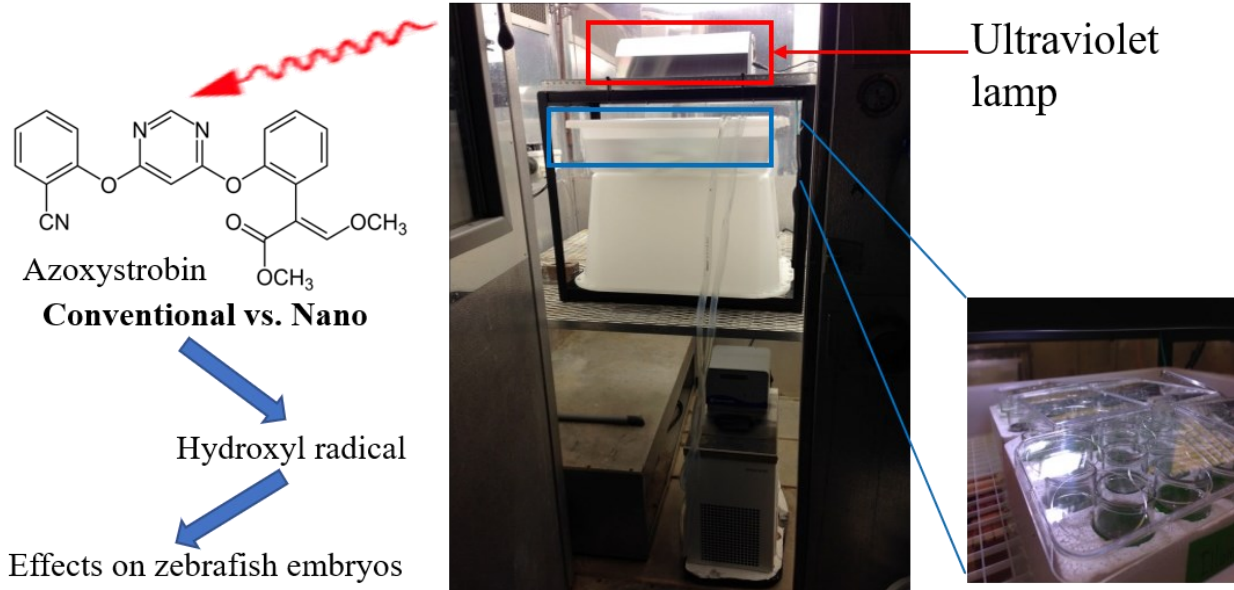
azoxystrobin on zebrafish

3.1 Introduction

The pesticide industry has been continuously discovering and developing novel formulations to provide better crop protection and minimize environmental impacts.[148, 149] Fungicides are the second most used pesticides after herbicides and widely used to protect crops from fungal infection.[150] Strobilurins are one major group of novel synthetic fungicides. The most popular strobilurin, azoxystrobin, was first launched in Europe in 1996 and has become the best-selling fungicide worldwide with over $1.2 billion in annual sales and occupies approximately 10% of the global fungicide market.[150-152] Azoxystrobin was discovered in the mushrooms *Oudemansiella mucide* and *Strobilurus tenacellus* which possess the ability to release natural strobilurin to fight yeasts and other fungi.[148, 153] Azoxystrobin inhibits the respiratory electron transport chain (ETC) in the mitochondria by blocking the mitochondria Q_o (ubiquinol oxidizing) site of complex III to prevent electron transfer between cytochrome b and cytochrome c1, thereby reducing cellular respiration and synthesis of adenosine triphosphate (ATP) in eukaryotes.[148, 150, 153, 154] Inhibition of the ETC results in oxidative stress due to increases in reactive oxygen species (ROS).[148, 150, 154] Azoxystrobin is considered to have relatively low toxicity to birds, mammals, bees and humans but is classified as highly toxic to aquatic organisms.[148, 150, 155] The half-life of azoxystrobin varies greatly in different media and can be significantly affected by environmental factors including temperature, pH and ultraviolet (UV) light.[148, 151, 152] The average half-life in the aquatic environment is estimated to be between 8.7 and 13.9 days at around pH 7.[148, 151] Azoxystrobin has been detected in groundwater, surface water and streams in many countries.[151, 152] In the US, 45% of 103 water samples collected from 29 streams in 13 states contained azoxystrobin which was the most frequent of all 12 different fungicides tested.[156] The average detected residual concentration ranged from 0.15 µg L^{-1} to 29.7 µg L^{-1} in surface waters and streams close to agricultural regions across the US and Europe.[151, 152]

54

The highest levels in the river were detected in China where the mean concentration reached 34 μg L^{-1}.[151] However, the mean detected concentration in the water close to application sites can stay above 0.1 mg L^{-1}, even 10 days after a runoff event.[151] Studies have suggested that azoxystrobin exposure had significant effects on gene expression profiles in zebrafish (*Danio rerio*) and Atlantic salmon (*Salmo salar L.*), antioxidant enzymes in juvenile grass carp (*Ctenopharyngodon idella*), decreased reproduction in zebrafish and induced oxidative stress in several other aquatic organisms.[150-152, 154] As a synthetic organic molecule, azoxystrobin has an octanol/water partition coefficient ($LogK_{ow}$) of 2.5 and has relatively low solubility in water (6.7 mg L^{-1} at pH 5.2 to 7) so it requires multiple foliar applications in agriculture practice. Multiple applications in the growing season prolong exposure in addition to increasing the overall exposure concentration in the nearby water systems.[148, 152, 157] Therefore, azoxystrobin may pose a major risk to aquatic organisms at environmentally relevant concentration during and after the applications. Currently, there is a large data gap on the sub-lethal effects of azoxystrobin on aquatic species since most studies have focused on lethality (LC_{50}) while few have investigated sub-lethal effects. There are even fewer integrated studies on the mechanisms of its toxicity in fish species.[148, 150-152, 154]

Nanotechnology has been widely used in many fields including electronics, medical imaging, drug delivery, personal care products and research.[7, 11, 149, 158] Nanomaterials can have unique properties that provide them with advantages in applications when compared to conventional counterparts.[7, 158, 159] For example, high surface area to volume ratio at the nanometer scale makes them highly efficient and effective in many applications including nano-biosensor in cell imaging and nano-sized photocatalyst in wastewater treatment plants.[149, 159] The rapid rise in global population requires higher food production to keep up with the growing daily

demands while the agricultural land remains limited.[159] Therefore, new technological innovations

and agricultural practices are necessary to increase the yield of agriculture production.[149, 159]

Recently, the use of nanoparticles (NPs) and the development of nano-enabled formulations have

been applied in agriculture to reduce their global footprint.[159, 160] Vive Crop Protection Inc. has

developed a nano-enabled azoxystrobin formulation (nAz) which includes a nano-sized

azoxystrobin core with a negatively charged polyacrylic acid (PAA) coating. The resulting nAz

has a better dispersibility than the conventional azoxystrobin (Az) due to its PAA coating and

can be applied as either a seed coating or via direct in-furrow soil application. The nAz provides

better absorption and longer pest protection and can reduce usage rate by approximately 50%.[158]

However, this new formulation will be inevitably released into the environment, raising concerns

regarding potential risks to living organisms.[149, 158] It also challenges the current regulatory

guidelines which have been created for conventional materials and therefore, the nano-enabled

forms require specific research protocols to evaluate the potential risks.[149, 158] Current knowledge

on the ecotoxicity of nano-enabled pesticides and the influences of environmental factors on

their toxicity is extremely limited.

Sunlight is known to be a mediating factor in toxicity due to its ability to induce ROS

production with the particular toxicant. It is well known that some specific compounds

containing aromatic rings and conjugated double bonds can absorb photons and generate ROS

directly.[161-164] Given the structure of azoxystrobin with its two aromatic rings flanking an aryl

pyrazole ring, the potential for sunlight-induced ROS requires investigation. Therefore, the

purpose of this comprehensive study was to 1) investigate the lethal and sub-lethal effects of nAz

on the development of zebrafish embryo and compare it to its conventional counterpart in

different biological levels including molecular, biochemical, morphological and organismal

levels; 2) determine if environmental factors like UV light can affect the toxicity of azoxystrobin.

3.2 Methods

3.2.1. Chemicals

Conventional azoxystrobin (18.46 weight percent, wt%; VCP-06-007, lot#001), nAz (18.54 wt%; VCP-06-007, lot#002), input polymer (17.14 wt%; B-002, lot#001) and Allosperse (12 wt%; B-001, lot#001) manufactured and donated by Vive Crop Protection Inc (Toronto Canada) were used in this study. Allosperse consists of polyacrylic acid polymers crosslinked by using charge-specific reduction or ionizing radiation.[165] Suspensions of nAz and Az were diluted to make stock solutions at a nominal concentration of 3 mg L^{-1}. Stock Az was suspended in 0.01% methanol due to its low solubility in the water while stock nAz was suspended in reverse osmosis (RO) water with 1% weight/volume seawater salt mix added back to give the ions.

3.2.2 Water chemistry

Water samples of each nominal concentration used in the LC_{50} experiment were stored in an amber glass bottle (250 mL) and transported to Agriculture and Agri-Food Canada, Lethbridge, Alberta, Canada at 4°C for analysis (see Supplementary Text A3-1). The concentrations of stock solutions used in sub-lethal experiments were measured to be 1081 ± 37 $\mu g\ L^{-1}$ for nAz and 1133 ± 19 $\mu g\ L^{-1}$ for Az. The nAz solutions were prepared based on the mass of azoxystrobin core within the Allosperse to match the relative mass of azoxystrobin in Az.

3.2.3 Characterization of nano-enabled azoxystrobin

Nano-enabled azoxystrobin formulations at 20 and 100 ug L^{-1} (diluted in double distilled water, ddH_2O) were characterized by Dynamic Light Scattering (DLS). Full details of the method are available in Supplementary Text A3-2.

3.2.4 Zebrafish maintenance and collection of viable embryos

Wild type strain AB adult zebrafish (aged 6 to 18 months) were housed in 20 L tanks (pH: 7.2-7.4, conductivity: 1100-1200 μS cm^{-1}, temperature: 28 °C, dissolved oxygen: 7.0 mg L^{-1}, general hardness: 100 mg L^{-1} as $CaCO_3$, salinity: 0.6 ppt, 14 h light: 10 h dark). Two female and one male zebrafish were placed in a hatching tank in which they were separated by a splitter and acclimated overnight. The next morning, the splitter was removed allowing zebrafish to spawn under the stimulation of the start of the light cycle. Fertilized embryos were collected after 1 h.

3.2.5 Lethal effects of azoxystrobin exposure to zebrafish

The experimental setup was modified based on the previous study.[166] Viable embryos (24 hours post fertilization, hpf) were rinsed three times with RO water and then randomly distributed into six-well plates and four wells were used for each concentration (Sarstedt, Nümbrecht, Germany; 20 embryos per well). Embryos were exposed to various nominal concentrations of 100, 200, 300, 400 or 500 μg L^{-1} of nAz, or 100, 200, 300, 400, 500, 1000, 1500, 2000 or 3000 μg L^{-1} Az in 0.01% methanol. Embryos in RO water were used as negative

control and embryos in 0.01% methanol as vehicle control for Az. Half of the embryos were placed in a container of water regulated by a digital refrigerated bath (Isotemp 3016D, Fisher Scientific) placed 17 cm under a UV lamp (UVA: 0.64 ± 0.12 W m^{-2}, UVB: 0.31 ± 0.11 W m^{-2}) for 8 h per day for 4 consecutive days while the other half were placed in an incubator (Exo Terra PT2499; 28 ± 0.1°C) under laboratory light (14 h light:10 h dark). The temperatures in both light conditions were kept at 27 ± 0.5 °C. RO water (0.375 mL) was added into each well of the plates under UV exposure every hour to compensate for water loss due to evaporation. Only 0.1 mL water was added into each well of the plates each day under laboratory light. The UV exposed embryos were removed from UV light after 8 h exposure each day and placed into the same incubator. All azoxystrobin suspensions were renewed after 48 h exposure (at 72 hpf) during the experiment period. Survival and hatching success of zebrafish were recorded every 12 h by using a dissecting microscope. Zebrafish were considered dead if they lacked movement, heartbeat or transparency and removed from wells.[167] Plates with $\geq$ a 90% survival rate in the control group were analyzed. Survival and hatching rates were calculated every 12h. The median lethal concentration (LC$_{50}$) values were calculated at 120 hpf.

3.2.6 Sub-lethal effects of azoxystrobin exposure to zebrafish

AB zebrafish embryos were collected following the procedure mentioned in section 3.2.4. Viable embryos at 24 hpf were rinsed three times with RO water and then randomly distributed into six-well plates. Embryos were exposed to input polymer (polymer control) or Allosperse (coating control), nAz and Az at a nominal concentration of either 20 or 100 µg L^{-1} (diluted from pre-prepared stock solution mentioned above). Embryos in RO water were used as control and a

parallel 0.01% methanol was also performed as vehicle control for the Az. The exposure procedure followed the lethality experiment in section 3.2.5. Survival and hatching rates were recorded and calculated during the exposure period every 12 h as for the lethality experiments. At 120 hpf, larvae were rinsed three times with RO water, transferred to an Eppendorf tube (10 embryos per tube), snap-frozen in liquid nitrogen and stored at -80°C until further analyses.

3.2.6.1 Morphological effects

Malformation including pericardial edema, yolk sac edema and spinal curvature was recorded, and the side view and ventral view were captured (see Supplementary Text A3-3) at 120 hpf following the sub-lethal experiment. The yolk sac volume was estimated according to the following equation and is based on the assumption that the yolk sac is ellipsoid at 120 hpf (Figure S3-1).

Volume= π*a*b*c/3

Where: a = height of yolk sack at widest point (side view)

b= length from anterior of yolk sac to the mid-point of a (side view)

c= maximum width of yolk sac (dorsal view)

3.2.6.2 Metabolic effects

Following the sub-lethal experiment setup as section 3.2.6, the oxygen consumption of embryos/larvae (two pooled for each measurement) was measured at 48, 72, 96 and 120 hpf.

Embryo respiratory analyses were carried out using a Loligo O_2 sensing microplate system (Product #SY25020; HS code: 90273000; see Supplementary Text A3-4).

3.2.6.3 Biochemical effects

All biochemical assays (SOC, catalase, BCA assay for [protein], PCR) were tested using both capsule and nAz nanomaterials to ensure no inhibition in the presence of nanomaterials occurred at the concentrations tested, following the procedures as outlined by Ong et al.[168] Sod and catalase assays followed manufacturer's instructions (see Supplementary Text A3-5).

3.2.6.5 Molecular effects

RNA isolation and cDNA synthesis of zebrafish larvae followed the manufacturer's recommendations (see Supplementary Text A3-6). Primers for zebrafish *elongation factor 1 alpha* (*ef1α*), *catalase* (*cat*), *superoxide dismutase 1* (*sod1*), *sod2*, *glutathione peroxidase 1a* (*gpx1a*) and *gpx1b* were designed using National Center for Biotechnology Information (NCBI) Primer-BLAST software and validated by BLAST. Primer information is listed in Table S3-1. The expression of target genes (*cat*, *sod1*, *sod2*, *gpx1a* and *gpx1b*) and housekeeping gene (*ef1α*) were measured through quantitative polymerase chain reaction (qPCR) by Applied Biosystems 7500 Fast Real-Time PCR System (version. 1.4.) with reaction conditions as follows: 95°C for 2 min, and then 40 thermal cycles of 95°C for 15 s and 60°C for 1 min, then followed by dissociation phase of 95 °C for 15 s, 60 °C for 1 min, 95 °C for 15 s and 60 °C for 15 s. The efficiency of all primers was also determined based on the same method and was used to

calculate the changes in gene expression based on the comparative CT (-ΔΔCT) method[169] The

results were normalized to endogenous control gene *ef1α* based on the results of McCurley and

Callard[170] and *ef1α* was found to be stable among all the treatment and control groups (Figure

S3-8).

3.2.6.6 Lipid peroxidation

The presence and abundance of 4-hydroxynonenal or 4-hydroxy-2-nonenal (4-HNE) in

each group was determined by Western blotting analysis (see Supplementary Text A3-7).

3.2.7 Generation of free radicals

Generation of hydroxyl radicals (•OH) in the water was measured by using the modified

method described in a previous study (see Supplementary Text A3-8).[85]

3.2.8 Statistical analysis

GraphPad Prism (Version. 6.0, GraphPad Software Inc.) was used for statistical analysis

and creating graphs. The normality and homoscedasticity were evaluated by Shapiro-Wilk and

Breusch-Pagan ($\alpha=0.05$) tests, respectively. Two-way analysis of variance (ANOVA, $\alpha=0.05$)

followed by Tukey's multiple comparison tests ($\alpha=0.05$) was used to compare laboratory light

and UV light stimulated groups at different concentrations. Two-way repeated-measures

ANOVA ($\alpha=0.05$) was used to compare the hydrodynamic diameters (HD), polydispersity index

and zeta-potentials of nAz between 20 and 100 μg L^{-1}. Generalized linear regression was used to determine if slopes of the linear regression lines between nominal concentration and measured concentration at both light conditions are significantly different (R version 3.5.3). All data are presented as mean ± standard error of the mean (SEM).

3.3 Results

3.3.1 Water chemistry and DLS results

The measured concentrations of nAz and Az were not significantly different at either a nominal concentration of 20 or 100 μg L^{-1} under either light condition (Figure S3-2). The slope of the linear regression line of the relationship between measured concentrations and nominal concentrations of nAz was significantly higher than Az in laboratory light (p=0.021) and UV light (p=0.048; Table S3-2). The hydrodynamic diameters (HD) of nAz at the nominal concentration of 20 μg L^{-1} and 100 μg L^{-1} were all significantly affected by time (p < 0.001, Figure S3-3A) but there was no significant difference between the two concentrations. HD at 20 μg L^{-1} was significantly increased at 4 (p=0.0057) and 8 h (p=0.015) while HD at 100 μg L^{-1} was significantly decreased at 96 h (p=0.0335). The average zeta-potential at 100 μg L^{-1} was significantly more negative than 20 μg L^{-1} over 96 h (p=0.0007) but remained relatively constant with a slight decrease at 24 and 72 h (Figure S3-3B). Nano-enabled azoxystrobin was highly polydispersed at both nominal concentrations and no significant differences were detected between the two concentrations (Figure S3-3C).

3.3.2 Lethal effects (LC$_{50}$) and hatching success

The 96h-LC$_{50}$ values in Table 3-1 were calculated based on the equation of each regression line in Figure 3-1 and the values were very close to the results from Probit analysis in Table S3-3. The 96h-LC$_{50}$ value of Az on zebrafish embryos was estimated to be 1031 µg L^{-1} while nAz was 334 µg L^{-1} under laboratory light. UV light significantly decreased 96h-LC$_{50}$ values of Az and nAz to 349 µg L^{-1} and 174 µg L^{-1} respectively (Figure 3-1). The survival rate of zebrafish embryos exposed to nAz started to have a significant decrease at the nominal concentration of 500, 400 and 300 µg L^{-1} starting at 72, 84 and 108 hpf respectively, without UV exposure (Figure S3-4A). Interestingly, under UV stimulation, the survival rate was significantly reduced at the nominal concentration of 400 and 500 µg L^{-1} starting at 72 hpf, 300 µg L^{-1} at 84 hpf and 200 µg L^{-1} at 96 hpf (Figure S3-4B). The survival rate of zebrafish embryos exposed to Az in laboratory light began to show a significant reduction only at the nominal concentration of 1000, 1500, 2000 and 3000 µg L^{-1} starting at 96, 84, 72 and 60 hpf respectively (Figure S3-4C) while the survival rate with UV exposure was only significantly decreased at a nominal concentration of 400 and 500 µg L^{-1} starting at 96 and 48 hpf respectively (Figure S3-4D).

In laboratory light conditions, pre-mature hatching was observed in the zebrafish embryos exposed to nAz at 300 µg L^{-1} at 60 and 72 hpf while both nominal concentrations of 400 and 500 µg L^{-1} significantly decreased hatching success starting at 60 hpf (Figure S3-5A). UV light significantly reduced hatching success at nominal concentrations of 200 µg L^{-1} starting at 96 hpf, 300 µg L^{-1} at 84 hpf, and 300, 400 and 500 at 72 hpf (Figure S3-5B). Co-exposure of nAz and UV also significantly reduced hatching at all concentrations at 60 hpf and nominal concentration of 20 µg L^{-1} at 72 hpf but did not affect their final hatching success (Figure S3-5B). Hatching success was significantly reduced at a nominal concentration of 1000, 1500 and 2000 µg L^{-1} of

Az starting at 96, 84 and 60 hpf without UV light while not a single embryo was able to hatch at a nominal concentration of 3000 $\mu g\ L^{-1}$ (Figure S3-5C). UV light significantly reduced the hatching rate at a nominal concentration of 400 $\mu g\ L^{-1}$ starting at 72 hpf and zero hatching success was observed at 500 $\mu g\ L^{-1}$ throughout 96 h exposure (Figure S3-5D).

3.3.3 Morphological effects

No gross morphological alterations including yolk sac edema, pericardial edema and spinal deformity were observed in control groups or during the exposure of either nAz or Az in either light conditions (Figure S3-6&S3-7). However, yolk consumption during the exposure period was significantly reduced in zebrafish embryos exposed to nAz and Az at the nominal concentration of 20 and 100 $\mu g\ L^{-1}$ under either light condition when comparing control, vehicle control, coating control and polymer control ($p < 0.001$). However, embryos exposed to Az at a nominal concentration of 20 $\mu g\ L^{-1}$ had higher yolk consumption than that in the other three treatment groups in both light conditions ($p < 0.05$; Figure 3-2).

3.3.4 Metabolic effects

The oxygen consumption rate of zebrafish embryos and larvae showed no significant differences between control, vehicle control (0.01% methanol), polymer control (input polymer) and coating control (Allosperse) in either light condition ($p > 0.92$; Figure 3-3A). However, under UV light, the oxygen consumption rate of zebrafish larvae was significantly reduced by nAz at nominal concentrations of either 20 or 100 $\mu g\ L^{-1}$ ($p < 0.03$; Figure 3-3B). In addition, a

decreasing trend was observed in nAz at 100 μg L^{-1} without UV exposure (p=0.0653 compared to control). However, no significant differences were detected between azoxystrobin treated groups.

The heart rate of zebrafish larvae at 120 hpf did not have any significant difference between the control group, vehicle control (0.01% methanol), polymer control (input polymer) or coating control (Allosperse) in either light condition (p > 0.99; Figure 3-4). The heart rate was significantly decreased by nAz at nominal concentrations of 20 and 100 μg L^{-1} and Az at nominal concentrations of 100 μg L^{-1} under laboratory light (p = 0.0023, 0.0001 and 0.0044 respectively) and UV light (p = 0.0002, 0.0001 and 0.0023 respectively) when compared to the control group (Figure 3-4). However, the heart rate of larvae exposed to Az at nominal concentrations of 20 μg L^{-1} in both light conditions (p = 0.0012 under laboratory light and p= 0.0007 under UV light) were significantly higher than the one of larvae exposed to nAz at nominal concentrations of 100 μg L^{-1} under UV (Figure 3-4).

3.3.5 Biochemical effects

In laboratory light, a significant increase in catalase activity was only observed in embryos exposed to nAz at a nominal concentration of 100 μg L^{-1} (p < 0.0001; Figure 3-5A). UV light significantly reduced catalase activity in all the groups (p < 0.001; Figure 3-5A), but increased sod activity in embryos exposed to nAz at nominal concentrations of 100 μg L^{-1} (p=0.0054; Figure 3-5B). The increase in sod activity caused by co-exposure of Az at a nominal concentration of 100 μg L^{-1} and UV light was only significantly higher than the control groups (p=0.0041; Figure 3-5B).

3.3.6 Molecular effects

Neither nAz nor Az altered *catalase* expression in either lighting conditions (Figure 3-6A). nAz had no effect on *sod1*, *sod2* or *gpx1b* gene expression in either UV illuminated or non-illuminated groups while co-exposure of Az at a nominal concentration of 100 µg L^{-1} and UV light significantly upregulated *sod1* ($p<0.0001$), *sod2* ($p<0.0001$) or *gpx1b* ($p<0.0001$) expression in 120 hpf zebrafish larvae (Figure 3-6B, C&E). Both nano-enabled and conventional Az at both 20 and 100 µg L^{-1} significantly reduced *gpx1a* gene expression in both light conditions ($p<0.05$) and there was no significant difference between illuminated groups non-illuminated groups (Figure 3-6D).

3.3.7 Lipid peroxidation

Western blot analysis showed that the amount of 4-HNE protein was significantly increased in zebrafish larvae at 120 hpf after being exposed to either nAz at a nominal concentration of 100 µg L^{-1} ($p<0.0001$) or Az at a nominal concentration of 20 µg L^{-1} ($p=0.0044$). The amount of 4-HNE was not further increased by UV light in the larvae exposed to Az at 20 µg L^{-1} ($p>0.999$). However, UV light significantly induced 4-HNE protein in the larvae exposed to nAz ($p<0.0001$) and Az ($p=0.0025$) at 100 µg L^{-1} (Figure 3-7).

3.3.8 Generation of free radicals

The generation of •OH by azoxystrobin in RO water was UV and concentration-dependent (Figure 3-8). The production of •OH at a nominal concentration of 10 mg L^{-1} nAz

(0.23 ± 0.12 nmol 1,1,3,3-tetraethoxypropane (TEP) Equivalent mL^{-1}) and Az (0.32 ± 0.12 nmol TEP Equivalent mL^{-1}) was significantly induced by UV light after 30 min exposure when compared to the control group (p<0.001).

3.4 Discussion

This study demonstrates the lethal and sub-lethal toxicity of nAz and Az in zebrafish embryos and larvae during their early developmental stages. Moreover, it illuminates an interactive and novel effect of UV light exposure on azoxystrobin toxicity. The LC$_{50}$ results demonstrate that nAz had higher lethality when compared to Az and that UV light significantly increased the toxicity of both Az and nAz. While nAz at 100 µg L^{-1} had a greater reduction in oxygen consumption and higher lipid peroxidation compared to Az, mainly due to higher bioavailability of nAz, other sub-lethal endpoints showed little to no biological difference between the two exposures. UV light exacerbated both Az and nAz toxicity and further induced greater changes in oxygen consumption, sod activity and lipid peroxidation compared to those embryos exposed to laboratory light.

3.4.1 Water chemistry and DLS

The measured concentrations of nAz at both light conditions were higher than measured concentrations of Az at high nominal concentrations (Table 3-1) while no significant differences were seen in the low nominal concentration treatment group (Figure S3-2). This is likely due to the fact that nAz is designed to be more dispersible in water and the result is a higher

bioavailability in the water column over the experimental period. DLS result shows that nAz had a broad size distribution. The increase in HD at 4 and 8 h at 20 µg L^{-1} also show that particles started with relatively small size but aggregated to larger particles when their zeta-potential rose towards zero. The primary size of individual materials (nAz and capsule) is reported as <50 nm and the distribution analysis within the DLS shows that there are nano-sized materials (< 100 nm) in each exposure. The aggregations noticed in DLS may be overestimated since the mathematical algorithms in DLS tend to be biassed towards reporting larger aggregates, especially with particles without a high enough density to diffract light. Zeta-potential measures the electrostatic interaction between particles.[62, 110] When zeta-potential is closer to zero, there are fewer repulsive forces present between particles and this results in greater aggregation of particles.[62] The low zeta-potential of nAz in our study resulted in increasing aggregation over time. These larger aggregates tend to sediment to the bottom and thereby increase the bioavailability to the organisms in (or on) the sediments.[19]

3.4.2 Survival and Hatching success

The 96h-LC$_{50}$ of Az (1031 µg L^{-1} nominal concentration) without UV exposure was similar to the published 96h-LC$_{50}$ value (1230 µg L^{-1}) for zebrafish embryos[171] while the 96h-LC$_{50}$ of nAz (334 µg L^{-1}) was found to be much lower. The published LC$_{50}$ of 1230 µg/L was based on nominal concentrations and this is why we have included our nominal concentration for comparison. However, the LC$_{50}$ values of nAz and Az based on measured concentrations were lower than those for nominal concentrations. This suggests that regulations should follow an LC$_{50}$ with measured concentrations. The hatching success was significantly decreased when

zebrafish embryos were exposed to the concentrations close to or above LC_{50} value mainly due to the death of embryos at those concentrations while no significant reduction in final hatching success was observed at low concentrations (Figure S3-5). Therefore, the direct effect of azoxystrobin on zebrafish hatching success is negligible.

3.4.3 Metabolic stress

It is well known that the mode of action for azoxystrobin is to block Q_o site of complex III in mitochondria to disrupt electrons transfer in ETC during cellular respiration.[150, 153, 154] All the eukaryotes, including fish, share the same ETC, which makes fish the potential indirect target of azoxystrobin when it leaches and/or runoff into the water.[150, 155] However, very few studies have focused on the metabolic effects of azoxystrobin, especially on aquatic organisms.[150, 172] One study found that both mitochondria activity and ATP concentration in zebrafish larvae at 98 hpf were significantly reduced compared to the control group after being exposed to Az at a nominal concentration of 0.2 mg L^{-1} for 96 h.[172] The current study showed that the co-exposure of UV light and nAz significantly reduced oxygen consumption by more than 40% at 120 hpf compared to the control group while other treatments also decreased oxygen consumption (Figure 3-3B). Therefore, inhibiting mitochondrial respiration and decreasing ATP production is the mechanism of nAz and Az toxicity on zebrafish embryos.

The fish heart is an important organ to circulate blood to provide nutrients and O_2, and remove waste from all the tissues. The heart has been demonstrated to be a target for various toxicants, including organic compounds and NPs, in the environment.[154, 173, 174] An ~10% reduction in heart rate (HR) was observed in nAz at a nominal concentration of 20 and 100 μg L^-

^{1} and Az at 100 μg L^{-1}. This finding suggested that both forms of azoxystrobin are bioavailable and can act to reduce zebrafish heart rate. Both nAz and Az showed a similar reduction in HR at the higher concentration while nAz had greater effects (lower HR) compared to Az at a lower concentration. Similar effects on HR for Az have been observed previously.[154] The HR was significantly reduced in juvenile grass carp (*Ctenopharyngodon idella*) after exposure to Az for 48 h at nominal concentrations of 0.16, 0.25, 0.40 and 0.63 mg L^{-1}.[154] Therefore, changes in the heartbeat of fish embryos and larvae when they are exposed to environmental toxicants may be an early response and a simple endpoint to measure for toxicity studies.[173, 174]

3.4.4 Morphological alternations

Common morphological malformations were not observed at 120 hpf embryos in the current study suggesting that azoxystrobin is not a teratogenic toxicant in zebrafish at ecologically relevant concentrations[148, 171, 172, 175] although tests at an experimentally high level (more than 500 μg L^{-1} for 144 h exposure) have found teratogenic effects.[171] In our study, the remaining yolk sac volume in larvae exposed to azoxystrobin at 120 hpf was increased when at both concentrations under both light conditions. The reduction of yolk consumption is likely associated with the combination of a decrease in the HR and decreased oxygen consumption mentioned above resulting in reduced or delayed use of yolk sac contents during development. The yolk is the only source of food to provide energy and nutrients for embryos and larvae during these early stages of development before they can feed exogenously.[176, 177] Malabsorption of yolk can lead to lack of nutrients for embryos during critical development phases, which may reduce growth, alter the endocrine system and metabolism, decrease reproduction, and cause

disease during and beyond the development stage.[177, 178] This suggests that examination of chronic and transgenerational exposures are necessary to provide information on the prolonged effects of azoxystrobin on aquatic organisms.

3.4.5 Oxidative stress

Previous research has demonstrated that azoxystrobin can alter the expression of antioxidant, oxidative stress, growth and apoptosis-related genes in various organisms.[148, 150, 154, 172, 179] In the current study, *catalase* expression was not affected by azoxystrobin. Significant up-regulation of antioxidant-related genes including *sod1*, *sod2* and *gpx1b* was only observed in zebrafish embryos exposed to the highest concentrations of Az (100 µg L^{-1}) and only when the embryo was exposed to UV light. However, *gpx1a* expression was decreased in the embryos exposed to Az and nAz at both light conditions in all treatments. These results were perplexing given that they are not in agreement with other studies on Az.[172, 179] One study showed that there were no effects of azoxystrobin exposure on *gpx* while *catalase* and *sod2* were significantly up-regulated at 50 and 200 µg L^{-1} of Az at 98 hpf. In the same study, *sod1* was only significantly increased at the highest concentration of 200 µg L^{-1}.[172] A second study found that *copper/zinc-sod* expression in zebrafish larvae was significantly reduced at 0.1, 1, 10 and 100 µg L^{-1} while *catalase* and *gpx* were only up-regulated at 0.1, 1 and 10 µg L^{-1} at 120 hpf after exposure to Az for 48 h.[179] This study also showed that *sod*, *catalase* and *gpx* were all up-regulated at 144 hpf when larvae at 72 hpf exposed to Az at 0.1 µg L^{-1} for 72 h but all down-regulated when exposed to higher concentrations.[179] The result is that each study provided unique/inconsistent results suggesting that the expression of antioxidant and oxidative stress-related genes may not be ideal

markers for azoxystrobin exposure. Differences in experimental design including dose and timing may have contributed to this variation in gene response.[172, 179] Moreover, it should be noted that gene expression can only partially predict protein expression, and in most cases, the correlation between protein abundance and mRNA expression is lower than 50%.[180, 181] Therefore, better or more consistent markers than simply gene expression are required to evaluate if exposure of zebrafish to azoxystrobin results in oxidative stress.

ROS is a naturally derived chemical species in normal metabolism and are highly reactive molecules due to their unpaired electron.[80, 81] Mitochondria utilize oxygen to generate energy through oxidative phosphorylation.[182] In normal conditions, about 0.1 to 4 % of the oxygen in the cell is incompletely reduced to superoxide ion ($O_2^{-\bullet}$) instead of H_2O in Complex I and III of mitochondria.[182, 183] Since ROS is a naturally occurring and cell generated substance, organisms have developed strong antioxidant defense systems to rapidly degrade ROS generated from these endogenous reactions.[110, 133, 172] Previous studies have demonstrated that the inhibition of ETC in mitochondria by Az will increase the number of electrons escaping from ETC, leading to a much higher production of ROS (mainly $O_2^{-\bullet}$ and H_2O_2) and increased activity for antioxidant enzymes including catalase.[150, 154, 179]

Experiments conducted in laboratory light revealed that catalase activity was only induced by nAz at the higher concentration (100 µg L^{-1}) which matches similar trends observed in other studies.[154, 172] For example, catalase activity was increased in zebrafish larvae at 98 hpf after exposed to Az at a nominal concentration of 0.2 mg L^{-1} for 96 h.[172] Similarly, a second study showed that catalase activity in juvenile grass carp was induced at 0.05 and 0.25 mg L^{-1} of Az in a concentration-dependent manner after 24 hour exposure period. However, the induction of catalase activity at the 48-hour exposure period was lower compared to 24 h at both

concentrations.[154] It should be noted that one study did not find any significant increase in catalase activity in zebrafish larvae exposed to Az.[179] Therefore, the induction of catalase by Az may be both concentration- and time-dependent.

One important finding is that catalase activity was significantly decreased by exposure to UV light in all the groups. This is likely due to the absorption of UV energy by the chromophore of catalase resulting in the oxidation of tryptophan residues, aggregation of the protein and eventually, breakdown of the enzyme.[110, 184, 185]

Exposure to either nAz or Az at 100 μg L^{-1} under UV light increased sod activity by approximately 15%. However, exposure to Az alone (in lab light) did not affect sod activity. The substantial effects of UV light exposure on sod activity indicate that azoxystrobin absorbed the UV light with resultant secondary production of $O_2^{-\bullet}$. This would explain the up-regulation of sod activity in UV-treated Az exposure embryos. The induction of sod by Az may be both concentration- and time-dependent. Studies of Az exposure under lab conditions have shown no changes or a significant decrease in sod activity at a nominal concentration ranging from 0.05 mg L^{-1} to 0.25 mg L^{-1} in zebrafish and grass carp after 48 hour exposure[154, 179] while one study reported a significant increase in larval and adult zebrafish after 96 and 192 h exposure.[172]

Excess ROS exposure in organisms is thought to act by overwhelming the natural antioxidant cellular defenses resulting in damaged cellular constituents such as RNA, DNA, protein and lipids.[110, 133, 152, 172, 179] Lipid peroxidation occurs when uncontrolled free radicals take electrons from polyunsaturated fatty acyl groups present in the lipids in the cellular membranes.[132, 133, 182, 186] Lipid peroxidation results in the degradation of the cell membrane and production of aldehydes, alkenals and hydroxylalkenals including malondialdehyde (MDA) and

4-hydroxy-2-nonenal (4-HNE).[132, 133, 182, 186] Both MDA and 4-HNE have been intensively studied and widely used to evaluate the level of lipid peroxidation in various organisms and cell lines.[186-188] In our study in laboratory light conditions, the level of 4-HNE was significantly increased by nAz at 100 μg L^{-1} and Az at both 20 and 100 μg L^{-1} compared to the control group. Therefore, the zebrafish embryos and larvae experienced oxidative stress induced by nAz and Az, especially at 100 μg L^{-1}. This result is supported by previous studies showing increases in lipid peroxidation with Az exposure.[152, 171, 172] In these studies, the MDA content/concentration was significantly increased by Az at the concentration of 100 μg L^{-1}, 25 μg L^{-1} and 0.05 mg L^{-1} in adult zebrafish liver,[152] larvae at 96 hpf[171] and larvae at 98 hpf respectively.[172] Interestingly, we have also shown that the presence of UV light further exacerbates the lipid peroxidation by demonstrated further increases in 4-HNE level in both nAz and Az at 100 μg L^{-1} with UV light exposure. This study is the first to demonstrate that UV light can further increase oxidative stresses by inducing even higher lipid peroxidation than that associated with nAz and Az exposure alone. However, the next question to address was whether this enhanced lipid peroxidation was a direct effect of UV light on Az or a secondary effect of UV on Az damaged/impaired mitochondria.

3.4.6 Generation of free radicals

We decided to determine if azoxystrobin itself (in the absence of fish) could generate ROS when exposed to UV light. Surprisingly, UV stimulation of either nAz or Az containing water showed an increased production of •OH as measured by the 2-DR assay. This demonstrated that •OH was generated from both nAz and Az by UV light. We could only

measure an increase in •OH at a nominal concentration of 10 mg L^{-1}, 2 mg L^{-1} did not show any significant increase compared to the control group, likely because the amount of •OH generated at 2 mg L^{-1} was lower than the detection limit of 2-DR TBARS assay.[110] Studies on photo-induced toxicity of other organic compounds on aquatic species are very limited. A previous study examining the effect of exposure to 11 types of polycyclic aromatic hydrocarbons (PAHs) on the immobility of *Daphnia magna* neonates showed that UV light significantly decreased 48-h EC_{50} but the authors did not report lipid peroxidation of other oxidative stress markers.[189] A study of reproduction in *Ceriodaphnia dubia* exposed to Az at measured concentrations of 10, 18 and 26 μg L^{-1} reported that 4-h UV exposure per day for 7 days significantly reduced the fecundity.[190] However, no toxicity studies to date have provided a plausible mechanism of photo-induced toxicity for azoxystrobin. This study is the first and only one to demonstrate photo-inducible properties of azoxystrobin. One possible mechanism is through direct UV-induced generation of •OH by azoxystrobin. Organic chemicals containing conjugated π electrons, especially in the aromatic ring(s) and aryl pyrazole ring(s), have been reported to be able to absorb light.[161-164] When the π electron on the highest occupied molecular orbital (HOMO) absorbs light, it can overcome energy gap (HOMO-LUMO gap) and jump to the lowest unoccupied molecular orbital (LUMO) becoming a free electron. This free electron is able to react with nearby oxygen and water molecules to produce ROS.[161-163] Compounds with more aromatic/aryl pyrazole rings and more conjugated π electrons have a lower HOMO-LUMO gap, which makes it easier for π electrons on HOMO to be excited by UV light.[161, 163] Since azoxystrobin has the same numbers of aromatic ring and aryl pyrazole ring as pyraclostrobin, the HOMO-LUMO gap (E_{gap}) in azoxystrobin should be close to 0.179 a.u. (=4.87 eV) in pyraclostrobin.[164] Therefore, azoxystrobin is indeed able to absorb light with the wavelength of

approximately 255 nm (calculated by $\lambda=hc/E_{gap}$) and excite electrons to directly generate •OH or other ROS. This mimics the electron on the valence band that absorbs light and jumps over the band gap to reach the conduction band as occurs during the photo-excitation of metal and metal oxide semiconductors.[17, 38] However, the ROS generated by co-exposure of UV and azoxystrobin was much lower than metal oxide nanoparticles tested in other studies.[85, 110] In summary, the results suggest the production of ROS directly by azoxystrobin during photo-excitation as a key but understudied mechanism of azoxystrobin and perhaps other organic molecule toxicities.

3.5 Conclusion

This is the first comprehensive study to evaluate the toxicity of nAz and compare the effects of nAz to its conventional form. In general, the small differences in toxicity at the lower concentration are likely due to differences in bioavailability. Nano-enabled forms of pesticides are designed to improve water dispersibility and therefore likely to have higher bioavailability at lower concentrations compared to their conventional forms. An important finding in the present study is the exacerbation of toxicity by UV light. We provide a mechanism whereby the azoxystrobin molecule itself may generate •OH under UV exposure. Given that these pesticides are intended for field applications, this aspect of photo-induced toxicity for pesticides having aromatic ring(s) has not been thoroughly explored. In fact, the potential for UV-induced exacerbation of toxicity for a variety of organic compounds should be further investigated. The current study will provide much-needed data of acute and medium-term hazards of nAz for its implementation in agriculture. Moreover, this study clearly demonstrates the importance of considering environmental factors (e.g. UV light) in modulating toxicity.
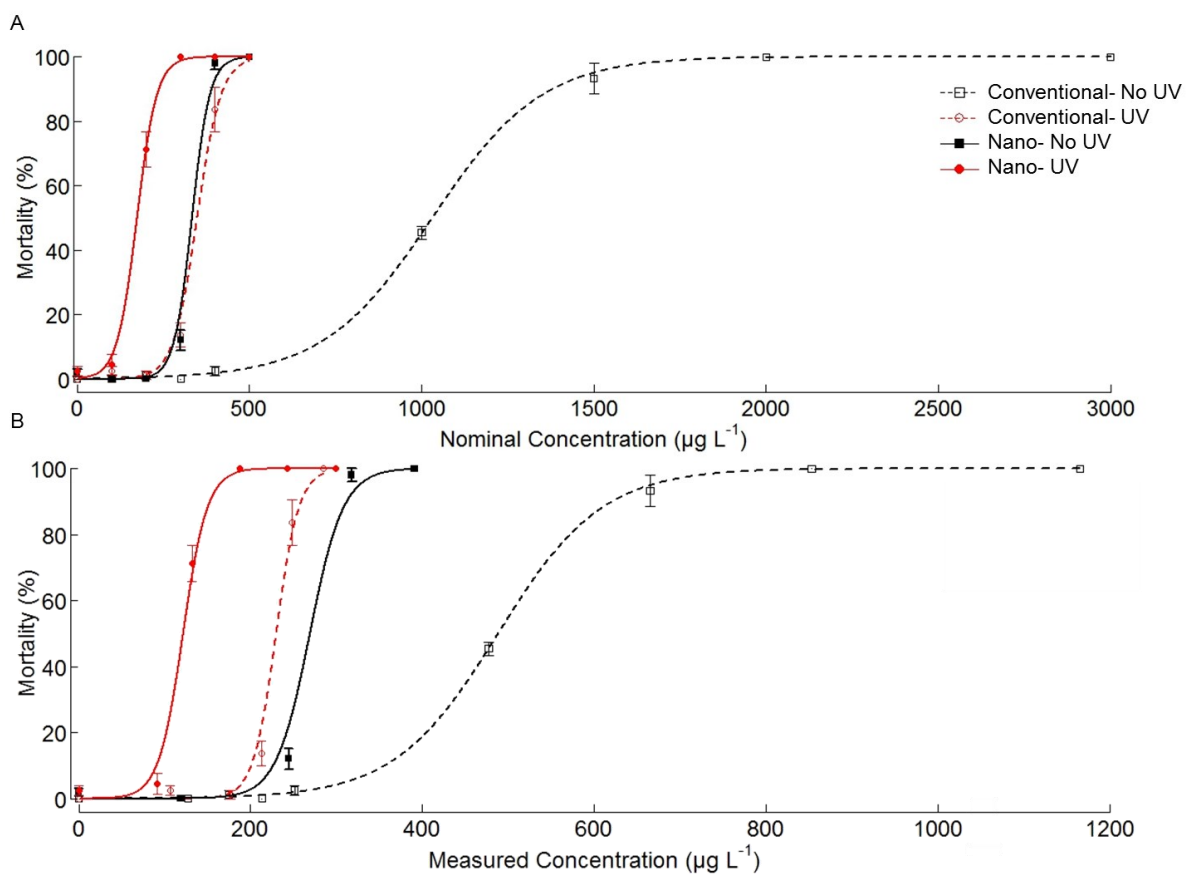
Figure 3-1. Mortality of nAz (solid line) and Az (dashed line) azoxystrobin at various nominal concentrations (A) and measured concentrations (B) on zebrafish embryo/larvae from 24 hpf to 120 hpf with (red) or without (black) UV exposure. Values are mean ± SEM. n=4.
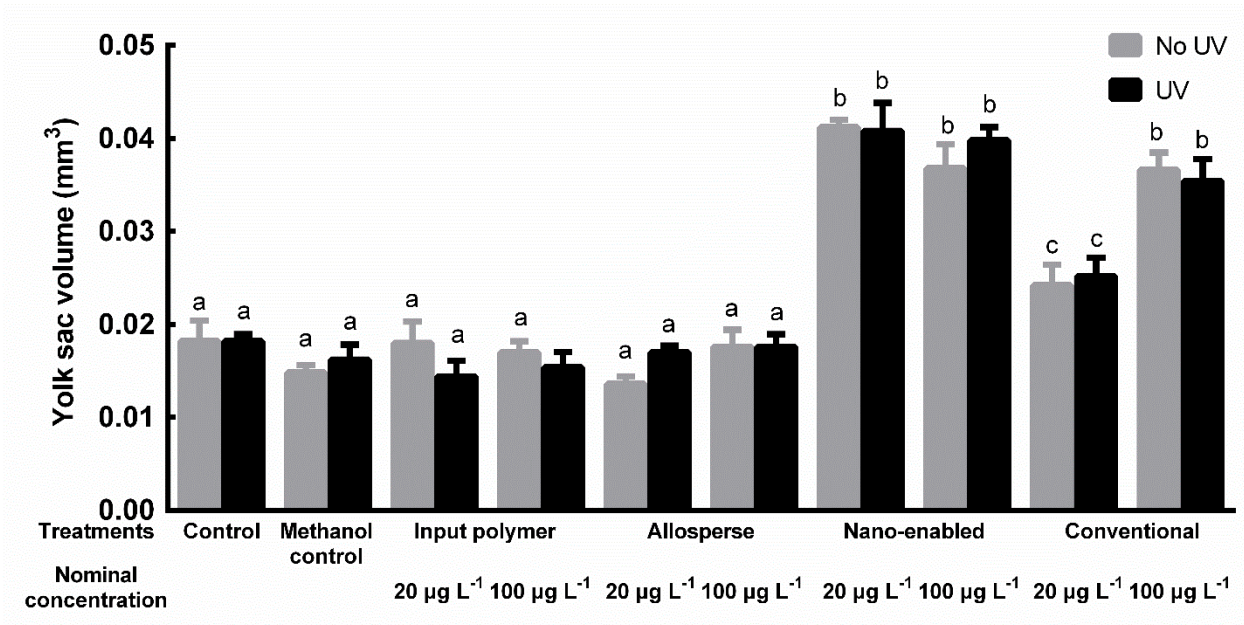
Figure 3-2. Yolk sac volume of zebrafish larvae at 120 hpf in the control groups and treatment groups after exposure from 24 to 120 hpf. Means sharing the same letter are not significantly different from each other (p>0.05). Values are mean ± SEM. n=5.
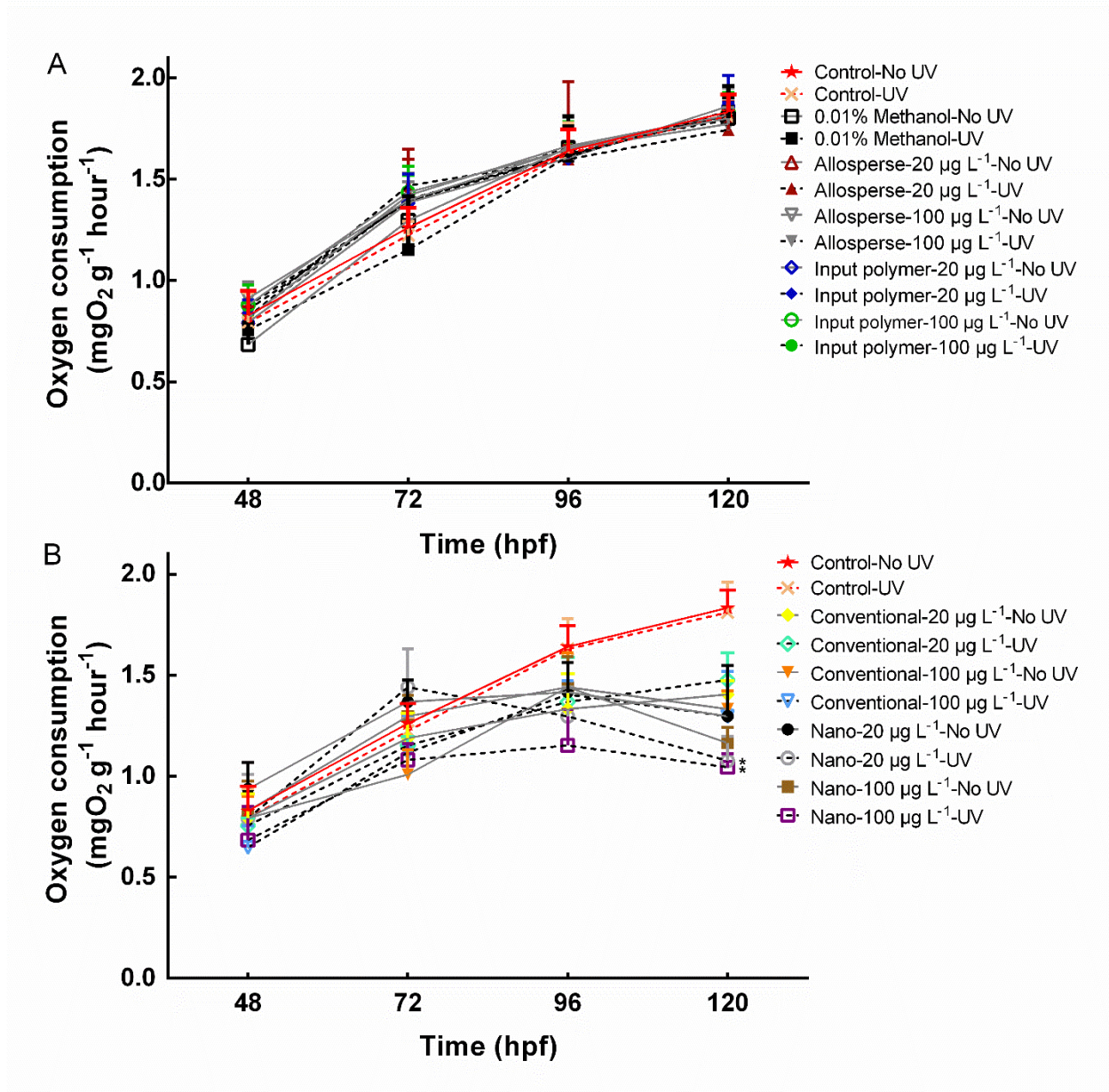
Figure 3-3. Oxygen consumption of zebrafish embryos and larvae exposed to all control groups (A) and all treatment groups (B) between 48 hpf and 120 hpf. Asterisk (*) indicates a significant difference between treatments and control. Values are mean ± SEM. n=5.
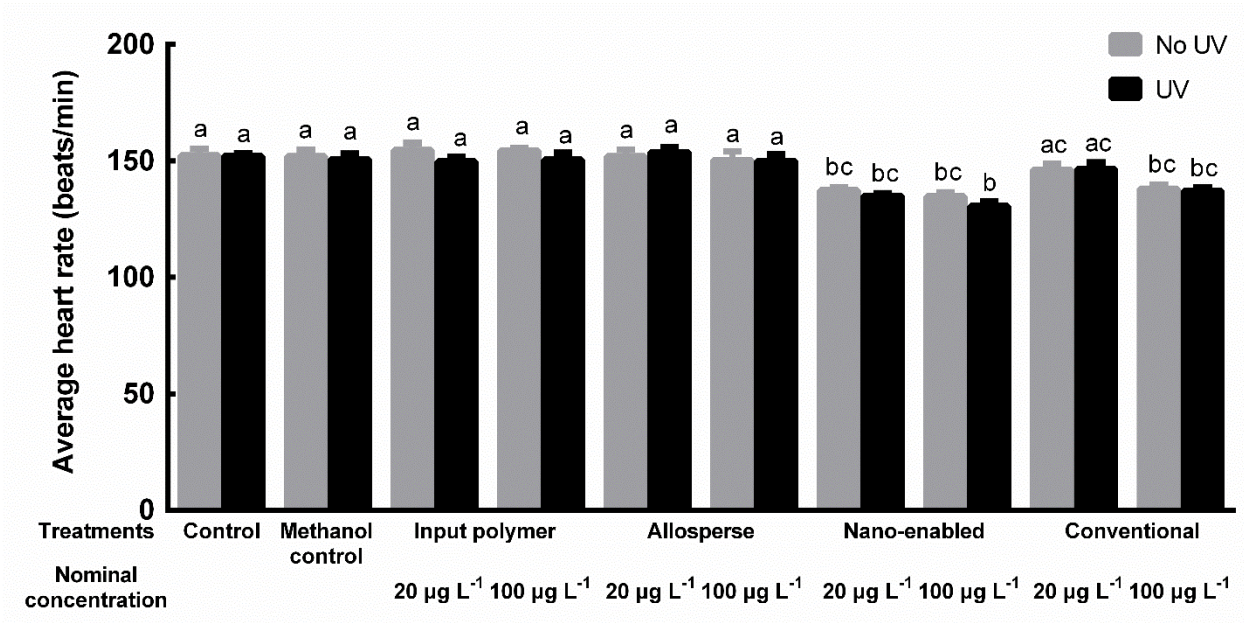
Figure 3-4. The average heartbeats of zebrafish larvae at 120 hpf after exposure to all control groups and treatment groups from 24 to 120 hpf. Means sharing the same letter are not significantly different from each other (p>0.05). Values are mean ± SEM. n=5.
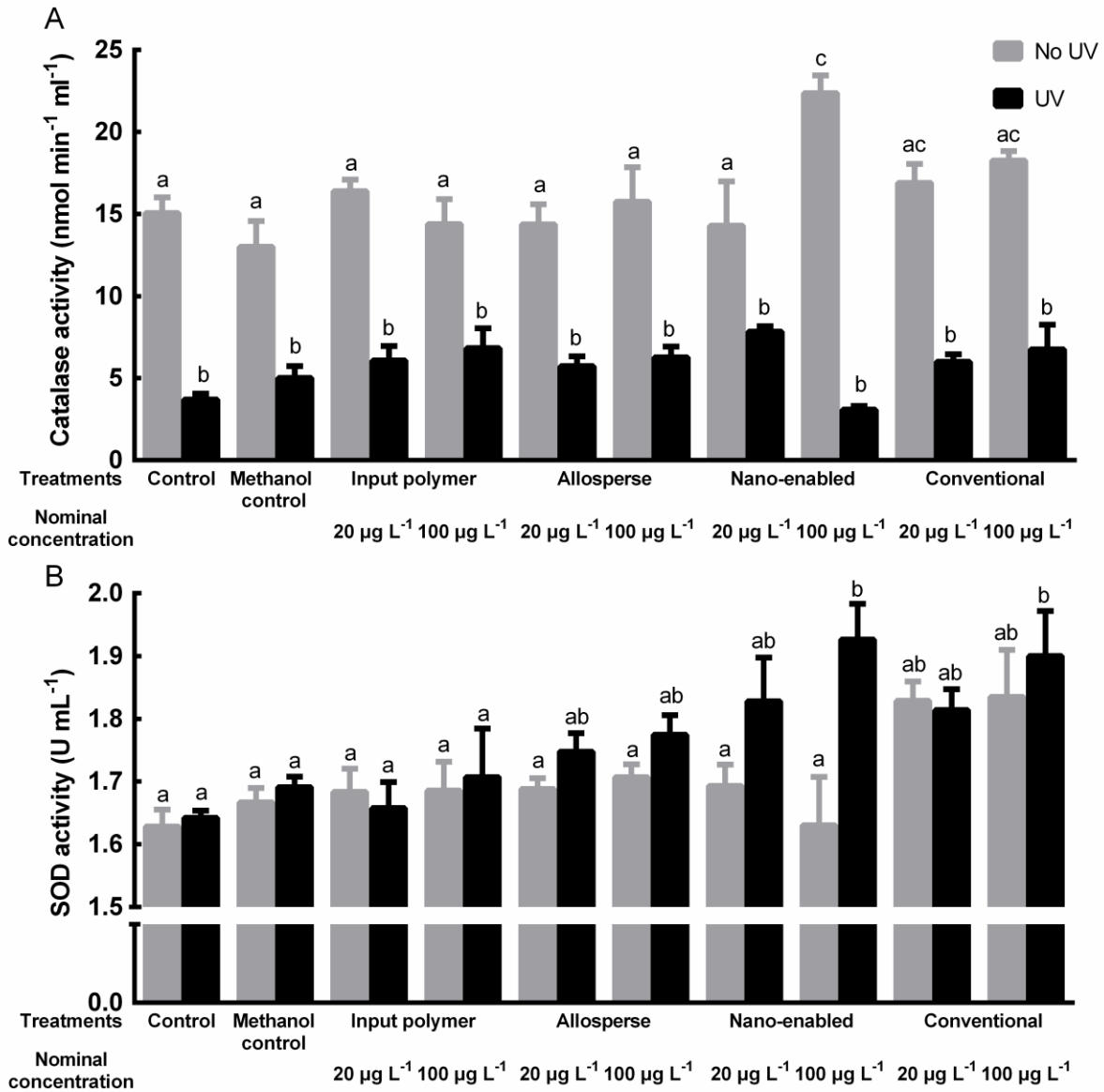
Figure 3-5. Catalase (A) and superoxide dismutase (B) activities in zebrafish larvae at 120 hpf after exposure to all control groups and treatment groups from 24 to 120 hpf. Means sharing the same letter are not significantly different from each other ($p > 0.05$). Values are mean $\pm$ SEM. n=5.
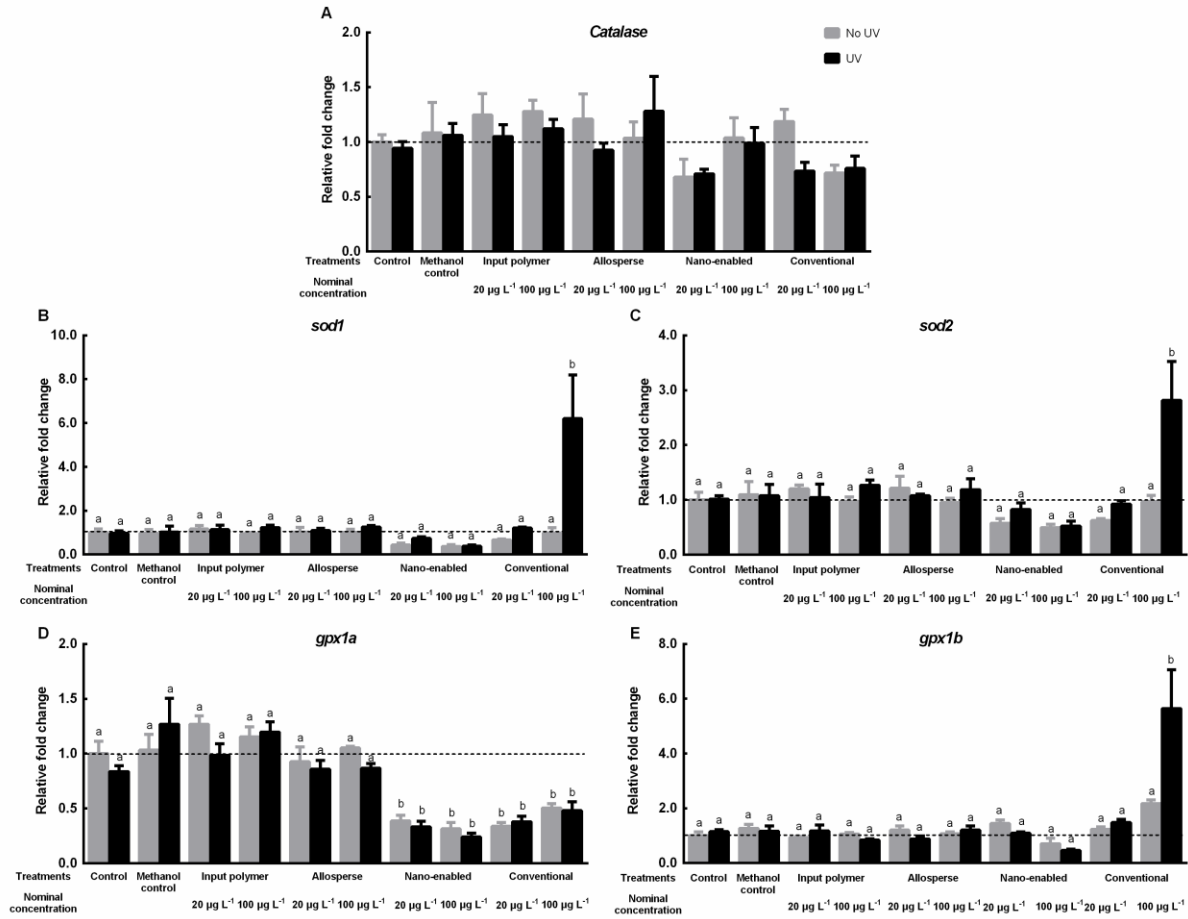
Figure 3-6. Relative fold change in gene expressions of *catalase* (A), *sod1* (B), *sod2* (C), *gpx1a* (D) and *gpx1b* (E) relative to ef1α in zebrafish larvae at 120 hpf after 96-hour exposure from 24 hpf under either laboratory light or UV light. Means sharing the same letter are not significantly different from each other (p>0.05). Values are mean ± SEM. n=4.
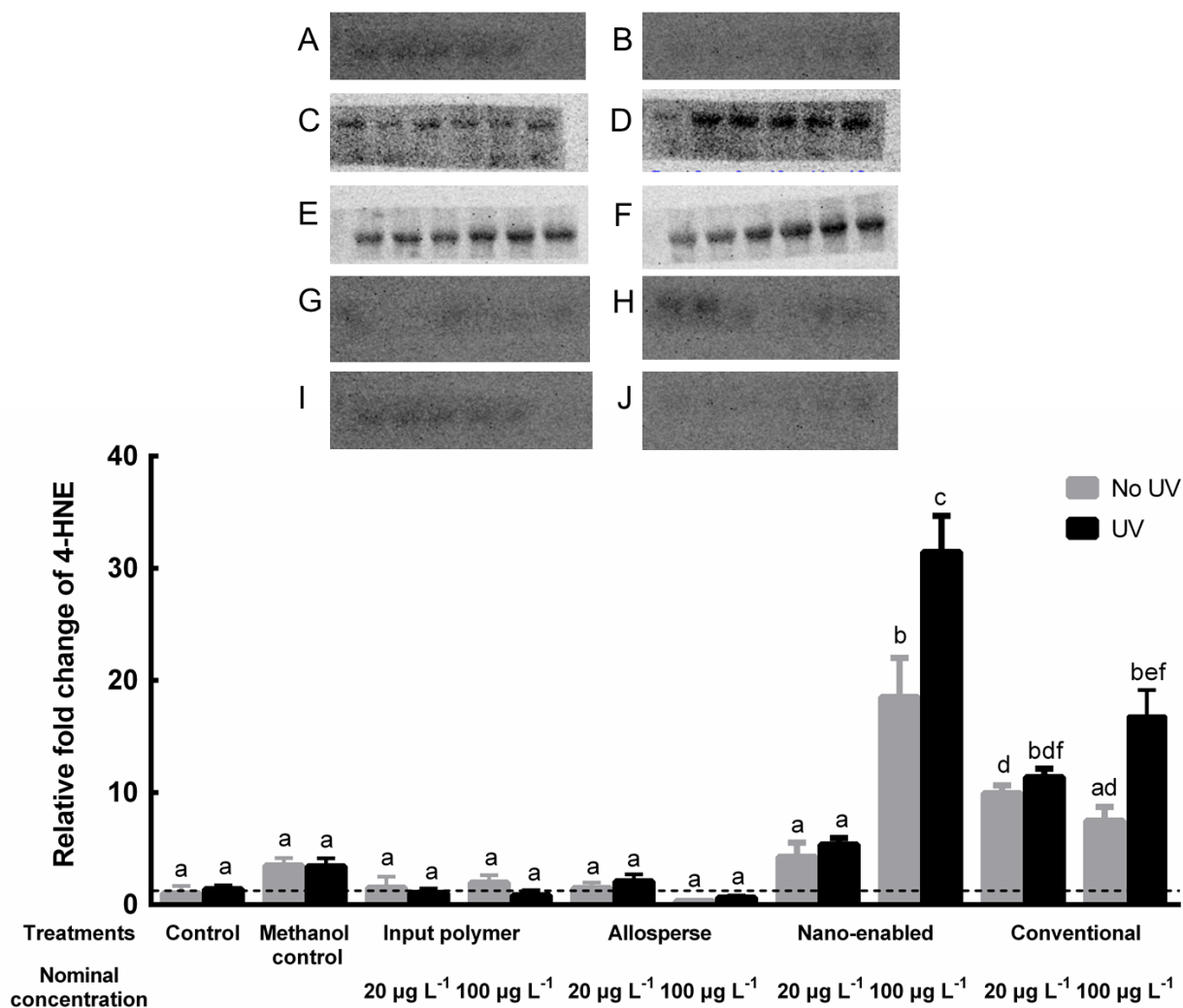
Figure 3-7. Western blot images (Top) of 4-HNE expression in zebrafish larvae at 120 hpf in control (A), vehicle control (B), nAz at 20 μg L^{-1} (C) and 100 μg L^{-1} (D), Az at 20 μg L^{-1} (E) and 100 μg L^{-1} (F), input polymer at 20 μg L^{-1} (G) and 100 μg L^{-1} (H), and Allosperse at 20 μg L^{-1} (I) and 100 μg L^{-1} (J) under laboratory light (lane 1, 2 and 3) and UV light (lane 4, 5 and 6), and western blot analysis (Bottom) of 4-HNE relative fold change to control group without UV exposure in zebrafish larvae at 120 hpf after 96-hour exposure from 24 hpf under either laboratory light or UV light. Means sharing the same letter are not significantly different from each other (p>0.05). Values are mean ± SEM. n=3.
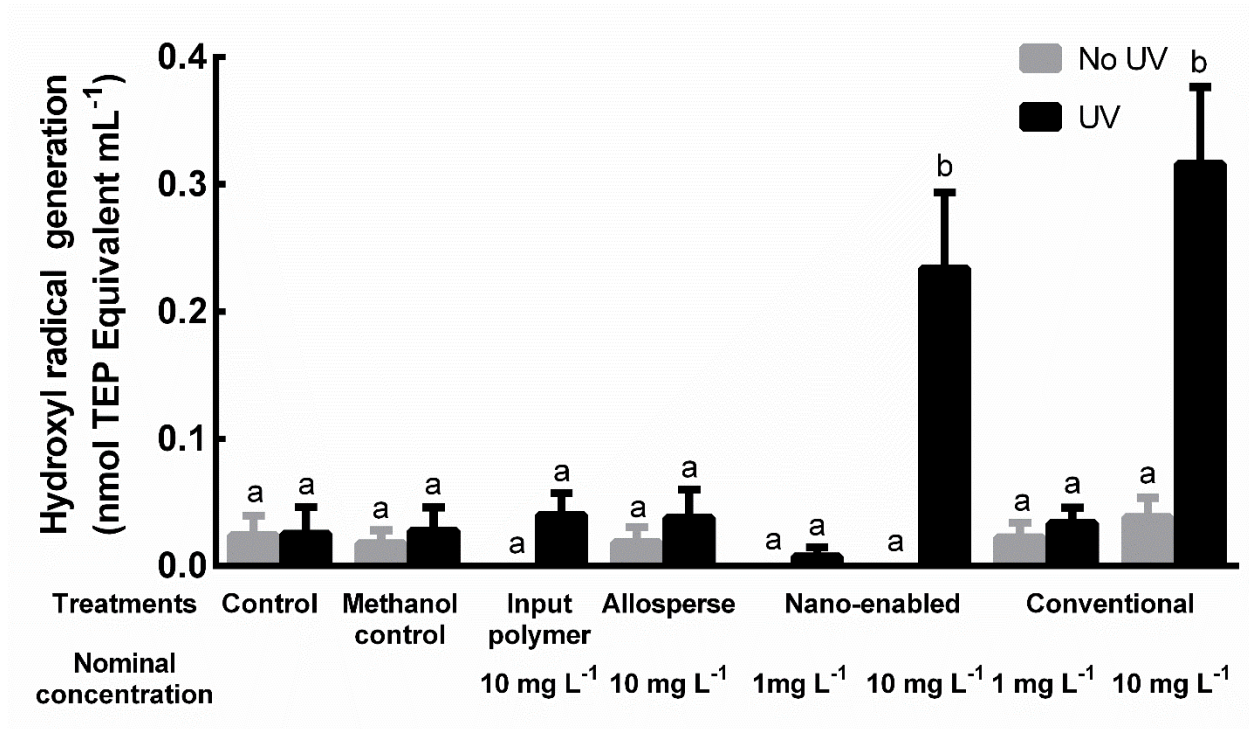
Figure 3-8. Generation of •OH by nAz at a nominal concentration of 1 or 10 mg L^{-1}, Az at a nominal concentration of 1 or 10 mg L^{-1}, input polymer at a nominal concentration of 10 mg L^{-1} or Allosperse at a nominal concentration of 10 mg L^{-1} RO water and 0.01% methanol in the presence (black bar) and absence (grey bar) of UV light. Means sharing the same letter are not significantly different from each other (p>0.05). Values are mean ± SEM. n=4.
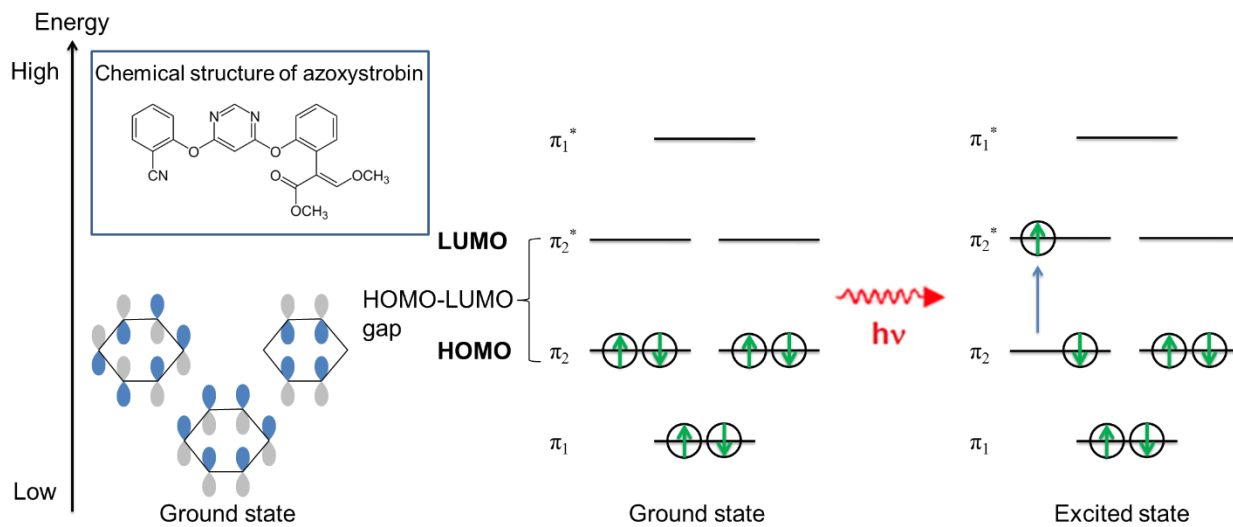
Figure 3-9. Simplified molecular orbital and HOMO-LUMO diagram of π system of a single aromatic ring, and the excitation of electron on HOMO by UV light to LUMO.

Table 3-1. LC$_{50}$ values of nano-enabled and conventional Az under laboratory light and UV light at nominal concentration and measured concentration. Values are mean ± SEM.

Azoxystrobin	Concentration	No UV	UV
Nano-enabled	Nominal	$334 \pm 13 \ \mu g \ L^{-1}$	$174 \pm 12 \ \mu g \ L^{-1}$
	Measured	$261 \pm 4.3 \ \mu g \ L^{-1}$	$135 \pm 3.2 \ \mu g \ L^{-1}$
Conventional	Nominal	$1031 \pm 64 \ \mu g \ L^{-1}$	$349 \pm 13 \ \mu g \ L^{-1}$
	Measured	$488 \pm 12 \ \mu g \ L^{-1}$	$223 \pm 2.4 \ \mu g \ L^{-1}$

Chapter 4

Potentiation of polycyclic aromatic hydrocarbon uptake in zebrafish embryos by nanoplastics
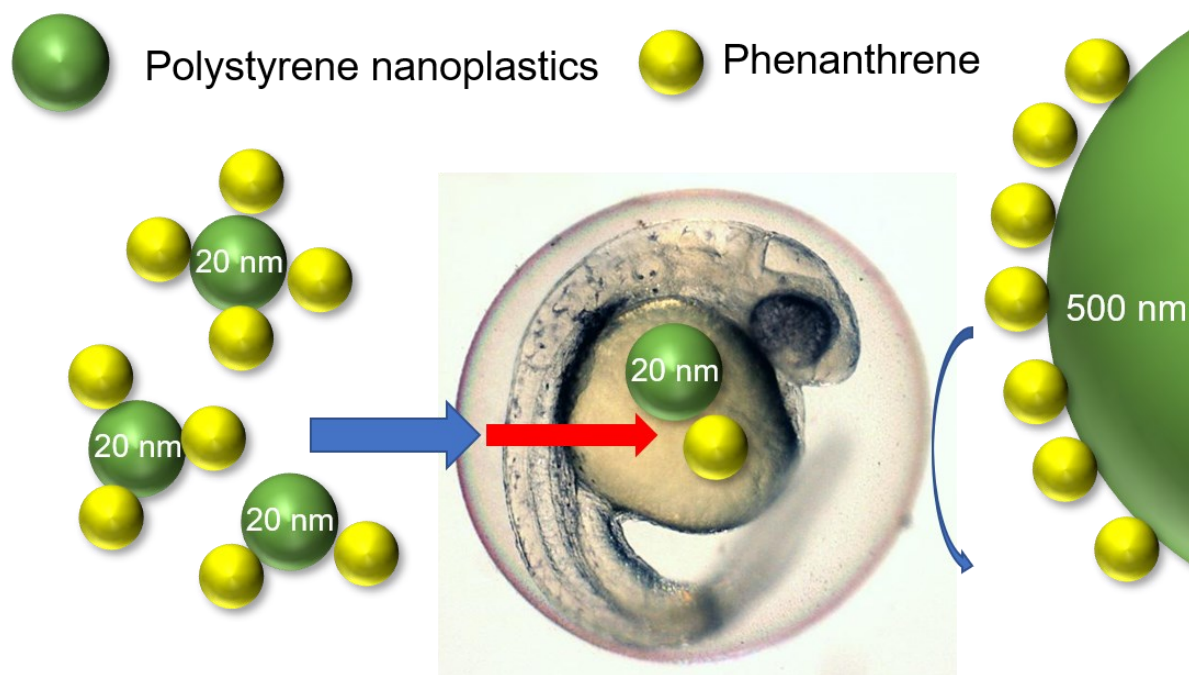
4.1 Introduction

Modern plastics have been mass-produced as early as the 1940s and global production has expanded greatly since the 1970s.[3, 191] Annual production was estimated to be over 320 million tonnes in 2015 which consumed about 8% of global crude oil production.[191] Unfortunately, ~50% of plastics manufactured are for single-use purpose and approximately 10% of annually produced plastics are expected to reach the ocean eventually.[3, 192, 193] Studies have also estimated that plastics contribute more than 60% of marine litter worldwide, making them one of the most significant pollutants in the aquatic environment.[3, 194] These plastics are known to break down over time with both UV light and mechanical action to produce microplastics (MPs; less than 5 mm, defined by The National Oceanic and Atmospheric Administration)[3, 195] which have become a significantly studied environmental concern.[191, 194, 196] The most common exposure route of MPs in invertebrates, fish and seabirds is through ingestion.[197, 198] When ingested, MPs can act in several ways to induce their toxicological effects. These include physical blockage which may cause pseudo-satiation, leaching of toxic plastic additives and release of chemicals sorbed onto the MP into these tissues.[197, 199]

Further degradation of microplastics by UV radiation, mechanical force, and microbiological activity will generate even smaller plastics with an exponentially higher surface area/gram plastic.[3, 196, 200] The particles smaller than 100 nm are considered to be nanoplastics (NPLs)[3, 196] and the potential toxicity of nanoplastics is beginning to attract more attention in recent years but have been relatively understudied.[191, 196] Various studies have demonstrated sub-lethal effects associated with nanoplastics exposure in aquatic species, including reduced growth and photosynthesis in *Scenedesmus obliquus*,[201] decreased body size and reproduction in

Daphnia magna,[201] increased feeding time[202] and alterations in the metabolism of liver and muscle in nanoplastics exposed *Carassius carassius.*[203]

A variety of hydrophobic persistent organic pollutants (POPs), including polycyclic aromatic hydrocarbons (PAHs), present in the aquatic system have been shown to adhere and concentrate on the surface of MPs.[193, 197, 204, 205] It has been proposed that one potential mechanism of toxicity is the sorption of organic pollutants onto the surface of plastics which then facilitates the transport of those POPs into the animal.[3, 193, 197, 205] Given that nanoplastics are much smaller than MPs with a much larger specific surface area (SSA), it is hypothesized that NPLs may have a significantly higher potential to deliver organic pollutants to exposed animals.[3, 191, 205] Also, given their small size, NPLs may be able to pass through biological membranes and have even higher bioavailability to aquatic organisms due to a "Trojan horse" effect allowing even greater uptake of POPs.[196, 206] The few studies that have examined this hypothesis have demonstrated higher tissue concentrations of POPs in NPLs and POPs co-exposed *D. magna*[205] and digestive tract of sea urchin embryos[207] but the direct demonstration of increased POP/NPLs uptake has not been performed.

Zebrafish are widely used as an aquatic animal model in acute toxicity tests.[208] Adults can produce a large number of embryos that are sensitive to environmental pollutants at relatively low concentrations.[208] Moreover, the small size of embryos allows the dosing medium and the transparent chorion is suitable for studying developmental malformations.[208] The chorion also contains pore canals with a diameter between 200 and 500 nm has been previously demonstrated to allow NPLs with a small size to pass through.[165, 209] During early developmental stages, zebrafish consume yolk as their sole energy and nutrient source and do not ingest food or water from the environment, which makes them a suitable model to study contaminant uptake

without the confounding effects of ingestion.[176, 177] Therefore, zebrafish embryos are the proper model to study co-contaminant transport and direct uptake of nanoplastics and POPs.

In this study, we developed a novel method to track organic co-contaminant uptake using radiolabelled phenanthrene to track the fate and transport of the organic and quantitatively assess unidirectional uptake rates. The purpose of this study was 1) to investigate the sorption of a radioactive labeled model compound of PAHs, ^{14}C-phenanthrene, onto two different sized NPLs; 2) to evaluate if the presence of NPLs can potentiate phenanthrene both passing through zebrafish embryo chorion and direct uptake by the larvae; and 3) to determine the lethality of two different sizes NPLs on zebrafish embryos, including differentiating the effects of different size NPLs on both the lethality and sub-lethal effects of phenanthrene on zebrafish embryos.

4.2 Methods

4.2.1 Chemicals

Yellow-green fluorescently labeled carboxylated polystyrene nanoplastics (PS-NPLs) at 500 nm (505 nm excitation, 515 nm emission; ThermoFisher, Catalog#F8813) and 20 nm (505 nm excitation, 515 nm emission; ThermoFisher, Catalog#F8787) were purchased for this study. Both PS-NPLs were suspended in water (2% solid) with 2 mM sodium azide (NaN_3).

Both PS-NPLs stock suspensions were dialyzed in double-distilled water (ddH$_2$O) for 7 days using Slide-A-Lyzer Dialysis Cassettes (2000 molecular weight cut-off, ThermoFisher, Catalog#PI66203) to remove NaN_3. The ddH$_2$O was changed every 1 h in the first 12 h and every 12 h for the next 6 days. Dynamic light scattering (DLS; Zetasizer Nano Series, Malvern

Instruments Ltd.) was used to characterize hydrodynamic diameter and polydispersity index (PDI) and zeta-potential of two PS-NPLs before and after dialysis.

4.2.2 Zebrafish maintenance and collection of viable embryos

Wild type strain TL adult zebrafish (aged 6 to 18 months) were housed in 20 L tanks (pH: 7.2-7.4, conductivity: 1100-1200 μS cm^{-1}, temperature: 28 °C, dissolved oxygen: 7.0 mg L^{-1}, general hardness: 100 mg L^{-1} as CaCO$_3$, salinity: 0.6 ppt, 14 h light: 10 h dark). Two female and one male zebrafish were placed in a hatching tank in which they were separated by a splitter and acclimated overnight. The next morning, the splitter was removed allowing zebrafish to spawn under the stimulation of the start of the light cycle. Fertilized embryos were collected after 1 h.

4.2.3 Sorption of phenanthrene onto the surface of nanoplastics

The stock [9-^{14}C]-labeled phenanthrene (^{14}C-phenanthrene; 55 mCi mmol^{-1}, ARC0867) were diluted 1 in 10 with ddH$_2$O. Two μL of this diluted ^{14}C-phenanthrene was then added into 1 mL of either 20 nm or 500 nm PS-NPLs suspensions at concentrations of 100 mg L^{-1} to make a solution of ^{14}C-phenanthrene at a final concentration of 648 μg L^{-1}. We used a high concentration of ^{14}C-phenanthrene to ensure complete saturation of sorption. In addition, to match the total theoretical surface area (Table S4-1) of 20 nm PS-NPLs suspensions at a concentration of 100 mg L^{-1}, 2 μl ^{14}C-phenanthrene was added into 1 mL diluted 500 nm PS-NPLs suspension at a concentration of 1780 mg L^{-1}. All experiments were performed in glass vials and achieved a final concentration of 0.1 mCi mL^{-1} ^{14}C-phenanthrene (initial solution, n=3 for each treatment). Two

μL of diluted ^{14}C-phenanthrene in 1mL ddH$_2$O was used as control and PS-NPLs suspensions without ^{14}C-phenanthrene were used as a negative control. The mixtures were then incubated at room temperature in the dark for 10, 30, 60 and 120 min. After incubation, mixtures were transferred into 10 kDa molecular weight cut-off Amicon filter vials (Millipore Sigma, Catalog#UFC201024) and centrifuged in swinging bucket rotor at 3200 g for 10 min where the organic-coated plastics remained on the top surface of the filter, ^{14}C-phenanthrene that was either unbound or loosely bound was then washed off by adding 1 mL of ddH$_2$O to the vials, incubating for 5 min and then centrifugation at 3200 g for 10 min. This procedure was repeated two more times until no phenanthrene was detected in the filtrate. The organic-coated plastics were then recovered from the top surface of the vial by adding 1 mL ddH$_2$O, resuspending gently by pipetting up and down and then the vials were inverted and then centrifuged 3200 g for 10 min to recover PS-NPLs with^{14}C-phenanthrene sorbed onto their surface. To determine how much phenanthrene was bound to the plastics, the recovered PS-NPLs were transferred into scintillation vials, 5 mL Ultima Gold AB (PerkinElmer, Catalog#6013309) added and incubated in the dark for 2 h. Counts per minute (cpm) were measured using a HITACHI AccuFLEX LSC-8000 beta counter. The percentage of ^{14}C-phenanthrene sorption was calculated from the cpm and specific activity (SA) according to the following equation:

$$\text{Percent } ^{14}\text{C-phenanthrene sorption (\%)} = \frac{\frac{\text{cpm of recovered solution}}{\text{SA}} \div \frac{\text{cpm of initial solution}}{\text{SA}}}{} \times 100\% =$$

$$\frac{\text{cpm of recovered solution}}{\text{cpm of initial solution}} \times 100\%$$

4.2.4 Zebrafish embryo uptake

The first half of this experiment was to determine if the presence of 20 or 500 nm PS-NPLs can facilitate ^{14}C-phenanthrene passing through the chorion. The stock ^{14}C-phenanthrene was diluted 1 in 100 with ddH$_2$O. Two µL of this diluted ^{14}C-phenanthrene (initial exposing medium) was added into 1 mL either diluted 20 nm or 500 nm PS-NPLs suspensions at a concentration of 10 mg L^{-1} to make a solution of ^{14}C-phenanthrene at a final concentration of 64.8 µg L^{-1}. Ten zebrafish embryos (at 24 hours post fertilization, hpf) were randomly selected and added to each well of 24-well plate with 2 mL of reverse osmosis (RO) water with 1% weight/volume seawater salt mix added back to give the ions, ^{14}C-phenanthrene, 20 nm PS-NPLs, 500 nm PS-NPLs, 20 nm PS-NPLs with ^{14}C-phenanthrene or 500 nm PS-NPLs with ^{14}C-phenanthrene (n=4 for each treatment) and incubated in the dark for 0.5, 1, 2 and 4 h. After incubation, the exposure medium was removed, and then embryos were washed thrice with non-radioactive phenanthrene prepared in methanol at the concentration of 10 mg L^{-1} and RO H$_2$O once. The high concentration of non-radioactive phenanthrene was used to wash off loosely bound or unbound ^{14}C-phenanthrene on the surface of chorions. Embryos were digested in 1 mL HNO$_3$ (1 M) in scintillation vials at 65 °C for 24 h. After the digestion, 5 mL Ultima gold was added into each vial and then incubated for 2 h before measuring cpm.

To confirm if the presence of 20 or 500 nm PS-NPLs can facilitate the uptake of ^{14}C-phenanthrene into embryos, embryos exposed to the same exposure scheme mentioned above for 1, 4, 8 and 24 h. After incubation, the exposure medium was removed, and then embryos were washed thrice with non-radioactive phenanthrene prepared in methanol at the concentration of 10 mg L^{-1} and RO H$_2$O once. Once the chorion was removed under dissection microscopy, the larvae were washed thrice with non-radioactive phenanthrene at the concentration of 10 mg L^{-1} and RO H$_2$O once. Larvae were digested in 1 mL HNO$_3$ (1 M) in scintillation vials at 65 °C for

24 h. After the digestion, 5 mL Ultima gold was added into each vial and incubated for 2 h before measuring cpm.

To calculate the uptake rate of phenanthrene, the wet weight of 10 zebrafish embryos or 10 dechorionated embryos at 4 hpf and 24 hpf were determined by patting dry on Kimwipes and then weighed using a Cahn C-35 Ultra-Microbalance (Thermo Electron Corporation, Model# BLN-09-5990). The average weight was used in each calculation.

The percentage of ^{14}C-phenanthrene cross chorion and uptake was calculated from cpm, SA and wet weight of 10 zebrafish embryos (W) as defined by the following equation:

$$\text{Percent } ^{14}\text{C-phenanthrene passing through chorion (\%)} = \frac{\text{cpm of recovered embryos}}{\text{SAxW}} \div$$

$$\frac{\text{cpm of initial exposing medium}}{\text{SAxW}} \times 100\% = \frac{\text{cpm of recovered embryos}}{\text{cpm of initial exposing medium}} \times 100\%$$

The percentage of ^{14}C-phenanthrene uptake was calculated from the cpm, SA, and W as defined by the following equation:

$$\text{Percent } ^{14}\text{C-phenanthrene sorption (\%)} = \frac{\text{cpm of recovered dechorionated embryos}}{\text{SAxW}} \div$$

$$\frac{\text{cpm of initial exposing medium}}{\text{SAxW}} \times 100\% = \frac{\text{cpm of recovered dechorionated embryos}}{\text{cpm of initial exposing medium}} \times 100\%$$

The rate of phenanthrene passing through chorion and uptake by larvae ($\mu g\ kg^{-1}\ h^{-1}$) were calculated as follows:

$$\text{The rate of phenanthrene crossing chorion or uptake per embryo} = \frac{\text{cpm of tissue}}{\text{SAxWx}\Delta\text{T0}}$$

4.2.5 Imaging of PS-NPLs accumulation

Ten zebrafish embryos at 24 hpf were randomly placed into 50 mL glass beakers with 10 mL of either RO water, 10 mg L^{-1} 20 nm PS-NPLs or 10 mg L^{-1} 500 nm PS-NPLs and incubated in an incubator (Exo Terra PT2499; 28±0.1°C) under laboratory light (14 h light:10 h dark) for 24 h. After the incubation period, embryos from each beaker were anesthetized with 10 mg L^{-1} tricaine methanesulfonate (TMS) for 15 min, rinsed thrice with phosphate-buffered saline (PBS). Five embryos from each beaker were transferred into a 12-well plate and fixed with 1 mL 4% paraformaldehyde at 4 °C for 12 h. The chorions of the other five embryos were removed under a dissection microscope and then the larvae were rinsed thrice with PBS, transferred into a 12-well plate and fixed with 1 mL 4% paraformaldehyde at 4 °C for 12 h. After fixation, all embryos/ larvae were washed with PBS for 8 h and PBS was renewed every 30 min at first 2 h. Images were captured by using a fluorescence microscope (Leica Microsystems, Germany, Model#DM2500).

4.2.6 Lethal effects of PS-NPLs exposure to zebrafish

A 96h acute toxicity test was modified based on a previous study.[210] Viable embryos at 24 hpf were rinsed thrice with RO water and then randomly distributed into 50 mL glass beakers and four beakers were used for each concentration. Embryos were exposed to various nominal concentrations of 3.125, 6.25, 12.5, 25 or 50 mg L^{-1} non-dialyzed 20 nm PS-NPLs, or 6.25, 12.5, 25, 50, 100 or 125 mg L^{-1} dialyzed 20 nm PS-NPLs for 96 h. Embryos were exposed to various nominal concentrations of 0.08125, 0.1625, 0.325, 0.65 and 1.3 mg L^{-1} NaN$_3$ to match the concentrations in non-dialyzed 20 PS-NPLs (100 mg L^{-1} contains 1.3 mg L^{-1} NaN$_3$) to determine

if the toxicity of non-dialyzed PS-NPLs is associated with plastics alone or NaN_3 alone or both. After adding the NPLs, embryos were placed in the incubator and to compensate for the water loss due to evaporation, 0.1 mL RO water was added into each beaker every day. All exposing mediums were renewed after 48 h exposure (at 72 hpf) during the experiment period. Survival and hatching of zebrafish were recorded every 12 h under a dissecting microscope. Zebrafish were considered dead if they lacked movement, heartbeat or transparency and removed from beakers [167]. Embryos in RO water were used as a control group. Four control groups were carried out alongside each exposure and exposure with ≥ a 90% survival rate in the control groups were analyzed. The median lethal concentration (LC_{50}) values were calculated at 120 hpf.

4.2.7 Lethal effects of co-exposure of PS-NPLs and phenanthrene to zebrafish

Similar to section 4.2.6, viable embryos at 24 hpf were rinsed thrice with RO water and then randomly distributed into 50 mL glass beakers and four beakers were used for each concentration. Embryos were exposed to various nominal concentrations of phenanthrene at the presence (10 mg L^{-1}) or absence of either 20 nm or 500 nm PS-NPLs for 96 h. RO water was used as the control group and 0.1% dimethyl sulfoxide (DMSO) was used as vehicle control.

4.2.8 Zebrafish larvae Ethoxyresorufin-O-deethylase (EROD) assay

Fifteen embryos at 24 hpf were randomly distributed into 50 mL glass beaker (four beakers for each group) with 10 mL of either RO water (control group), 0.1% DMSO (vehicle control), 10 mg L^{-1} 20 nm PS-NPLs with or without 64.8 µg L^{-1} phenanthrene, or 10 mg L^{-1} 500

nm PS-NPLs with 0.1% DMSO with or without 64.8 μg L^{-1} phenanthrene. Embryos were placed in an incubator for 96 h. Dead embryos were removed every 12 h and the exposure medium was renewed at 72 hpf during this period. The EROD assay was modified based on a previous study. [211] At the end of 96 h exposure, 10 hatched larvae from each beaker were gently rinsed with RO water thrice and placed into a 24-well plate containing 2 mL of 7-ethoxyresorufin (7-ER) at a final concentration of 2.5 μmol L^{-1} in each well for 6 h. After 7-ER treatment, 250 μL of 7-ER treatment solution (four replicates) was transferred into each well of the 96-well black wall plate for EROD measurement using a VICTOR3V 1420 Multilabel Counter (PerkinElmer, MS, USA) at 535 nm (excitation) /585 nm (emission). A standard curve of Resorufin was also prepared by measuring the EROD fluorescence of Resorufin at various concentrations of 1000 pM, 500 pM, 250 pM, 125 pM, 62.5 pM, 31.3 pM, 15.6 pM, and control (RO water). The results of EROD activity in zebrafish larvae were expressed as fold change relative to the control group. Malformation including pericardial edema, yolk sac edema, and spinal curvature was recorded at 120 hpf following the sub-lethal exposure before EROD assay.

4.2.9 Statistical analysis

GraphPad Prism (Version. 6.0, GraphPad Software Inc.) was used for statistical analysis and creating graphs. The normality and homoscedasticity were evaluated by Shapiro-Wilk and Breusch-Pagan (α=0.05) tests, respectively. Two-way analysis of variance (ANOVA, α=0.05) followed by Tukey's multiple comparison tests (α=0.05) was used to compare the percentage sorption of phenanthrene onto the surface of different nanoplastics, the co-contaminant uptake of phenanthrene and nanoplastics at two different sizes by zebrafish embryos, and EROD activity in

zebrafish larvae exposed to a different medium. Two-way repeated-measures ANOVA ($\alpha=0.05$) was used to compare the hydrodynamic diameters (HD), polydispersity index and zeta-potentials of PS-NPLs before and after dialysis. Probit analysis was used to calculate the LC_{50} value and 95% confidence interval. All data are presented as mean ± standard error of the mean (SEM).

4.3 Results

4.3.1 Characterizations of PS-NPLs

The HD of non-dialyzed 20 nm PS-NPLs was 35.5 nm which was not significantly different from dialyzed PS-NPLs (37.7 nm) at 0 h. The HD of non-dialyzed 500 nm PS-NPLs was 527.2 nm which was not significantly different from dialyzed PS-NPLs (522.6 nm). This indicated that the aggregation of PS-NPLs in the stock suspensions was negligible, although the sizes were slightly larger than advertised by the manufacturer. The difference in HD of non-dialyzed and dialyzed 20 nm and 500 nm PS-NPLs was also negligible at 96 h and very close to the sizes at 0 h (Table S4-2).

4.3.2 Sorption of phenanthrene onto nanoplastics

The amount of ^{14}C-phenanthrene that is bound to the surface of the filtration apparatus (background binding) is represented by the black dot (Figure 4-1). This value was < 1% and unchanging with the time of sorption. When 20 nm PS-NPLs were added to the ^{14}C-phenanthrene containing solution, there was an increase in the sorption onto the surface over the first 30 minutes to approximately 13% followed by slight desorption to about 9% of the total

phenanthrene bound (red squares, Figure 4-1). If we examine the sorption only based on the gravimetric weight being equal, it appears that the larger 500 nm PS-NPLs have a lower binding capacity (~ 7-3%; gray circles). However, when corrected for surface area, the sorption of ^{14}C-phenanthrene was essentially identical to the 20 nm PS-NPLs with 13-10% bound (black triangles; Figure 4-1).

4.3.3 Zebrafish embryo uptake

The percent of ^{14}C-phenanthrene passed through chorion and accumulated inside zebrafish chorion was significantly higher in the presence of 20 nm PS-NPLs than either with ^{14}C- phenanthrene alone (p<0.001) or in the presence of the larger 500 nm PS-NPLs (p<0.001). This was consistent after each of the 1, 2, and 4 hour incubation periods and continued to increase over time with the 4 h period having a significantly greater accumulation compared to earlier time points (Figure 4-2A). The ^{14}C-phenanthrene accumulation in both ^{14}C-phenanthrene alone and 500 nm PS-NPLs groups were very close at any given incubation period tested. The percent of ^{14}C-phenanthrene uptake into zebrafish larvae themselves (chorion removed) did not show any significant difference between ^{14}C-phenanthrene alone and in the presence of PS-NPLs after 1, 4 and 8 h incubation period (Figure 4-2B). However, the accumulation of ^{14}C-phenanthrene in zebrafish larvae was only significantly higher after 24 h incubation in the presence of 20 nm PS-NPLs when compared to either the ^{14}C-phenanthrene alone (p=0.0175) or the 500 nm PS-NPLs (p=0.006, Figure 4-2B).

When the rate of ^{14}C-phenanthrene uptake either across the chorion (Figure 4-2C) or into the embryo itself (Figure 4-2D) was calculated, the presence of 20 nm PS-NPLs significantly

increased the rate of phenanthrene crossing through the chorion compared to 500 nm PS-NPLs (p<0.001) and phenanthrene alone (p<0.001, Figure 4-2C). The presence of 20 nm PS-NPLs significantly increased the uptake rate of phenanthrene by embryos compared to 500 nm PS-NPLs (p=0.008) and phenanthrene alone (p=0.015, Figure 4-2D).

The fluorescence images of the zebrafish embryos exposed to dialyzed 20 nm or 500 nm PS-NPLs to determine if the embryos can uptake the PS-NPLs (Figure 4-3). The images showed the dechorionated embryos exposed to 20 nm PS-NPLs at a nominal concentration of 10 mg L^{-1} had greater fluorescence intensity accumulating in the yolk sac, which means higher uptake of 20 nm PS-NPLs compared to 500 nm PS-NPLs.

4.3.4 Lethal effects (LC$_{50}$) of PS-NPLs

The 96h-LC$_{50}$ values in Table 4-1 were calculated based on the Probit Analysis. The 96h-LC$_{50}$ value of NaN$_3$ on zebrafish embryos was estimated to be 0.53 mg L^{-1}. The 96h-LC$_{50}$ value of non-dialyzed 20 nm PS-NPLs was 21.5 mg L^{-1} while the dialyzed PS-NPLs was 52.2 mg L^{-1}. The 500 nm PS-NPLs had a significantly higher LC$_{50}$ value compared to 20 nm PS-NPLs (Figure 4-4A). The 96h-LC$_{50}$ value of non-dialyzed 500 nm PS-NPLs was 78.3 mg L^{-1} while the dialyzed PS-NPLs cannot be calculated (> 100 mg L^{-1}).

4.3.5 Lethal effects of co-exposure of PS-NPLs and phenanthrene

The 96h-LC$_{50}$ values in Table 4-2 were calculated based on the Probit Analysis. The 96h-LC$_{50}$ value of phenanthrene alone was estimated to be 0.802 mg L^{-1}. The 96h-LC$_{50}$ value of

phenanthrene in the presence of 10 mg L^{-1} 20 nm PS-NPLs was 0.748 mg L^{-1} while the value in

the presence of 10 mg L^{-1} 500 nm PS-NPLs was 0.812 mg L^{-1}. These three LC$_{50}$ values were not

significantly different from each other (Figure 4-4B).

4.3.6 Sub-lethal effects

The presence of 20 nm PS-NPLs resulted in a delay in hatching in zebrafish embryos but

did not affect the final hatching success rate at 120 hpf (Figure 4-4C, D & E and Figure S4-3).

The hatching rate of zebrafish embryos exposed to 10 mg L^{-1} 20 nm PS-NPLs with an additional

0.156 mg L^{-1} phenanthrene was slightly reduced at 72 hpf (Figure S4-3A). Further decreases in

the hatching rate were observed when embryos exposed to phenanthrene at a nominal

concentration of either 0.313 or 0.625 mg L^{-1} in the presence of 10 mg L^{-1} 20 nm PS-NPLs at

each of 72, 84 and 96 hpf. No delay in hatching was observed in the 500 nm PS-NPLs or the

absence of PS-NPLs (Figure S4-3B&C). However, the hatching rate of zebrafish embryos

exposed to either 1.25 or 2.5 mg L^{-1} phenanthrene in the presence of 10 mg L-1 20 nm PS-NPLs

was slightly decreased at both 72 and 84 hpf (Figure S4-3D&E).

Neither control DMSO treatment, nor 20 nm or 500 nm PS-NPLs exposure at a nominal

concentration of 10 mg L^{-1} altered EROD activity in zebrafish (Figure 4-5). Phenanthrene at a

nominal concentration of 64.8 µg L^{-1}, did not significantly increase EROD activity after 96 h

exposure (p= 0.261, Figure 4-5). EROD activity was also not significantly increased by the co-

exposure of phenanthrene and 500 nm PS-NPLs (p=0.155) while co-exposure of phenanthrene

and 10 mg L^{-1} 20 nm PS-NPLs did result in an induction of EROD activity compared to both the

control group (p<0.001), and the co-exposure of phenanthrene with 500 nm PS-NPLs (p=0.0342, Figure 4-5).

4.4 Discussion

This study demonstrated the sorption of the model hydrophobic organic phenanthrene onto the surface of nano-sized PS-NPLs was greater compared to sub-micron sized materials. Moreover, the sorption of organics onto nano-sized plastics resulted in increased rates of transport across the chorion and potentiation of uptake into zebrafish larvae. Finally, we also demonstrated that smaller nano-sized plastics can also mediate the other sub-lethal effects including delays in hatching and potentiation of sub-lethal responses such as EROD induction.

4.4.1 Sorption of phenanthrene onto nanoplastics

It is well-known that organic pollutants adhere and concentrate on the surface of plastics.[197, 205, 212] The sorption of 10 different PAHs onto the surface of 70 nm polystyrene plastics was found to be non-linear in the aqueous phase where the sorption of PAHs plateaued at maximum binding capacity.[213] Our study demonstrated that while smaller particles (20 nm PS-NPLs) appear to have significantly higher sorption capacity for phenanthrene compared to 500 nm PS-NPLs at the same plastic concentration when we matched the exposed surface area rather than gravimetric mass, the sorption capacity of phenanthrene was not significantly different between 20 nm and 500 nm PS-NPLs. Moreover, when we calculated the sorption of phenanthrene per unit theoretical surface area between 20 nm and 500 nm PS-NPLs at the same concentration, the sorption capacity of phenanthrene per surface area in 500 nm PS-NPLs was

~5-10 times higher when compared to 20 nm PS-NPLs. However, a study has shown that the measured SSA of 50 nm PS-NPLs (63.4 m^2 g^{-1}) is much lower than the theoretical SSA (114.3 m^2 g^{-1}) while the measured SSA of larger 235 nm PS-NPLs (24.6 m^2 g^{-1}) is very close to their theoretical SSA (24.3 m^2 g^{-1}).[193] Furthermore, the distribution coefficient (K_d) decreased as particle size decreased from sub-micron to nanoscale due to less surface area can be accessed by larger phenanthrene molecules making the effective surface area even smaller than the measured SSA, especially in nanoplastics.[193] Therefore, in our study, the sorption capacity of phenanthrene per unit surface area in 500 nm PS-NPLs may be slightly higher (less than 2- 4 times) when compared to 20 nm PS-NPLs. Both particle size and the effective surface area may play a significant role in the sorption capacity of small plastics. Given that there is an increase in total surface area per gravimetric mass as particle diameter decreases,[214] with weathering of plastics and microplastics into nanoplastics, the increase in total surface area and decrease in particle size may result in exacerbation of total organic adsorption to NPLs.

4.4.2 Zebrafish embryo uptake

To this day, no studies have directly demonstrated the potentiation of hydrophobic organic pollutants transport across the chorion or the potentiation of dermal uptake by nanoplastics. A previously published paper has shown that the presence of 50 nm NPLs in the water increased the total accumulation of ^{14}C-phenanthrene in the entire *D. magna* after 2, 7 or 14 days when compared to when 10 µm microplastics were present. However, this study could not determine whether either (or both) of the nanoplastics or phenanthrene were directly taken up into *D. magna* tissues or if it remained in the gut tissues. Moreover, there was no direct

assessment of whether the rate of uptake or either phenanthrene or nanoplastics into the animal was occurring[205] The current study is the first to demonstrate that the presence of nano-sized plastics can directly facilitate the transport and uptake of hydrophobic organic pollutants. The rate of phenanthrene crossing chorion over 4h in the presence of dialyzed 20 nm PS-NPLs was approximately 5x higher when compared to either the 500 nm PS-NPLs and phenanthrene alone groups. The reasons for the increased transport likely include both the higher sorption capacity (per gravimetric mass) of phenanthrene onto the smaller 20 nm PS-NPLs surfaces and the fact that 20 nm PS-NPLs are smaller than the size of pores present on the chorion, thereby allowing the 20 nm PS-NPLs to pass through the chorion and have direct contact with the embryo.[165, 209] However, while the transport of 20 nm PS-NPLs was faster across the chorion, the relative uptake rate across the dermal surface of the embryo/larvae was much slower by comparison, although still greater in the 20 nm PS-NPLs compared to the 500 nm PS-NPLs.

Fluorescence microscopy of the chorionated and dechorionated embryos confirmed greater numbers of dialyzed 20 nm PS-NPLs pass through chorionic pores were not only on the surface of the embryo but also accumulated in the yolk sac of the embryos. Few, if any, 500 nm PS-MPs passed through the chorionic membrane and adhered to the surface of the embryo. The gills of zebrafish embryos only begin to develop at 2 days post fertilization (dpf) so the uptake of PS-NPLs between 24 and 48 hpf occurs transdermally.[215] Our results indicate that nano-sized PS-NPLs potentiate hydrophobic organic transfer from the water phase, through the chorion of fish embryos and can potentiate uptake across epithelia.

4.4.3 Lethal effects (LC$_{50}$) of PS-NPLs

While previous studies have demonstrated the lethality of nanoplastics on invertebrate aquatic organisms,[198, 200, 216] there is a potentially significant issue with the use of commercial preparations and the addition of potentially toxic additives such as NaN_3.[198] The NPLs used in this study were supplied in a stock solution containing 2 mM NaN_3 which means a dilution of 200 mg L^{-1} non-dialyzed PS-NPLs would have ~1.3 mg L^{-1} NaN_3. We found that the 96h-LC_{50} value of non-dialyzed 20 nm PS-NPLs was 21.5 mg L^{-1} (containing 0.14 mg L^{-1} NaN_3) while the value of dialyzed NaN_3-free PS-NPLs was 52.2 mg L^{-1}. This indicated that the toxicity on zebrafish embryos was from the combination of 20 nm PS-NPLs and NaN_3. Our 96h-LC_{50} value of non-dialyzed 500 nm PS-NPLs was 78.3 mg L^{-1} (nominal concentration of NaN_3 was estimated to be ~0.51 mg L^{-1}) which was similar to the zebrafish embryo 96h-LC_{50} value of NaN_3 alone (0.53 mg L^{-1} NaN_3). However, dialyzed 500 nm PS-NPLs showed negligible toxicity on zebrafish even at the highest concentrations. This demonstrates that removal of stabilizers and other chemicals in the stock plastics suspensions is essential and also clearly demonstrates that only nano-sized polystyrene plastics and not sub-micro-sized have significant toxicity to zebrafish embryos.

4.4.4 Lethal effects and sub-lethal effects of co-exposure of PS-NPLs and phenanthrene

This study also demonstrates that the presence of nanoplastics does not itself alter the LC_{50} value of phenanthrene. While the 96h-LC_{50} value of phenanthrene in the presence of 20 nm PS-NPLs was slightly lower, but it was not statistically significant when compared to both phenanthrene alone or phenanthrene in the presence of 10 mg L^{-1} 500 nm PS-NPLs. Approximately 0.04 mg more phenanthrene accumulated in the embryos in the presence of 20

nm PS-NPLs over 96 h exposure when compared to the control group and 500 nm PS-NPLs based on our uptake results. The 0.04 mg increase of phenanthrene accumulation is much smaller compared to the 96-LC_{50} value of phenanthrene (0.802 mg L^{-1}) and the differences cannot be detected. However, perhaps chronic exposure in the presence of 20 nm PS-NPLs will cause a much higher accumulation of phenanthrene and may lead to a significant increase in toxicity (i.e. decreased LC_{50} value). Our study findings suggested that the presence of nanoplastics does not alter the acute lethal effects of organic pollutants but studies have shown nano-plastics potentiating sub-lethal markers of organic pollutants toxicity.[4, 205] For example, the 48h-EC_{50} of phenanthrene, using immobilization of *D. magna* as an endpoint, was significantly decreased in the presence of 50 nm NPLs.[205] However, the calculation of EC_{50} in the presence of 50 nm NPLs was performed on non-dialyzed materials which likely overestimates the NPLs' toxicity since stabilizers were not removed prior to analysis. Similarly, EROD is widely used as a biomarker for evaluating exposure to PAHs through activation of cytochrome P450 1A enzyme activity.[211, 217] Our findings of significantly increased EROD activity in phenanthrene with 20 nm PS-NPLs exposed zebrafish embryos compared to either phenanthrene alone or with 500 nm PS-NPLs support facilitation of organic uptake by nano-sized polystyrene plastics.

In our study, phenanthrene in the absence of NPLs resulted in a delay in hatching, with increased delays noted at phenanthrene concentration increased. This delay was exacerbated in the presence of 20 nm PS-NPsL with greater delays seen at the 72, 84 and 96 hpf when embryos exposed to 0.313 and 0.625 mg L^{-1} of phenanthrene. The delays in the presence of 500 nm PS-NPLs were not significantly different from phenanthrene alone. Delays in hatching have been noted as significant effects of smaller sized NPLs through interaction and inhibition of hatching

enzymes[218] which likely explains the exacerbation of hatching delay, however, a mechanism for phenanthrene-induced hatching delay is unknown.

4.5 Conclusion

This is the first comprehensive study to simultaneously evaluate the sorption of hydrophobic organic pollutants onto the surface of nanoplastics, the effects of particle size on the sorption of associated organics, and the potential impact on toxicity to organisms. We clearly demonstrate that the presence of 20 nm PS-NPLs can facilitate the transport and uptake of phenanthrene when compared to both the absence of plastics or with larger sub-micron sized PS-NPLs. Given the near-ubiquity of larger plastics and microplastics in our oceans and freshwater environments, and the further weathering of these into nano-sized particles plastics,[3, 191, 196, 200] we predict that the effects of nano-sized plastics in potentiation organic-mediated toxicity will be of significant concern.
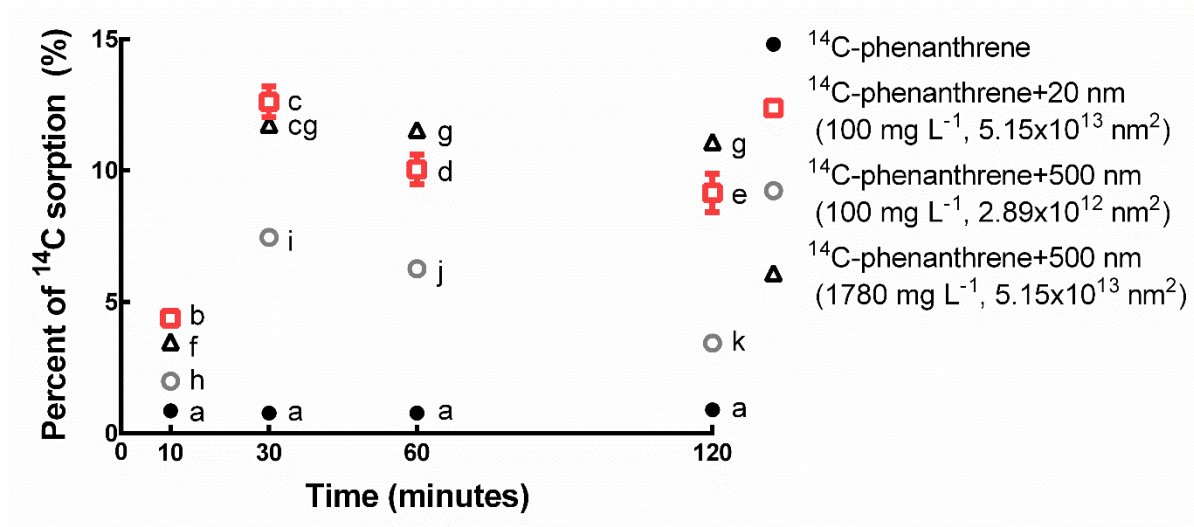
Figure 4-1. Percentage of initial ^{14}C-phenanthrene detected in the recovered medium above the membrane after incubation for various periods in control (^{14}C-phenanthrene alone no PS-NPLs), or in the presence of 100 mg L^{-1} of either 20 nm PS-NPLs (surface area 5.15x10^3 nm^2), 500 nm PS-NPLs (surface are of 2.89x10^{12} nm^2), or 1780 mg L^{-1} of 500 nm PS-NPLs (surface area 5.15x10^{13} nm^2). Means sharing the same letter are not significantly different from each other (p>0.05). Values are mean ± SEM. n=3.
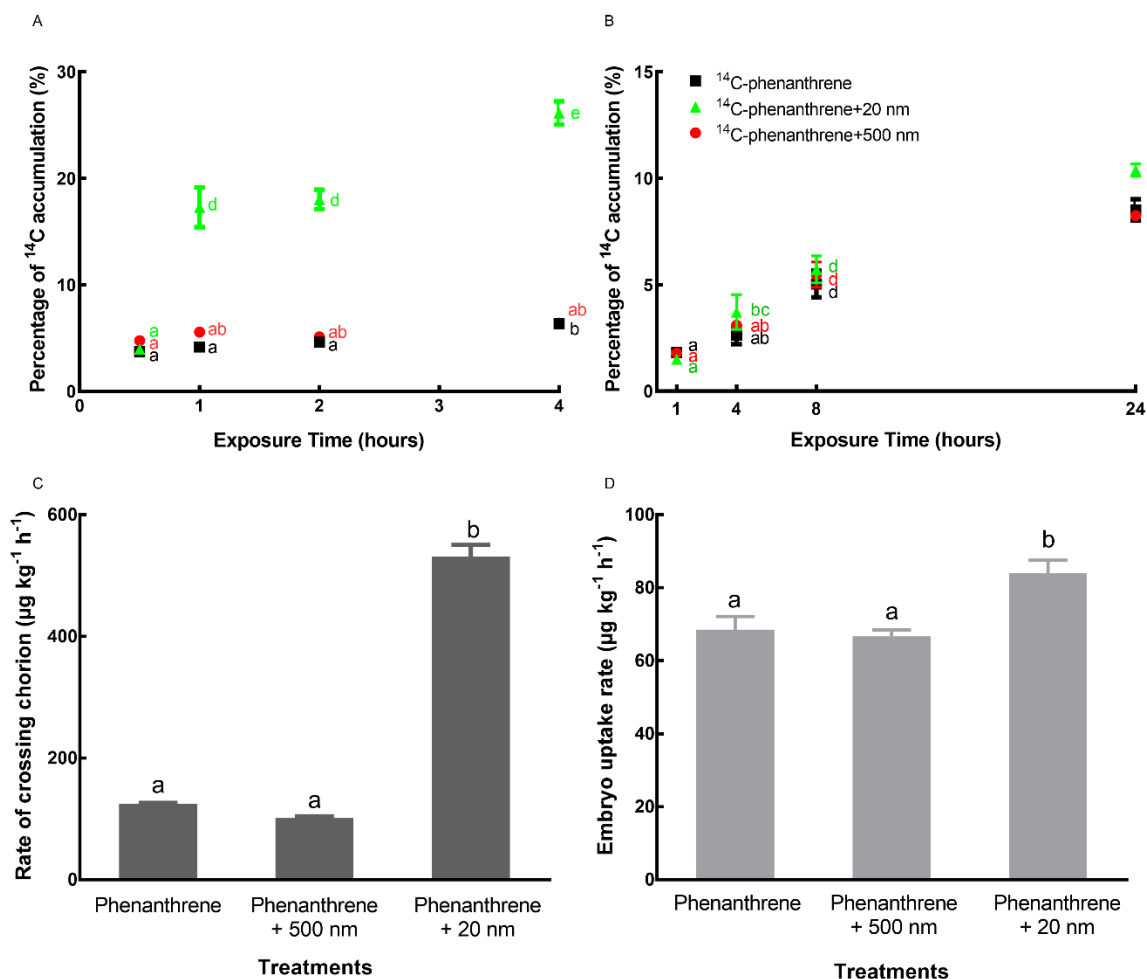
Figure 4-2. Percentage of initial ^{14}C-phenanthrene that either passed through chorionic membrane of zebrafish embryos (A), or accumulated in zebrafish larvae (B) after the incubation for various periods in control (^{14}C-phenanthrene alone no PS-NPLs), in the presence of 20 nm PS-NPLs at 10 mg L^{-1}, or 500 nm PS-NPLs at 10 mg L^{-1}. The rate (μg kg^{-1} h^{-1}) of ^{14}C-phenanthrene crossing zebrafish embryo chorion over 4h (C) and uptake by larvae over 24h (D) with or without 20 nm or 500 nm PS-NPLs. Means sharing the same letter are not significantly different from each other ($p > 0.05$). Values are mean $\pm$ SEM. n=4.
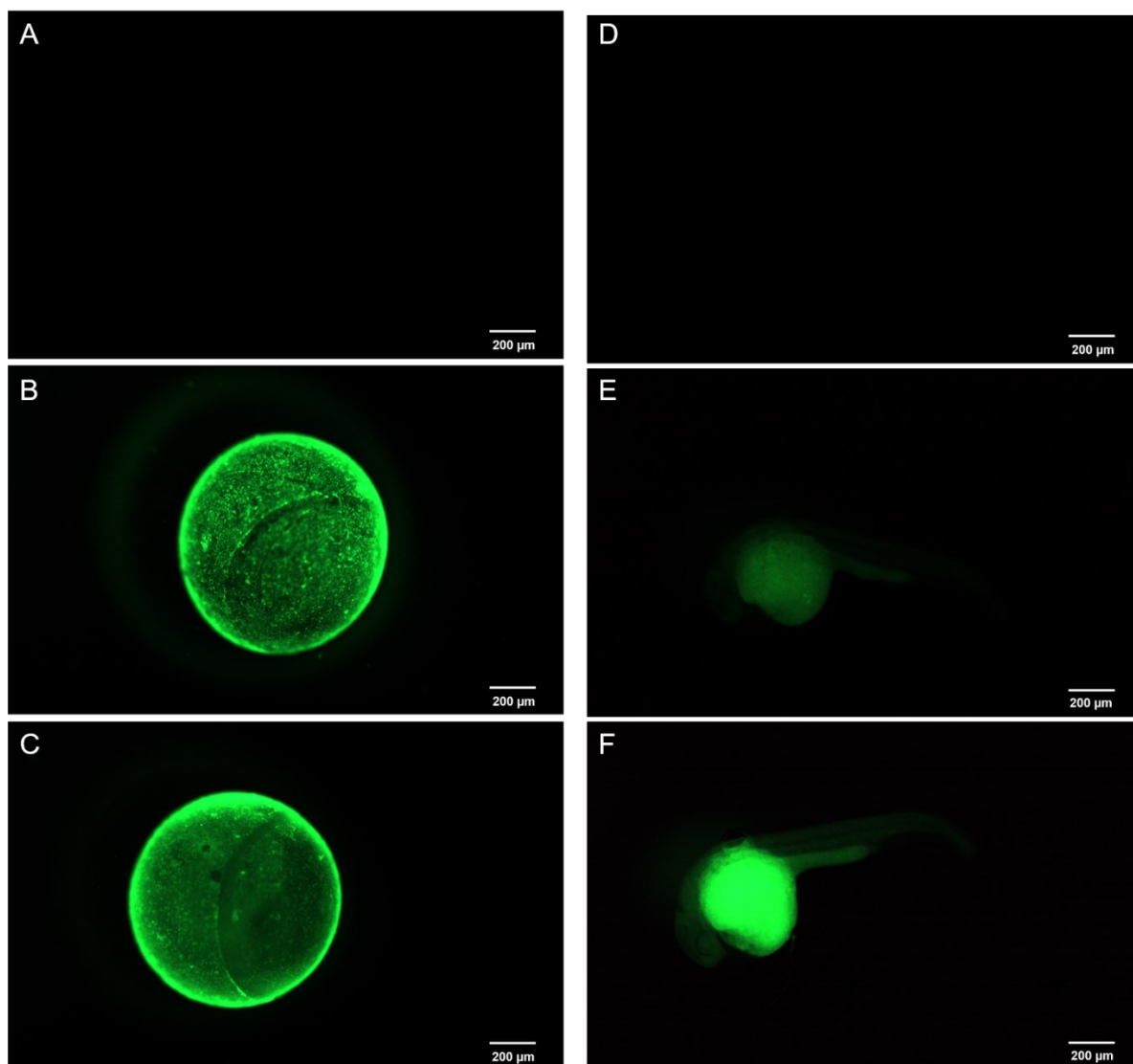
Figure 4-3. Fluorescence images of zebrafish embryos (A, B & C) and dechorionated embryos (D, E & F) at 48 hpf after 24-h exposure to RO water (A & D), dialyzed 500 nm PS-NPLs at 10 mg L^{-1} (B & E) and dialyzed 20 nm PS-NPLs at 10 mg L^{-1} (C & F).
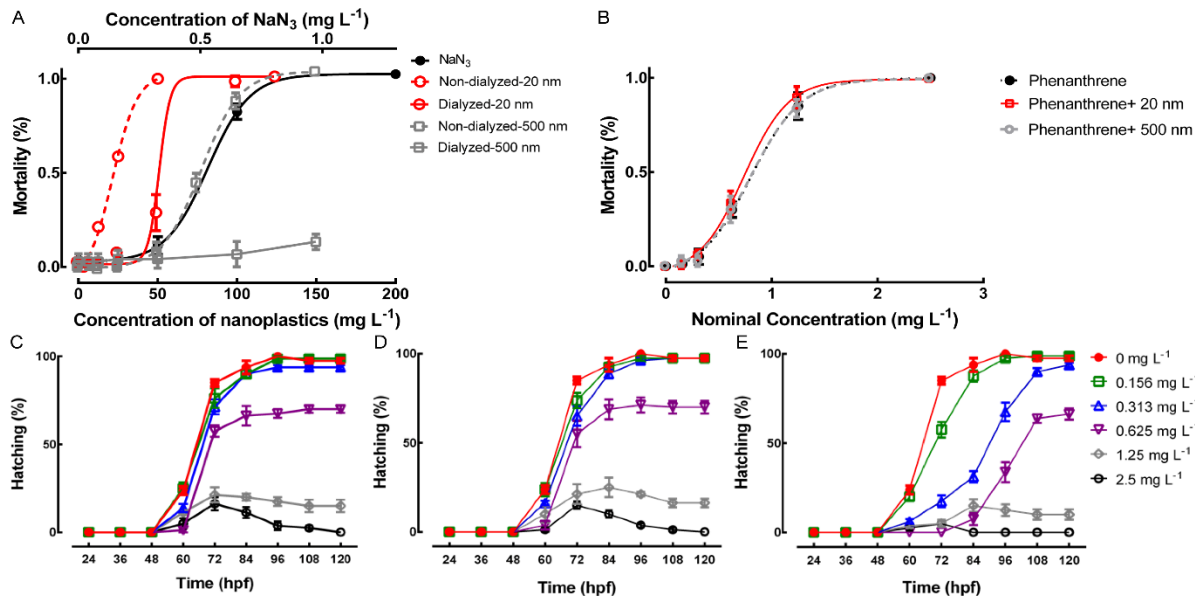
Figure 4-4. Mortality of NaN$_3$ (solid black line), dialyzed 20 nm PS-NPLs (solid red line), non-dialyzed 20 nm PS-NPLs (dashed red line), dialyzed 500 nm PS-NPLs (solid grey line) and non-dialyzed 500 nm PS-NPLs (dashed grey line) (A), and phenanthrene (black dot line), phenanthrene with 10 mg L^{-1} 20 nm PS-NPLs (red solid line) and phenanthrene with 10 mg L^{-1} 500 nm PS-NPLs (grey dashed line) (B) at various nominal concentrations on zebrafish embryos/larvae from 24 hpf to 120 hpf. Hatching success of zebrafish embryos exposed to phenanthrene (C), phenanthrene with 10 mg L^{-1} 500 nm PS-NPLs (D) and phenanthrene with 10 mg L^{-1} PS-NPLs (E) at various nominal concentrations from 24 hpf to 120 hpf. Values are mean ± SEM. n=4.
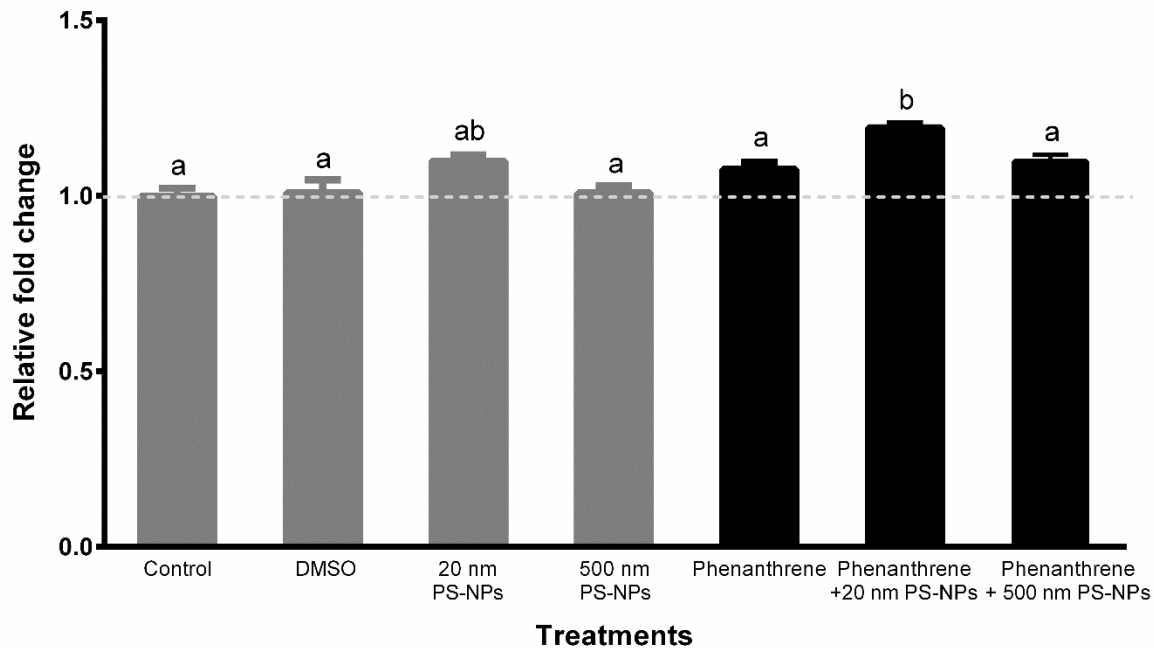
Figure 4-5. Relative fold change in EROD activity induced by exposure to RO water (control group), 0.1% DMSO, 10 mg L^{-1} 20 nm PS-NPLs, 10 mg L^{-1} 500 nm PS-NPLs with 64.8 μg L^{-1} phenanthrene, 64.8 μg L^{-1} phenanthrene, 10 mg L^{-1} 20 nm PS-NPLs with 64.8 μg L^{-1} phenanthrene and 10 mg L^{-1} 500 nm PS-NPLs with 64.8 μg L^{-1} phenanthrene relative to control group in zebrafish larvae at 120 hpf after 96-hour exposure from 24 hpf. Means sharing the same letter are not significantly different from each other (p>0.05). Values are mean ± SEM. n=5.

Table 4-1. Probit analysis of LC_{50} values of NaN_3, non-dialyzed and dialyzed PS-NPLs at 20 nm and 500 nm at the nominal concentration on zebrafish embryos/larvae from 24 hpf to 120 hpf. Values are mean. Ranges are 95% confidence interval (95% CI).

	LC_{50} (95% CI)
NaN_3	0.53 mg L^{-1} (0.51-0.55)
Non-dialyzed 20 nm PS-NPLs	21.5 mg L^{-1} (20.0-22.9)
Dialyzed 20 nm PS-NPLs	52.2 mg L^{-1} (46.4-55.1)
Non-dialyzed 500 nm PS-NPLs	78.3 mg L^{-1} (76.5-80.2)
Dialyzed 500 nm PS-NPLs	>100 mg L^{-1}

Table 4-2. Probit analysis of LC_{50} values of phenanthrene, phenanthrene with 10 mg L^{-1} 20 nm PS-NPLs and phenanthrene with 10 mg L^{-1} 500 nm PS-NPLs at nominal concentrations on zebrafish embryos/larvae from 24 hpf to 120 hpf.

	LC_{50} (95% CI)
Phenanthrene	0.802 mg L^{-1} (0.747-0.857)
Phenanthrene + 20 nm PS-NPLs	0.748 mg L^{-1} (0.703-0.794)
Phenanthrene + 500 nm PS-NPLs	0.812 mg L^{-1} (0.750-0.874)

Chapter 5

The "Trojan Horse" Effect of Nanoplastics: Potentiation of Polycyclic Aromatic Hydrocarbon Uptake in Rainbow trout and the Mitigating Effects of Natural Organic Matter

5.1 Introduction

Plastics have been widely used in various fields and consumer goods for decades. The global production of plastics has surpassed 310 million tonnes in 2014 and is growing by approximately 7% every year.[216, 219] Approximately one-tenth of plastics manufactured each year will reach the aquatic environment eventually.[193, 220] These plastics can persist in the aquatic environment for an extremely long time due to the slow degradation process.[204, 216, 221] During the degradation and fragmentation, large plastic debris is eventually broken down by ultraviolet (UV) radiation, mechanical force, microbiological activity and other factors into to smaller pieces termed microplastics and microfibres (less than 5 μm, microplastics, MPs).[204, 222] The biological fate of MPs have been well studied in several organisms and several relevant environmental scenarios.[3, 201-203, 223] The primary mechanism of MP toxicity is associated with ingestion by organisms whereby MPs have been shown to form a physical blockage to alter feeding behaviour.[5, 197, 204, 224] Further breakdowns of MPs by environmental processes can produce even smaller nanoplastics (NPLs; defined as less than 100 nm) with exponentially increased specific surface areas (SAA) when compared to MPs.[3-5] Concerns on the potential impact of NPLs has encouraged more researchers to focus on NPL biological fate and possible effects on aquatic species. A wide range of effects associated with NPL exposure have been reported in various aquatic species, including accumulation of polystyrene (PS) NPLs in the yolk sac, heart, brain and other organs during the developmental stage of zebrafish (*Danio rerio*) embryos and led to hypoactivity,[224] reduced reproduction performance (delayed first eggs and clutch and decreased total offspring), induction of stress defense genes in *Daphnia pulex*,[216] and increased production of reactive oxygen species, lipid peroxidation and DNA damage in grass carp (*Ctenopharyngodon idella*).[220]

Polycyclic aromatic hydrocarbons (PAHs) are ubiquitous contaminants in the aquatic environment due to the incomplete combustion of petroleum-related products.[225, 226] PAHs are lipophilic, which allow them to pass through the lipid membranes of the gill or gut and bioaccumulated in various tissues.[226] However, PAHs can be metabolized by Cytochrome P450 1A (CYP1A) enzymes to significantly reduce their concentration in the tissues.[226, 227] The toxicological profile of many PAHs and their metabolites have been well studied[225, 228] but the interaction between PAHs and contaminants of emerging concern, such as microplastics and nanoplastics, are not well understood. A few studies have demonstrated that plastics' hydrophobic nature can allow MPs and NPLs to function as a vector for the uptake of hydrophobic persistent organic pollutants (POPs), including PAHs. Recent research has demonstrated that PAHs can adsorb and concentrate on the surface of plastics and can act to increase the bioavailability of POPs.[205, 219, 229, 230] Compared to MPs, NPLs not only have a higher adsorption capacity for organic pollutants due to the much larger surface area but also can penetrate cell membranes due to their smaller size when compared to MPs.[3, 191, 223] These properties of NPL have been demonstrated to enhance the "Trojan Horse" effects and further increase the uptake of organic pollutants by aquatic species.[3, 191, 223]

Natural organic matter (NOM) is an anionic heterogeneous matrix of carbon-based compounds,[2] is ubiquitous in all aquatic environments and is considered a natural colloid.[16, 19, 113] It is well known that NOM can sorb onto the surface of engineered nanoparticles (ENPs) and organic pollutants to provide a negative surface charge which can subsequently alter the repulsion between particles.[221, 231] This behavior has the potential to change particles' aggregation, stability, bioavailability and toxicity.[58, 221, 232] However, only a few studies have

focused on the effects of NOM on NPLs[221, 222] and there is a significant knowledge gap about if the presence of NOM can alter the "Trojan Horse" effects of NPLs for POPs.

In this study, we used the method developed in our lab for the previous study[229] to track the uptake, distribution, and depuration of organics using radiolabelled compounds. This exquisitely sensitive technique allows for the measurement of organic uptake at environmentally relevant concentrations. In this study, we used rainbow trout (*Oncorhynchus mykiss*) fingerlings, a widely used freshwater model species for regulatory science, to measure ^{14}C-radiolabelled phenanthrene (^{14}C-Phe) uptake, distribution, and depuration.[233] The aims of this study were 1) to determine if NPLs can facilitate the uptake and the distribution of phenanthrene in rainbow trout using induction of CYP1A activity as an indicator and 2) to investigate if the presence of NOM can alter the carrier function of NPLs for phenanthrene.

5.2 Methods

5.2.1 Chemicals

The stock [9-^{14}C]-labeled phenanthrene was purchased from American Radiolabeled Chemical, Inc. (^{14}C-Phe; 55 mCi mmol^{-1}, ARC0867). Yellow-green fluorescently labeled (505 nm excitation, 515 nm emission) carboxylated polystyrene nanoplastics (PS-NPLs) at 20 nm (Catalog#F8787) and 500 nm (Catalog#F8813) were purchased from Thermo Fisher Scientific. PS-NPLs were suspended in water (2% solid) with 2 mM sodium azide (NaN$_3$). Both PS-NPLs stock suspensions were dialyzed to remove NaN$_3$ following the protocol according to our previous study.[229] The dialysis had negligible effects on the characterization of PS-NPLs.[229] Dialyzed 20 nm and 500 nm PS-NPLs were diluted in reverse osmosis (RO) water (with 1%

weight/volume seawater salt mix added back to give the ions) to make suspensions at a final concentration of 200 µg L^{-1} with or without humic acid (0.5 mg L^{-1}, Sigma-Aldrich, 1415-93-6). Hydrodynamic diameter (HD) and polydispersity index (PDI) and zeta-potential of both PS-NPLs suspensions were measured by Dynamic light scattering (DLS; Zetasizer Nano Series, Malvern Instruments Ltd.) at 0, 4, and 24 h.

5.2.2 Animals and maintenance

Rainbow trout (*Oncorhynchus mykiss*) were obtained from fertilized eggs from Raven Brood Trout Station (Caroline, AB, Canada) and maintained in 300 L flow-through tanks with dechlorinated tap water from the City of Edmonton ([Na$^+$] = 14.5 ppm, [Ca^{2+}] = 56.0 ppm, [Mg^{2+}] = 15.0 ppm, [K$^+$] = 2.5 ppm, titratable alkalinity $\approx$ 119 mg L^{-1} as CaCO$_3$, pH $\approx$ 7.4, hardness $\approx$ 180 mg L^{-1} as CaCO$_3$, conductivity $\approx$ 385 µS cm^{-1}). Fish were kept in 10 ± 0.5 °C with a light: dark cycle of 14: 10 hours and fed ground dry trout pellets daily. Animal use was approved by the Animal Ethics Committee of the University of Alberta and the Canadian Council on Animal Care Committee under protocol AUP00000001 and all experimental procedures were performed following the guidelines and regulations.

5.2.3 Rainbow trout uptake

One µL of the stock ^{14}C-Phe was added into 200 mL non-radioactive phenanthrene (4.86 µg L^{-1}) in a 500 mL glass beaker to make a solution at a final concentration of 6.48 µg L^{-1} (initial exposing medium). To determine if the presence of PS-NPLs can potentiate uptake of

phenanthrene through gills and transport inside fish tissues, 2.5 µL of either 20 nm or 500 nm PS-NPLs was added into beakers to make a final concentration of 200 µg L^{-1}. ^{14}C-Phe without PS-NPLs was used as the comparison. The solutions were kept at 9 °C in the dark for 1 h to ensure stable sorption of phenanthrene onto PS-NPLs.[229] Rainbow trout fingerlings (one fish per beaker, N=4 per group; 0.95 ± 0.10 g) were randomly selected and added into each beaker and oxygen saturation was kept above 90% by aeration. Fish were maintained for 4 and 24 h at 9 ± 1 °C using a refrigerated chiller (Isotemp 3016 D, Fisher Scientific). Groups of fish exposed for 24 h were transferred into freshwater without added phenanthrene and allowed to recover for 24 h. At the end of each treatment period, to remove any loosely bound surficial ^{14}C-Phe, fish were washed thrice with non-radioactive phenanthrene (1 mg L^{-1}) prepared in 1% methanol and then in RO water thrice. The fish were then anesthetized in 50 mg L^{-1} tricaine methanesulfonate (TMS; Aqualife, DIN02168510). Gills and livers were removed and rewashed with the non-radioactive phenanthrene thrice and RO H$_2$O trice. The wet weight of whole fish, gills and livers were measured. Gills and livers were digested in 1 mL HNO$_3$ (1 M) in 20 mL scintillation vials at 65 °C for 24 h. After the digestion, 5 mL Ultima gold was added into each vial and then incubated for 2 h before measuring cpm (HITACHI AccuFLEX LSC-8000).[229]

Humic-like substances are the most abundant NOM and account for more than 60% (up to 80% in some aquatic environments) of the total NOM in freshwater and marine environment.[19, 113] We used humic acid in the current study to simplify the complexity of NOM. To determine if the presence of NOM can mitigate the uptake and transport of ^{14}C-Phe and/or PS-NPLs, humic acid was added into the treatment and control groups described above to make a final concentration of 0.5 mg L^{-1}. Beakers were placed on a shaking platform at 9°C in the dark

for 1 h to ensure sufficient interaction. Fish were transferred into each beaker and followed the methods described above.

The rate of ^{14}C-Phe passing through and accumulate in the gill (μg kg^{-1} h^{-1}) was calculated from cpm, specific activity (SA) and wet weight of the tissues (W) as defined by the following equation:

The SA of ^{14}C-Phe = cpm of initial exposing medium/concentration of phenanthrene

The rate of ^{14}C-Phe uptake/accumulation in gill $= \dfrac{\text{cpm of tissue}}{\text{SAxWx}\Delta\text{T}}$

5.2.4 Ethoxyresorufin-O-deethylase (EROD) activity

Phenanthrene is a weak CYP1A inducer when compared to other well-studied PAHs such as Bezo[a]pyrene (BaP),[225, 227] and therefore a higher concentration of phenanthrene (non-radioisotope labeled) at 60 μg L^{-1} (dissolved in RO water with 0.05% DMSO) was used to examine the interactive effects of NPLLs and NOM on phenanthrene uptake. At the end of each exposure time, fish were washed thrice with RO water and then anesthetized in 50 mg L^{-1} tricaine methanesulfonate to collect gill and liver samples for EROD assay. The gill EROD assay was modified from the method described by Jonsson et al.[234] and the liver EROD assay was modified from the method described by Hodson et al.[235] (See Supplementary Information for details).

5.2.5 Confocal imaging

Rainbow trout fingerlings were randomly placed into 500 mL glass beakers with 200 mL of control or treatment solutions described in uptake experiment as above but using non-radioisotope labeled phenanthrene and incubated at 9 ± 1 °C for 4 and 24h. Groups of fish exposed for 24 h were transferred into fresh RO water and allowed to recover for 24 h. After the incubation period, fish were anesthetized in 50 mg L^{-1} TMS and rinsed thrice with phosphate-buffered saline (PBS). Gills and livers were removed and rinsed thrice with PBS for fixation and slide preparation (See supplementary for slide preparation for confocal imaging).

Fixed tissue samples were imaged by a laser scanning confocal microscope (Zeiss LSM 710, Germany) with a Plan-Apochromat 40x/1.3 numerical aperture oil objective lens. A diode laser (405 nm) was used to excite Hoechst 33342 and emissions were collected by a band-pass filter of 410-493 (blue) at 451 nm. For cell membrane stain detection, a solid-state laser (561 nm) was used to excite CellMask™ Orange Plasma membrane Stain (CMO) and emissions were captured by a band-pass filter of 562-638 nm (red) at 600 nm. PS-NPLs fluorescence was excited with an argon laser (488 nm) and emission was recorded by a band-pass filter of 493-552 nm (green) at 522 nm. The detector gain and offset of each channel selected were kept constant in all the samples. Multi-color split images were captured with 1 airy unit pinhole.

5.2.6 Statistical analysis

Prism 8 (Version. 8.2, GraphPad Software Inc.) was used for graphing and statistical analysis. The normality and homoscedasticity were evaluated by Shapiro-Wilk and Breusch-Pagan (α=0.05) tests, respectively. Two-way analysis of variance (ANOVA, α=0.05) followed by Tukey's multiple comparison tests (α=0.05) was used to compare the accumulation of ^{14}C-Phe in

uptake experiment and used to compare the EROD activity between groups at different time points. Fuji-ImageJ was used to process confocal images. All data are presented as mean ± standard error of the mean (SEM).

5.3 Results

5.3.1 Characterization of PS-NPs

The HD and PDI of 20 nm and 500 nm PS-NPLs had a slight but non-significant increase from 0 to 24 h (Table S5-1). The zeta-potential of 20 nm PS-NPLs at 24 h was significantly lower than that at 0 h by 0.6 while the zeta-potential of 500 nm PS-NPLs did not have any significant change over 24 h. The presence of NOM significantly decreased the zeta-potential of 20 nm PS-NPLs but did not cause a significant shift in HD or PDI. However, NOM significantly reduced the HD of 500 nm PS-NPLs at 0, 4 and 24 h and slightly decreased PDI and zeta-potential.

5.3.2 Phenanthrene uptake by rainbow trout

The amount of ^{14}C-Phe accumulated in the gills was significantly higher in the presence of 20 nm PS-NPLs at 4 and 24 h when compared to gills either exposed to ^{14}C-Phe alone or in the presence of 500 nm PS-NPLs (Figure 5-1). The presence of NOM significantly reduced the ^{14}C-Phe accumulation in the gills in the presence of 20 nm PS-NPLs at 4 h (p=0.0114). The ^{14}C-Phe accumulation was significantly increased in the presence of 20 nm PS-NPLs at 24h when compared to 4h (p<0.001), while 500 nm PS-NPLs showed a slight but non-significant increase

in ^{14}C-Phe accumulation (p=0.392). The presence of NOM significantly reduced the ^{14}C-Phe at 24 h than that at 4h in all ^{14}C-Phe treated groups. After 24h of recovery in clean RO water, ^{14}C-Phe accumulation markedly decreased in all the groups (Figure 5-1).

The amount of ^{14}C-Phe accumulated in the liver was similar in all the groups at 4h (Figure 5-2). The presence of 20 nm significantly increased ^{14}C-Phe accumulated at 24h when compared to ^{14}C-Phe only group (p=0.0124). However, none of the groups at 24h showed significant changes compared to 4h, except ^{14}C-Phe with NOM which had a significant decrease in ^{14}C-Phe at 24h. Similar to gills, ^{14}C-Phe accumulation significantly reduced to a very low level after 24h recovery (Figure 5-2).

5.3.3 EROD activity

None of the groups induced significant increases in branchial EROD activity in gills of rainbow trout fingerlings at 4h (Figure 5-3). However, at 24 h post-exposure, phenanthrene induced a significant EROD activity in both the absence and presence of PS-NPLs (4-, 6-, 4- fold change by phenanthrene alone, the presence of 20 nm PS-NPLs and in the presence of 500 nm PS-NPs, respectively). 20 nm PS-NPLs alone also had a markedly higher EROD activity than the control group (p<0.001). The presence of NOM only significantly reduced EROD activity in the gills exposed to phenanthrene in the presence of 20 nm PS-NPs. However, EROD activity was still significantly higher than the control group at 24 h (Figure 5-3). After 24h of recovery in clean RO water, gill EROD activity dropped back to the control values.

Hepatic EROD activity was also not significantly affected by 4 h for any of the exposure regimes (Figure 5-4). Similar to the gill results, after 24h exposure, hepatic EROD activity was

125

significantly induced when fish exposed to phenanthrene in the presence of 20 nm PS-NPLs (p=0.006). However, the rest treatment groups showed only slight but non-significant induction of EROD activity. After 24h recovery in clean RO water, both phenanthrene alone (p=0.0038) and phenanthrene with 500 nm PS-NPLs (0.0285) induced a significantly higher hepatic EROD activity compared to the control group but still much lower than phenanthrene with 20 nm PS-NPLs treated group. The presence of NOM significantly decreased the hepatic EROD activity only in the phenanthrene with 20 nm PS-NPLs treated group (Figure 5-4).

5.3.4 Confocal imaging

PS-NPLs fluorescence was excited with an argon laser at 488 nm, which only had 61% relative intensity compared to peak excitation at 505 nm. Fuji-ImageJ was used to standardize the brightness of all PS-NPLs fluorescence images. Control, NOM and 500 nm PS-NPLs with or without NOM showed a low level of auto-fluorescence. However, in fish exposed to 20 nm PS-NPLs (with or without NOM) had much stronger fluorescence in both primary and secondary lamellae as early as 4 h after exposure, with strong fluorescence persisting even after 24 h transferring into clean RO water (Figure 5-5). In the liver, no apparent fluorescence was observed at 4 h after exposure while control and 500 nm PS-NPLs with or without NOM had weak auto-fluorescence when compared to the intense green fluorescence in 20 nm PS-NPLs exposed fish (with or without NOM) at either 24 h exposure or after 24 h recovery clean RO water (Figure 5-6).

5.4 Discussion

The current study demonstrates that nano-sized polystyrene plastics can facilitate the uptake of a model hydrophobic organic pollutant, phenanthrene, by rainbow trout fingerlings, thereby demonstrating the "Trojan Horse" effect for these nanoplastics. This is demonstrated by both an increase in ^{14}C-Phe uptake in the presence of 20 nm PS-NPLs and increased induction of EROD activity in gill and liver compared to control ^{14}C-Phe uptake without NPLs. Furthermore, the presence of NOM partially mitigated the potentiation of phenanthrene uptake by nano-sized plastics and also mitigated the induction of gill EROD activity. Last, our study also demonstrates that 20 nm nano-sized plastics are indeed taken up across the epithelia and found in the gill and liver of rainbow trout after 24 h of exposure. These 20 nm NPLs are then maintained in those tissues after 24 h of depuration while phenanthrene is largely depurated after 24 h in fresh clean water.

5.4.1 Fate and behavior of NP in exposure media

The HD, PDI and zeta-potential of 20 nm PS-NPLs were not significantly affected by NOM at 0 and 24 h while HD of 500 nm PS-NPLs was decreased in the presence of NOM but only by ~5%. This reflects negligible effects of HA at low concentration on the aggregation and stability of negatively charged PS-NPLs, especially smaller PS-NPLs. A similar result was reported in other studies.[221, 236] For example, the HD of negatively charged amino-modified PS-NPLs (~ 50 nm), PS-NPLs (100 nm) and carboxyl-modified PS-NPLs (300 nm) was not affected by the presence of HA at concentrations ranging from 0 to 50 mg L^{-1}. Moreover, the zeta-potential of PS-NPLs became significantly more negative when HA concentration was above 4 mg L^{-1}.[221]

5.4.2 Uptake and depuration of ^{14}C-Phe

^{14}C-Phe was detected in both gills and livers of rainbow trout fingerlings after 4 h exposure and continued increasing from 4 h to 24 h exposure. However, the net ^{14}C-Phe accumulation rate in these tissues from 4 h to 24 h was much lower than from 0 h to 4 h. During the depuration phase, the amount of ^{14}C-Phe in gills and livers dropped considerably after only 24 h of recovery in clean RO water. The much slower accumulation rate between 4 and 24 h and a significant drop after 24 h recovery indicated that there is likely an upregulation of excretion-related mechanisms. The rapid induction of CYP1A activity by phenanthrene is consistent with the apparent slower rate of increase in the 4-24 h period when compared to the 0-4 h period as Phe entering was metabolized rapidly by CYP1A and excreted.[234] These results also demonstrate the relatively high capacity of rainbow trout to metabolize and rapidly depurate and remove Phe from the gill and liver once placed in clean water.

5.4.3 Co-contaminant transport and the "Trojan Horse" effect by nanoplastics

In recent years, studies have demonstrated that NPLs have a higher sorption ability/capacity for environmental pollutants due to their surface hydrophobicity and much higher SSA when compared to MPs.[193, 230] This has resulted in the "Trojan horse" hypothesis whereby it has been hypothesized that the increased mobility and transport of nano-sized plastics across animal epithelia result in a potentiation of sorbed co-contaminant uptake into the animal.[237, 238] Recent results suggest that indeed, plastics can serve to increase co-contaminant uptake and release once inside the fish. Our results support the "Trojan horse" hypothesis in that the presence of 20 nm PS-NPLs significantly enhanced the uptake of ^{14}C-Phe in gills by ~ 40%

and 200% at 4 and 24 h of exposure, respectively, and by ~ 55% in livers at 24 h when compared to ^{14}C-Phe alone and the 500 nm PS-NPLs group. These results are consistent with not only our previous study[229] but also other recently published research[219, 230] demonstrating that smaller NPLs have a higher potential to facilitate the uptake and transport of hydrophobic organic pollutants in aquatic organisms. It is known that smaller particles display greater mobility in solutions, thereby rendering them more bioavailable[26] while other research in nanoparticles has demonstrated that smaller particles (< 50 nm) can be taken up across the cell membrane, whereas larger particles do not transverse epithelia readily.[25, 27]

5.4.4 Impact of NOM on co-contaminant uptake

NOM is ubiquitous in the aquatic environment and can alter particles' aggregation and stability, which can change particles' bioavailability and hence, toxicity.[58, 221, 222] While NOM and PAHs are the intensively studied compounds with regards to toxicology. Most studies have focused either on the interaction between NOM and organic pollutants,[231] the interaction between NOM and MPs/NPLs,[221, 222, 239] or the potential for "Trojan Horse" effects of NPLs.[219, 221, 222] To our knowledge, this is the first comprehensive study to investigate the impacts of NOM on the carrier function of NPLs for hydrophobic organic pollutants. Our results demonstrated that the presence of NOM significantly decreased ^{14}C-Phe uptake in rainbow trout gills as early as 4 h exposure (20% decrease in the presence of 20 nm PS-NPLs). After 24 h exposure, all groups exposed to ^{14}C-Phe in the presence of NOM had significantly lower ^{14}C-Phe uptake, especially in 20 nm PS-NPLs (~70% reduction vs. 30% in ^{14}C-Phe alone group and 40% in 500 nm PS-NPLs group). The 40% difference in the reduction of ^{14}C-Phe uptake between 20 nm PS-NPLs and

phenanthrene alone group at 24 h may be due to the presence of NOM competing with PAH binding to the NPL surface, thereby reducing ^{14}C-Phe sorption onto the surface of the PS-NPLs. This consequently would decrease the amount of PAHs transferring across the epithelia and into the fish.[221, 240] While humic acids are overall negatively charged at ecologically relevant pHs,[222, 236] they possess both positively charged domains and hydrophobic fractions that may allow sorption to the PS-NPLs used in the current study.[2, 88] Therefore, in this study, we suggest that NOM sorbs to the surface of PS-NPLs, reducing ^{14}C-Phe sorption.[236]

5.4.5 EROD induction as a measure of co-contaminant uptake

A common measure of exposure to PAHs is the induction of CYP1A activity.[225, 226] CYP1A metabolizes planar hydrocarbons like some PAHs to allow for eventual excretion of PAH metabolites and concomitant reduction of concentration in various tissues.[241] Therefore, CYP1A catalyzed ethoxy-resorufin-o-deethylase (EROD) activity is a widely used biomarker to measure the sub-lethal exposure to PAHs in aquatic species.[225, 234, 241] The CYP1A response varies depending on species, exposure durations, pollutants and concentrations.[225-227, 234, 241] In our study, only phenanthrene in combination with 20 nm PS-NPs had a slight but non-significant CYP1A induction (p=0.0842) in gill after 4 h exposure. After 24 h exposure to phenanthrene, EROD activity in gills was significantly elevated by 6-fold in the presence of 20 nm PS-NPLs. In contrast, phenanthrene alone and 500 nm PS-NPs group only had an approximately 4-fold increase. EROD activity in liver tissues was only significantly increased in the presence of 20 nm PS-NPLs, by ~2-fold. The further elevation of EROD activity in gills and liver at 24 h by 20 nm PS-NPLs demonstrated that phenanthrene uptake from the water was potentiated by the presence

of the NPLs. Fish gills are approximately 70% of the total surfaced area in rainbow and continuously contact water.[242] Gills are also the major site for the transport of oxygen and compounds into the fish through direct absorption.[234, 241] In this study, we assume that the gills are the dominant site of phenanthrene uptake although small contributions from other integuments (buccal epithelia and intestinal epithelia cannot be ruled out). Therefore, gills may have higher CYP1A inducibility and are more sensitive to waterborne pollutants. High gill EROD activity may act to metabolize PAHs rapidly to reduce liver exposure.[241] Together, these functions likely resulted in higher EROD activity induction in gills than that in livers after 24 h exposure.

During the depuration phase post-exposure, branchial EROD activity dropped back to control level in all groups within 24 h after the fish transferred to clean RO water. A similar result was observed by Jonsson et al. who demonstrated that BaP induced EROD activity in various rainbow trout tissues (gill and liver) decreased rapidly after a 2-day recovery.[234] The rapid decrease in branchial EROD activity is likely associated with fast induction of CYP1A.[234] However, in their study, branchial EROD activity remained slightly elevated after a 2-day recovery when compared to the control group. In our study, phenanthrene concentration in gills and livers both decreased dramatically after 24 h recovery in clean RO water, although the liver still had slightly higher phenanthrene concentration than gills, especially in the presence of 20 nm PS-NPLs (Figure S5-1). The slower but long-lasting hepatic EROD activity indicates the redistribution of phenanthrene from gills to other internal tissues including the liver and the lower turnover rate in the liver.[219, 234] The presence of NOM had less pronounced mitigating effects on EROD activity than for phenanthrene uptake. NOM only significantly reduced EROD activity in the presence of 20 nm PS-NPLs in the gill after 24 h exposure and in the liver 24 h

following transfer to clean RO water. Even though EROD activity is known to be concentration-dependent, many studies have demonstrated that EROD activity does not significantly change until exposure concentration reaches a specific threshold.[226, 241] For example, hepatic EROD activity was found to be similar in *Liza aurata* exposed to either 0.3 or 0.9 μM of phenanthrene, while gill EROD activity did not have a significant change in zebrafish exposed to either 0.1 or 1 nM of BaP.[226, 241] Therefore, while NOM reduced phenanthrene uptake, the phenanthrene concentration in tissues was still above the threshold in both the phenanthrene alone and 500 nm PS-NPLs group while the NOM acted to decrease phenanthrene concentration in the 20 nm PS-NPLs group below a threshold to have a significant reduction in EROD activity.

5.4.6 Uptake and retention of 20 nm PS particles

Confocal microscopy showed rapid epithelial uptake of 20 nm PS-NPLs via gill and accumulation of NPLs in the gill as early as 4 h exposure to 20 nm PS-NPs while no apparent uptake of 20 nm PS-NPLs in the liver was observed until 24 h after exposure. This demonstrated that smaller PS-NPLs (20 nm) have a much higher ability to pass through the cell membrane than larger plastic particles at the sub-micron level (500 nm).[3, 191, 193, 223] Confocal microscopy images of liver tissues only found a prominent accumulation of 20 nm PS-NPs at 24 h, indicating that small 20 nm NPL particles are taken up across the gills and redistributed to the gills. While we cannot rule out transintestinal uptake and transport to the liver via the portal circulation, the fact that the fish were not fed and that freshwater fish do not drink[243] argues against this route of transport. Interestingly, while ^{14}C-Phe activity was depurated from the liver and gill by 24 post-exposure, both the gill and liver confocal imaging at 24 h following recovery showed significant

amounts of 20 nm PS-NPLs persisted in the tissues. Studies have shown the accumulation of PS-NPLs in aquatic organisms.[219, 244] For example, in a study conducted by Chen et al. (2017), the measured concentrations PS-NPLs in adult zebrafish head, liver, gill and muscle found significantly increased after 24 h of exposure to 50 nm PS-NPLs. However, no study has focused on if nanoplastics can persist in the tissues during the depuration phase. The lack of depuration of NPL's from liver tissues is similar to that found in goldfish kidneys and livers where 5 nm TiO_2 particles persisted for >30 days after an initial infusion (Ortega et al., 2021- submitted). This is likely the result of a lack of an evolved mechanism to deal with particles of concern and suggests that exposure to NPL may accumulate over time.
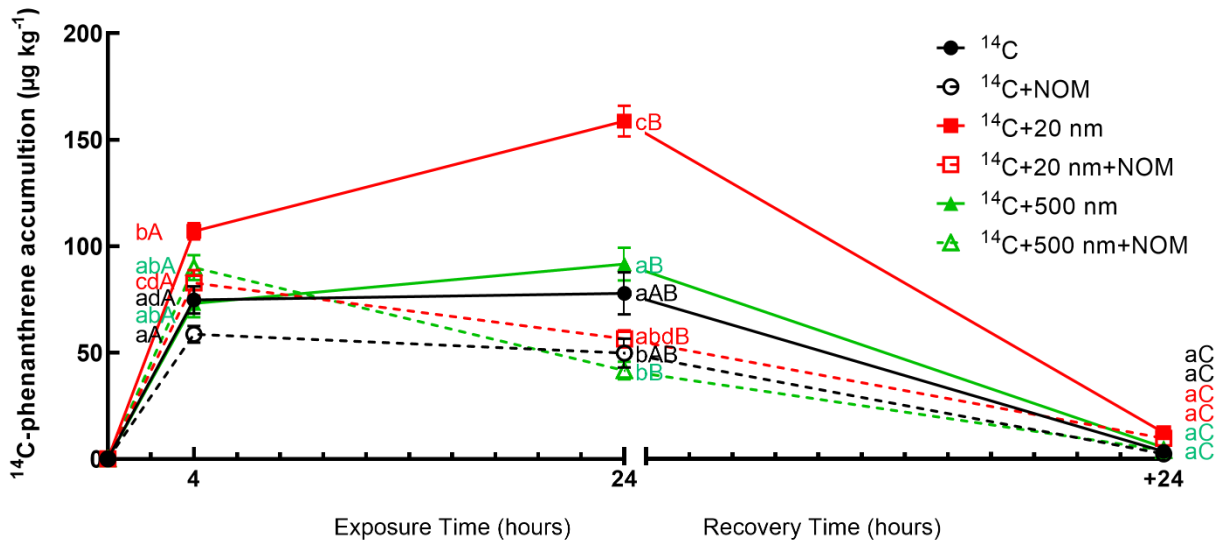
Figure 5-1. Accumulation of ^{14}C-labeled phenanthrene detected in rainbow trout fingerlings gills after exposure for various periods in ^{14}C-labeled phenanthrene alone, ^{14}C-labeled phenanthrene with NOM or in the presence of either 20 nm PS-NPLs or 500 nm PS-NPLs with or without NOM. Lowercase letters indicate different groups at the same time point. Uppercase letters indicate the same group at different time points. Means sharing the same letter are not significantly different from each other (p > 0.05). Values are mean ± SEM. n = 4.
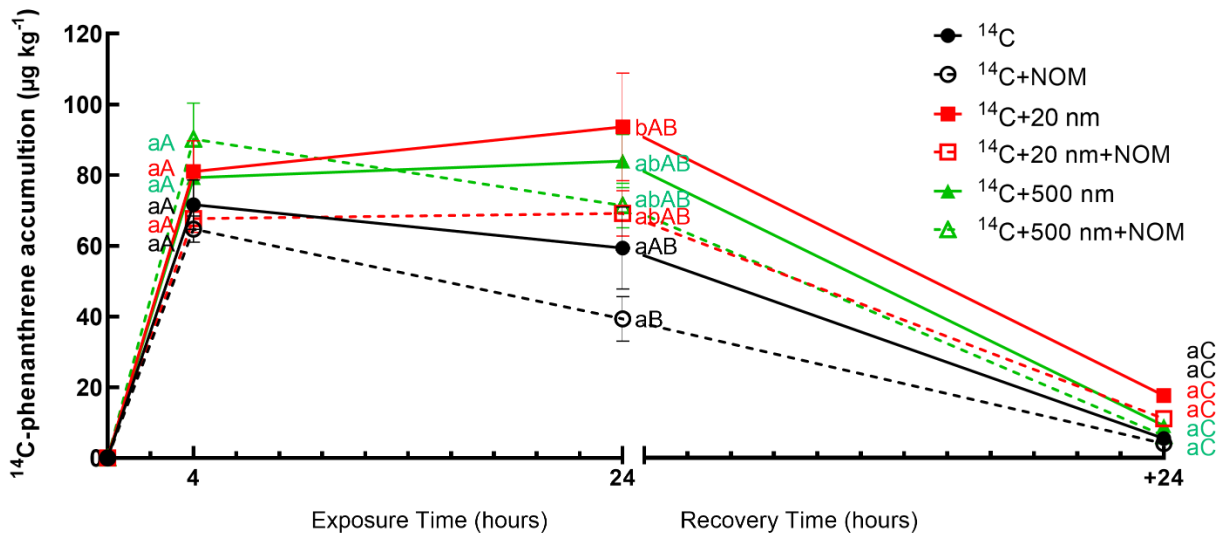
Figure 5-2. Accumulation of ^{14}C-labeled phenanthrene detected in rainbow trout fingerlings livers after exposure for various periods in ^{14}C-labeled phenanthrene alone, ^{14}C-labeled phenanthrene with NOM or in the presence of either 20 nm PS-NPLs or 500 nm PS-NPLs with or without NOM. Lowercase letters indicate different groups at the same time point. Uppercase letters indicate the same group at different time points. Means sharing the same letter are not significantly different from each other ($p > 0.05$). Values are mean ± SEM. n = 4.
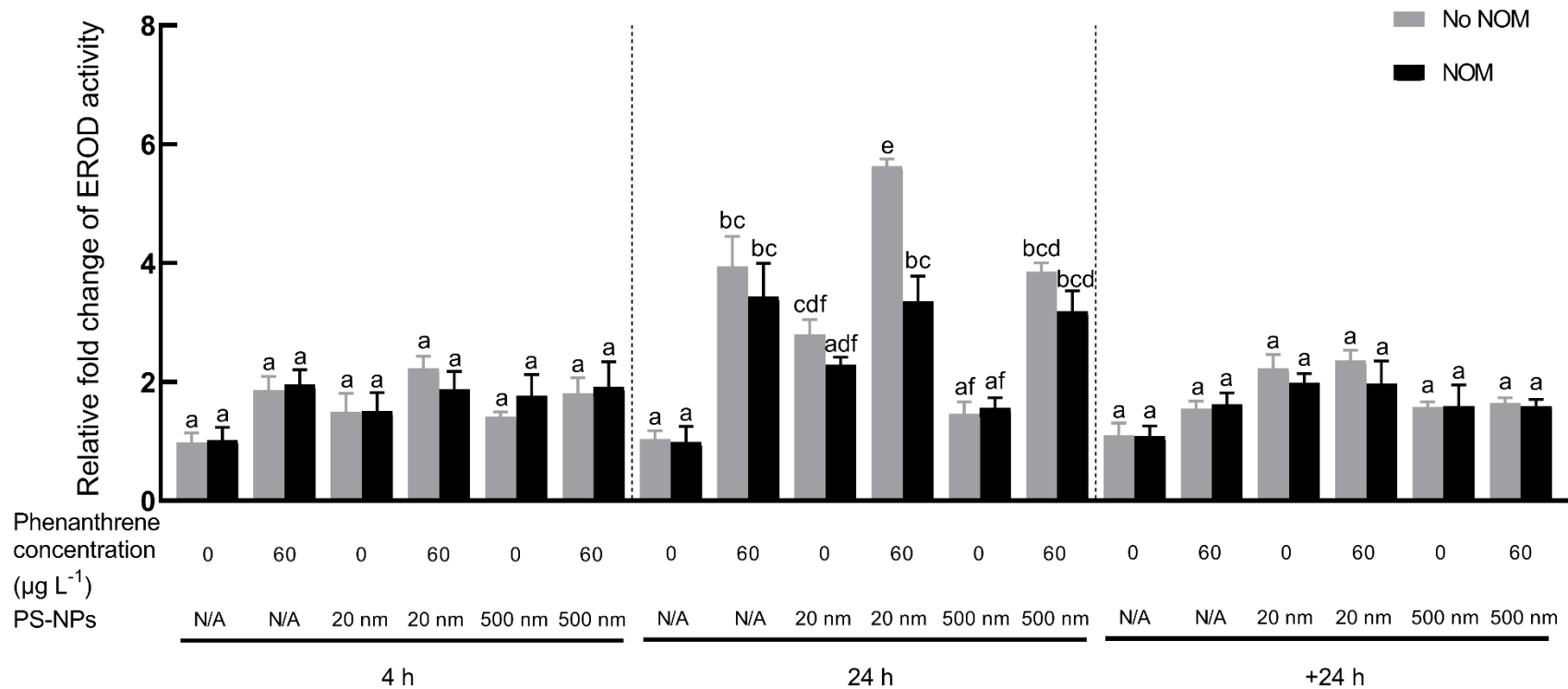
Figure 5-3. Relative fold change to control group (RO water) in EROD activity in gills induced by exposure to 0.05% DMSO, 20 nm PS-NPLs, 20 nm PS-NPLs with phenanthrene, 500 nm PS-NPLs, or 500 nm PS-NPLs with phenanthrene in the presence of NOM (black bar) or the absence of NOM (grey bar) at various period. Means sharing the same letter are not significantly different from each other ($p > 0.05$). Values are mean ± SEM. n = 5.
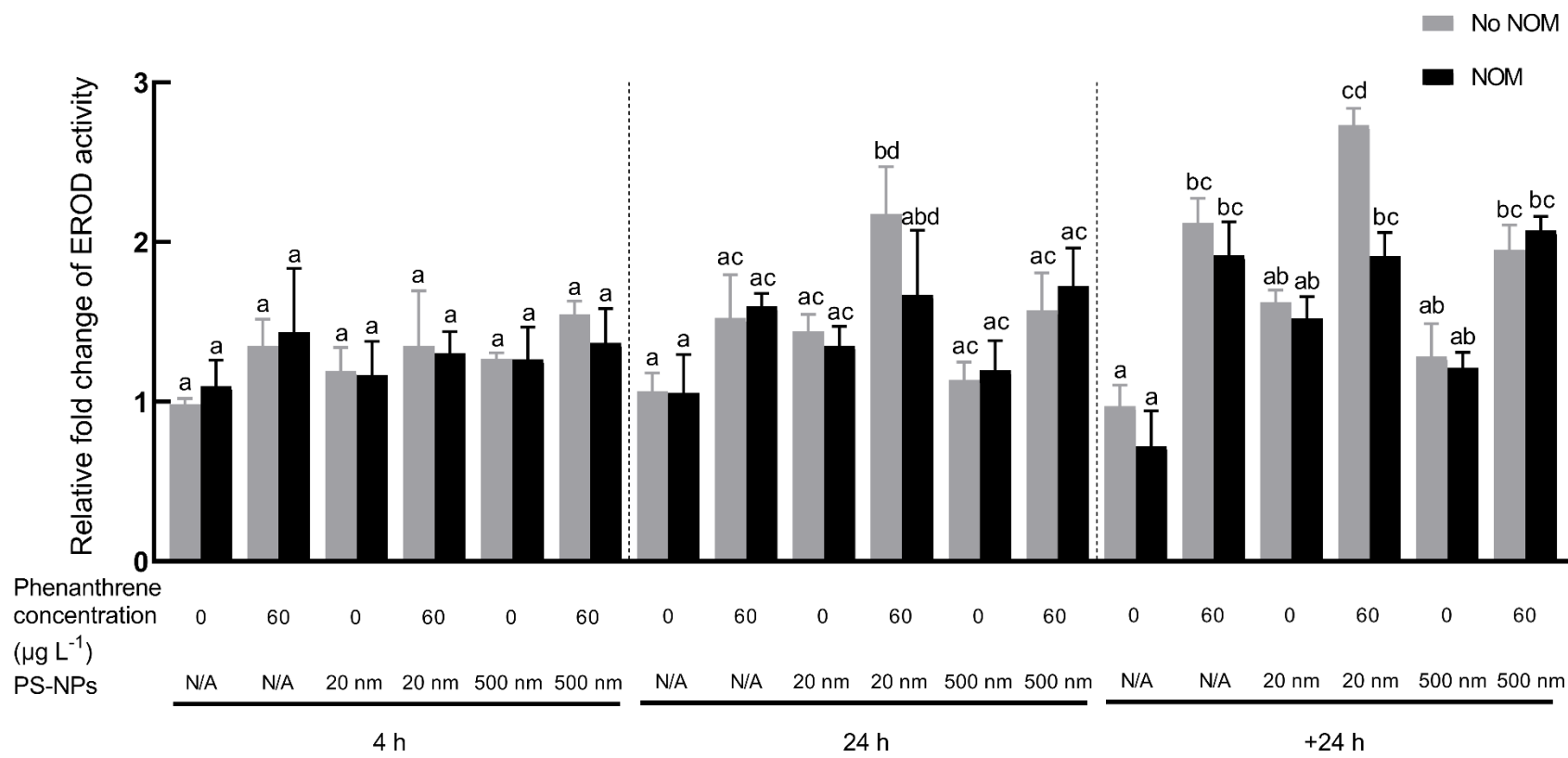
Figure 5-4. Relative fold change to control group (RO water) in EROD activity in livers induced by exposure to 0.05% DMSO, 20 nm PS-NPLs, 20 nm PS-NPLs with phenanthrene, 500 nm PS-NPLs, or 500 nm PS-NPLs with phenanthrene in the presence of NOM (black bar) or the absence of NOM (grey bar) at various period. Means sharing the same letter are not significantly different from each other ($p > 0.05$). Values are mean ± SEM. n = 5.

A   Bright field   PS-NPLs
Hoechst+CMO

Control

NOM

Phe+20 nm

Phe+20 nm
+ NOM

Phe+500 nm

Phe+500 nm
+ NOM

B

Bright field
Hoechst+CMO

PS-NPLs

Control

NOM

Phe+20 nm

Phe+20 nm
+ NOM

Phe+500 nm

Phe+500 nm
+ NOM

C | Bright field Hoechst+CMO | PS-NPLs

Control

NOM

Phe+20 nm

Phe+20 nm + NOM

Phe+500 nm

Phe+500 nm + NOM
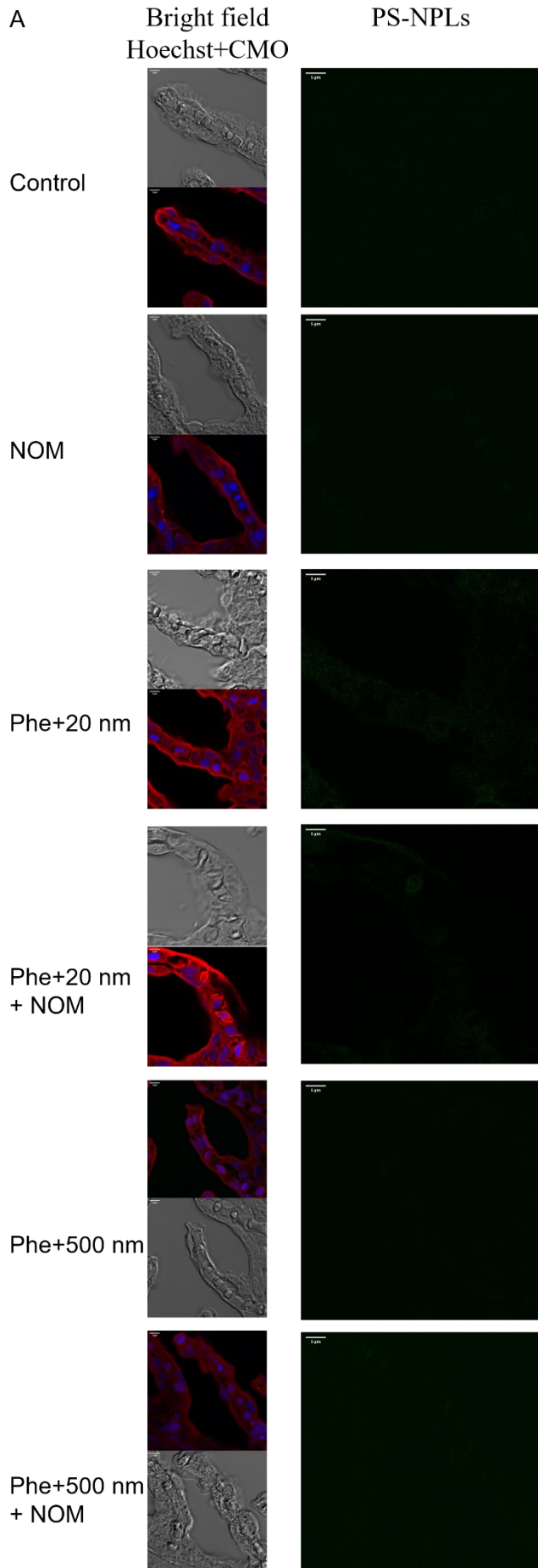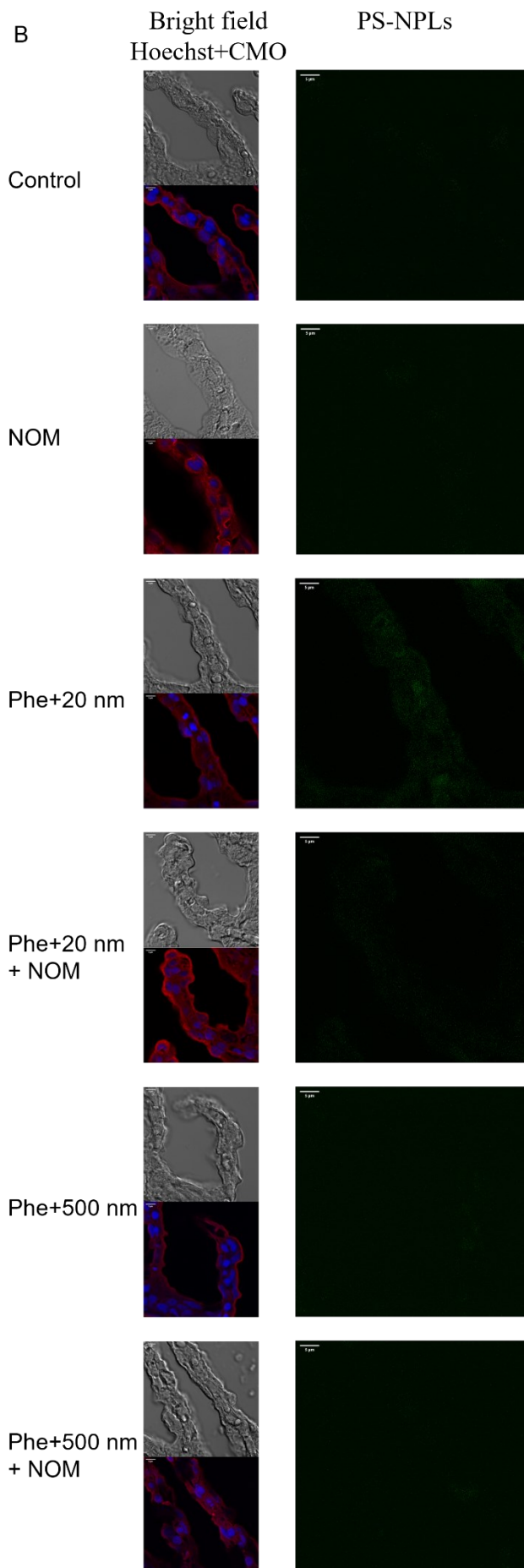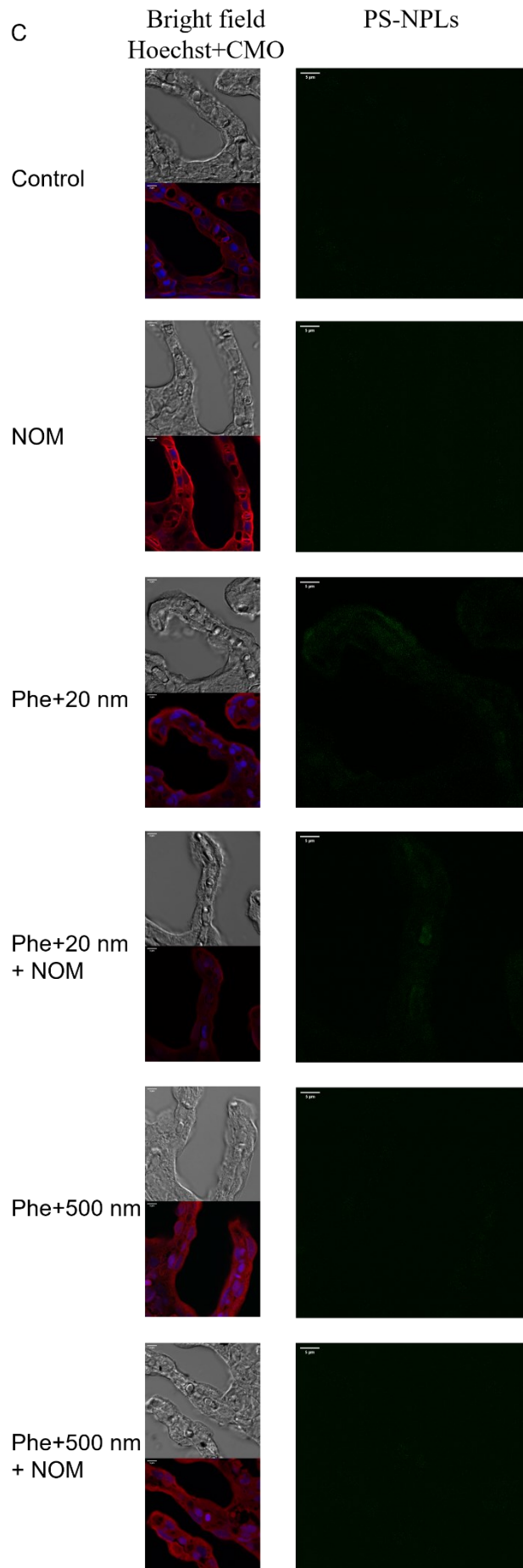
Figure 5-5. Processed confocal images (bright-field (top), Hoechst and CMO overlay (bottom) on the left side, PS-NPLls fluorescence on the right side) of gills of rainbow trout fingerlings exposed to control, NOM, phenanthrene in the presence of 20 nm PS-NPLs with or without NOM and phenanthrene in the presence of 500 nm PS-NPLs with or without NOM at 4h (A), 24h (B) and 24 h after recovery (C). Scale bars are 5 μm.

A   Bright field   PS-NPLs

Hoechst+CMO

Control

NOM

Phe+20 nm

Phe+20 nm
+ NOM

Phe+500 nm

Phe+500 nm
+ NOM

Bright field   PS-NPLs

B

Bright field
Hoechst+CMO

PS-NPLs

Control

NOM

Phe+20 nm

Phe+20 nm
+ NOM

Phe+500 nm

Phe+500 nm
+ NOM

Bright field
Hoechst+CMO

PS-NPLs

C	Bright field Hoechst+CMO	PS-NPLs
Control		
NOM		
Phe+20 nm		
Phe+20 nm + NOM		
Phe+500 nm		
Phe+500 nm + NOM		
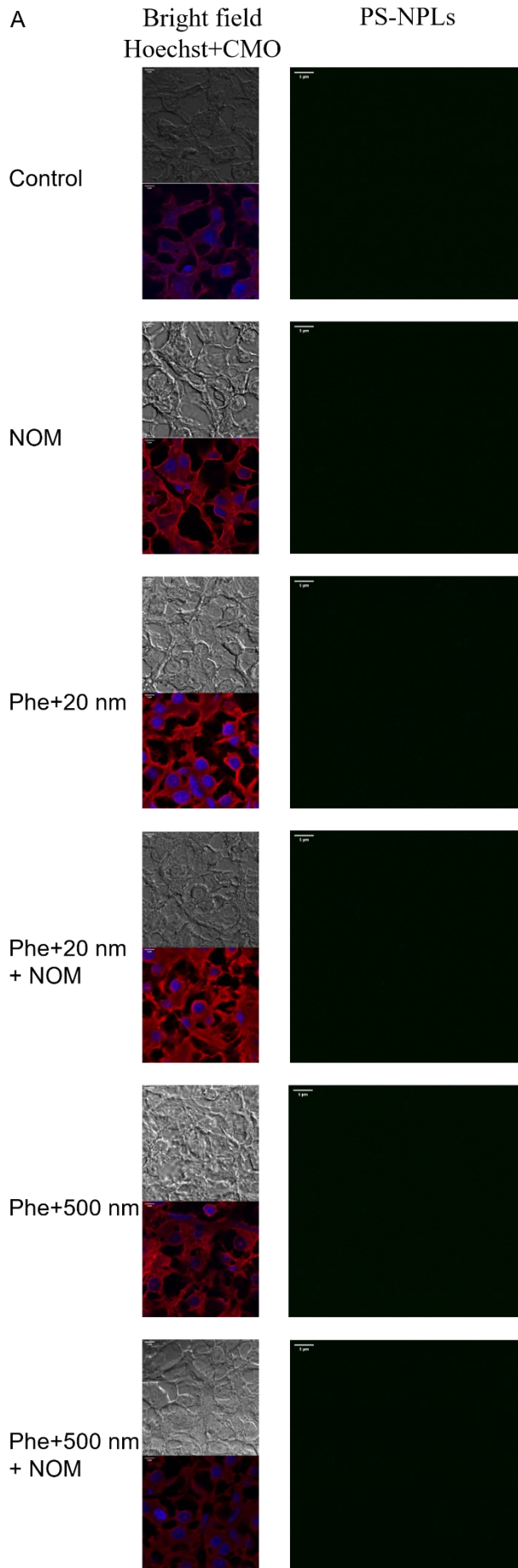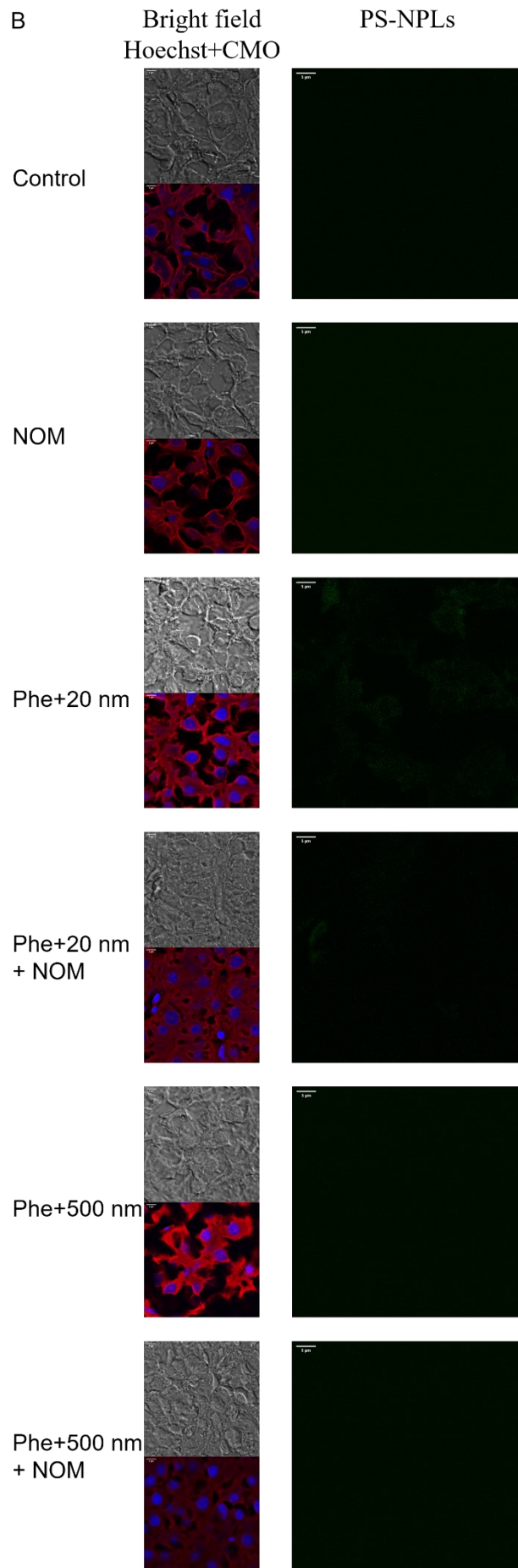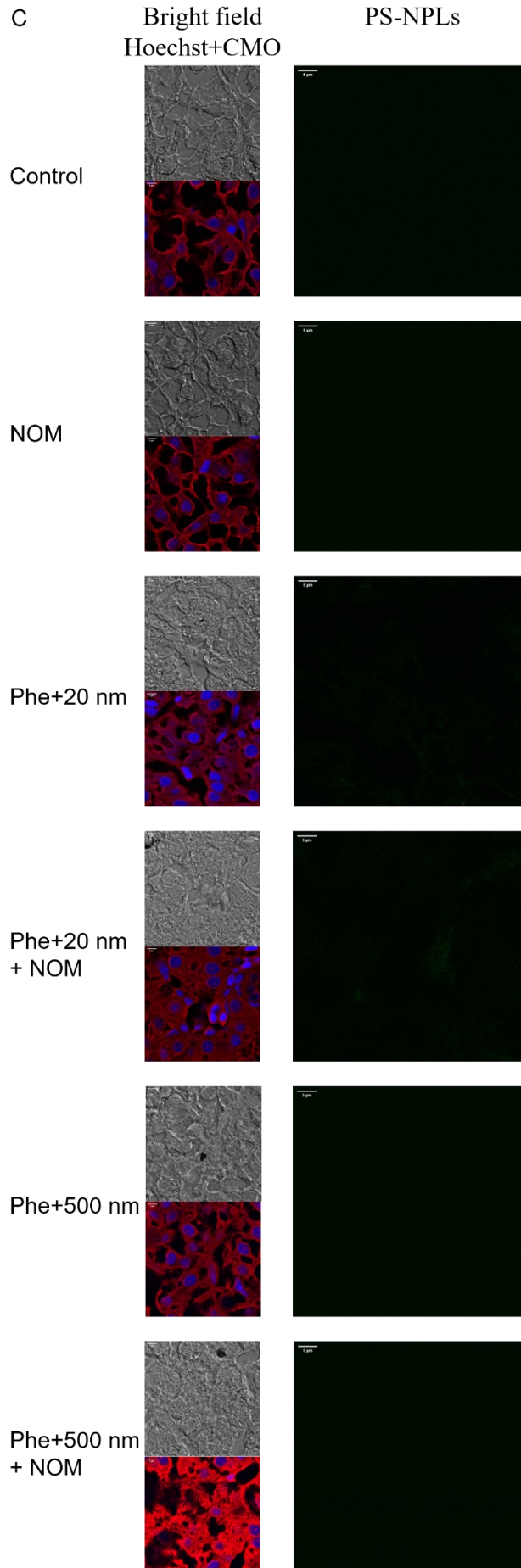
Figure 5-6. Processed confocal images (bright-field (top), Hoechst and CMO overlay (bottom) on the left side, PS-NPLs fluorescence on the right side) of livers of rainbow trout fingerlings exposed to control, NOM, phenanthrene in the presence of 20 nm PS-NPLs with or without NOM and phenanthrene in the presence of 500 nm PS-NPLs with or without NOM at 4h (A), 24h (B) and 24 h after recovery (C). Scale bars are 5 μm.

Chapter 6

Conclusions and future directions

6.1 General conclusions

My doctoral thesis investigated the physicochemical characteristics of CeO_2 NPs, nano-enabled azoxystrobin and NPLs and their lethal and sub-lethal effects on various *in vivo* aquatic species models, including cardinal tetra, zebrafish embryos/larvae and rainbow trout. These experiments addressed four main objectives: 1) to determine if environmental factors, including UV light and NOM, can modulate the lethal and sub-lethal effects of NMs on aquatic organisms, 2) to evaluate the toxicological effects of metal oxide nanoparticles, nano-enabled pesticides and nanoplastics on various aquatic organisms at multiple biological levels of organization, 3) to determine the carrier function of NPLs for hydrophobic organic pollutants uptake, 4) to investigate the mechanisms of toxicity. I have used and developed several *in vivo* methods to accurately assess the potential toxicity associated with NMs exposure. Briefly, I improved a UV light simulator built by a previous Ph.D. and used it to test the photo-induced toxicity of CeO_2 NPs on cardinal tetra over 96 h and evaluated the mitigating effects of NOM at high concentration on the photo-induced toxicity of CeO_2 NPs at low pH ($\sim$ 4.5) under ecologically relevant conditions (see Chapter 2). Secondly, I developed a technique to quantify the effects of azoxystrobin on the yolk sac volume of zebrafish larvae and a protocol for Western Blotting to quantify oxidative stress associated with azoxystrobin exposure by measuring the abundance of 4-HNE (see Chapter 3). Lastly, I developed a novel method to track and quantitatively assess the organic pollutant uptake (with and without NPLs) by zebrafish embryos/ larvae and rainbow trout using ^{14}C-radiolabelled phenanthrene (see Chapter 4 and 5).

The toxicity of NMs depends on the intrinsic properties, such as size, shape, surface charge, crystal structure, and dissolution, and is affected by a variety of environmental factors, including pH, UV light, NOM, and ionic strength.[20-23] My thesis emphasizes the impacts of environmental factors, especially UV light, on the toxicity of NMs with semiconductor properties. To achieve the first two objectives of my thesis, I examined lethal and sub-lethal effects associated with acute exposure of both metal oxide NPs and nano-enabled fungicides in different fish species at the whole-organismal, biochemical, cellular, and molecular levels. The CeO_2 NPs used in Chapter 2 are metal oxide semiconductor similar as TiO_2 NPs which has been intensively studied in the past decade.[16-18, 82, 120] The specific species (Cardinal tetra), low pH (~ 4.5) and high NOM concentration used in Chapter 2 represent the unique properties of Rio Negro Amazon River water.[105-108] Very little metal ion was released at pH around 4.5 during the experimental period, indicating the toxicity was associated with CeO_2 NPs itself, not the free ions. These results demonstrated that UV light significantly potentiated the toxicity of CeO_2 NPs due to the induction of •OH radicals while the presence of NOM in the exposure media showed protective properties, reducing the adverse effects associated with co-exposure of NPs and UV light. In Chapter 3, an organic fungicide with aromatic rings, azoxystrobin, was tested to evaluate whether its semiconductor property based on the HOMO-LUMO theory altered its toxicity in the presence of UV light. UV light was shown to increase the lethality on zebrafish embryos/larvae and also induce effects at sub-lethal levels of azoxystrobin due to the induction of •OH radicals. Furthermore, results suggested that nano-enabled azoxystrobin have higher adverse impacts on zebrafish embryos/larvae when compared to conventional azoxystrobin formulations, especially at a

lower nominal concentration. The abovementioned findings in CeO_2 NPs and nAZ demonstrated that 1) smaller size of NMs increases their bioavailability, 2) higher SSA allows more electrons on the surface of NMs to be excited by UV light to produce more •OH, which increases its adverse effects.

To achieve the last two objectives of my thesis, I developed a technique to examine the sorption of phenanthrene onto the surface of nano-sized (20 nm) and sub-micron-sized (500 nm) PS-NPLs. I then was able to measure the rate of phenanthrene transport across the chorion and quantify dermal uptake into zebrafish larvae. Both lethality and sub-lethal effects on zebrafish embryos/larvae with or without the presence of PS-NPLs were measured. Lastly, I evaluated the interactive effects of NOM on the carrier function of PS-NPLs for phenanthrene in rainbow trout fingerlings. The sorption experiment in Chapter 4 demonstrated that smaller PS-NPLs with a higher SSA have a higher sorption capacity per gravimetric mass for phenanthrene. This is the primary reason that smaller PS-NPLs (20 nm) can facilitate greater phenanthrene passing through chorion and uptake by both zebrafish larvae and by the gill of rainbow trout fingerlings when compared to 500 nm PS-NPLs or phenanthrene alone. While the presence of PS-NPLs did not affect the LC_{50} of phenanthrene on zebrafish embryos, it resulted in a delay in hatching when embryos were also exposed at 0.156 or 0.313 mg L^{-1}. Both Chapter 4 and Chapter 5 suggested that phenanthrene-coated 20 nm PS-NPLs also induced a higher EROD activity in both zebrafish larvae and gill and liver tissues of rainbow trout. Results in Chapter 5 suggested rapid upregulation of metabolism and excretion of phenanthrene in both gill and liver of exposed fish, while the 20 nm PS-NPLs that we found in the liver after 24 h persisted in both the gill and liver for 24 h even after fish

were transferred into clean water. Furthermore, Chapter 5 also demonstrated the mitigating effects of NOM on aquatic pollutants. The presence of NOM reduced both phenanthrene uptake and EROD activity, most prominently in the presence of 20 nm PS-NPLs.

In general, my research demonstrated 1) photo-induced toxicity of CeO_2 NPs and azoxystrobin, 2) that nano-enabled azoxystrobin has higher lethal and sub-lethal effects when compared to conventional counterpart, 3) that smaller PS-NPLs has higher ability to facilitate the uptake of phenanthrene due to higher sorption capacity and induces higher EROD activity, 4) the mitigating effects of NOM on UV light and "Trojan horse" effect. Overall, my thesis 1) provides much-needed data for acute and medium-term hazard assessment of metal oxide NPs, nAz and nanoplastics, 2) demonstrates the importance of environmental factors in conducting toxicity experiments and 3) facilitates the improvement of current nanotoxicity tests and regulatory guidelines.

6.2 Future research

While this thesis provides valuable data on the environmental factors that affect the toxicity of various NMs, much more research is required to have a better understanding of their hazard and potential environmental impact. There are still large knowledge gaps about the effects of environmental factors on the potential toxicity of NMs.

6.2.1 Chronic exposure under environmentally relevant conditions

148

In recent years, the impact of various NMs has been intensively studied *in vivo* and *in vitro* models to better understand their toxicological profiles to the environment and human health.[245-247] However, the knowledge about the interaction between NMs and environmental factors and the long-term impact of NMs is still lacking.[7, 245] The laboratory setting may not reflect all the environmental conditions in nature. For example, CeO_2 NPs are considered to have very low to no toxicity to aquatic species due to their very poor dispersiveness in moderate environmental conditions (pH>6.8), moderately hard water, low NOM concentration and low UV intensity.[76, 100, 104, 121] However, Chapter 2 demonstrated that high NOM concentration and low pH in Rio Negro Amazon River water significantly increased the dispersiveness and reduced aggregation of CeO_2 NPs, which helped NPs stay in the water column longer without aggregation. The increased bioavailability coupled with high UV intensity in the region then enhanced the toxicity of CeO_2 NPs to the aquatic organisms. Many current studies used acute exposure at high concentrations which are not ecologically relevant.[12] Furthermore, many environmental factors show temporal and spatial variation.[2, 76, 108] Therefore, future toxicology studies should examine the toxicity of NMs in chronic exposure at both lower concentrations that are environmentally relevant and include more environmentally relevant factors to represent more realistic exposure conditions.

6.2.2 Investigate the toxicity and mechanism of nano-enabled pesticides

In past decades, many companies have developed and manufactured pesticides using nanoformulation to replace conventional pesticides to meet the increasing food demands

while reducing their environmental footprint.[149, 159] However, the current regulatory guidelines are based on the studies done only on conventional pesticides. Chapter 3 has clearly shown that while nano-enabled azoxystrobin still has the same mechanism associated with toxicity as its conventional counterpart, the nano-enabled formulation has potentially a higher adverse impact on aquatic organisms. On the other hand, a parallel study from our lab has demonstrated that nanoencapsulation of bifenthrin shows lower lethality in rainbow trout and similar sub-lethal effects as its conventional counterpart.[248] Therefore, there is no one-size-fits-all answer to the difference in toxicity between nano-formulations and their conventional counterparts. Extrapolation or read- across from other nano-enabled pesticides or current data and guidelines based on conventional pesticides could either underestimate or overestimate the environmental impacts of these novel nano-enabled pesticides. This challenges the current regulations and indicates that the nanoformulation of pesticides itself requires more targeted research to investigate their environmental risk under environmentally realistic conditions.

6.2.3 Evaluate the different type of nanoplastics and weathered nanoplastics

As an emerging pollutant, nanoplastics have attracted increasing attention in the past few years. Most research so far has heavily focused on polystyrene (PS), which accounted for over 54% of total research publications.[230] The reason is the nano-sized PS particles are readily available from commercial suppliers while other plastics are not readily available. However, PS only accounts for approximately 6% of the total global production of plastics

each year.[249] As a result, it is highly recommended that research focuses on different types of nanoplastics, especially polypropylene (PP) and polyethylene (PE), to verify the potential for a "Trojan horse" effect and induction of increased toxicity. Furthermore, the majority of current published studies only examine acute exposure of pristine nanoplastics, either purchased from manufacturers or produced in the lab.[196, 236] Nanoplastics in the aquatic environment are known to be persistent over a long time, are weathered by UV radiation and mechanical forces, and develop their own eco-corona.[250] The weathering process alters the surface, shape and functional groups on the surface of nanoplastics, which likely affects their sorption capacity and toxicity.[230, 251] Therefore, it is important to conduct research using chronic exposure of the weathered nanoplastics to understand better their sorption capacity for hydrophobic organic pollutants, behavior, and biological fate in the aquatic environment.

6.3 Outlook

In the past two decades, the intensive studies on NMs have tremendously improved the knowledge of their intrinsic properties, environmental and biological fate, hazard and applications of NMs and provided updated data for risk assessments and regulation guidelines.[252, 253] The Organisation for Economic Co-operation and Development (OECD) established a Working Party on Manufactured Nanomaterials (WPMN) in 2006 to provide a global platform for advising environment, health, and safety-related issues. The WPMN monitored the testing and assessment of a variety of NMs and suggested that the majority of guideline and testing for conventional chemicals is suitable for NMs but few adaptations

were required, mainly focusing on Ag and TiO$_2$ NPs in 2009.[252, 254] The last major update on guideline was in 2013 and 2014 when two meetings organized by OECD further discussed and updated test guidelines of NMs.[254] Although significant progress on testing method and guidelines has been achieved to date, increasing numbers of newly developed NMs and the limitations on existing instruments challenges current guidelines. Furthermore, the emerging concern on microplastics and especially nanoplastics in the past few years requires much more effort from agencies and nanotoxicologists to catch up with the rapid development of NMs. This requires collaboration from all fields including regulatory agencies, nanotoxicologists and engineers, to improve current methods and develop new methods to fit the unique properties of NMs. Nanotechnology has shown its tremendous advantages in many fields and a promising future for providing solutions in many applications.

References

1. S. J. Klaine, P. J. Alvarez, G. E. Batley, T. F. Fernandes, R. D. Handy, D. Y. Lyon, S. Mahendra, M. J. McLaughlin and J. R. Lead, Nanomaterials in the environment: behavior, fate, bioavailability, and effects, *Environmental toxicology and chemistry*, 2008, **27**, 1825-1851 DOI: https://doi.org/10.1897/08-090.1

2. R. Grillo, A. H. Rosa and L. F. Fraceto, Engineered nanoparticles and organic matter: a review of the state-of-the-art, *Chemosphere*, 2015, **119**, 608-619 DOI: https://doi.org/10.1016/j.chemosphere.2014.07.049.

3. K. Mattsson, L.-A. Hansson and T. Cedervall, Nano-plastics in the aquatic environment, *Environmental Science: Processes & Impacts*, 2015, **17**, 1712-1721 DOI: 10.1039/C5EM00227C.

4. J. A. Pitt, J. S. Kozal, N. Jayasundara, A. Massarsky, R. Trevisan, N. Geitner, M. Wiesner, E. D. Levin and R. T. Di Giulio, Uptake, tissue distribution, and toxicity of polystyrene nanoparticles in developing zebrafish (Danio rerio), *Aquatic Toxicology*, 2018, **194**, 185-194 DOI: https://doi.org/10.1016/j.aquatox.2017.11.017.

5. M. Sendra, P. Pereiro, M. P. Yeste, L. Mercado, A. Figueras and B. Novoa, Size matters: Zebrafish (Danio rerio) as a model to study toxicity of nanoplastics from cells to the whole organism, *Environmental Pollution*, 2020, **268**, 115769 DOI: https://doi.org/10.1016/j.envpol.2020.115769.

6. R. P. Feynman, in *Handbook of Nanoscience, Engineering, and Technology, Third Edition*, CRC Press, 2012, pp. 26-35.

7. A. G. Schultz, D. Boyle, D. Chamot, K. J. Ong, K. J. Wilkinson, J. C. McGeer, G. Sunahara and G. G. Goss, Aquatic toxicity of manufactured nanomaterials: challenges and recommendations for future toxicity testing, *Environmental Chemistry*, 2014, **11**, 207-226 DOI: http://dx.doi.org/10.1071/EN13221.

8. E. Inshakova and O. Inshakov, 2017.

9. X. He, P. Fu, W. G. Aker and H.-M. Hwang, Toxicity of engineered nanomaterials mediated by nano–bio–eco interactions, *Journal of Environmental Science and Health, Part C*, 2018, **36**, 21-42 DOI: https://doi.org/10.1080/10590501.2017.1418793.

10. StatNano, Database: Products, 2018.

11. G. Bystrzejewska-Piotrowska, J. Golimowski and P. L. Urban, Nanoparticles: their potential toxicity, waste and environmental management, *Waste Management*, 2009, **29**, 2587-2595 DOI: http://dx.doi.org/10.1016/j.wasman.2009.04.001.

12. D. M. Mitrano, S. Motellier, S. Clavaguera and B. Nowack, Review of nanomaterial aging and transformations through the life cycle of nano-enhanced products, *Environment international*, 2015, **77**, 132-147 DOI: https://doi.org/10.1016/j.envint.2015.01.013.

13. Y. Zhang, Y. Chen, P. Westerhoff and J. Crittenden, Impact of natural organic matter and divalent cations on the stability of aqueous nanoparticles, *Water Research*, 2009, **43**, 4249-4257 DOI: http://dx.doi.org/10.1016/j.watres.2009.06.005.

14. A. A. Keller, H. Wang, D. Zhou, H. S. Lenihan, G. Cherr, B. J. Cardinale, R. Miller and Z. Ji, Stability and aggregation of metal oxide nanoparticles in natural aqueous matrices, *Environmental science & technology*, 2010, **44**, 1962-1967 DOI: 10.1021/es902987d.

15. M. J. Clift, S. Bhattacharjee, D. M. Brown and V. Stone, The effects of serum on the

toxicity of manufactured nanoparticles, *Toxicology letters*, 2010, **198**, 358-365 DOI: https://doi.org/10.1016/j.toxlet.2010.08.002.

16. A. M. Wormington, J. Coral, M. M. Alloy, C. L. Damare, C. M. Mansfield, S. J. Klaine, J. H. Bisesi and A. P. Roberts, Effect of natural organic matter on the photo-induced toxicity of titanium dioxide (TiO2) nanoparticles, *Environmental Toxicology and Chemistry*, 2016, **36(6)**, 1661-1666 DOI: 10.1002/etc.3702.

17. H. Ma, A. Brennan and S. A. Diamond, Phototoxicity of TiO2 nanoparticles under solar radiation to two aquatic species: Daphnia magna and Japanese medaka, *Environmental Toxicology and Chemistry*, 2012, **31**, 1621-1629 DOI: https://doi.org/10.1002/etc.1858.

18. M. Zhu, H. Wang, A. A. Keller, T. Wang and F. Li, The effect of humic acid on the aggregation of titanium dioxide nanoparticles under different pH and ionic strengths, *Science of the Total Environment*, 2014, **487**, 375-380 DOI: https://doi.org/10.1016/j.scitotenv.2014.04.036.

19. M. Baalousha, A. Manciulea, S. Cumberland, K. Kendall and J. R. Lead, Aggregation and surface properties of iron oxide nanoparticles: influence of pH and natural organic matter, *Environmental toxicology and chemistry*, 2008, **27**, 1875-1882 DOI: https://doi.org/10.1897/07-559.1.

20. J. Jiang, G. Oberdörster and P. Biswas, Characterization of size, surface charge, and agglomeration state of nanoparticle dispersions for toxicological studies, *Journal of Nanoparticle Research*, 2009, **11**, 77-89 DOI: 10.1007/s11051-008-9446-4.

21. C. Ren, X. Hu and Q. Zhou, Influence of environmental factors on nanotoxicity and knowledge gaps thereof, *NanoImpact*, 2016, **2**, 82-92 DOI: https://doi.org/10.1016/j.impact.2016.07.002.

22. S. K. Misra, S. Nuseibeh, A. Dybowska, D. Berhanu, T. D. Tetley and E. Valsami-Jones, Comparative study using spheres, rods and spindle-shaped nanoplatelets on dispersion stability, dissolution and toxicity of CuO nanomaterials, *Nanotoxicology*, 2014, **8**, 422-432 DOI: https://doi.org/10.3109/17435390.2013.796017.

23. L. K. Braydich-Stolle, N. M. Schaeublin, R. C. Murdock, J. Jiang, P. Biswas, J. J. Schlager and S. M. Hussain, Crystal structure mediates mode of cell death in TiO2 nanotoxicity, *Journal of Nanoparticle Research*, 2009, **11**, 1361-1374 DOI: 10.1007/s11051-008-9523-8.

24. L. Shang, K. Nienhaus and G. U. Nienhaus, Engineered nanoparticles interacting with cells: size matters, *Journal of nanobiotechnology*, 2014, **12**, 5 DOI: https://doi.org/10.1186/1477-3155-12-5.

25. N. Oh and J.-H. Park, Endocytosis and exocytosis of nanoparticles in mammalian cells, *International journal of nanomedicine*, 2014, **9**, 51 DOI: 10.2147/IJN.S26592.

26. L. C. Felix, V. A. Ortega and G. G. Goss, Cellular uptake and intracellular localization of poly (acrylic acid) nanoparticles in a rainbow trout (Oncorhynchus mykiss) gill epithelial cell line, RTgill-W1, *Aquatic toxicology*, 2017, **192**, 58-68 DOI: https://doi.org/10.1016/j.aquatox.2017.09.008.

27. J. Farkas, P. Christian, J. A. Gallego-Urrea, N. Roos, M. Hassellöv, K. E. Tollefsen and K. V. Thomas, Uptake and effects of manufactured silver nanoparticles in rainbow trout (Oncorhynchus mykiss) gill cells, *Aquatic Toxicology*, 2011, **101**, 117-125 DOI: https://doi.org/10.1016/j.aquatox.2010.09.010.

28. J. Rejman, V. Oberle, I. S. Zuhorn and D. Hoekstra, Size-dependent internalization of particles via the pathways of clathrin-and caveolae-mediated endocytosis, *Biochemical Journal*, 2004, **377**, 159-169 DOI: 10.1042/bj20031253.

29. A. J. Wyrwoll, P. Lautenschläger, A. Bach, B. Hellack, A. Dybowska, T. A. Kuhlbusch, H. Hollert, A. Schäffer and H. M. Maes, Size matters–the phototoxicity of TiO2 nanomaterials, *Environmental Pollution*, 2016, **208**, 859-867 DOI: https://doi.org/10.1016/j.envpol.2015.10.035.

30. T. M. Scown, E. M. Santos, B. D. Johnston, B. Gaiser, M. Baalousha, S. Mitov, J. R. Lead, V. Stone, T. F. Fernandes and M. Jepson, Effects of aqueous exposure to silver nanoparticles of different sizes in rainbow trout, *Toxicological Sciences*, 2010, **115**, 521-534 DOI: https://doi.org/10.1093/toxsci/kfq076.

31. O. J. Osborne, S. Lin, C. H. Chang, Z. Ji, X. Yu, X. Wang, S. Lin, T. Xia and A. E. Nel, Organ-specific and size-dependent Ag nanoparticle toxicity in gills and intestines of adult zebrafish, *ACS nano*, 2015, **9**, 9573-9584 DOI: 10.1021/acsnano.5b04583.

32. P. Ganguly, A. Breen and S. C. Pillai, Toxicity of Nanomaterials: Exposure, Pathways, Assessment, and Recent Advances, *ACS Biomater. Sci. Eng.*, 2018, **4**, 2237-2275 DOI: 10.1021/acsbiomaterials.8b00068.

33. A. Varki and R. Schauer, Sialic acids, 2009.

34. L. Kou, J. Sun, Y. Zhai and Z. He, The endocytosis and intracellular fate of nanomedicines: Implication for rational design, *Asian Journal of Pharmaceutical Sciences*, 2013, **8**, 1-10 DOI: https://doi.org/10.1016/j.ajps.2013.07.001.

35. T.-G. Iversen, T. Skotland and K. Sandvig, Endocytosis and intracellular transport of nanoparticles: present knowledge and need for future studies, *Nano Today*, 2011, **6**, 176-185 DOI: https://doi.org/10.1016/j.nantod.2011.02.003.

36. G. A. Dominguez, S. E. Lohse, M. D. Torelli, C. J. Murphy, R. J. Hamers, G. Orr and R. D. Klaper, Effects of charge and surface ligand properties of nanoparticles on oxidative stress and gene expression within the gut of Daphnia magna, *Aquatic Toxicology*, 2015, **162**, 1-9 DOI: 10.1016/j.aquatox.2015.02.015.

37. T. Silva, L. R. Pokhrel, B. Dubey, T. M. Tolaymat, K. J. Maier and X. Liu, Particle size, surface charge and concentration dependent ecotoxicity of three organo-coated silver nanoparticles: comparison between general linear model-predicted and observed toxicity, *Science of the total environment*, 2014, **468**, 968-976 DOI: https://doi.org/10.1016/j.scitotenv.2013.09.006.

38. P. P. Fu, Q. Xia, H.-M. Hwang, P. C. Ray and H. Yu, Mechanisms of nanotoxicity: generation of reactive oxygen species, *Journal of food and drug analysis*, 2014, **22**, 64-75 DOI: https://doi.org/10.1016/j.jfda.2014.01.005.

39. J. Fabrega, S. N. Luoma, C. R. Tyler, T. S. Galloway and J. R. Lead, Silver nanoparticles: behaviour and effects in the aquatic environment, *Environment international*, 2011, **37**, 517-531 DOI: https://doi.org/10.1016/j.envint.2010.10.012.

40. S. K. Misra, A. Dybowska, D. Berhanu, S. N. Luoma and E. Valsami-Jones, The complexity of nanoparticle dissolution and its importance in nanotoxicological studies, *Science of the total environment*, 2012, **438**, 225-232 DOI: https://doi.org/10.1016/j.scitotenv.2012.08.066.

41. C. Ispas, D. Andreescu, A. Patel, D. V. Goia, S. Andreescu and K. N. Wallace, Toxicity

and developmental defects of different sizes and shape nickel nanoparticles in zebrafish, *Environmental science & technology*, 2009, **43**, 6349-6356 DOI: 10.1021/es9010543.

42. R. Bacchetta, N. Santo, I. Valenti, D. Maggioni, M. Longhi and P. Tremolada, Comparative toxicity of three differently shaped carbon nanomaterials on Daphnia magna: does a shape effect exist?, *Nanotoxicology*, 2018, **12**, 201-223 DOI: 10.1080/17435390.2018.1430258.

43. F. Nasser, A. Davis, E. Valsami-Jones and I. Lynch, Shape and Charge of Gold Nanomaterials Influence Survivorship, Oxidative Stress and Moulting of Daphnia magna, *Nanomaterials*, 2016, **6**, 13 DOI: 10.3390/nano6120222.

44. L. Clement, C. Hurel and N. Marmier, Toxicity of TiO2 nanoparticles to cladocerans, algae, rotifers and plants - Effects of size and crystalline structure, *Chemosphere*, 2013, **90**, 1083-1090 DOI: 10.1016/j.chemosphere.2012.09.013.

45. M. L. Avramescu, P. E. Rasmussen, M. Chenier and H. D. Gardner, Influence of pH, particle size and crystal form on dissolution behaviour of engineered nanomaterials, *Environmental Science and Pollution Research*, 2017, **24**, 1553-1564 DOI: 10.1007/s11356-016-7932-2.

46. L. E. Oi, M.-Y. Choo, H. V. Lee, H. C. Ong, S. B. A. Hamid and J. C. Juan, Recent advances of titanium dioxide (TiO 2) for green organic synthesis, *Rsc Advances*, 2016, **6**, 108741-108754 DOI: 10.1039/C6RA22894A.

47. A. Menard, D. Drobne and A. Jemec, Ecotoxicity of nanosized TiO2. Review of in vivo data, *Environmental Pollution*, 2011, **159**, 677-684 DOI: https://doi.org/10.1016/j.envpol.2010.11.027.

48. J. Ji, Z. Long and D. Lin, Toxicity of oxide nanoparticles to the green algae Chlorella sp, *Chemical Engineering Journal*, 2011, **170**, 525-530 DOI: https://doi.org/10.1016/j.cej.2010.11.026.

49. M. Buchalska, M. Kobielusz, A. Matuszek, M. Pacia, S. Wojtyła and W. Macyk, On oxygen activation at rutile-and anatase-TiO2, *ACS Catalysis*, 2015, **5**, 7424-7431 DOI: 10.1021/acscatal.5b01562.

50. Y. Kakuma, A. Y. Nosaka and Y. Nosaka, Difference in TiO 2 photocatalytic mechanism between rutile and anatase studied by the detection of active oxygen and surface species in water, *Physical Chemistry Chemical Physics*, 2015, **17**, 18691-18698 DOI: https://doi.org/10.1039/C5CP02004B.

51. P. R. Paquin, R. C. Santore, K. B. Wu, C. D. Kavvadas and D. M. Di Toro, The biotic ligand model: a model of the acute toxicity of metals to aquatic life, *Environmental Science & Policy*, 2000, **3**, 175-182 DOI: https://doi.org/10.1016/S1462-9011(00)00047-2.

52. D. M. Di Toro, H. E. Allen, H. L. Bergman, J. S. Meyer, P. R. Paquin and R. C. Santore, Biotic ligand model of the acute toxicity of metals. 1. Technical basis, *Environmental toxicology and chemistry*, 2001, **20**, 2383-2396 DOI: https://doi.org/10.1002/etc.5620201034

53. T. A. Blewett and E. M. Leonard, Mechanisms of nickel toxicity to fish and invertebrates in marine and estuarine waters, *Environmental pollution*, 2017, **223**, 311-322 DOI: https://doi.org/10.1016/j.envpol.2017.01.028.

54. H. Ma, P. L. Williams and S. A. Diamond, Ecotoxicity of manufactured ZnO

nanoparticles–a review, *Environmental Pollution*, 2013, **172**, 76-85 DOI: https://doi.org/10.1016/j.envpol.2012.08.011.

55. M. Baalousha, M. Sikder, A. Prasad, J. Lead, R. Merrifield and G. T. Chandler, The concentration-dependent behaviour of nanoparticles, *Environmental Chemistry*, 2016, **13**, 1-3 DOI: 10.1071/en15142.

56. M. Sikder, E. Eudy, G. T. Chandler and M. Baalousha, Comparative study of dissolved and nanoparticulate Ag effects on the life cycle of an estuarine meiobenthic copepod, Amphiascus tenuiremis, *Nanotoxicology*, 2018, **12**, 375-389 DOI: https://doi.org/10.1080/17435390.2018.1451568.

57. S.-W. Bian, I. A. Mudunkotuwa, T. Rupasinghe and V. H. Grassian, Aggregation and dissolution of 4 nm ZnO nanoparticles in aqueous environments: influence of pH, ionic strength, size, and adsorption of humic acid, *Langmuir*, 2011, **27**, 6059-6068 DOI: 10.1021/la200570n.

58. F. M. Omar, H. A. Aziz and S. Stoll, Aggregation and disaggregation of ZnO nanoparticles: influence of pH and adsorption of Suwannee River humic acid, *Science of the total environment*, 2014, **468**, 195-201 DOI: http://dx.doi.org/10.1016/j.scitotenv.2013.08.044.

59. J. T. Dahle, K. Livi and Y. Arai, Effects of pH and phosphate on CeO2 nanoparticle dissolution, *Chemosphere*, 2015, **119**, 1365-1371 DOI: https://doi.org/10.1016/j.chemosphere.2014.02.027.

60. T. Xia, Y. Zhao, T. Sager, S. George, S. Pokhrel, N. Li, D. Schoenfeld, H. Meng, S. Lin and X. Wang, Decreased dissolution of ZnO by iron doping yields nanoparticles with reduced toxicity in the rodent lung and zebrafish embryos, *ACS nano*, 2011, **5**, 1223-1235 DOI: 10.1021/nn1028482.

61. S. George, S. Pokhrel, T. Xia, B. Gilbert, Z. Ji, M. Schowalter, A. Rosenauer, R. Damoiseaux, K. A. Bradley and L. Mädler, Use of a rapid cytotoxicity screening approach to engineer a safer zinc oxide nanoparticle through iron doping, *ACS nano*, 2009, **4**, 15-29 DOI: 10.1021/nn901503q.

62. A. M. E. Badawy, T. P. Luxton, R. G. Silva, K. G. Scheckel, M. T. Suidan and T. M. Tolaymat, Impact of Environmental Conditions (pH, Ionic Strength, and Electrolyte Type) on the Surface Charge and Aggregation of Silver Nanoparticles Suspensions, *Environmental Science & Technology*, 2010, **44**, 1260-1266 DOI: 10.1021/es902240k.

63. R. A. Sperling and W. J. Parak, Surface modification, functionalization and bioconjugation of colloidal inorganic nanoparticles, *Philosophical Transactions of the Royal Society A: Mathematical, Physical and Engineering Sciences*, 2010, **368**, 1333-1383 DOI: https://doi.org/10.1098/rsta.2009.0273.

64. T. Yin, H. W. Walker, D. Chen and Q. Yang, Influence of pH and ionic strength on the deposition of silver nanoparticles on microfiltration membranes, *Journal of Membrane Science*, 2014, **449**, 9-14 DOI: https://doi.org/10.1016/j.memsci.2013.08.020.

65. K.-T. Kim, L. Truong, L. Wehmas and R. L. Tanguay, Silver nanoparticle toxicity in the embryonic zebrafish is governed by particle dispersion and ionic environment, *Nanotechnology*, 2013, **24**, 115101 DOI: doi:10.1088/0957-4484/24/11/115101.

66. I. Römer, T. A. White, M. Baalousha, K. Chipman, M. R. Viant and J. R. Lead, Aggregation and dispersion of silver nanoparticles in exposure media for aquatic

toxicity tests, *Journal of Chromatography A*, 2011, **1218**, 4226-4233 DOI: https://doi.org/10.1016/j.chroma.2011.03.034.

67. I. Römer, A. J. Gavin, T. A. White, R. C. Merrifield, J. K. Chipman, M. R. Viant and J. R. Lead, The critical importance of defined media conditions in Daphnia magna nanotoxicity studies, *Toxicology letters*, 2013, **223**, 103-108 DOI: https://doi.org/10.1016/j.toxlet.2013.08.026.

68. N. Garcia-Reyero, C. Thornton, A. D. Hawkins, L. Escalon, A. J. Kennedy, J. A. Steevens and K. L. Willett, Assessing the exposure to nanosilver and silver nitrate on fathead minnow gill gene expression and mucus production, *Environmental nanotechnology, monitoring & management*, 2015, **4**, 58-66 DOI: https://doi.org/10.1016/j.enmm.2015.06.001.

69. N. Tripathy, T.-K. Hong, K.-T. Ha, H.-S. Jeong and Y.-B. Hahn, Effect of ZnO nanoparticles aggregation on the toxicity in RAW 264.7 murine macrophage, *Journal of Hazardous Materials*, 2014, **270**, 110-117 DOI: https://doi.org/10.1016/j.jhazmat.2014.01.043.

70. F. Seitz, R. R. Rosenfeldt, K. Storm, G. Metreveli, G. E. Schaumann, R. Schulz and M. Bundschuh, Effects of silver nanoparticle properties, media pH and dissolved organic matter on toxicity to Daphnia magna, *Ecotoxicology and environmental safety*, 2015, **111**, 263-270 DOI: https://doi.org/10.1016/j.ecoenv.2014.09.031.

71. V. K. Sharma, Aggregation and toxicity of titanium dioxide nanoparticles in aquatic environment—a review, *Journal of Environmental Science and Health Part A*, 2009, **44**, 1485-1495 DOI: https://doi.org/10.1080/10934520903263231.

72. M. Ates, J. Daniels, Z. Arslan and I. O. Farah, Effects of aqueous suspensions of titanium dioxide nanoparticles on Artemia salina: assessment of nanoparticle aggregation, accumulation, and toxicity, *Environmental monitoring and assessment*, 2013, **185**, 3339-3348 DOI: 10.1007/s10661-012-2794-7.

73. S. W. Wong, P. T. Leung, A. Djurišić and K. M. Leung, Toxicities of nano zinc oxide to five marine organisms: influences of aggregate size and ion solubility, *Analytical and bioanalytical chemistry*, 2010, **396**, 609-618 DOI: 10.1007/s00216-009-3249-z.

74. C. E. Williamson, R. G. Zepp, R. M. Lucas, S. Madronich, A. T. Austin, C. L. Ballaré, M. Norval, B. Sulzberger, A. F. Bais and R. L. McKenzie, Solar ultraviolet radiation in a changing climate, *Nature Climate Change*, 2014, **4**, 434.

75. S. Safari, S. Eshraghi Dehkordy, M. Kazemi, H. Dehghan and B. Mahaki, Ultraviolet radiation emissions and illuminance in different brands of compact fluorescent lamps, *International Journal of Photoenergy*, 2015, **2015** DOI: http://dx.doi.org/10.1155/2015/504674.

76. J. T. Dahle and Y. Arai, Environmental geochemistry of cerium: applications and toxicology of cerium oxide nanoparticles, *International journal of environmental research and public health*, 2015, **12**, 1253-1278 DOI: 10.3390/ijerph120201253.

77. K. Apel and H. Hirt, Reactive oxygen species: metabolism, oxidative stress, and signal transduction, *Annu. Rev. Plant Biol.*, 2004, **55**, 373-399 DOI: 10.1146/annurev.arplant.55.031903.141701.

78. P. Riley, Free radicals in biology: oxidative stress and the effects of ionizing radiation, *International journal of radiation biology*, 1994, **65**, 27-33 DOI:

https://doi.org/10.1080/09553009414550041.

79. P. Ježek and L. Hlavatá, Mitochondria in homeostasis of reactive oxygen species in cell, tissues, and organism, *The international journal of biochemistry & cell biology*, 2005, **37**, 2478-2503 DOI: https://doi.org/10.1016/j.biocel.2005.05.013.

80. S. Di Meo, T. T. Reed, P. Venditti and V. M. Victor, Role of ROS and RNS sources in physiological and pathological conditions, *Oxidative Medicine and Cellular Longevity*, 2016, **2016** DOI: http://dx.doi.org/10.1155/2016/1245049.

81. C. Kohchi, H. Inagawa, T. Nishizawa and G.-I. Soma, ROS and innate immunity, *Anticancer research*, 2009, **29**, 817-821.

82. O. Bar-Ilan, K. M. Louis, S. P. Yang, J. A. Pedersen, R. J. Hamers, R. E. Peterson and W. Heideman, Titanium dioxide nanoparticles produce phototoxicity in the developing zebrafish, *Nanotoxicology*, 2012, **6**, 670-679 DOI: https://doi.org/10.3109/17435390.2011.604438.

83. R. J. Miller, S. Bennett, A. A. Keller, S. Pease and H. S. Lenihan, TiO2 nanoparticles are phototoxic to marine phytoplankton, *PloS one*, 2012, **7**, e30321 DOI: https://doi.org/10.1371/journal.pone.0030321.

84. M. J. Behrenfeld, R. T. O'Malley, D. A. Siegel, C. R. McClain, J. L. Sarmiento, G. C. Feldman, A. J. Milligan, P. G. Falkowski, R. M. Letelier and E. S. Boss, Climate-driven trends in contemporary ocean productivity, *Nature*, 2006, **444**, 752 DOI: 10.1038/nature05317.

85. Y. Zhang, T. A. Blewett, A. L. Val and G. G. Goss, UV-induced toxicity of cerium oxide nanoparticles (CeO 2 NPs) and the protective properties of natural organic matter (NOM) from the Rio Negro Amazon River, *Environmental Science: Nano*, 2018, **5**, 476-486 DOI: 10.1039/C7EN00842B.

86. J. A. Nason, S. A. McDowell and T. W. Callahan, Effects of natural organic matter type and concentration on the aggregation of citrate-stabilized gold nanoparticles, *Journal of Environmental Monitoring*, 2012, **14**, 1885-1892 DOI: 10.1039/C2EM00005A

87. J. A. Gallego-Urrea, J. P. Holmberg and M. Hassellöv, Influence of different types of natural organic matter on titania nanoparticle stability: effects of counter ion concentration and pH, *Environmental Science: Nano*, 2014, **1**, 181-189 DOI: 10.1039/C3EN00106G.

88. I. Levchuk, J. J. R. Marquez and M. Sillanpaa, Removal of natural organic matter (NOM) from water by ion exchange - A review, *Chemosphere*, 2018, **192**, 90-104 DOI: 10.1016/j.chemosphere.2017.10.101.

89. J. T. Quik, I. Lynch, K. Van Hoecke, C. J. Miermans, K. A. De Schamphelaere, C. R. Janssen, K. A. Dawson, M. A. C. Stuart and D. Van De Meent, Effect of natural organic matter on cerium dioxide nanoparticles settling in model fresh water, *Chemosphere*, 2010, **81**, 711-715 DOI: http://dx.doi.org/10.1016/j.chemosphere.2010.07.062.

90. K. Van Hoecke, K. A. De Schamphelaere, P. Van der Meeren, G. Smagghe and C. R. Janssen, Aggregation and ecotoxity of CeO 2 nanoparticles in synthetic and natural waters with variable pH, organic matter concentration and ionic strength, *Environmental Pollution*, 2011, **159**, 970-976 DOI: http://dx.doi.org/10.1016/j.envpol.2010.12.010.

91. J. Gao, S. Youn, A. Hovsepyan, V. L. Llaneza, Y. Wang, G. Bitton and J.-C. J. Bonzongo,

Dispersion and toxicity of selected manufactured nanomaterials in natural river water samples: effects of water chemical composition, *Environmental science & technology*, 2009, **43**, 3322-3328 DOI: 10.1021/es803315v.

92. C. Cerrillo, G. Barandika, A. Igartua, O. Areitioaurtena and G. Mendoza, Towards the standardization of nanoecotoxicity testing: Natural organic matter 'camouflages' the adverse effects of TiO2 and CeO2 nanoparticles on green microalgae, *Science of the Total Environment*, 2016, **543**, 95-104 DOI: 10.1016/j.scitotenv.2015.10.137.

93. D. Westmeier, R. H. Stauber and D. Docter, The concept of bio-corona in modulating the toxicity of engineered nanomaterials (ENM), *Toxicology and applied pharmacology*, 2016, **299**, 53-57 DOI: https://doi.org/10.1016/j.taap.2015.11.008.

94. A. Quigg, W.-C. Chin, C.-S. Chen, S. Zhang, Y. Jiang, A.-J. Miao, K. A. Schwehr, C. Xu and P. H. Santschi, Direct and indirect toxic effects of engineered nanoparticles on algae: role of natural organic matter, *ACS Sustainable Chemistry & Engineering*, 2013, **1**, 686-702 DOI: 10.1021/sc400103x.

95. S. Li, H. Ma, L. K. Wallis, M. A. Etterson, B. Riley, D. J. Hoff and S. A. Diamond, Impact of natural organic matter on particle behavior and phototoxicity of titanium dioxide nanoparticles, *Science of the Total Environment*, 2016, **542**, 324-333 DOI: https://doi.org/10.1016/j.scitotenv.2015.09.141.

96. T. Heitmann, T. Goldhammer, J. Beer and C. Blodau, Electron transfer of dissolved organic matter and its potential significance for anaerobic respiration in a northern bog, *Global Change Biology*, 2007, **13**, 1771-1785 DOI: 10.1111/j.1365-2486.2007.01382.x.

97. D. T. Scott, D. M. McKnight, E. L. Blunt-Harris, S. E. Kolesar and D. R. Lovley, Quinone moieties act as electron acceptors in the reduction of humic substances by humics-reducing microorganisms, *Environmental Science & Technology*, 1998, **32**, 2984-2989 DOI: 10.1021/es980272q.

98. W. Jacobs, L. Pegler, M. Reis and H. Pereira, Amazon shipping, commodity flows and urban economic development: the case of Belém and Manaus, *Cadernos Metrópole*, 2013, **15**, 389-410 DOI: http://dx.doi.org/10.1590/2236-9996.2013-3002

99. A. s. L. Schmid and C. A. A. Hoffmann, Replacing diesel by solar in the Amazon: short-term economic feasibility of PV-diesel hybrid systems, *Energy Policy*, 2004, **32**, 881-898 DOI: https://doi.org/10.1016/S0301-4215(03)00014-4.

100. F. R. Cassee, E. C. van Balen, C. Singh, D. Green, H. Muijser, J. Weinstein and K. Dreher, Exposure, health and ecological effects review of engineered nanoscale cerium and cerium oxide associated with its use as a fuel additive, *Critical reviews in toxicology*, 2011, **41**, 213-229 DOI: http://dx.doi.org/10.3109/10408444.2010.529105.

101. K. V. Hoecke, J. T. Quik, J. Mankiewicz-Boczek, K. A. D. Schamphelaere, A. Elsaesser, P. V. d. Meeren, C. Barnes, G. McKerr, C. V. Howard and D. V. D. Meent, Fate and effects of CeO2 nanoparticles in aquatic ecotoxicity tests, *Environmental science & technology*, 2009, **43**, 4537-4546 DOI: 10.1021/es9002444.

102. M. Tella, M. Auffan, L. Brousset, E. Morel, O. Proux, C. Chaneac, B. Angeletti, C. Pailles, E. Artells, C. Santaella, J. Rose, A. Thiery and J. Y. Bottero, Chronic dosing of a simulated pond ecosystem in indoor aquatic mesocosms: fate and transport of CeO2 nanoparticles, *Environmental Science: Nano*, 2015, **2**, 653-663 DOI: 10.1039/C5EN00092K.

103. K. M. Dunnick, R. Pillai, K. L. Pisane, A. B. Stefaniak, E. M. Sabolsky and S. S. Leonard, The effect of cerium oxide nanoparticle valence state on reactive oxygen species and toxicity, *Biological trace element research*, 2015, **166**, 96-107 DOI: 10.1007/s12011-015-0297-4.

104. J. Labille and J. Brant, Stability of nanoparticles in water, *Nanomedicine*, 2010, **5**, 985-998 DOI: 10.2217/nnm.10.62.

105. K. Furch, in *The Amazon*, Springer, 1984, DOI: 10.1007/978-94-009-6542-3_6, pp. 167-199.

106. A. L. Val, R. J. Gonzalez, C. M. Wood, R. W. Wilson, M. L. Patrick, H. L. Bergman and A. Narahara, Effects of water pH and calcium concentration on ion balance in fish of the Rio Negro, Amazon, *Physiological Zoology*, 1998, **71**, 15-22 DOI: 10.1086/515893.

107. O. E. Johannsson, D. S. Smith, H. Sadauskas-Henrique, G. Cimprich, C. M. Wood and A. L. Val, Photo-oxidation processes, properties of DOC, reactive oxygen species (ROS), and their potential impacts on native biota and carbon cycling in the Rio Negro (Amazonia, Brazil), *Hydrobiologia*, 2017, **789**, 7-29 DOI: 10.1007/s10750-016-2687-9.

108. U. F. Rodríguez-Zuniga, D. M. B. P. Milori, W. T. L. Da Silva, L. Martin-Neto, L. C. Oliveira and J. C. Rocha, Changes in optical properties caused by UV-irradiation of aquatic humic substances from the amazon river basin: Seasonal variability evaluation, *Environmental science & technology*, 2008, **42**, 1948-1953 DOI: 10.1021/es702156n.

109. K. J. Ong, L. C. Felix, D. Boyle, J. D. Ede, G. Ma, J. G. Veinot and G. G. Goss, Humic acid ameliorates nanoparticle-induced developmental toxicity in zebrafish, *Environmental Science: Nano*, 2017, **4(1)**, 127-137 DOI: 10.1039/C6EN00408C.

110. L. C. Felix, E. J. Folkerts, Y. He and G. G. Goss, Poly (acrylic acid)-coated titanium dioxide nanoparticle and ultraviolet light co-exposure has minimal effect on developing zebrafish (Danio rerio), *Environmental Science: Nano*, 2017, **4(3)**, 658-669 DOI: 10.1039/C6EN00436A

111. S. George, H. Gardner, E. K. Seng, H. Chang, C. Wang, C. H. Yu Fang, M. Richards, S. Valiyaveettil and W. K. Chan, Differential effect of solar light in increasing the toxicity of silver and titanium dioxide nanoparticles to a fish cell line and zebrafish embryos, *Environmental science & technology*, 2014, **48**, 6374-6382 DOI: 10.1021/es405768n.

112. Y. Xue, Q. Luan, D. Yang, X. Yao and K. Zhou, Direct evidence for hydroxyl radical scavenging activity of cerium oxide nanoparticles, *The Journal of Physical Chemistry C*, 2011, **115**, 4433-4438 DOI: 10.1021/jp109819u.

113. M. Delay, T. Dolt, A. Woellhaf, R. Sembritzki and F. H. Frimmel, Interactions and stability of silver nanoparticles in the aqueous phase: Influence of natural organic matter (NOM) and ionic strength, *Journal of Chromatography A*, 2011, **1218**, 4206-4212 DOI: http://dx.doi.org/10.1016/j.chroma.2011.02.074.

114. N. Sani-Kast, J. Labille, P. Ollivier, D. Slomberg, K. Hungerbühler and M. Scheringer, A network perspective reveals decreasing material diversity in studies on nanoparticle interactions with dissolved organic matter, *Proceedings of the National Academy of Sciences*, 2017, DOI: 10.1073/pnas.1608106114, 201608106 DOI: 10.1073/pnas.1608106114.

115. L. Beheregaray, L. Möller, T. Schwartz, N. Chao and A. Caccone, Microsatellite markers for the cardinal tetra Paracheirodon axelrodi, a commercially important fish from central Amazonia, *Molecular Ecology Notes*, 2004, **4**, 330-332 DOI: 10.1111/j.1471-8286.2004.00686.x.

116. R. M. Duarte, D. S. Smith, A. L. Val and C. M. Wood, Dissolved organic carbon from the upper Rio Negro protects zebrafish (Danio rerio) against ionoregulatory disturbances caused by low pH exposure, *Scientific reports*, 2016, **6** DOI: 10.1038/srep20377.

117. A. Kumar, S. Babu, A. S. Karakoti, A. Schulte and S. Seal, Luminescence properties of europium-doped cerium oxide nanoparticles: role of vacancy and oxidation states, *Langmuir*, 2009, **25**, 10998-11007 DOI: 10.1021/la901298q.

118. S. G. DePalma, W. R. Arnold, J. C. McGeer, D. G. Dixon and D. S. Smith, Effects of dissolved organic matter and reduced sulphur on copper bioavailability in coastal marine environments, *Ecotoxicology and environmental safety*, 2011, **74**, 230-237 DOI: http://dx.doi.org/10.1016/j.ecoenv.2010.12.003.

119. D. R. Janero, Malondialdehyde and thiobarbituric acid-reactivity as diagnostic indices of lipid peroxidation and peroxidative tissue injury, *Free Radical Biology and Medicine*, 1990, **9**, 515-540 DOI: 10.1016/0891-5849(90)90131-2.

120. H. Linhua, W. Zhenyu and X. Baoshan, Effect of sub-acute exposure to TiO2 nanoparticles on oxidative stress and histopathological changes in Juvenile Carp (Cyprinus carpio), *Journal of Environmental Sciences*, 2009, **21**, 1459-1466 DOI: http://dx.doi.org/10.1016/S1001-0742(08)62440-7.

121. A. Rundle, A. B. Robertson, A. M. Blay, K. M. Butler, N. I. Callaghan, C. A. Dieni and T. J. MacCormack, Cerium oxide nanoparticles exhibit minimal cardiac and cytotoxicity in the freshwater fish Catostomus commersonii, *Comparative Biochemistry and Physiology Part C: Toxicology & Pharmacology*, 2016, **181**, 19-26 DOI: https://doi.org/10.1016/j.cbpc.2015.12.007.

122. B. Collin, E. Oostveen, O. V. Tsyusko and J. M. Unrine, Influence of natural organic matter and surface charge on the toxicity and bioaccumulation of functionalized ceria nanoparticles in Caenorhabditis elegans, *Environmental science & technology*, 2014, **48**, 1280-1289 DOI: 10.1021/es404503c.

123. J. Y. Ma, H. Zhao, R. R. Mercer, M. Barger, M. Rao, T. Meighan, D. Schwegler-Berry, V. Castranova and J. K. Ma, Cerium oxide nanoparticle-induced pulmonary inflammation and alveolar macrophage functional change in rats, *Nanotoxicology*, 2011, **5**, 312-325 DOI: http://dx.doi.org/10.3109/17435390.2010.519835.

124. J. Gao, K. Powers, Y. Wang, H. Zhou, S. M. Roberts, B. M. Moudgil, B. Koopman and D. S. Barber, Influence of Suwannee River humic acid on particle properties and toxicity of silver nanoparticles, *Chemosphere*, 2012, **89**, 96-101 DOI: http://dx.doi.org/10.1016/j.chemosphere.2012.04.024.

125. S. M. Hirst, A. S. Karakoti, R. D. Tyler, N. Sriranganathan, S. Seal and C. M. Reilly, Anti-inflammatory Properties of Cerium Oxide Nanoparticles, *Small*, 2009, **5**, 2848-2856 DOI: 10.1002/smll.200901048.

126. I. Celardo, M. De Nicola, C. Mandoli, J. Z. Pedersen, E. Traversa and L. Ghibelli, Ce3+ ions determine redox-dependent anti-apoptotic effect of cerium oxide nanoparticles,

Acs Nano, 2011, **5**, 4537-4549 DOI: 10.1021/nn200126a.

127. N. Meems, C. Steinberg and C. Wiegand, Direct and interacting toxicological effects on the waterflea (Daphniamagna) by natural organic matter, synthetic humic substances and cypermethrin, *Science of the total environment*, 2004, **319**, 123-136 DOI: http://dx.doi.org/10.1016/S0048-9697(03)00445-5.

128. J. F. Reeves, S. J. Davies, N. J. Dodd and A. N. Jha, Hydroxyl radicals (OH) are associated with titanium dioxide (TiO 2) nanoparticle-induced cytotoxicity and oxidative DNA damage in fish cells, *Mutation Research/Fundamental and Molecular Mechanisms of Mutagenesis*, 2008, **640**, 113-122 DOI: http://dx.doi.org/10.1016/j.mrfmmm.2007.12.010.

129. A. Nel, T. Xia, L. Mädler and N. Li, Toxic potential of materials at the nanolevel, *science*, 2006, **311**, 622-627 DOI: 10.1126/science.1114397.

130. R. D. Handy, T. B. Henry, T. M. Scown, B. D. Johnston and C. R. Tyler, Manufactured nanoparticles: their uptake and effects on fish—a mechanistic analysis, *Ecotoxicology*, 2008, **17**, 396-409 DOI: 10.1007/s10646-008-0205-1.

131. T. Xia, N. Li and A. E. Nel, Potential health impact of nanoparticles, *Annual review of public health*, 2009, **30**, 137-150 DOI: 10.1146/annurev.publhealth.031308.100155.

132. Q. Kong and C.-l. G. Lin, Oxidative damage to RNA: mechanisms, consequences, and diseases, *Cellular and Molecular Life Sciences*, 2010, **67**, 1817-1829 DOI: 10.1007/s00018-010-0277-y.

133. E. Niki, Y. Yoshida, Y. Saito and N. Noguchi, Lipid peroxidation: mechanisms, inhibition, and biological effects, *Biochemical and biophysical research communications*, 2005, **338**, 668-676 DOI: http://dx.doi.org/10.1016/j.bbrc.2005.08.072.

134. B. Halliwell and S. Chirico, Lipid peroxidation: its mechanism, measurement, and significance, *The American journal of clinical nutrition*, 1993, **57**, 715S-724S.

135. S. P. Wolff, A. Garner and R. T. Dean, Free radicals, lipids and protein degradation, *Trends in Biochemical Sciences*, 1986, **11**, 27-31 DOI: https://doi.org/10.1016/0968-0004(86)90228-8.

136. J. E. Biaglow, Y. Manevich, F. Uckun and K. D. Held, Quantitation of hydroxyl radicals produced by radiation and copper-linked oxidation of ascorbate by 2-deoxy-D-ribose method, *Free Radical Biology and Medicine*, 1997, **22**, 1129-1138 DOI: http://dx.doi.org/10.1016/S0891-5849(96)00527-8.

137. G. Federici, B. J. Shaw and R. D. Handy, Toxicity of titanium dioxide nanoparticles to rainbow trout (Oncorhynchus mykiss): gill injury, oxidative stress, and other physiological effects, *Aquatic Toxicology*, 2007, **84**, 415-430 DOI: http://dx.doi.org/10.1016/j.aquatox.2007.07.009.

138. D. Saglam, G. Atli, Z. Dogan, E. Baysoy, C. Gurler, A. Eroglu and M. Canli, Response of the antioxidant system of freshwater fish (Oreochromis niloticus) exposed to metals (Cd, Cu) in differing hardness, *Turkish Journal of Fisheries and Aquatic Sciences*, 2014, **14**, 43-52 DOI: 10.4194/1303-2712-v14_1_06.

139. J. Chen, X. Dong, Y. Xin and M. Zhao, Effects of titanium dioxide nano-particles on growth and some histological parameters of zebrafish (Danio rerio) after a long-term exposure, *Aquatic Toxicology*, 2011, **101**, 493-499 DOI:

http://dx.doi.org/10.1016/j.aquatox.2010.12.004.

140. G. A. Al-Bairuty, B. J. Shaw, R. D. Handy and T. B. Henry, Histopathological effects of waterborne copper nanoparticles and copper sulphate on the organs of rainbow trout (Oncorhynchus mykiss), *Aquatic Toxicology*, 2013, **126**, 104-115 DOI: http://dx.doi.org/10.1016/j.aquatox.2012.10.005.

141. R. J. Griffitt, R. Weil, K. A. Hyndman, N. D. Denslow, K. Powers, D. Taylor and D. S. Barber, Exposure to copper nanoparticles causes gill injury and acute lethality in zebrafish (Danio rerio), *Environmental Science & Technology*, 2007, **41**, 8178-8186 DOI: 10.1021/es071235e.

142. R. J. Griffitt, K. Hyndman, N. D. Denslow and D. S. Barber, Comparison of molecular and histological changes in zebrafish gills exposed to metallic nanoparticles, *Toxicological Sciences*, 2009, **107**, 404-415 DOI: https://doi.org/10.1093/toxsci/kfn256.

143. T. L. McBryan, T. M. Healy, K. L. Haakons and P. M. Schulte, Warm acclimation improves hypoxia tolerance in Fundulus heteroclitus, *Journal of Experimental Biology*, 2016, **219**, 474-484 DOI: 10.1242/jeb.133413.

144. T. Ostaszewska, M. Chojnacki, M. Kamaszewski and E. Sawosz-Chwalibóg, Histopathological effects of silver and copper nanoparticles on the epidermis, gills, and liver of Siberian sturgeon, *Environmental Science and Pollution Research*, 2016, **23**, 1621-1633 DOI: 10.1007/s11356-015-5391-9.

145. E. Farmen, H. Mikkelsen, Ø. Evensen, J. Einset, L. Heier, B. Rosseland, B. Salbu, K. Tollefsen and D. Oughton, Acute and sub-lethal effects in juvenile Atlantic salmon exposed to low μg/L concentrations of Ag nanoparticles, *Aquatic Toxicology*, 2012, **108**, 78-84 DOI: http://dx.doi.org/10.1016/j.aquatox.2011.07.007.

146. D. G. Kinniburgh, W. H. van Riemsdijk, L. K. Koopal, M. Borkovec, M. F. Benedetti and M. J. Avena, Ion binding to natural organic matter: competition, heterogeneity, stoichiometry and thermodynamic consistency, *Colloids and Surfaces A: Physicochemical and Engineering Aspects*, 1999, **151**, 147-166 DOI: http://dx.doi.org/10.1016/S0927-7757(98)00637-2.

147. J. Brame, M. Long, Q. Li and P. Alvarez, Inhibitory effect of natural organic matter or other background constituents on photocatalytic advanced oxidation processes: Mechanistic model development and validation, *Water research*, 2015, **84**, 362-371 DOI: http://dx.doi.org/10.1016/j.watres.2015.07.044.

148. E. T. Rodrigues, I. Lopes and M. Â. Pardal, Occurrence, fate and effects of azoxystrobin in aquatic ecosystems: a review, *Environment international*, 2013, **53**, 18-28 DOI: http://dx.doi.org/10.1016/j.envint.2012.12.005.

149. M. Kah, S. Beulke, K. Tiede and T. Hofmann, Nanopesticides: state of knowledge, environmental fate, and exposure modeling, *Critical Reviews in Environmental Science and Technology*, 2013, **43**, 1823-1867 DOI: https://doi.org/10.1080/10643389.2012.671750.

150. P. A. Olsvik, F. Kroglund, B. Finstad and T. Kristensen, Effects of the fungicide azoxystrobin on Atlantic salmon (Salmo salar L.) smolt, *Ecotoxicology and environmental safety*, 2010, **73**, 1852-1861 DOI: http://dx.doi.org/10.1016/j.ecoenv.2010.07.017.

151. F. Cao, L. Zhu, H. Li, S. Yu, C. Wang and L. Qiu, Reproductive toxicity of azoxystrobin

to adult zebrafish (Danio rerio), *Environmental Pollution*, 2016, DOI: http://dx.doi.org/10.1016/j.envpol.2016.09.015.

152. Y. Han, T. Liu, J. Wang, J. Wang, C. Zhang and L. Zhu, Genotoxicity and oxidative stress induced by the fungicide azoxystrobin in zebrafish (Danio rerio) livers, *Pesticide Biochemistry and Physiology*, 2016, DOI: http://dx.doi.org/10.1016/j.pestbp.2016.03.011.

153. A.-H. Gao, Y.-Y. Fu, K.-Z. Zhang, M. Zhang, H.-W. Jiang, L.-X. Fan, F.-J. Nan, C.-G. Yuan, J. Li and Y.-B. Zhou, Azoxystrobin, a mitochondrial complex III Q o site inhibitor, exerts beneficial metabolic effects in vivo and in vitro, *Biochimica et Biophysica Acta (BBA)-General Subjects*, 2014, **1840**, 2212-2221 DOI: https://doi.org/10.1016/j.bbagen.2014.04.002.

154. L. Liu, C. Jiang, Z.-Q. Wu, Y.-X. Gong and G.-X. Wang, Toxic effects of three strobilurins (trifloxystrobin, azoxystrobin and kresoxim-methyl) on mRNA expression and antioxidant enzymes in grass carp (Ctenopharyngodon idella) juveniles, *Ecotoxicology and environmental safety*, 2013, **98**, 297-302 DOI: http://dx.doi.org/10.1016/j.ecoenv.2013.10.011.

155. L. F. Jorgensen, J. Kjaer, P. Olsen and A. E. Rosenbom, Leaching of azoxystrobin and its degradation product R234886 from Danish agricultural field sites, *Chemosphere*, 2012, **88**, 554-562 DOI: 10.1016/j.chemosphere.2012.03.027.

156. W. A. Battaglin, M. W. Sandstrom, K. M. Kuivila, D. W. Kolpin and M. T. Meyer, Occurrence of Azoxystrobin, Propiconazole, and Selected Other Fungicides in US Streams, 2005-2006, *Water Air Soil Pollut.*, 2011, **218**, 307-322 DOI: 10.1007/s11270-010-0643-2.

157. R. P. A. van Wijngaarden, D. J. M. Belgers, M. I. Zafar, A. M. Matser, M. C. Boerwinkel and G. H. P. Arts, CHRONIC AQUATIC EFFECT ASSESSMENT FOR THE FUNGICIDE AZOXYSTROBIN, *Environmental Toxicology and Chemistry*, 2014, **33**, 2775-2785 DOI: 10.1002/etc.2739.

158. G. W. Walker, R. S. Kookana, N. E. Smith, M. Kah, C. L. Doolette, P. T. Reeves, W. Lovell, D. J. Anderson, T. W. Turney and D. A. Navarro, Ecological risk assessment of nano-enabled pesticides: a perspective on problem formulation, *Journal of agricultural and food chemistry*, 2017, **66**, 6480-6486 DOI: 10.1021/acs.jafc.7b02373.

159. H. Chhipa and P. Joshi, *Nanofertilisers, Nanopesticides and Nanosensors in Agriculture*, Springer, New York, 2016.

160. M. Kah and T. Hofmann, Nanopesticide research: current trends and future priorities, *Environment international*, 2014, **63**, 224-235 DOI: https://doi.org/10.1016/j.envint.2013.11.015.

161. J.-i. Aihara, Reduced HOMO−LUMO Gap as an Index of Kinetic Stability for Polycyclic Aromatic Hydrocarbons, *The Journal of Physical Chemistry A*, 1999, **103**, 7487-7495 DOI: 10.1021/jp990092i.

162. J.-L. Bredas, Mind the gap!, *Materials Horizons*, 2014, **1**, 17-19 DOI: 10.1039/C3MH00098B

163. Y. Ruiz-Morales, HOMO−LUMO Gap as an Index of Molecular Size and Structure for Polycyclic Aromatic Hydrocarbons (PAHs) and Asphaltenes: A Theoretical Study. I, *The Journal of Physical Chemistry A*, 2002, **106**, 11283-11308 DOI:

10.1021/jp021152e.

164.   Y. Liu, K. Lv, Y. Li, Q. Nan and J. Xu, Synthesis, fungicidal activity, structure-activity relationships (SARs) and density functional theory (DFT) studies of novel strobilurin analogues containing arylpyrazole rings, *Scientific reports*, 2018, **8** DOI: 10.1038/s41598-018-26154-5.

165.   L. C. Felix, V. A. Ortega, J. D. Ede and G. G. Goss, Physicochemical Characteristics of Polymer-Coated Metal-Oxide Nanoparticles and their Toxicological Effects on Zebrafish (Danio rerio) Development, *Environmental Science & Technology*, 2013, **47**, 6589-6596 DOI: 10.1021/es401403p.

166.   L. C. Felix, E. J. Folkerts, Y. He and G. G. Goss, Poly (acrylic acid)-coated titanium dioxide nanoparticle and ultraviolet light co-exposure has minimal effect on developing zebrafish (Danio rerio), *Environmental Science: Nano*, 2017, **4**, 658-669 DOI: 10.1039/C6EN00436A.

167.   S. Ali, H. G. Van Mil and M. K. Richardson, Large-scale assessment of the zebrafish embryo as a possible predictive model in toxicity testing, *PLoS one*, 2011, **6**, e21076 DOI: https://doi.org/10.1371/journal.pone.0021076.

168.   K. J. Ong, T. J. MacCormack, R. J. Clark, J. D. Ede, V. A. Ortega, L. C. Felix, M. K. Dang, G. Ma, H. Fenniri and J. G. Veinot, Widespread nanoparticle-assay interference: implications for nanotoxicity testing, *PLoS One*, 2014, **9**, e90650 DOI: http://dx.doi.org/10.1371/journal.pone.0090650.

169.   K. J. Livak and T. D. Schmittgen, Analysis of relative gene expression data using real-time quantitative PCR and the $2-\Delta\Delta CT$ method, *methods*, 2001, **25**, 402-408 DOI: https://doi.org/10.1006/meth.2001.1262.

170.   A. T. McCurley and G. V. Callard, Characterization of housekeeping genes in zebrafish: male-female differences and effects of tissue type, developmental stage and chemical treatment, *BMC molecular biology*, 2008, **9**, 102 DOI: https://doi.org/10.1186/1471-2199-9-102.

171.   W. Jia, L. Mao, L. Zhang, Y. Zhang and H. Jiang, Effects of two strobilurins (azoxystrobin and picoxystrobin) on embryonic development and enzyme activities in juveniles and adult fish livers of zebrafish (Danio rerio), *Chemosphere*, 2018, DOI: https://doi.org/10.1016/j.chemosphere.2018.05.138.

172.   F. Cao, P. Wu, L. Huang, H. Li, L. Qian, S. Pang and L. Qiu, Short-term developmental effects and potential mechanisms of azoxystrobin in larval and adult zebrafish (Danio rerio), *Aquatic Toxicology*, 2018, **198**, 129-140 DOI: https://doi.org/10.1016/j.aquatox.2018.02.023.

173.   D. S. Antkiewicz, C. G. Burns, S. A. Carney, R. E. Peterson and W. Heideman, Heart malformation is an early response to TCDD in embryonic zebrafish, *Toxicological Sciences*, 2005, **84**, 368-377 DOI: https://doi.org/10.1093/toxsci/kfi073.

174.   P. Asharani, Y. Lianwu, Z. Gong and S. Valiyaveettil, Comparison of the toxicity of silver, gold and platinum nanoparticles in developing zebrafish embryos, *Nanotoxicology*, 2011, **5**, 43-54 DOI: https://doi.org/10.3109/17435390.2010.489207.

175.   D. Li, M. Liu, Y. Yang, H. Shi, J. Zhou and D. He, Strong lethality and teratogenicity of strobilurins on Xenopus tropicalis embryos: Basing on ten agricultural fungicides, *Environmental Pollution*, 2016, **208**, 868-874 DOI:

https://doi.org/10.1016/j.envpol.2015.11.010.

176. D. Jardine and M. Litvak, Direct yolk sac volume manipulation of zebrafish embryos and the relationship between offspring size and yolk sac volume, *Journal of Fish Biology*, 2003, **63**, 388-397 DOI: https://doi.org/10.1046/j.1095-8649.2003.00161.x.

177. S. M. Kalasekar, E. Zacharia, N. Kessler, N. A. Ducharme, J.-Å. Gustafsson, I. A. Kakadiaris and M. Bondesson, Identification of environmental chemicals that induce yolk malabsorption in zebrafish using automated image segmentation, *Reproductive Toxicology (Elmsford, N.Y.)*, 2015, **55**, 20-29 DOI: 10.1016/j.reprotox.2014.10.022.

178. Y. Huang and S. E. Linsen, Partial depletion of yolk during zebrafish embryogenesis changes the dynamics of methionine cycle and metabolic genes, *BMC genomics*, 2015, **16**, 427 DOI: https://doi.org/10.1186/s12864-015-1654-6.

179. J. Jiang, Y. Shi, R. Yu, L. Chen and X. Zhao, Biological response of zebrafish after short-term exposure to azoxystrobin, *Chemosphere*, 2018, **202**, 56-64 DOI: https://doi.org/10.1016/j.chemosphere.2018.03.055.

180. A. Koussounadis, S. P. Langdon, I. H. Um, D. J. Harrison and V. A. Smith, Relationship between differentially expressed mRNA and mRNA-protein correlations in a xenograft model system, *Scientific reports*, 2015, **5**, 10775 DOI: 10.1038/srep10775.

181. C. Vogel and E. M. Marcotte, Insights into the regulation of protein abundance from proteomic and transcriptomic analyses, *Nature reviews genetics*, 2012, **13**, 227 DOI: 10.1038/nrg3185.

182. K. S. Echtay and M. D. Brand, 4-hydroxy-2-nonenal and uncoupling proteins: an approach for regulation of mitochondrial ROS production, *Redox Report*, 2007, **12**, 26-29 DOI: https://doi.org/10.1179/135100007X162158.

183. J. L. Campian, M. Qian, X. Gao and J. W. Eaton, Oxygen tolerance and coupling of mitochondrial electron transport, *Journal of Biological Chemistry*, 2004, **279**, 46580-46587 DOI: 10.1074/jbc.M406685200.

184. S. Zigman, J. Reddan, J. B. Schultz and T. McDaniel, Structural and functional changes in catalase induced by near-UV radiation, *Photochemistry and photobiology*, 1996, **63**, 818-824 DOI: https://doi.org/10.1111/j.1751-1097.1996.tb09637.x.

185. G. Formicki and R. Stawarz, Ultraviolet influence on catalase activity and mineral content in eyeballs of gibel carp (Carassius auratus gibelio), *Science of the total environment*, 2006, **369**, 447-450 DOI: https://doi.org/10.1016/j.scitotenv.2006.07.021.

186. A. Ayala, M. F. Muñoz and S. Argüelles, Lipid peroxidation: production, metabolism, and signaling mechanisms of malondialdehyde and 4-hydroxy-2-nonenal, *Oxidative medicine and cellular longevity*, 2014, **2014** DOI: http://dx.doi.org/10.1155/2014/360438.

187. H. Esterbauer and K. H. Cheeseman, in *Methods in enzymology*, Elsevier, 1990, vol. 186, pp. 407-421.

188. S. Dalleau, M. Baradat, F. Gueraud and L. Huc, Cell death and diseases related to oxidative stress: 4-hydroxynonenal (HNE) in the balance, *Cell death and differentiation*, 2013, **20**, 1615 DOI: 10.1038/cdd.2013.138.

189. M. A. Lampi, J. Gurska, K. I. McDonald, F. Xie, X. D. Huang, D. G. Dixon and B. M. Greenberg, Photoinduced toxicity of polycyclic aromatic hydrocarbons to Daphnia magna: Ultraviolet-mediated effects and the toxicity of polycyclic aromatic

hydrocarbon photoproducts, *Environmental Toxicology and Chemistry: An International Journal*, 2006, **25**, 1079-1087 DOI: https://doi.org/10.1897/05-276R.1.

190. J. L. Kunz, C. G. Ingersoll, K. L. Smalling, A. A. Elskus and K. M. Kuivila, Chronic toxicity of azoxystrobin to freshwater amphipods, midges, cladocerans, and mussels in water-only exposures, *Environmental toxicology and chemistry*, 2017, **36**, 2308-2315 DOI: 10.1002/etc.3764.

191. I. Brandts, M. Teles, A. Gonçalves, A. Barreto, L. Franco-Martinez, A. Tvarijonaviciute, M. Martins, A. Soares, L. Tort and M. Oliveira, Effects of nanoplastics on Mytilus galloprovincialis after individual and combined exposure with carbamazepine, *Science of The Total Environment*, 2018, **643**, 775-784 DOI: https://doi.org/10.1016/j.scitotenv.2018.06.257.

192. K. Chidambarampadmavathy, O. P. Karthikeyan and K. Heimann, Sustainable bio-plastic production through landfill methane recycling, *Renewable and Sustainable Energy Reviews*, 2017, **71**, 555-562 DOI: https://doi.org/10.1016/j.rser.2016.12.083.

193. J. Wang, X. Liu, G. Liu, Z. Zhang, H. Wu, B. Cui, J. Bai and W. Zhang, Size effect of polystyrene microplastics on sorption of phenanthrene and nitrobenzene, *Ecotoxicology and Environmental Safety*, 2019, **173**, 331-338 DOI: https://doi.org/10.1016/j.ecoenv.2019.02.037.

194. Q. Chen, M. Gundlach, S. Yang, J. Jiang, M. Velki, D. Yin and H. Hollert, Quantitative investigation of the mechanisms of microplastics and nanoplastics toward zebrafish larvae locomotor activity, *Science of the Total Environment*, 2017, **584**, 1022-1031 DOI: https://doi.org/10.1016/j.scitotenv.2017.01.156.

195. Y. Chae and Y.-J. An, Effects of micro-and nanoplastics on aquatic ecosystems: Current research trends and perspectives, *Marine Pollution Bulletin*, 2017, **124**, 624-632 DOI: https://doi.org/10.1016/j.marpolbul.2017.01.070.

196. J. P. da Costa, P. S. Santos, A. C. Duarte and T. Rocha-Santos, (Nano) plastics in the environment–sources, fates and effects, *Science of The Total Environment*, 2016, **566**, 15-26 DOI: https://doi.org/10.1016/j.scitotenv.2016.05.041.

197. M. Cole, P. Lindeque, C. Halsband and T. S. Galloway, Microplastics as contaminants in the marine environment: a review, *Marine Pollution Bulletin*, 2011, **62**, 2588-2597 DOI: https://doi.org/10.1016/j.marpolbul.2011.09.025.

198. O. Pikuda, E. G. Xu, D. Berk and N. Tufenkji, Toxicity Assessments of Micro-and Nanoplastics Can Be Confounded by Preservatives in Commercial Formulations, *Environmental Science & Technology Letters*, 2018, **6**, 21-25 DOI: https://doi.org/10.1021/acs.estlett.8b00614.

199. M. A. Browne, S. J. Niven, T. S. Galloway, S. J. Rowland and R. C. Thompson, Microplastic moves pollutants and additives to worms, reducing functions linked to health and biodiversity, *Current Biology*, 2013, **23**, 2388-2392 DOI: https://doi.org/10.1016/j.cub.2013.10.012.

200. L. Manfra, A. Rotini, E. Bergami, G. Grassi, C. Faleri and I. Corsi, Comparative ecotoxicity of polystyrene nanoparticles in natural seawater and reconstituted seawater using the rotifer Brachionus plicatilis, *Ecotoxicology and Environmental Safety*, 2017, **145**, 557-563 DOI: 10.1016/j.ecoenv.2017.07.068.

201. E. Besseling, B. Wang, M. Lürling and A. A. Koelmans, Nanoplastic affects growth of

S. obliquus and reproduction of D. magna, *Environmental Science & Technology*, 2014, **48**, 12336-12343 DOI: https://doi.org/10.1021/es503001d.

202. T. Cedervall, L.-A. Hansson, M. Lard, B. Frohm and S. Linse, Food chain transport of nanoparticles affects behaviour and fat metabolism in fish, *PloS one*, 2012, **7**, e32254 DOI: https://doi.org/10.1371/journal.pone.0032254.

203. K. Mattsson, M. T. Ekvall, L.-A. Hansson, S. Linse, A. Malmendal and T. Cedervall, Altered behavior, physiology, and metabolism in fish exposed to polystyrene nanoparticles, *Environmental Science & Technology*, 2014, **49**, 553-561 DOI: https://doi.org/10.1021/es5053655.

204. A. L. Andrady, Microplastics in the marine environment, *Marine Pollution Bulletin*, 2011, **62**, 1596-1605 DOI: 10.1021/es2031505.

205. Y. Ma, A. Huang, S. Cao, F. Sun, L. Wang, H. Guo and R. Ji, Effects of nanoplastics and microplastics on toxicity, bioaccumulation, and environmental fate of phenanthrene in fresh water, *Environmental Pollution*, 2016, **219**, 166-173 DOI: https://doi.org/10.1016/j.envpol.2016.10.061.

206. A. Binelli, L. Del Giacco, N. Santo, L. Bini, S. Magni, M. Parolini, L. Madaschi, A. Ghilardi, D. Maggioni and M. Ascagni, Carbon nanopowder acts as a Trojan-horse for benzo (α) pyrene in Danio rerio embryos, *Nanotoxicology*, 2017, **11**, 371-381 DOI: https://doi.org/10.1080/17435390.2017.1306130.

207. C. Della Torre, E. Bergami, A. Salvati, C. Faleri, P. Cirino, K. Dawson and I. Corsi, Accumulation and embryotoxicity of polystyrene nanoparticles at early stage of development of sea urchin embryos Paracentrotus lividus, *Environmental Science & Technology*, 2014, **48**, 12302-12311 DOI: https://doi.org/10.1021/es502569w.

208. A. J. Hill, H. Teraoka, W. Heideman and R. E. Peterson, Zebrafish as a model vertebrate for investigating chemical toxicity, *Toxicological Sciences*, 2005, **86**, 6-19 DOI: https://doi.org/10.1093/toxsci/kfi110.

209. S. Böhme, M. Baccaro, M. Schmidt, A. Potthoff, H.-J. Stärk, T. Reemtsma and D. Kühnel, Metal uptake and distribution in the zebrafish (Danio rerio) embryo: differences between nanoparticles and metal ions, *Environmental Science: Nano*, 2017, **4**, 1005-1015 DOI: 10.1039/C6EN00440G.

210. Y. Zhang, C. Sheedy, D. Nilsson and G. G. Goss, Evaluation of interactive effects of UV light and nano encapsulation on the toxicity of azoxystrobin on zebrafish, *Nanotoxicology*, 2019, 1-18 DOI: https://doi.org/10.1080/17435390.2019.1690064.

211. Y. He, S. L. Flynn, E. J. Folkerts, Y. Zhang, D. Ruan, D. S. Alessi, J. W. Martin and G. G. Goss, Chemical and toxicological characterizations of hydraulic fracturing flowback and produced water, *Water Research*, 2017, **114**, 78-87 DOI: https://doi.org/10.1016/j.watres.2017.02.027.

212. A. A. Koelmans, E. Besseling and W. J. Shim, in *Marine anthropogenic litter*, Springer, 2015, pp. 325-340.

213. L. Liu, R. Fokkink and A. A. Koelmans, Sorption of polycyclic aromatic hydrocarbons to polystyrene nanoplastic, *Environmental Toxicology and Chemistry*, 2016, **35**, 1650-1655 DOI: https://doi.org/10.1002/etc.3311.

214. M. R. Hamblin, P. Avci and T. Prow, *Nanoscience in dermatology*, Academic Press, 2016.

215. C. B. Kimmel, W. W. Ballard, S. R. Kimmel, B. Ullmann and T. F. Schilling, Stages of embryonic development of the zebrafish, *Developmental Dynamics*, 1995, **203**, 253-310 DOI: https://doi.org/10.1002/aja.100203030.

216. Z. Liu, P. Yu, M. Cai, D. Wu, M. Zhang, Y. Huang and Y. Zhao, Polystyrene nanoplastic exposure induces immobilization, reproduction, and stress defense in the freshwater cladoceran Daphnia pulex, *Chemosphere*, 2019, **215**, 74-81 DOI: https://doi.org/10.1016/j.chemosphere.2018.09.176.

217. U. Gündel, S. Kalkhof, D. Zitzkat, M. von Bergen, R. Altenburger and E. Küster, Concentration–response concept in ecotoxicoproteomics: Effects of different phenanthrene concentrations to the zebrafish (Danio rerio) embryo proteome, *Ecotoxicology and Environmental Safety*, 2012, **76**, 11-22 DOI: https://doi.org/10.1016/j.ecoenv.2011.10.010.

218. K. J. Ong, L. C. Felix, D. Boyle, J. D. Ede, G. Ma, J. G. Veinot and G. G. Goss, Humic acid ameliorates nanoparticle-induced developmental toxicity in zebrafish, *Environmental Science: Nano*, 2017, **4**, 127-137 DOI: 10.1039/C6EN00408C.

219. Q. Chen, D. Yin, Y. Jia, S. Schiwy, J. Legradi, S. Yang and H. Hollert, Enhanced uptake of BPA in the presence of nanoplastics can lead to neurotoxic effects in adult zebrafish, *Science of the Total Environment*, 2017, **609**, 1312-1321 DOI: https://doi.org/10.1016/j.scitotenv.2017.07.144.

220. A. T. B. Guimarães, F. N. Estrela, P. S. Pereira, J. E. de Andrade Vieira, A. S. de Lima Rodrigues, F. G. Silva and G. Malafaia, Toxicity of polystyrene nanoplastics in Ctenopharyngodon idella juveniles: A genotoxic, mutagenic and cytotoxic perspective, *Science of The Total Environment*, 2020, **752**, 141937 DOI: https://doi.org/10.1016/j.scitotenv.2020.141937.

221. J. Wu, R. Jiang, W. Lin and G. Ouyang, Effect of salinity and humic acid on the aggregation and toxicity of polystyrene nanoplastics with different functional groups and charges, *Environmental Pollution*, 2019, **245**, 836-843 DOI: https://doi.org/10.1016/j.envpol.2018.11.055.

222. I. Brandts, J. Balasch, A. Tvarijonaviciute, A. Barreto, M. Martins, L. Tort, M. Oliveira and M. Teles, 2019.

223. S. Gangadoo, S. Owen, P. Rajapaksha, K. Plastaid, S. Cheeseman, H. Haddara, V. K. Truong, S. T. Ngo, V. V. Vu and D. Cozzolino, Nano-plastics and their analytical characterisation and fate in the marine environment: From Source to Sea, *Science of The Total Environment*, 2020, 138792 DOI: https://doi.org/10.1016/j.scitotenv.2020.138792.

224. M. A. Browne, S. J. Niven, T. S. Galloway, S. J. Rowland and R. C. J. C. B. Thompson, Microplastic moves pollutants and additives to worms, reducing functions linked to health and biodiversity, 2013, **23**, 2388-2392 DOI: https://doi.org/10.1016/j.cub.2013.10.012.

225. K. Fent and R. Bätscher, Cytochrome P4501A induction potencies of polycyclic aromatic hydrocarbons in a fish hepatoma cell line: demonstration of additive interactions, *Environmental Toxicology and Chemistry: An International Journal*, 2000, **19**, 2047-2058 DOI: https://doi.org/10.1002/etc.5620190813.

226. M. Oliveira, M. Pacheco and M. Santos, Cytochrome P4501A, genotoxic and stress

responses in golden grey mullet (Liza aurata) following short-term exposure to phenanthrene, *Chemosphere*, 2007, **66**, 1284-1291 DOI: https://doi.org/10.1016/j.chemosphere.2006.07.024.

227. S. Billiard, N. Bols and P. Hodson, In vitro and in vivo comparisons of fish-specific CYP1A induction relative potency factors for selected polycyclic aromatic hydrocarbons, *Ecotoxicology and environmental safety*, 2004, **59**, 292-299 DOI: https://doi.org/10.1016/j.ecoenv.2004.06.009.

228. J. Mu, J. Wang, F. Jin, X. Wang and H. Hong, Comparative embryotoxicity of phenanthrene and alkyl-phenanthrene to marine medaka (Oryzias melastigma), *Marine pollution bulletin*, 2014, **85**, 505-515 DOI: https://doi.org/10.1016/j.marpolbul.2014.01.040.

229. Y. Zhang and G. G. Goss, Potentiation of polycyclic aromatic hydrocarbon uptake in zebrafish embryos by nanoplastics, *Environmental Science: Nano*, 2020, DOI: 10.1039/D0EN00163E DOI: 10.1039/D0EN00163E

230. J. Bhagat, N. Nishimura and Y. Shimada, Toxicological interactions of microplastics/nanoplastics and environmental contaminants: Current Knowledge and Future Perspectives, *Journal of Hazardous Materials*, 2020, DOI: https://doi.org/10.1016/j.jhazmat.2020.123913.

231. M. Aeschbacher, S. H. Brunner, R. P. Schwarzenbach and M. Sander, Assessing the effect of humic acid redox state on organic pollutant sorption by combined electrochemical reduction and sorption experiments, *Environmental science & technology*, 2012, **46**, 3882-3890 DOI: https://doi.org/10.1021/es204496d.

232. S. Noventa, D. Rowe and T. Galloway, Mitigating effect of organic matter on the in vivo toxicity of metal oxide nanoparticles in the marine environment, *Environ.-Sci. Nano*, 2018, **5**, 1764-1777 DOI: 10.1039/c8en00175h.

233. Y. He, E. J. Folkerts, Y. Zhang, J. W. Martin, D. S. Alessi and G. G. Goss, Effects on biotransformation, oxidative stress, and endocrine disruption in rainbow trout (Oncorhynchus mykiss) exposed to hydraulic fracturing flowback and produced water, *Environmental science & technology*, 2017, **51**, 940-947 DOI: https://doi.org/10.1021/acs.est.6b04695.

234. E. M. Jönsson, A. Abrahamson, B. Brunström and I. Brandt, Cytochrome P4501A induction in rainbow trout gills and liver following exposure to waterborne indigo, benzo [a] pyrene and 3, 3′, 4, 4′, 5-pentachlorobiphenyl, *Aquatic Toxicology*, 2006, **79**, 226-232 DOI: https://doi.org/10.1016/j.aquatox.2006.06.006.

235. P. V. Hodson, P. Kloepper-Sams, K. Munkittrick, W. Lockhart, D. Metner, P. Luxon, I. Smith, M. Gagnon, M. Servos and J. Payne, Protocols for measuring mixed function oxygenases of fish liver, 1991.

236. O. S. Alimi, J. Farner Budarz, L. M. Hernandez, N. J. E. s. Tufenkji and technology, Microplastics and nanoplastics in aquatic environments: aggregation, deposition, and enhanced contaminant transport, 2018, **52**, 1704-1724 DOI: https://doi.org/10.1021/acs.est.7b05559.

237. F. Abdolahpur Monikh, M. G. Vijver, Z. Guo, P. Zhang, G. K. Darbha and W. J. G. M. Peijnenburg, Metal sorption onto nanoscale plastic debris and trojan horse effects in Daphnia magna: Role of dissolved organic matter, *Water Research*, 2020, **186**, 116410

DOI: https://doi.org/10.1016/j.watres.2020.116410.

238. R. Trevisan, D. Uzochukwu and R. T. Di Giulio, PAH Sorption to Nanoplastics and the Trojan Horse Effect as Drivers of Mitochondrial Toxicity and PAH Localization in Zebrafish, *Frontiers in Environmental Science*, 2020, DOI: https://doi.org/10.3389/fenvs.2020.00078.

239. S. Chianese, A. Fenti, P. Iovino, D. Musmarra and S. Salvestrini, Sorption of organic pollutants by humic acids: A review, *Molecules*, 2020, **25**, 918 DOI: https://doi.org/10.3390/molecules25040918.

240. K. IKEDA, Y. SHIMIZU, T. OGURI and S. MATSUI, Sorption of Endocrine Disruptors onto Cell Membrane and the Effect of NOM, *ENVIRONMENTAL ENGINEERING RESEARCH*, 2003, **40**, 627-637 DOI: https://doi.org/10.11532/proes1992.40.627.

241. M. E. Jönsson, B. Brunström and I. Brandt, The zebrafish gill model: Induction of CYP1A, EROD and PAH adduct formation, *Aquatic Toxicology*, 2009, **91**, 62-70 DOI: https://doi.org/10.1016/j.aquatox.2008.10.010.

242. G. M. Hughes, Morphometrics of fish gills, *Respiration Physiology*, 1972, **14**, 1-25 DOI: https://doi.org/10.1016/0034-5687(72)90014-X.

243. G. Flik and P. M. Verbost, CALCIUM TRANSPORT IN FISH GILLS AND INTESTINE, *The Journal of Experimental Biology*, 1993, **184**, 17.

244. Z. Li, C. Feng, Y. Wu and X. Guo, Impacts of nanoplastics on bivalve: Fluorescence tracing of organ accumulation, oxidative stress and damage, *Journal of Hazardous Materials*, 2020, 122418 DOI: https://doi.org/10.1016/j.jhazmat.2020.122418.

245. A. B. Sengul and E. Asmatulu, Toxicity of metal and metal oxide nanoparticles: a review, *Environmental Chemistry Letters*, 2020, DOI: 10.1007/s10311-020-01033-6, 1-25 DOI: 10.1007/s10311-020-01033-6.

246. J. Jeevanandam, A. Barhoum, Y. S. Chan, A. Dufresne and M. K. Danquah, Review on nanoparticles and nanostructured materials: history, sources, toxicity and regulations, *Beilstein journal of nanotechnology*, 2018, **9**, 1050-1074.

247. M. Ajdary, M. A. Moosavi, M. Rahmati, M. Falahati, M. Mahboubi, A. Mandegary, S. Jangjoo, R. Mohammadinejad and R. S. Varma, Health concerns of various nanoparticles: a review of their in vitro and in vivo toxicity, *Nanomaterials*, 2018, **8**, 634 DOI: https://doi.org/10.3390/nano8090634.

248. T. A. Blewett, A. A. Qi, Y. Zhang, A. M. Weinrauch, S. D. Blair, E. J. Folkerts, C. Sheedy, D. Nilsson and G. G. Goss, Correction: Toxicity of nanoencapsulated bifenthrin to rainbow trout (Oncorhynchus mykiss), *Environmental Science: Nano*, 2019, **6**, 3171-3171 DOI: 10.1039/C9EN90052G.

249. R. Geyer, J. R. Jambeck and K. L. Law, Production, use, and fate of all plastics ever made, *Science advances*, 2017, **3**, e1700782 DOI: 10.1126/sciadv.1700782.

250. A. Turner, R. Arnold and T. Williams, Weathering and persistence of plastic in the marine environment: Lessons from LEGO, *Environmental Pollution*, 2020, 114299.

251. E. Fries, C. J. E. S. Zarfl and P. Research, Sorption of polycyclic aromatic hydrocarbons (PAHs) to low and high density polyethylene (PE), 2012, **19**, 1296-1304.

252. K. Rasmussen, H. Rauscher, P. Kearns, M. González and J. Riego Sintes, Developing OECD test guidelines for regulatory testing of nanomaterials to ensure mutual acceptance of test data, *Regulatory Toxicology and Pharmacology*, 2019, **104**, 74-83

DOI: https://doi.org/10.1016/j.yrtph.2019.02.008.

253. X. Gao and G. V. Lowry, Progress towards standardized and validated characterizations for measuring physicochemical properties of manufactured nanomaterials relevant to nano health and safety risks, *NanoImpact*, 2018, **9**, 14-30 DOI: https://doi.org/10.1016/j.impact.2017.09.002.

254. K. Hund-Rinke, A. Baun, D. Cupi, T. F. Fernandes, R. Handy, J. H. Kinross, J. M. Navas, W. Peijnenburg, K. Schlich, B. J. Shaw and J. J. Scott-Fordsmand, Regulatory ecotoxicity testing of nanomaterials – proposed modifications of OECD test guidelines based on laboratory experience with silver and titanium dioxide nanoparticles, *Nanotoxicology*, 2016, **10**, 1442-1447 DOI: 10.1080/17435390.2016.1229517.

Appendices

Supplemental Tables

Table S2-1. The concentrations (mg L^{-1}) of dissolved organic carbon (mg L^{-1}) in stock NOM water and NOM water without NPs at 48 hours and 96 hours with and without UV exposure. Values are mean ± standard deviation. Groups that share the same letter indicate no significance ($p > 0.05$).

Samples	UV exposure	Dissolved organic carbon (mg L^{-1})
Stock NOM	No	14.78±1.10[a]
NOM at 0 mg L^{-1}, 48 hours	Yes	14.07±0.69[a]
NOM at 0 mg L^{-1}, 48 hours	No	13.01±0.50[a]
NOM at 0 mg L^{-1}, 96 hours	Yes	13.50±0.56[a]
NOM at 0 mg L^{-1}, 96 hours	No	14.09±0.56[a]

Table S2-2. Absolute Fractions (arb units) of humic acid, fulvic acid, tryrosine and tryotophan- like fraction of experimental DOC's under Ultraviolet (UV) light and no UV light. Means are ± S.E.M (n=3 per treatment). Groups that share the same letter indicate no significance ($p > 0.05$).

Sample	Humic Acid	Fulvic Acid	Tyrosine	Tryptophan
Stock	2.9 ± 0.04[a]	1.2 ± 0.002[a]	0.11 ± 0.01[a]	0.15 ± 0.01[a]
48 hour No UV	2.9 ± 0.05[a]	1.30 ± 0.01[b]	0.1 ± 0.02[a]	0.15 ± 0.02[a]
48 hour UV	2.5±0.05[b]	1.60±0.007[c]	0.18±0.006[bd]	0.12±0.03[a]
96 hour No UV	3.0±0.02[a]	1.4±0.01[d]	0.13±0.004[ad]	0.20±0.007[a]
96 hour UV	2.3±0.0004[c]	1.85±0.0007[e]	0.21±0.007[bc]	0.19±0.008[a]

Table S2-3. The ICP-MS analysis of total cerium concentrations from the water samples collected during exposure of CeO$_2$ NPs at 0, 12, 48 and 96 hours. The results of the nominal concentration of 0.5 mg L^{-1} were not shown in the table because they were all below the detection limit (BDL, 0.048 mg L^{-1}).

Nominal Concentration (mg L^{-1})	Time (hours)	Water	UV	Detected concentration (mg L^{-1})
2	0	ddH$_2$O	No	0.73
2	12	ddH$_2$O	No	0.060
2	48	ddH$_2$O	No	BDL
2	96	ddH$_2$O	No	BDL
2	0	ddH$_2$O	Yes	0.56
2	12	ddH$_2$O	Yes	0.098
2	48	ddH$_2$O	Yes	0.28
2	96	ddH$_2$O	Yes	0.80
2	0	NOM	No	0.83
2	12	NOM	No	0.45
2	48	NOM	No	0.32
2	96	NOM	No	0.19
2	0	NOM	Yes	0.83
2	12	NOM	Yes	0.50
2	48	NOM	Yes	0.46
2	96	NOM	Yes	0.52
5	0	ddH$_2$O	No	2.2
5	12	ddH$_2$O	No	1.6
5	48	ddH$_2$O	No	0.98
5	96	ddH$_2$O	No	0.88
5	0	ddH$_2$O	Yes	1.8
5	12	ddH$_2$O	Yes	1.3
5	48	ddH$_2$O	Yes	1.2
5	96	ddH$_2$O	Yes	1.2
5	0	NOM	No	1.9
5	12	NOM	No	0.30
5	48	NOM	No	0.19
5	96	NOM	No	0.028
5	0	NOM	Yes	1.7
5	12	NOM	Yes	0.36
5	48	NOM	Yes	0.16
5	96	NOM	Yes	0.35

Table S2-4. The polydispersity index (PDI), PDI width (nm) and hydrodynamic diameter (HDD) of CeO$_2$ NPs at a nominal concentration of 0.5, 2 and 5 mg L^{-1} in ddH$_2$O (NOM-) measured by DLS at 0, 2, 4, 6, 12, 24, 48, 72 and 96 hours.

Time (hours)	Nominal concentration (mg/L)	Average PDI	Average PDI width (nm)	Average HDD (nm)	SEM PDI	SEM PDI width (nm)	SEM HDD (nm)
0	0.5	0.957	2965.7	2994.3	0.043	905.5	877.5
	2	1.000	3782.7	3783.3	0.000	1025.2	1025.7
	5	1.000	3120.0	3120.3	0.000	769.0	768.8
2	0.5	1.000	1991.0	1991.3	0.000	91.3	91.3
	2	0.964	2002.0	2025.0	0.036	615.3	600.3
	5	1.000	1738.0	1738.0	0.000	87.6	87.6
4	0.5	0.933	1795.7	1827.1	0.067	458.6	427.6
	2	0.967	2048.0	2074.7	0.033	327.5	306.4
	5	0.924	1572.7	1615.3	0.076	346.5	306.5
6	0.5	0.876	1189.9	1224.7	0.062	203.4	182.4
	2	0.893	1542.8	1603.1	0.074	434.9	400.1
	5	0.932	1323.3	1390.7	0.025	116.1	135.3
12	0.5	0.861	1166.8	1248.6	0.070	201.0	181.3
	2	0.799	819.2	908.1	0.088	133.8	98.1
	5	0.730	607.2	707.8	0.057	99.7	96.5
24	0.5	0.753	812.2	904.7	0.118	259.5	236.4
	2	0.592	501.1	646.8	0.056	73.2	64.4
	5	0.576	399.8	522.8	0.112	76.7	49.8
48	0.5	0.635	572.3	717.0	0.026	39.0	34.1
	2	0.561	392.9	516.4	0.097	90.9	73.8
	5	0.462	290.8	426.5	0.034	32.0	36.6
72	0.5	0.614	523.9	596.6	0.062	37.4	48.0
	2	0.639	540.9	676.7	0.046	40.4	36.7
	5	0.447	284.2	409.9	0.072	87.4	103.7
96	0.5	0.614	497.2	633.5	0.060	46.7	33.7
	2	0.612	527.1	665.9	0.073	101.9	87.1
	5	0.447	273.7	406.3	0.051	44.3	47.1

Table S2-5. The polydispersity index (PDI), PDI width (nm) and hydrodynamic diameter (HDD) of CeO$_2$ NPs at a nominal concentration of 0.5, 2 and 5 mg L^{-1} in Rio Negro water (NOM+) measured by DLS at 0, 2, 4, 6, 12, 24, 48, 72 and 96 hours.

Time (hours)	Nominal concentration (mg/L)	Average PDI	Average PDI width (nm)	Average HDD (nm)	SEM PDI	SEM PDI width (nm)	SEM HDD (nm)
0	0.5	0.688	674.9	797.5	0.087	178.9	161.6
	2	0.966	1742.6	1760.5	0.034	427.4	409.8
	5	0.997	1787.3	1789.0	0.003	293.3	291.9
2	0.5	0.673	574.2	713.9	0.069	95.2	75.9
	2	0.871	886.2	942.6	0.096	161.2	139.0
	5	0.831	673.3	733.3	0.085	122.2	104.6
4	0.5	0.627	500.3	622.2	0.104	104.3	88.6
	2	0.832	813.8	887.6	0.069	104.1	76.3
	5	0.838	728.5	793.6	0.034	150.3	155.9
6	0.5	0.707	546.8	646.0	0.116	98.6	82.2
	2	0.816	792.0	854.6	0.120	275.2	242.7
	5	0.695	508.0	601.8	0.038	98.5	102.4
12	0.5	0.645	574.3	514.3	0.058	62.3	54.8
	2	0.693	647.8	647.8	0.063	28.3	28.3
	5	0.753	718.4	718.4	0.128	120.1	120.1
24	0.5	0.583	473.7	473.7	0.083	15.3	15.3
	2	0.583	444.9	444.9	0.032	44.9	44.9
	5	0.488	346.1	346.1	0.044	22.2	22.2
48	0.5	0.347	302.4	302.4	0.014	20.8	20.8
	2	0.400	357.7	357.7	0.049	54.8	54.8
	5	0.363	317.4	317.4	0.044	27.5	27.5
72	0.5	0.452	355.9	355.9	0.052	60.6	60.6
	2	0.412	275.2	275.6	0.040	30.6	30.2
	5	0.367	229.5	229.5	0.024	19.3	19.3
96	0.5	0.420	193.6	303.7	0.055	19.3	40.6
	2	0.492	199.3	285.2	0.110	31.8	12.6
	5	0.440	142.1	214.2	0.053	12.9	6.8

Table S3-1. Gene-specific primers for zebrafish. Abbreviation of gene names, NCBI reference sequence, forward and reverse primer sequences

(5'-3'), amplicon size in base pairs and amplification efficiency measured by a quantitative polymerase chain reaction.

Gene	Accession no.	Forward primer 5'–3'	Reverse primer 5'–3'	Amplicon size (bp)	Eff.
ef1α	NM_131263.1	TTCTCAGGCTGACTGTGCTG	GGGTCTGTCCGTTCTTGGAG	83	2.02
cat	NM_130912.2	GAGAGAGTCGTGCATGCTAAA	GATCGGTGTCGTCTTTCCAATA	117	2.00
sod1	NM_131294	TCGGAGACCTGGGTAATGT	CACCATGGTCCTCCCAATAAT	113	2.02
sod2	NM_199976.1	GAGCCTCACATCTGTGCTGA	CTTGGCCAGAGCCTCTTGAT	111	1.98
gpx1a	NM_001007281.2	TTTACGACCTGTCCGCGAAA	CTGTTGTGCCTCAAAGCGAC	108	1.98
gpx1b	NM_001004634	GAGTCCCGTATGCAGAAATGA	TCAGGAATCTCCGGCTGTA	98	1.99

Table S3-2. The linear relationship between measured concentrations (y) and nominal

concentration (x) for two types of azoxystrobin under laboratory light and UV light.

Azoxystrobin	No UV	UV
Nano-enabled	y = 0.7113x + 23.798	y = 0.6184x + 22.341
	R^2 = 0.852	R^2 = 0.957
Conventional	y = 0.3768x + 99.825	y = 0.3493x + 101.2
	R^2 = 0.957	R^2 = 0.940

Table S3-3. Probit analysis of LC$_{50}$ values of nano-enabled and conventional azoxystrobin under laboratory light and UV light at nominal concentration and measured concentration. Values are mean. Ranges are 95% confidence interval (95% CI).

Azoxystrobin	Concentration	No UV (95%CI)	UV (95%CI)
Nano-enabled	Nominal	341 µg L^{-1} (328-356)	162 µg L^{-1} (147-181)
	Measured	267 µg L^{-1} (257-278)	131 µg L^{-1} (123-139)
Conventional form	Nominal	937 µg L^{-1} (820-1072)	404 µg L^{-1} (353-462)
	Measured	463 µg L^{-1} (422-509)	248 µg L^{-1} (228-271)

Table S3-4. The QA/QC measures for Azoxystrobin. All samples were run against a 10 point standard curve to ensure that the GC/MS/MS analysis is reporting standards and samples with the same internal condition. Characteristic accuracy for azoxystrobin R^2 was ~0.999.

	Level of Quantitation ($\mu g\ L^{-1}$)	Recovery %		Spiking Amounts ($\mu g\ L^{-1}$)	
		High	Low	High	Low
Azoxystrobin	0.113	111.5	103.5	116.21	23.24

Table S4-1. Characteristics of microplastics and nanoplastics.

	Primary diameter (nm)	Theoretical surface area (nm^2)	Number of particles per mL at 100 mg L^{-1}	Total theoretical surface area (nm^2)
20 nm PS-NPLs	27	2290	2.25×10^{11}	5.15×10^{14}
500 nm PS-NPLs	480	7.24×10^5	4.0×10^7	2.89×10^{13}

Table S4-2. The hydrodynamic diameters (HD), polydispersity index and zeta-potential of non-dialyzed and dialyzed PS-NPLs.

Values are mean ± SD. n=3.

PS-NPLs	HD (nm)		PDI		Zeta-potential (mV)	
	0 h	96 h	0 h	96 h	0 h	96 h
Non-dialyzed 20 nm	35.5±2	39.2±7	0.154±0.011	0.153±0.006	-11.9±0.2	-13.6±1
Dialyzed 20nm	37.7±4	40.3±6	0.147±0.006	0.163±0.004	-11.8±0.4	-13.0±0.3
Non-dialyzed 500 nm	527.2±10	542.7±24	0.149±0.014	0.226±0.017	-11.9±0.2	-12.4±0.4
Dialyzed 500nm	522.6±17	539.9±11	0.147±0.071	0.152±0.014	-12.2±0.3	-12.2±0.4

Table S4-3. Mean values (±S.D.) of the wet weight of 10 intact zebrafish embryos and 10 dechorionated embryos exposed to 20 nm or 500 nm PS-NPLs at 4 and 24 hpf (n=5).

		Wet weight (mg)	
		Intact embryo	Dechorionated embryo
No PS-NPLs	4 hpf	11.3 ± 0.58	3.74± 0.52
	24 hpf	11.1 ± 0.67	3.66 ± 0.64
20 nm PS-NPLs treated	4 hpf	10.9 ±0.64	3.61±0.55
	24 hpf	10.6 ±0.52	3.57±0.50
500 nm PS-NPLs treated	4 hpf	11.0 ±0.66	3.59±0.48
	24 hpf	10.7 ±0.59	3.62±0.76

Table S5-1. The hydrodynamic diameters (HD), polydispersity index, and zeta-potential of dialyzed PS-NPLs at 0, 4 and 24 h.

Lowercase letters were used to compare 20 nm with or without NOM, while uppercase letters were used to compare 500 nm with or without NOM. Means sharing the same letter are not significantly different from each other (p > 0.05). Values are mean ± SD. n=3.

PS-NPLs	HD (nm)			PDI			Zeta-potential (mV)		
	0 h	4 h	24h	0 h	4 h	24h	0 h	4 h	24h
20 nm	37.3 ± 1.0^a	37.6 ± 0.7^a	41.0 ± 1.5^a	0.148 ± 0.004^a	0.150 ± 0.002^a	0.159 ± 0.008^a	-12.1 ± 0.7^a	-12.3 ± 0.3^{ab}	-12.7 ± 0.3^{bc}
20 nm + NOM	35.6 ± 2.5^a	36.7 ± 0.4^a	40.4 ± 2.1^a	0.144 ± 0.005^a	0.145 ± 0.004^a	0.148 ± 0.004^a	-12.8 ± 0.4^{bc}	-12.6 ± 0.3^{bc}	-13.0 ± 0.3^c
500 nm	556 ± 8^A	560 ± 6^A	562 ± 5^A	0.158 ± 0.010^A	0.162 ± 0.003^A	0.168 ± 0.008^A	-12.1 ± 0.3^A	-12.2 ± 0.3^{AB}	-12.6 ± 0.4^{AB}
500nm + NOM	524 ± 14^B	526 ± 5^B	530 ± 8^B	0.149 ± 0.007^A	0.152 ± 0.002^A	0.155 ± 0.007^B	-11.9 ± 0.3^A	-12.4 ± 0.4^{AB}	-13.2 ± 0.3^B

Supplemental Figures
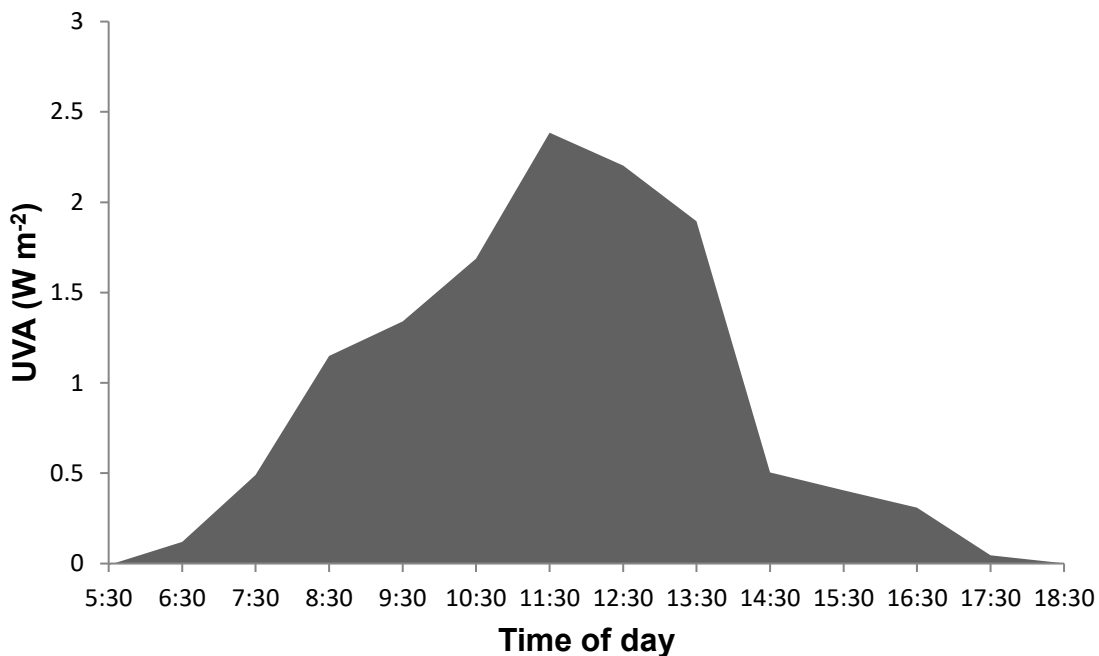
Figure S2-1. The average of UVA (W m^{-2}) in Rio Negro water (Brazil) from 5:30 to 18:30.
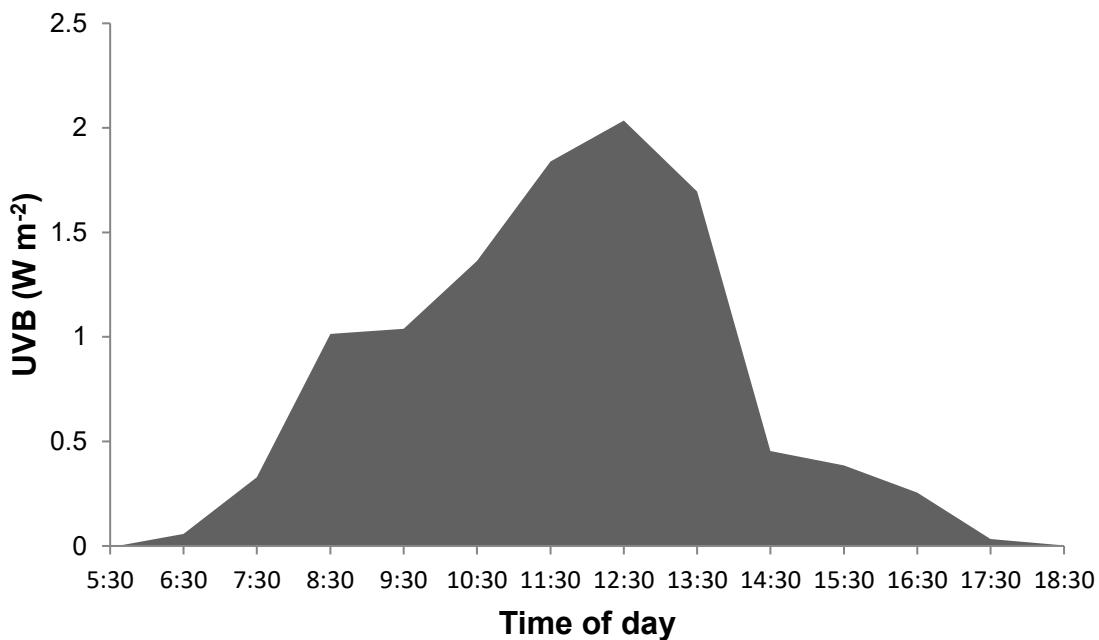
Figure S2-2. The average of UVB (W m^{-2}) in Rio Negro water (Brazil) from 5:30 to 18:30.
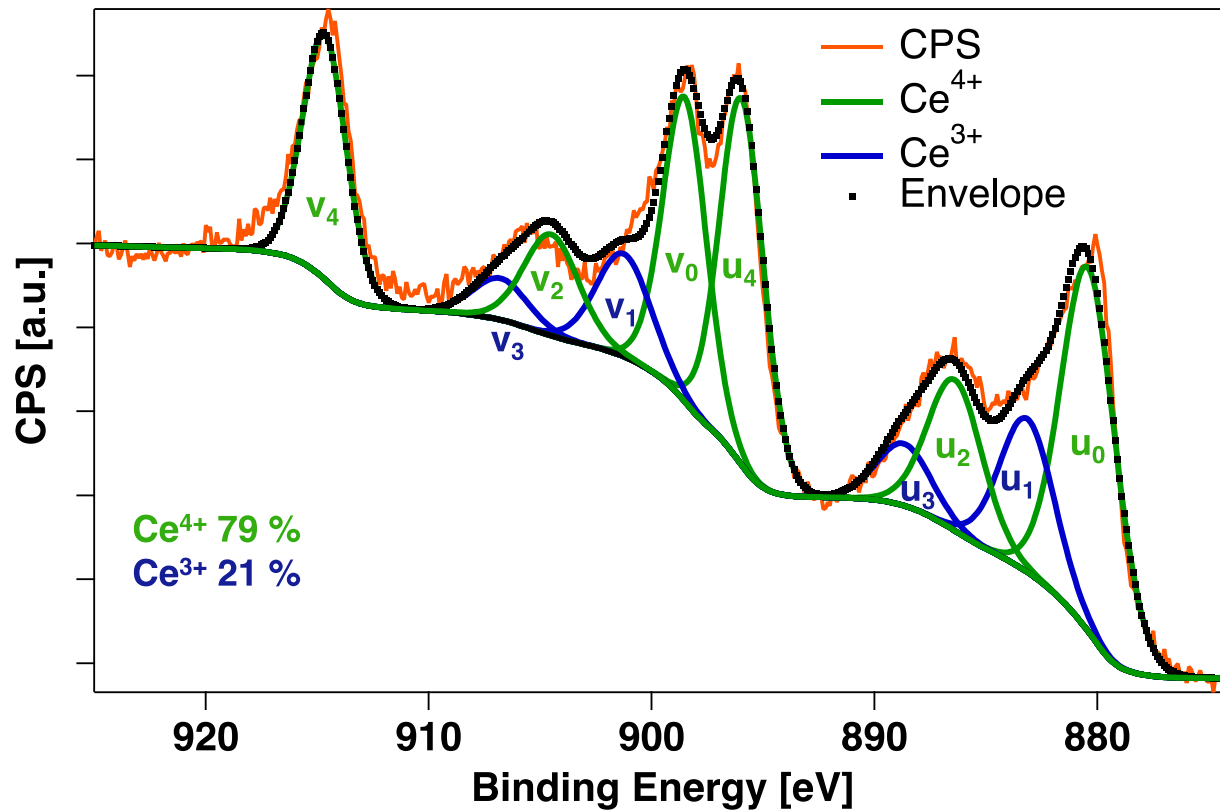
Figure S2-3. Narrow scan Ce 3d XPS spectrum of CeO$_2$ NPs samples. Three final states of Ce4+ are expressed as u0 (v0), u2 (v2) and u4 (v4), for Ce3d3/2 (Ce3d5/2). Two final states of Ce3+ are expressed as u1 (v1) and u3 (v3), for Ce3d3/2 (Ce3d5/2).
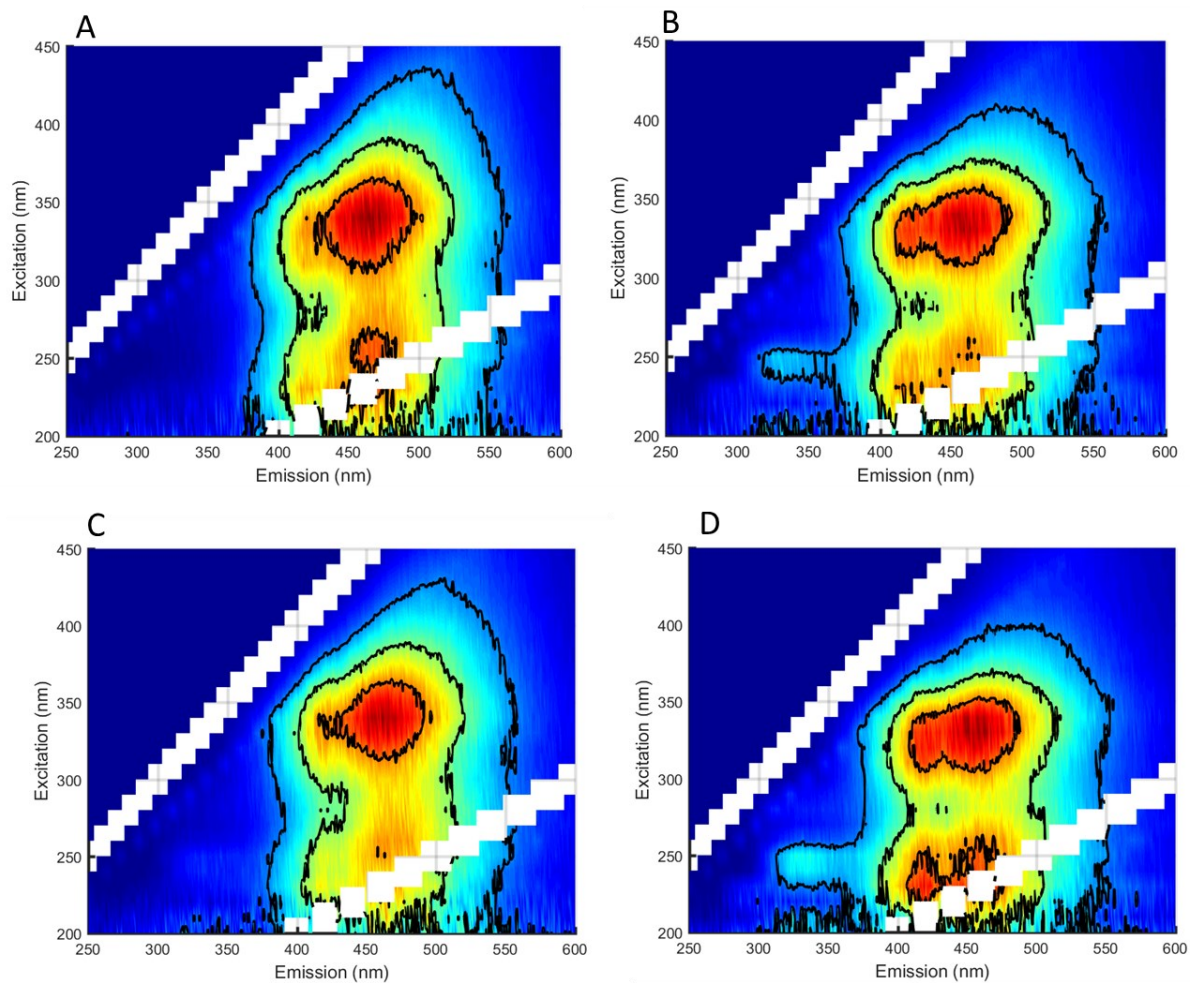
Figure S2-4. Fluorescence excitation-emission matrices (FEEM) were A) NOM no UV 48 hours; B) NOM UV 48 hours; C) NOM no UV 96 hours and D) NOM UV.
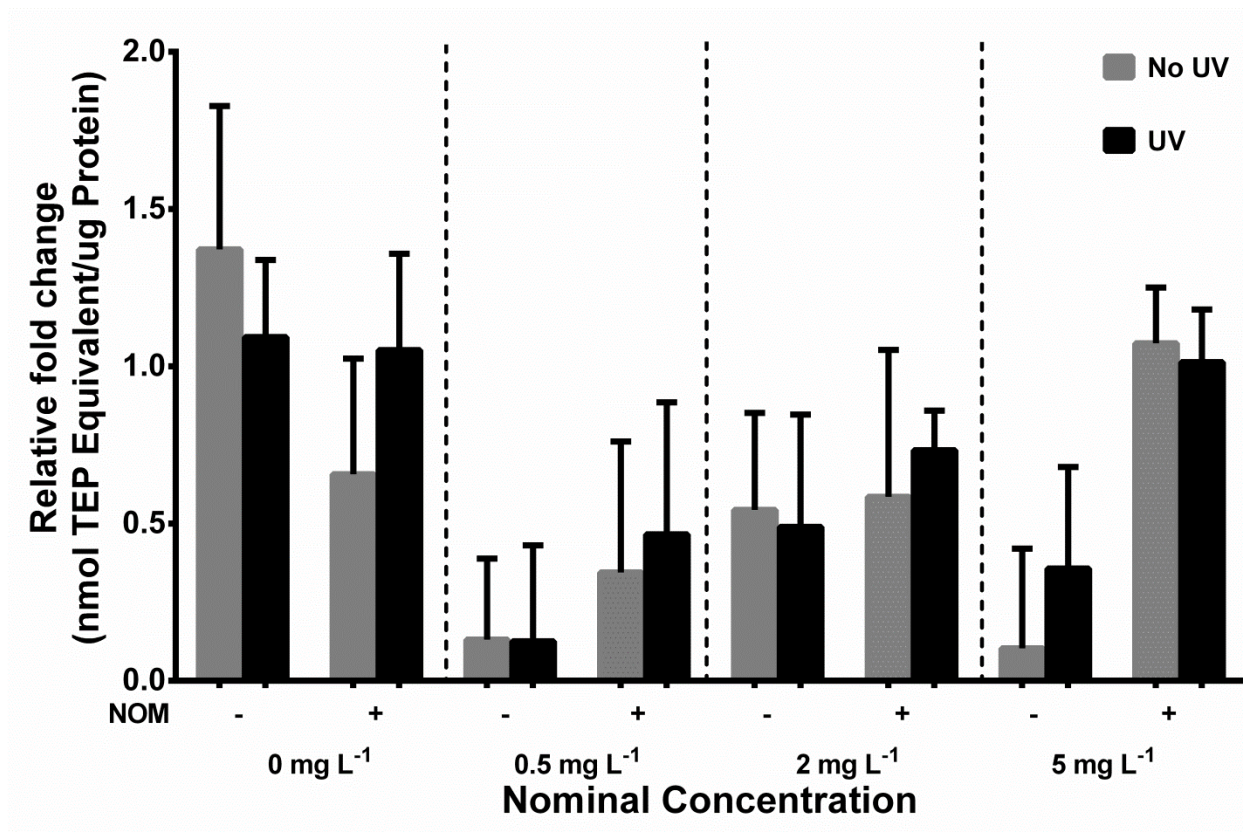
Figure S2-5. Lipid peroxidation in gills of cardinal tetras exposed to CeO_2 NPs suspension at nominal concentrations of 0, 0.5, 2 and 5 mg L^{-1} in ddH_2O (NOM-) and Rio Negro wa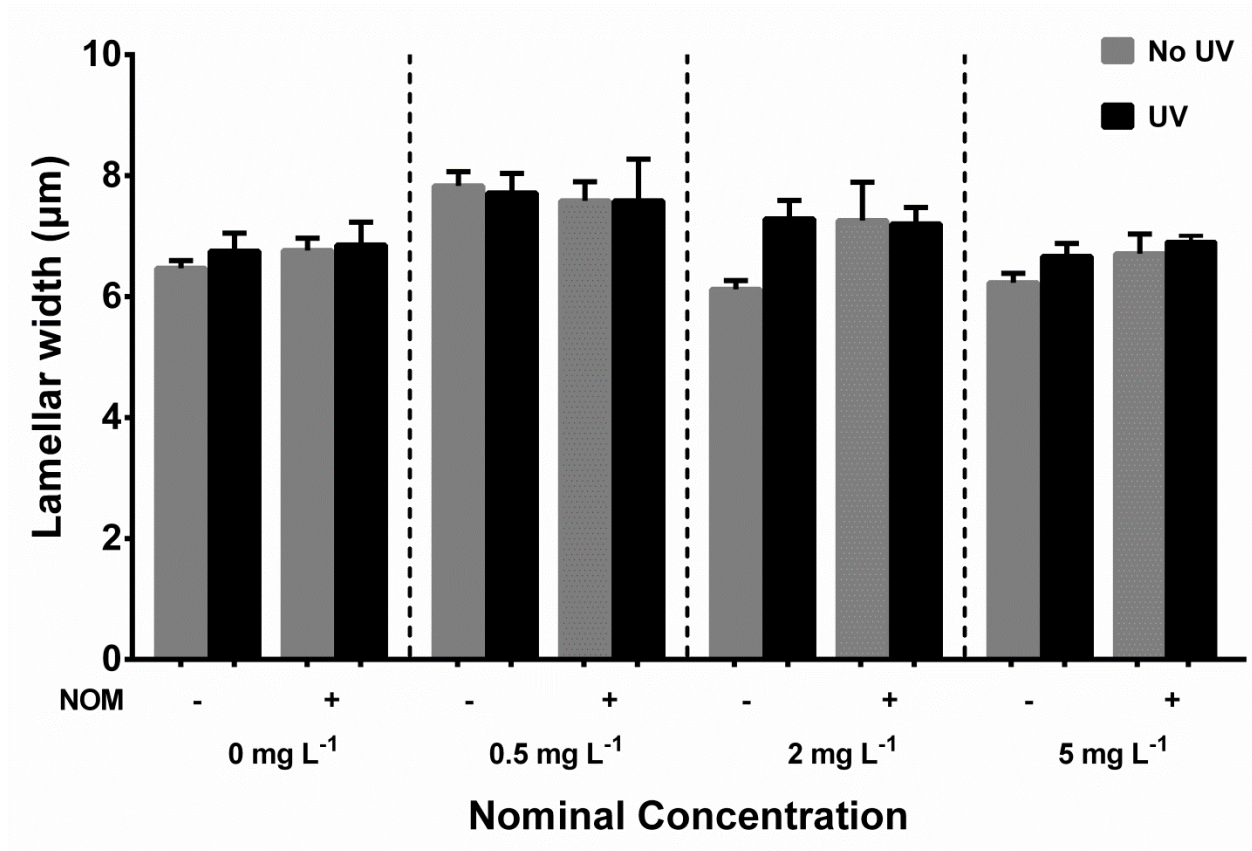ter (NOM+) with or without UV light for 96 hours (n=6). Relative fold change (NOM without UV at 0 mg L^{-1} were used as reference) of TBARS expressed as nmol TEP Equivalent/µg protein.
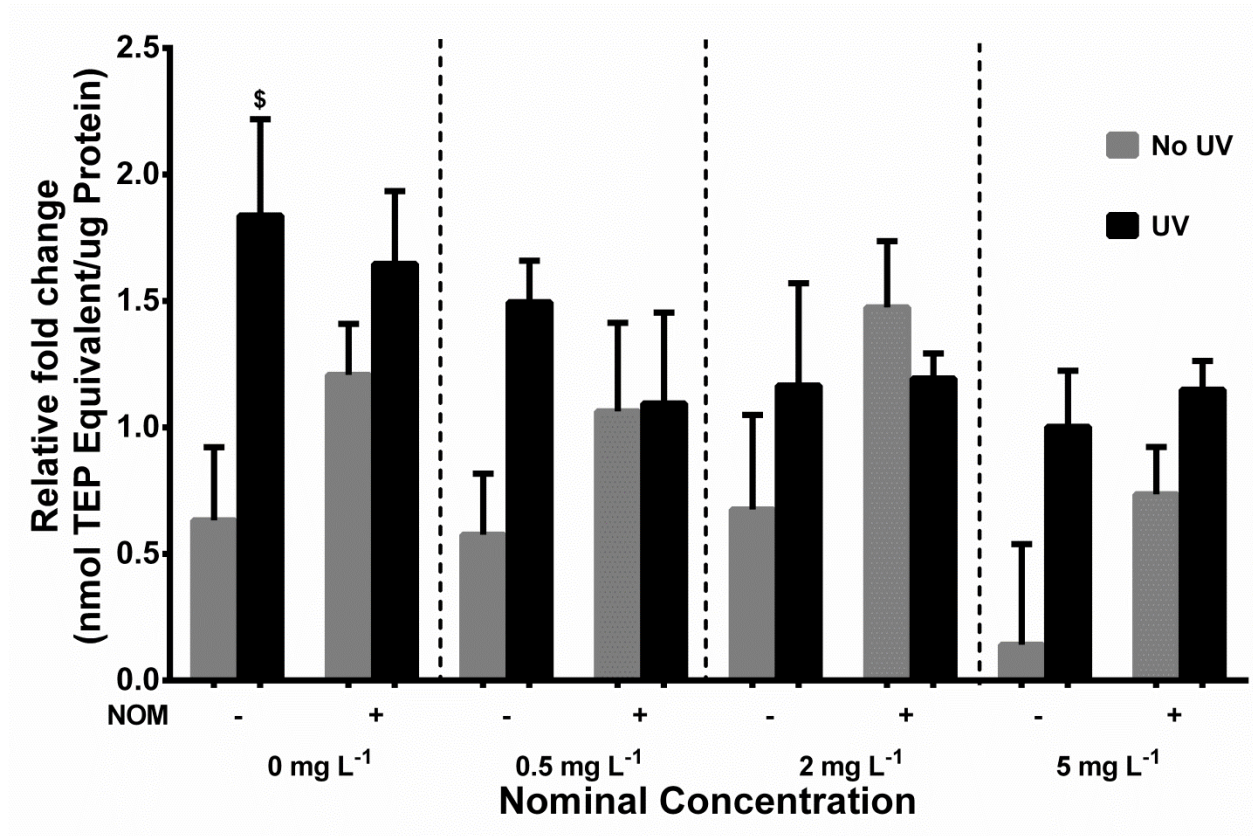
Figure S2-6. Lipid peroxidation in livers of cardinal tetras exposed to CeO_2 NPs suspension at nominal concentrations of 0, 0.5, 2 and 5 mg L^{-1} in ddH_2O (NOM-) and Rio Negro water (NOM+) with or without UV light for 96 hours (n=6). Relative fold change (NOM without UV at 0 mg L^{-1} were used as reference) of TBARS expressed as nmol TEP Equivalent/µg protein. Values are mean ± SEM.
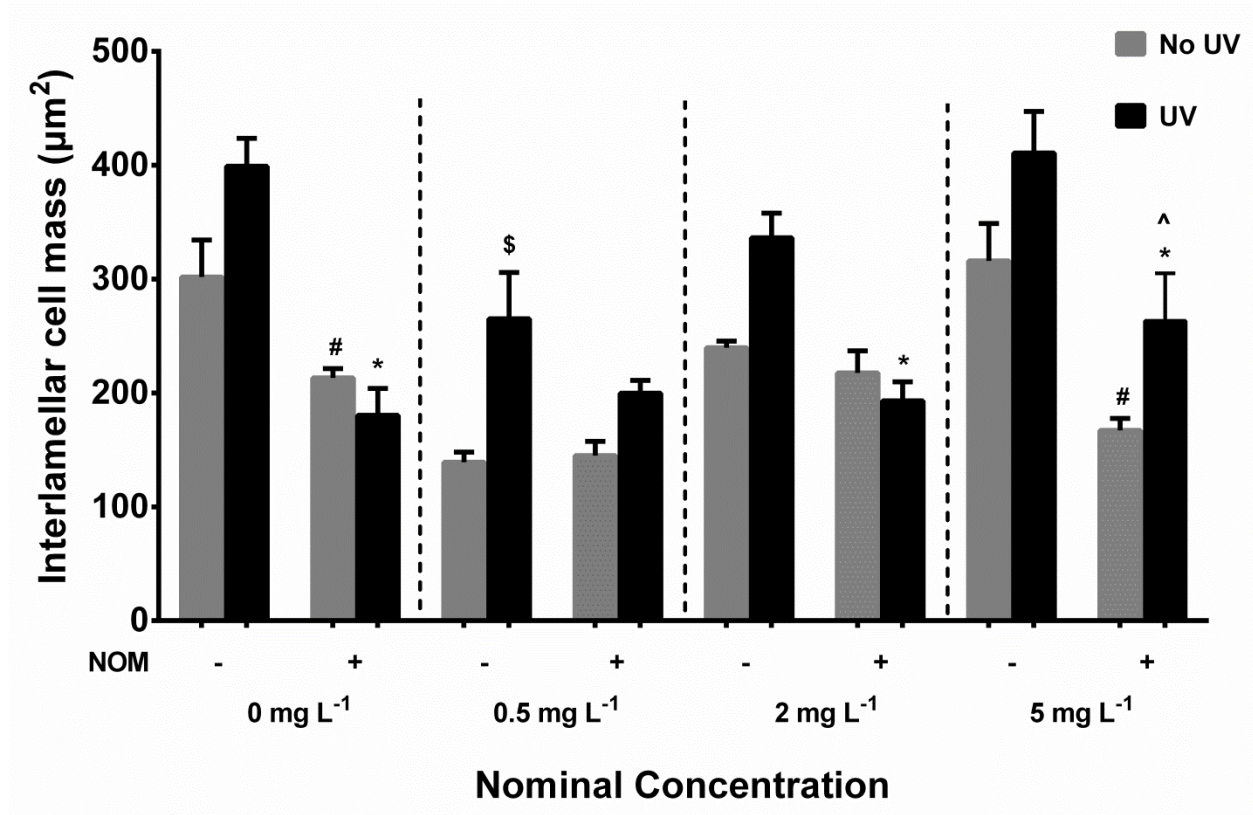
Figure S2-7. The interlamellar cell mass (μm^2) of gills of cardinal tetras exposed to CeO_2 NPs suspension at nominal concentrations of 0, 0.5, 2 and 5 mg L^{-1} in ddH_2O (NOM-) and Rio Negro water (NOM+) with or without UV light 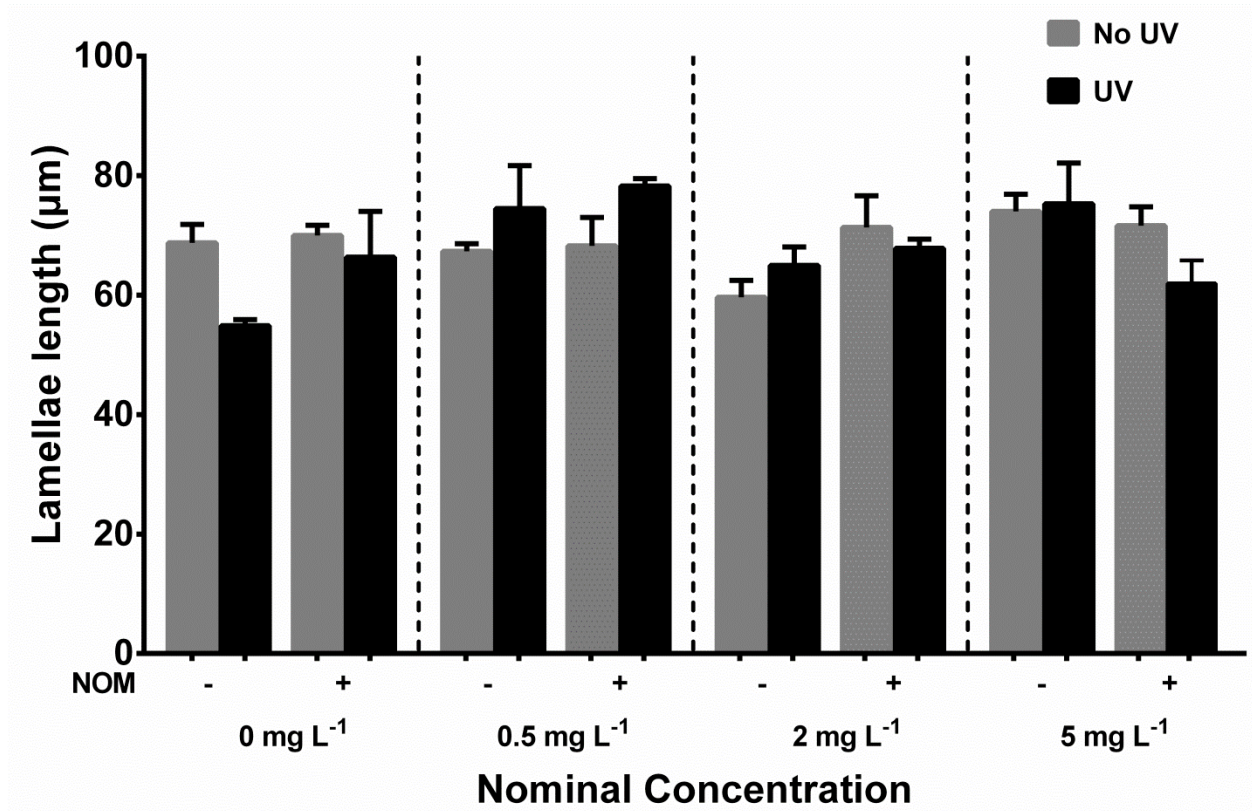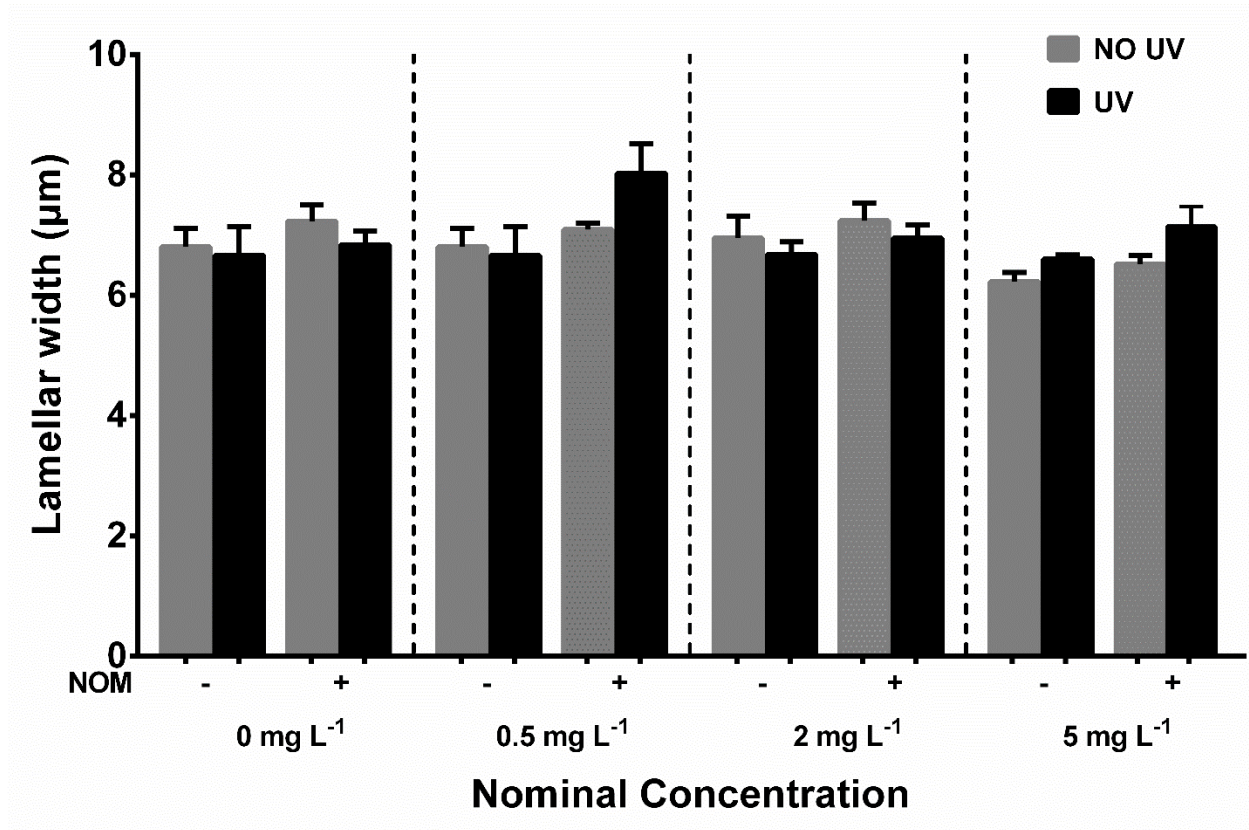for 96 hours (n=4). Values are mean ± SEM. * indicates NOM significantly reduces ILCM under UV light. # indicates NOM significantly reduces ILCM without UV light. $ indicates UV light significantly increases ILCM in ddH_2O.
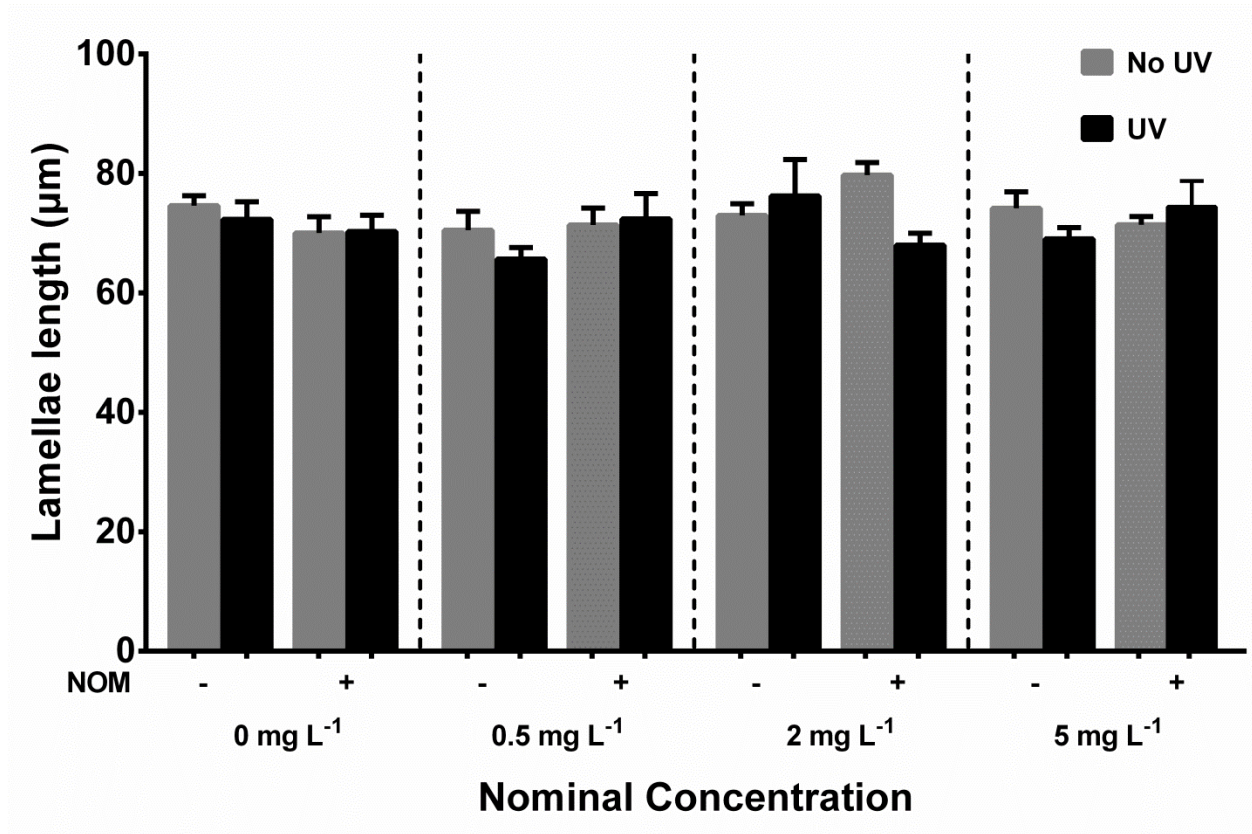
Figure S2-8. The lamellar length (μm) of gills of cardinal tetras exposed to CeO_2 NPs suspension at nominal concentrations of 0, 0.5, 2 and 5 mg L^{-1} in ddH$_2$O (NOM-) and Rio Negro water (NOM+) with or without UV light for 48 hours (n=4). Values are mean ± SEM.

Figure S2-9. The lamellar width (μm) of gills of cardinal tetras exposed to CeO_2 NPs suspension at nominal concentrations of 0, 0.5, 2 and 5 mg L^{-1} in ddH_2O (NOM-) and Rio Negro water (NOM+) with or without UV light for 48 hours (n=4). Values are mean ± SEM.

Figure S2-10. The lamellar length (μm) of gills of cardinal tetras exposed to CeO_2 NPs suspension at nominal concentrations of 0, 0.5, 2 and 5 mg L^{-1} in ddH_2O (NOM-) and Rio Negro water (NOM+) with or without UV light for 96 hours (n=4). Values are mean ± SEM.

Figure S2-11. The lamellar length (μm) of gills of cardinal tetras exposed to CeO_2 NPs suspension at nominal concentrations of 0, 0.5, 2 and 5 mg L^{-1} in ddH_2O (NOM-) and Rio Negro water (NOM+) with or without UV light for 96 hours (n=4). Values are mean ± SEM.
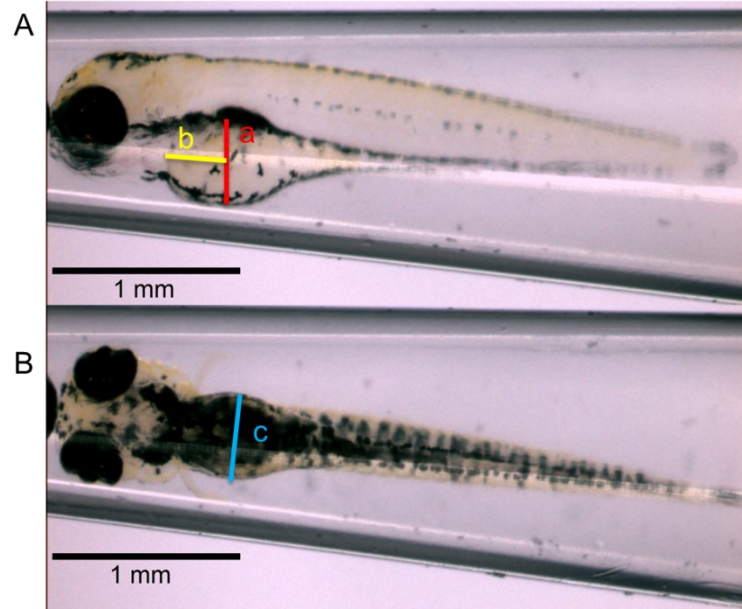
Figure S3-1. The side view (A) and the ventral view (B) of zebrafish larvae in at 120 hpf in control under laboratory light.
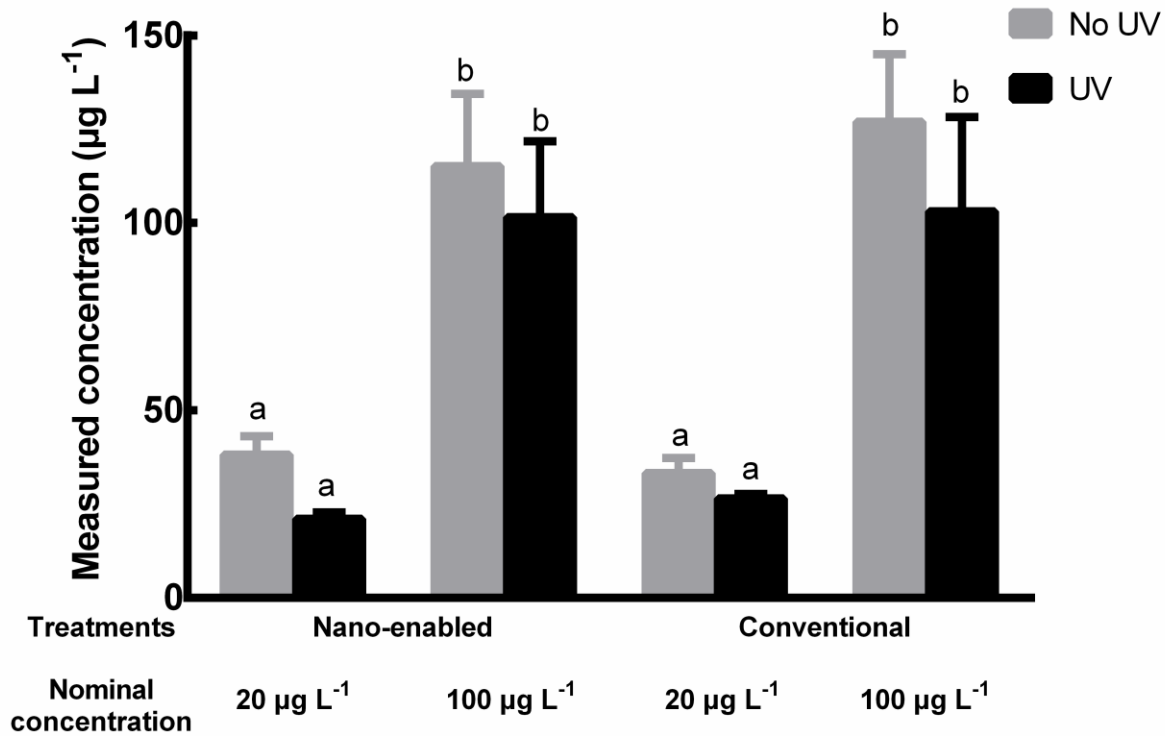
Figure S3-2. Measured concentrations of nano-enabled (A) and conventional (B) azoxystrobin at nominal concentrations of 20 and 100 μg L^{-1} under either laboratory light or UV light. Means sharing the same letter are not significantly different from each other (p>0.05). Values are mean ± SEM. n=3.
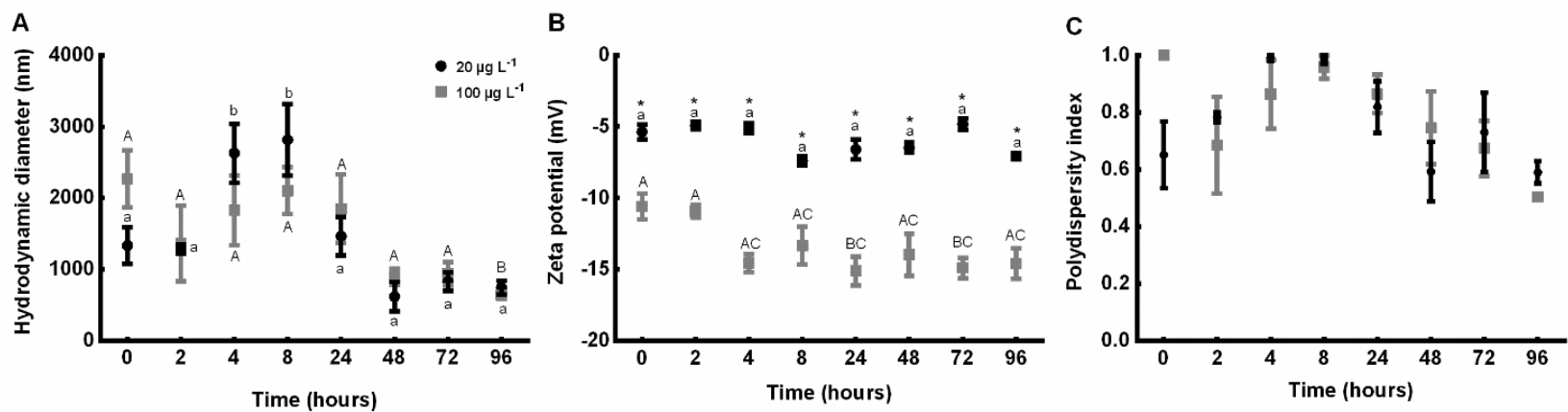
Figure S3-3. Average hydrodynamic diameter (A), zeta-potential (B) and polydispersity index (C) of nano-enabled azoxystrobin measured by DLS at 0, 2, 4, 8, 24, 48, 72 and 96 hours at a nominal concentration of 20 and 100 µg L⁻¹. * indicates measurement at 20 µg L⁻¹ is significantly different than 100 µg L⁻¹. Means sharing the same small letter are not significantly different from each other at 20 µg L⁻¹ (p>0.05). Means sharing the same capital letter are not significantly different from each other at 100 µg L⁻¹ (p>0.05). Values are mean ± SEM. n=3.
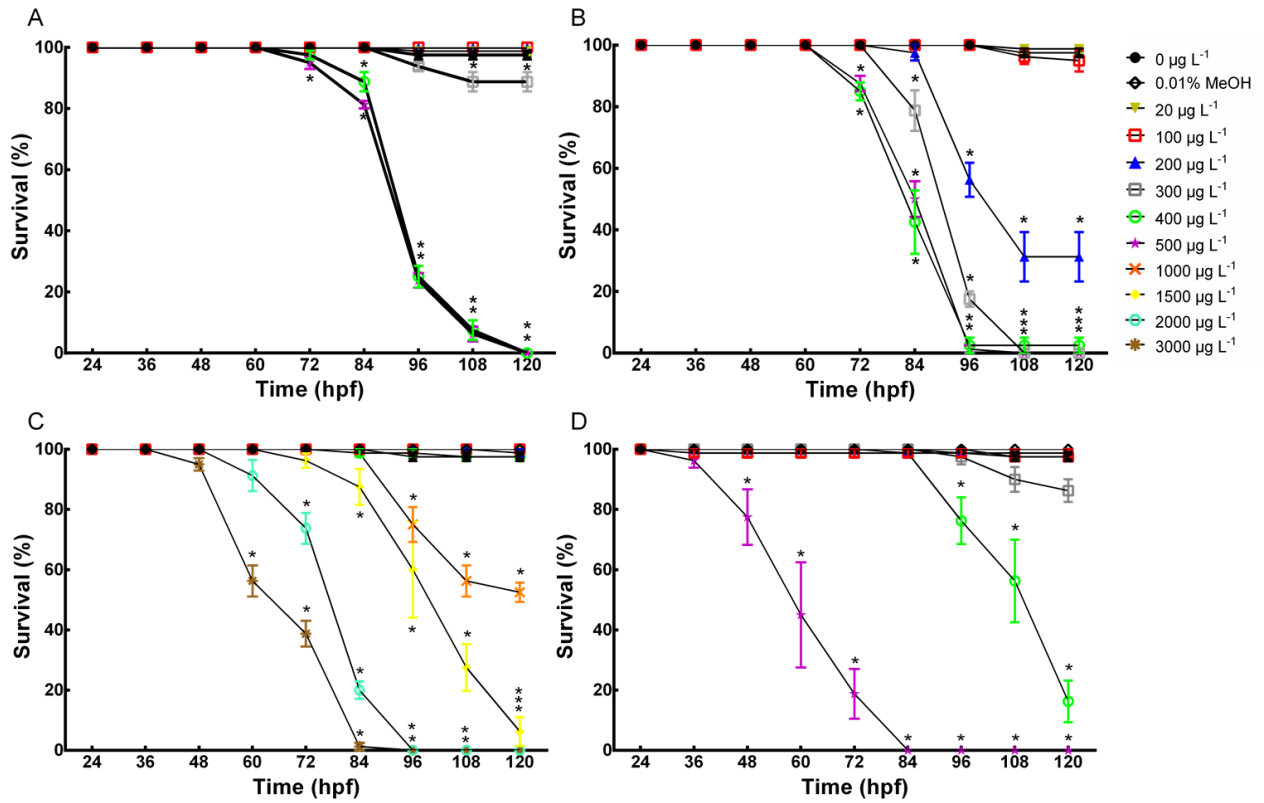
Figure S3-4. The survival rate of zebrafish embryos exposed to nano-enabled (A&B), conventional (C&D) azoxystrobin at various nominal concentrations, control and methanol control (0.01% MeOH) under fluorescent light (A&C) or UV light (B&D) from 24 hpf to 120 hpf. Asterisk (*) indicates a significant difference between treatments and control. Values are mean ± SEM. n=4.
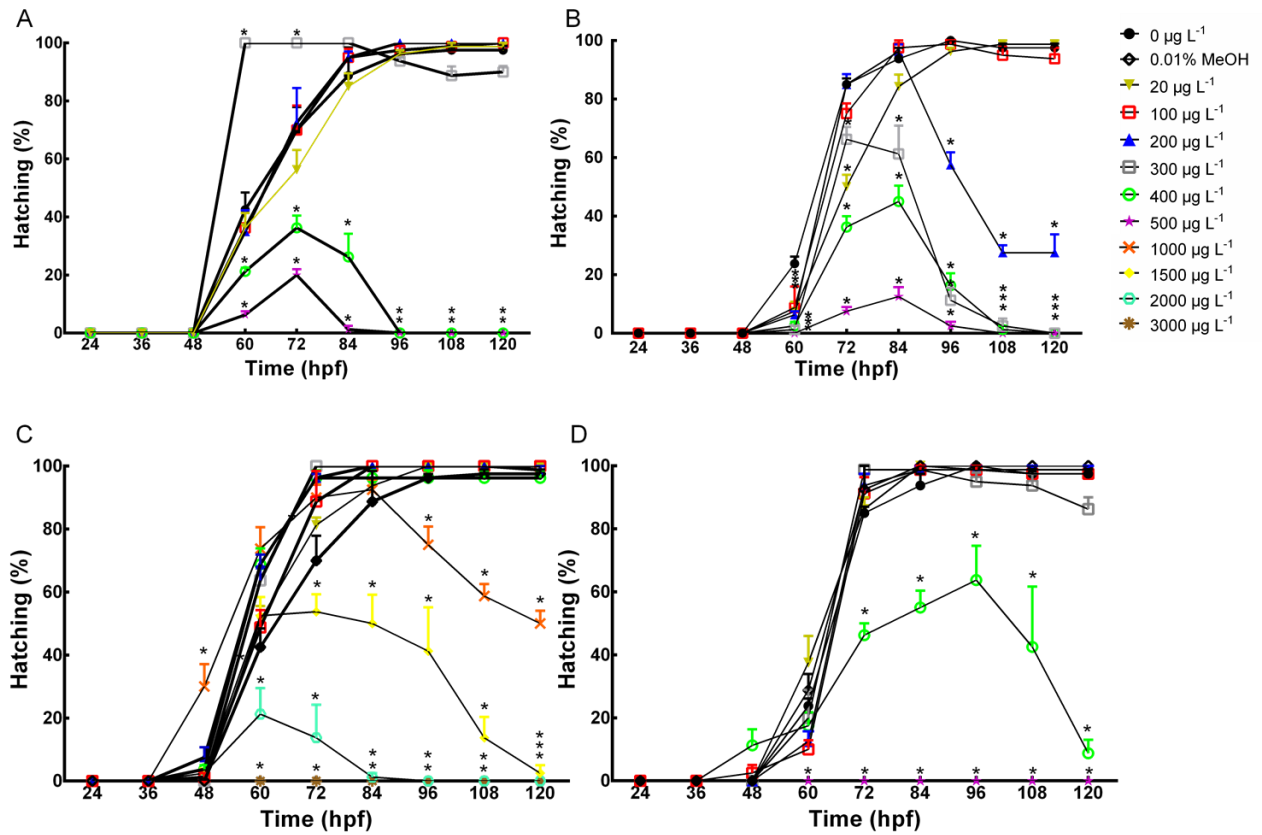
Figure S3-5. Hatching success of zebrafish embryos exposed to nano-enabled (A&B), conventional (C&D) azoxystrobin at various nominal concentrations, control and methanol control under fluorescent light (A&C) or UV light (B&D) from 24 hpf to 120 hpf. Asterisk (*) indicates a significant difference between treatments and control. Values are mean ± SEM. n=4.
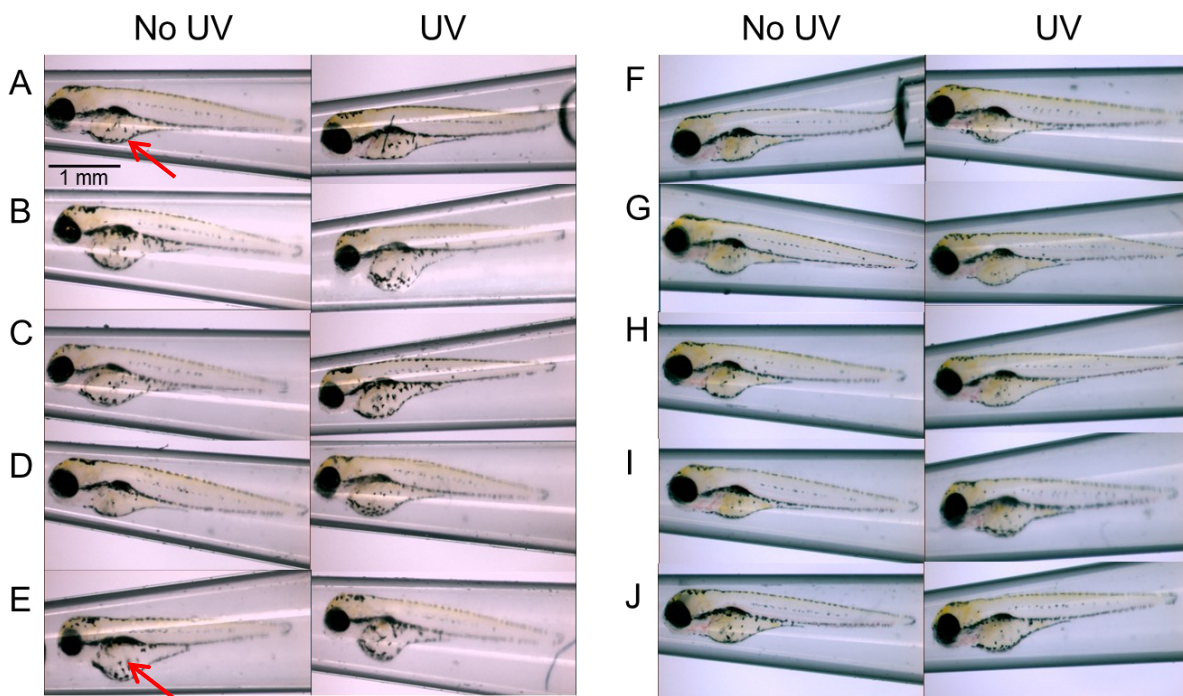
Figure S3-6. Side view of zebrafish larvae at 120 hpf in control (A), nAz at 20 µg L^{-1} (B) and 100 µg L^{-1} (C), Az at 20 µg L^{-1} (D) and 100 µg L^{-1} (E), vehicle control (F), input polymer at 20 µg L^{-1} (G) and 100 µg L^{-1} (H), and Allosperse at 20 µg L^{-1} (I) and 100 µg L^{-1} (J) under laboratory light and UV light. Arrows in A (control) and E (nAz at 100µg L^{-1}) illustrate the variation in yolk sac volume as reported in Fig 2. The scale is 1 mm in length.
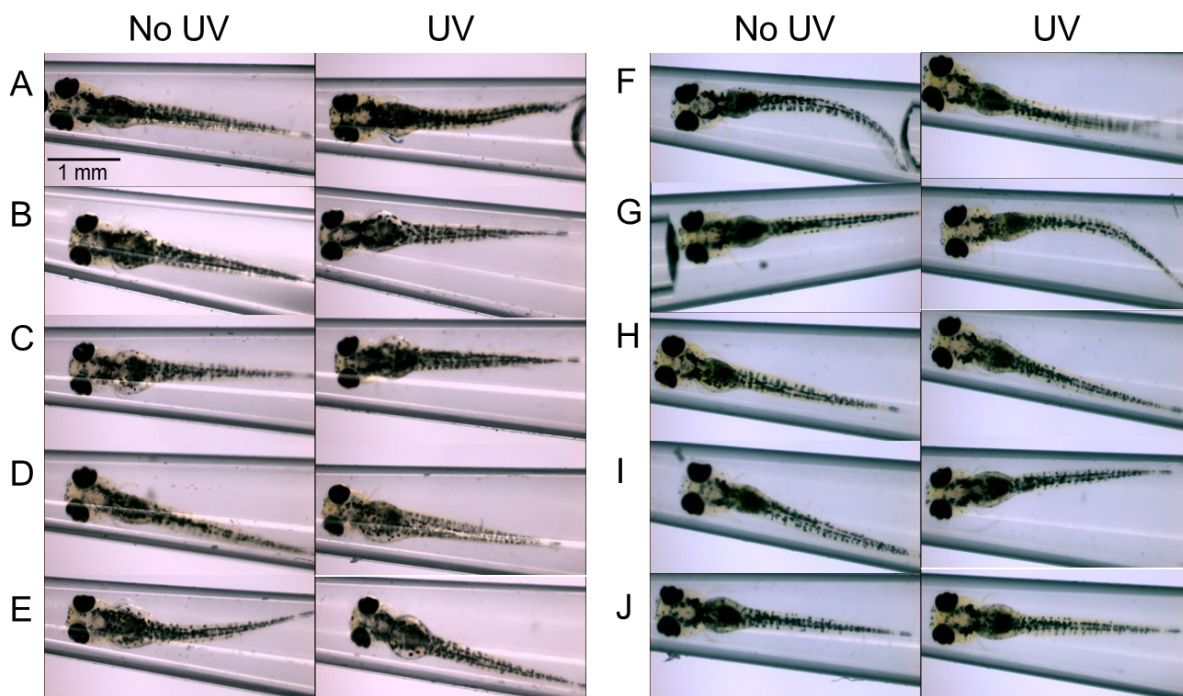
Figure S3-7. Ventral view of zebrafish larvae at 120 hpf in control (A), nAz at 20 µg L^{-1} (B) and 100 µg L^{-1} (C), Az at 20 µg L^{-1} (D) and 100 µg L^{-1} (E), vehicle control (F), input polymer at 20 µg L^{-1} (G) and 100 µg L^{-1} (H), and Allosperse at 20 µg L^{-1} (I) and 100 µg L^{-1} (J), and Allosperse at 20 µg L^{-1} (I) and 100 µg L^{-1} (J) under laboratory light and UV light. The scale is 1 mm in length.
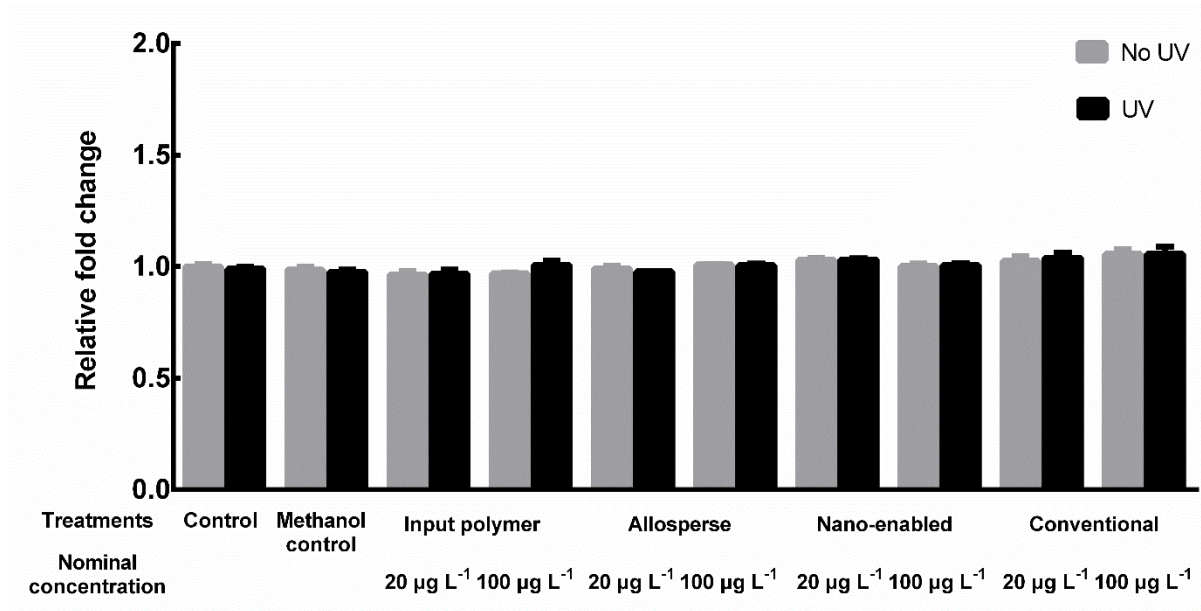
Figure S3-8. Relative fold change in gene expression of ef1α in zebrafish larvae at 120 hpf after 96-hour exposure from 24 hpf under either laboratory light or UV light. Values are mean ± SEM. n=4.
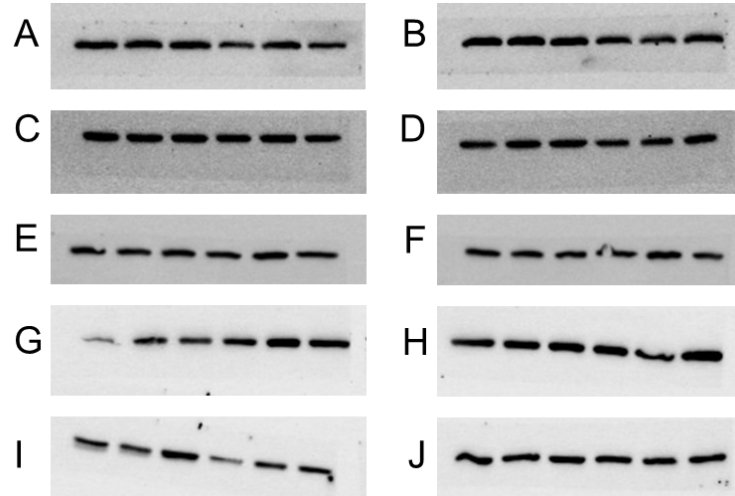
Figure S3-8. Western blot images of beta-actin expression n zebrafish larvae at 120 hpf in control (A), vehicle control (B), nano-enabled azoxystrobin at 20 μg L^{-1} (C) and 100 μg L^{-1} (D), conventional azoxystrobin at 20 μg L^{-1} (E) and 100 μg L^{-1} (F), input polymer at 20 μg L^{-1} (G) and 100 μg L^{-1} (H), and Allosperse at 20 μg L^{-1} (I) and 100 μg L^{-1} (J) under laboratory light (lane 1, 2 and 3) and UV light (lane 4, 5 and 6).
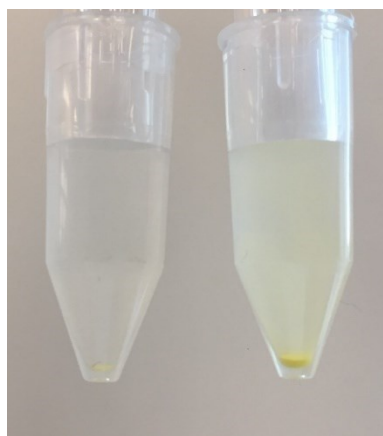
Figure S4-1. The recovered 20 nm PS-NPLs at 100 mg L^{-1} (left) and 500 nm PS-NPLs at 1780 mg L^{-1} (right) in the sorption experiment.
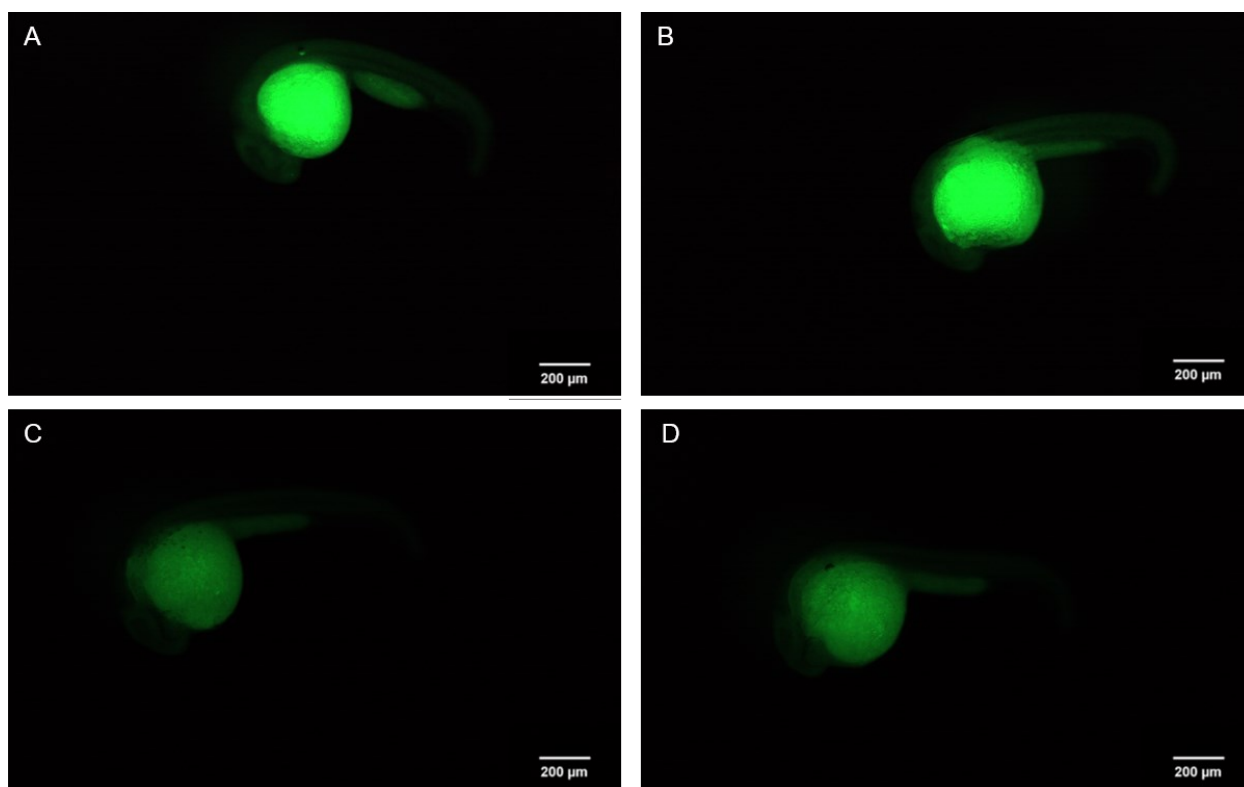

Figure S4-2. Fluorescence images of dechorionated embryos at 48 hpf after 24-h exposure to dialyzed 20 nm PS-NPLs at 10 mg L^{-1} (A & B) or dialyzed 500 nm PS-NPLs at 10 mg L^{-1} (C & D).
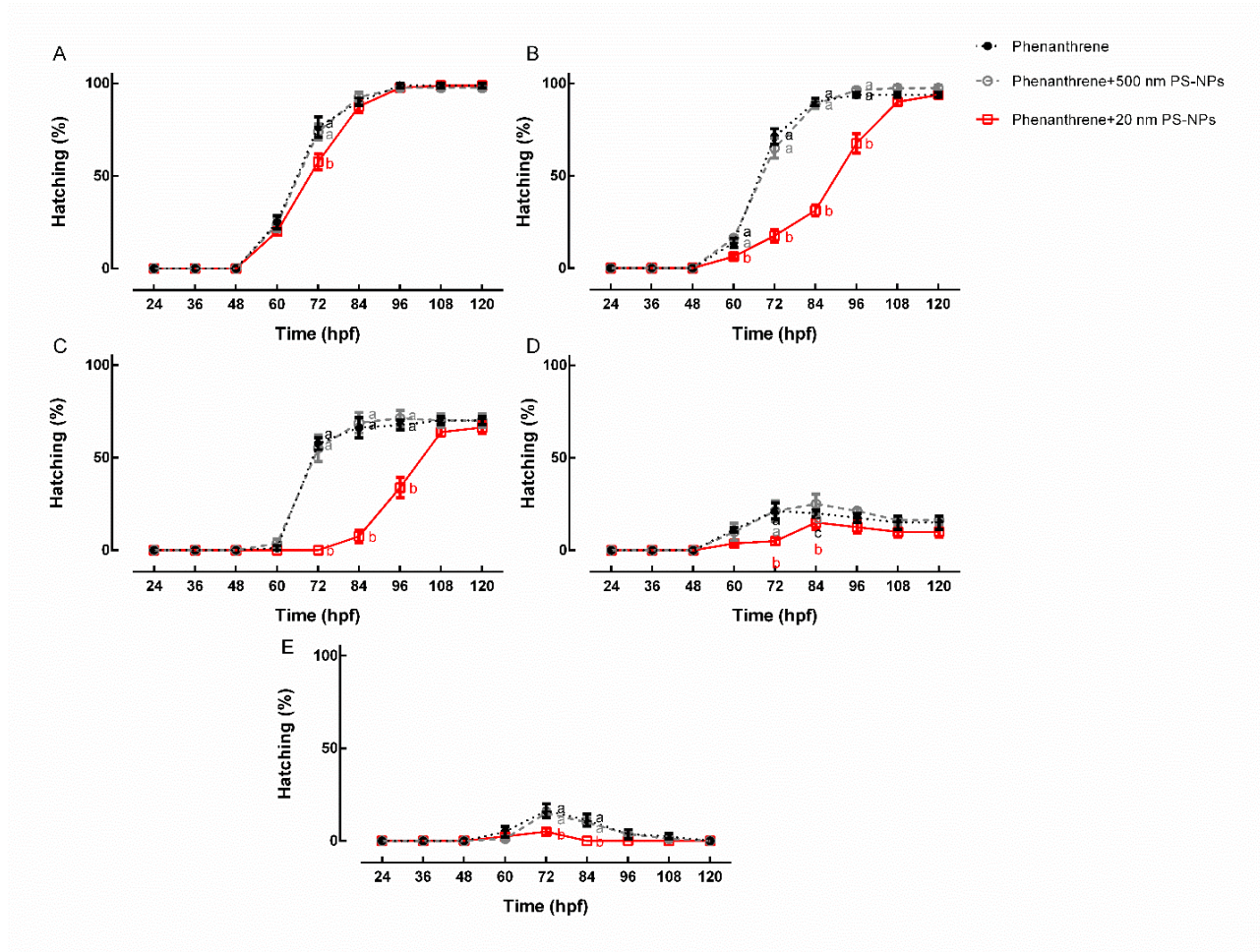
Figure S4-3. Hatching success of zebrafish embryos exposed to phenanthrene at various nominal concentrations including 0.156 mg L^{-1} (A), 0.313 mg L^{-1} (B), 0.625 mg L^{-1} (C), 1.25 mg L^{-1} (D) and 2.5 mg L^{-1} (E), without any PS-NPLs (black dots), in the presence of 10 mg L^{-1} 500 nm PS-NPLs (gray circles) or in the presence of 10 mg L^{-1} 20 nm PS-NPLs (red squares) from 24 hpf to 120 hpf. Means with different letters are significantly different from each other at a given time point (p<0.05). Means without any letters indicates there was no significant difference at the time point (p>0.05). Values are mean ± SEM. n=4.
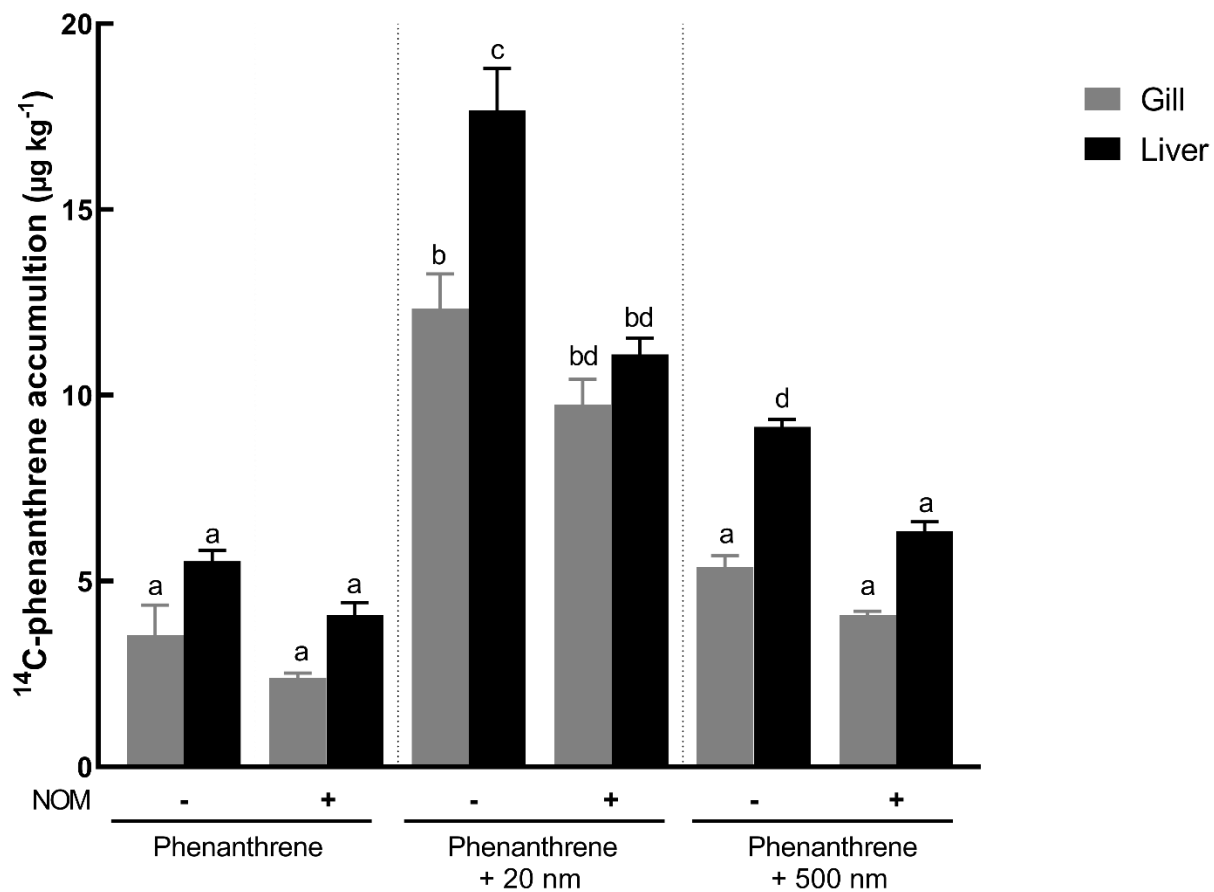
Figure S5-1. Residual ^{14}C-labeled phenanthrene detected in rainbow trout fingerlings gills and livers following 24 h recovery in clean RO water. Means sharing the same letter are not significantly different from each other (p > 0.05). Values are mean ± SEM. n = 4.

Figure S5-2. Confocal images (bright field, Hoechst+CMO, PS-NPL fluorescence, Hoechst+CMO+PS-NPLs fluorescence and overplay) of gills of rainbow trout fingerlings exposed to control, NOM, phenanthrene in the presence of 20 nm PS-NPLs with or without NOM and phenanthrene in the presence of 500 nm PS-NPLs with or without NOM at 4h. Scale bars are 5 μm.

Figure S5-3. Confocal images (bright field, Hoechst+CMO, PS-NPL fluorescence, Hoechst+CMO+PS-NPLs fluorescence and overplay) of gills of rainbow trout fingerlings exposed to control, NOM, phenanthrene in the presence of 20 nm PS-NPLs with or without NOM and phenanthrene in the presence of 500 nm PS-NPLls with or without NOM at 24h. Scale bars are 5 μm.

Figure S5-4. Confocal images (bright field, Hoechst+CMO, PS-NPL fluorescence, Hoechst+CMO+PS-NPLs fluorescence and overplay) of gills of rainbow trout fingerlings exposed to control, NOM, phenanthrene in the presence of 20 nm PS-NPLs with or without NOM and phenanthrene in the presence of 500 nm PS-NPLs with or without NOM at 24 h after recovery. Scale bars are 5 μm.
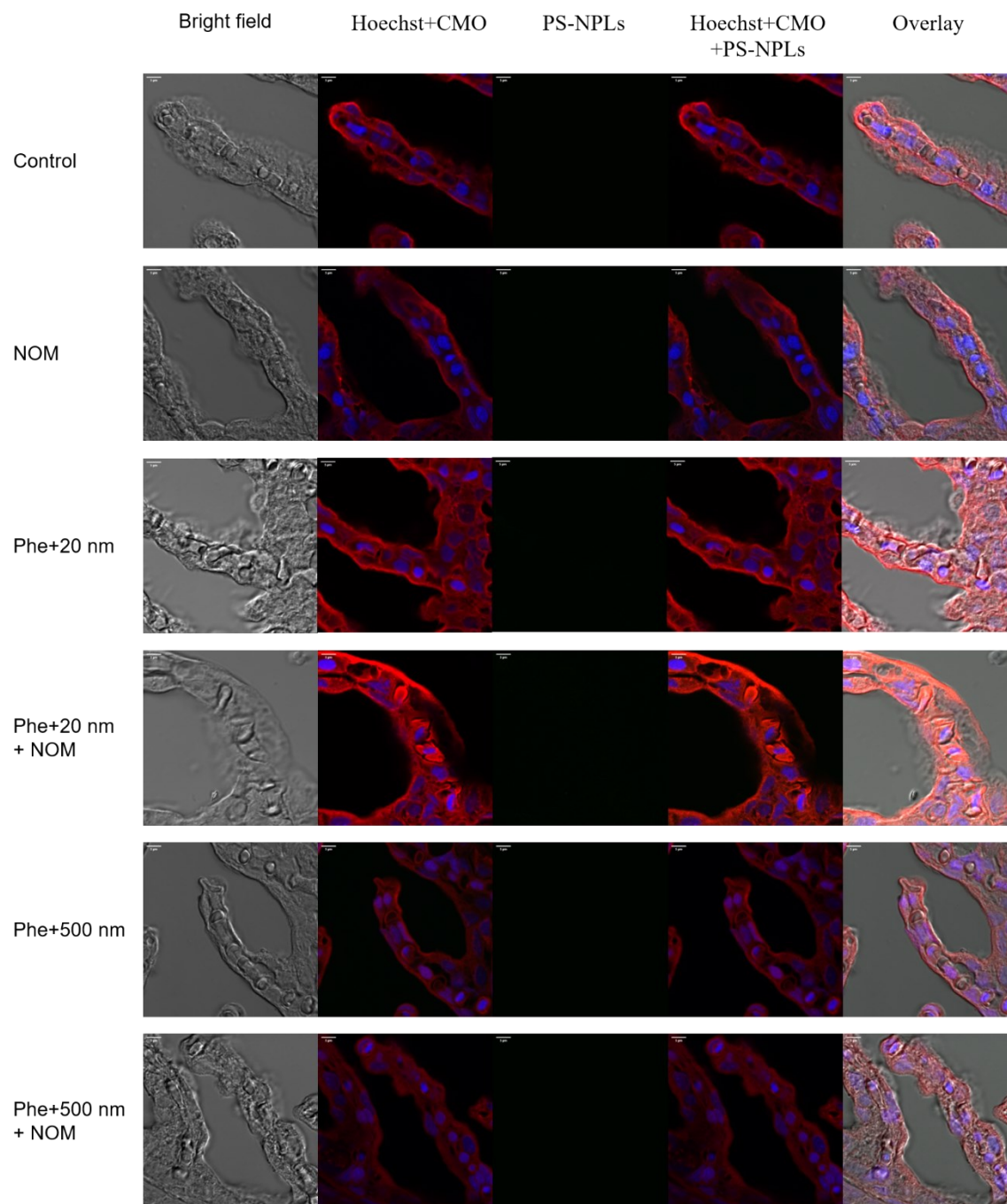
Figure S5-5. Confocal images (bright field, Hoechst+CMO, PS-NPL fluorescence, Hoechst+CMO+PS-NPLs fluorescence and overplay) of livers of rainbow trout fingerlings exposed to control, NOM, phenanthrene in the presence of 20 nm PS-NPLs with or without NOM and phenanthrene in the presence of 500 nm PS-NPLs with or without NOM at 4h. Scale bars are 5 μm.
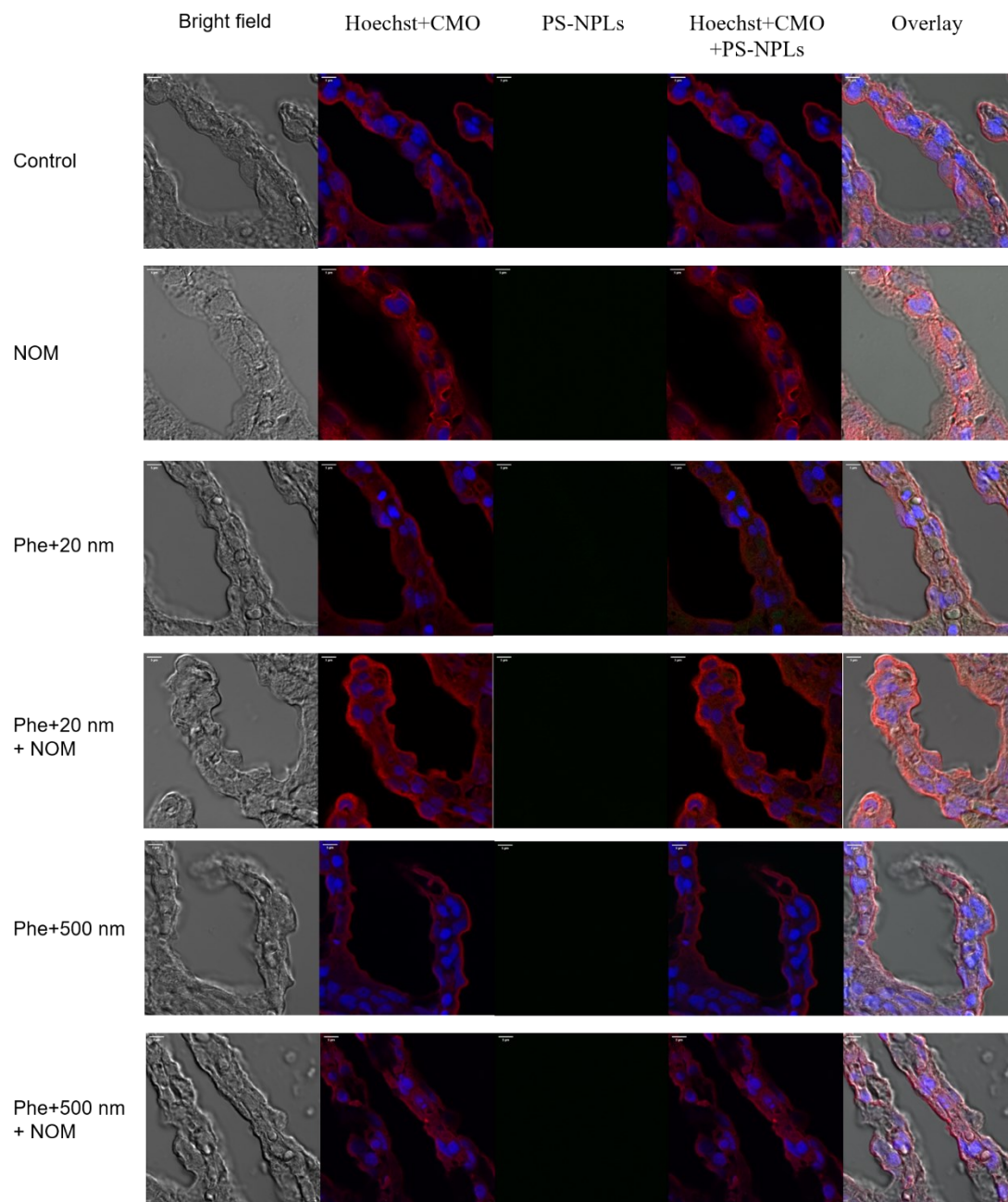
Figure S5-6. Confocal images (bright field, Hoechst+CMO, PS-NPL fluorescence, Hoechst+CMO+PS-NPLs fluorescence and overplay) of livers of rainbow trout fingerlings exposed to control, NOM, phenanthrene in the presence of 20 nm PS-NPLs with or without NOM and phenanthrene in the presence of 500 nm PS-NPLs with or without NOM at 24h. Scale bars are 5 μm.
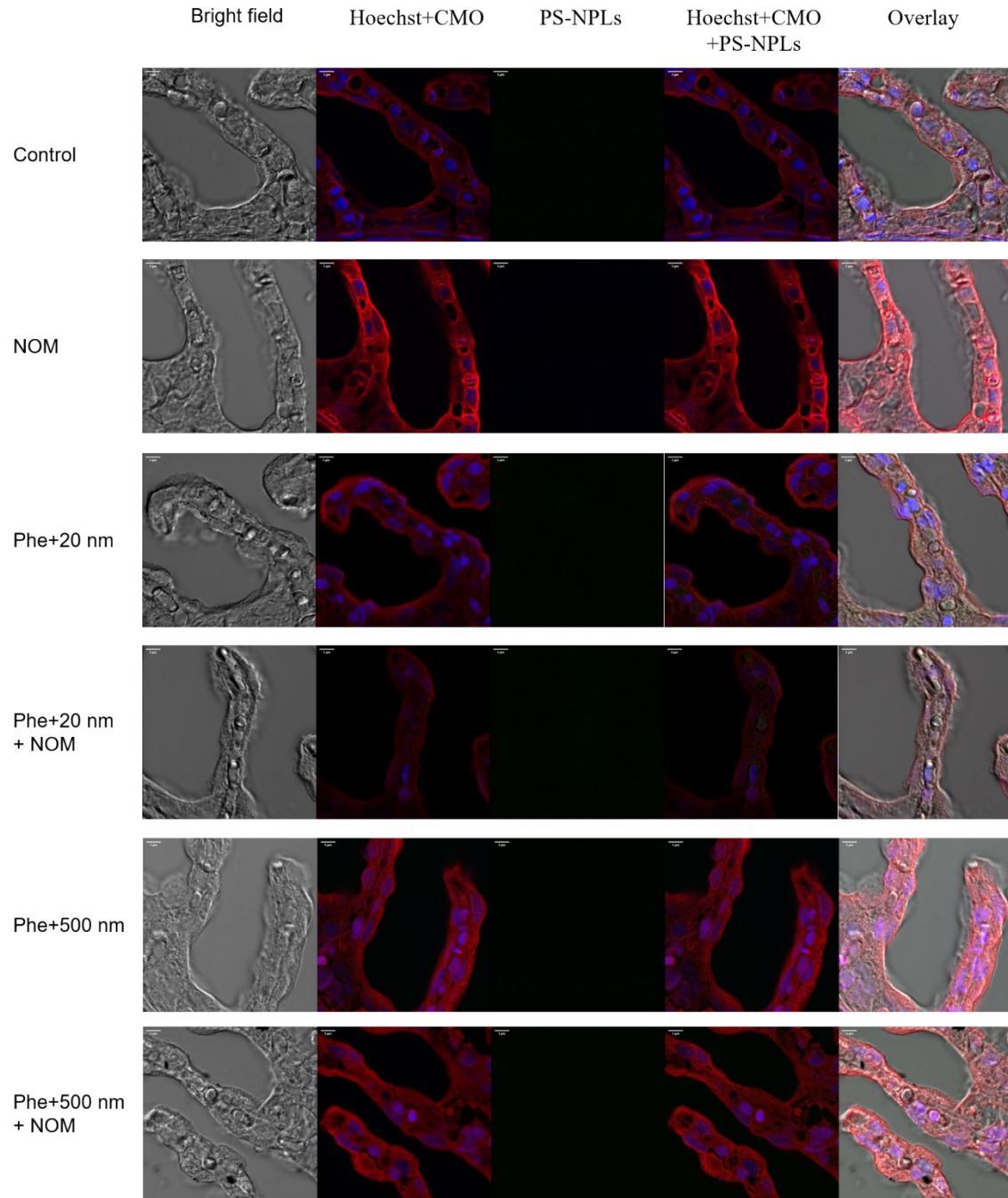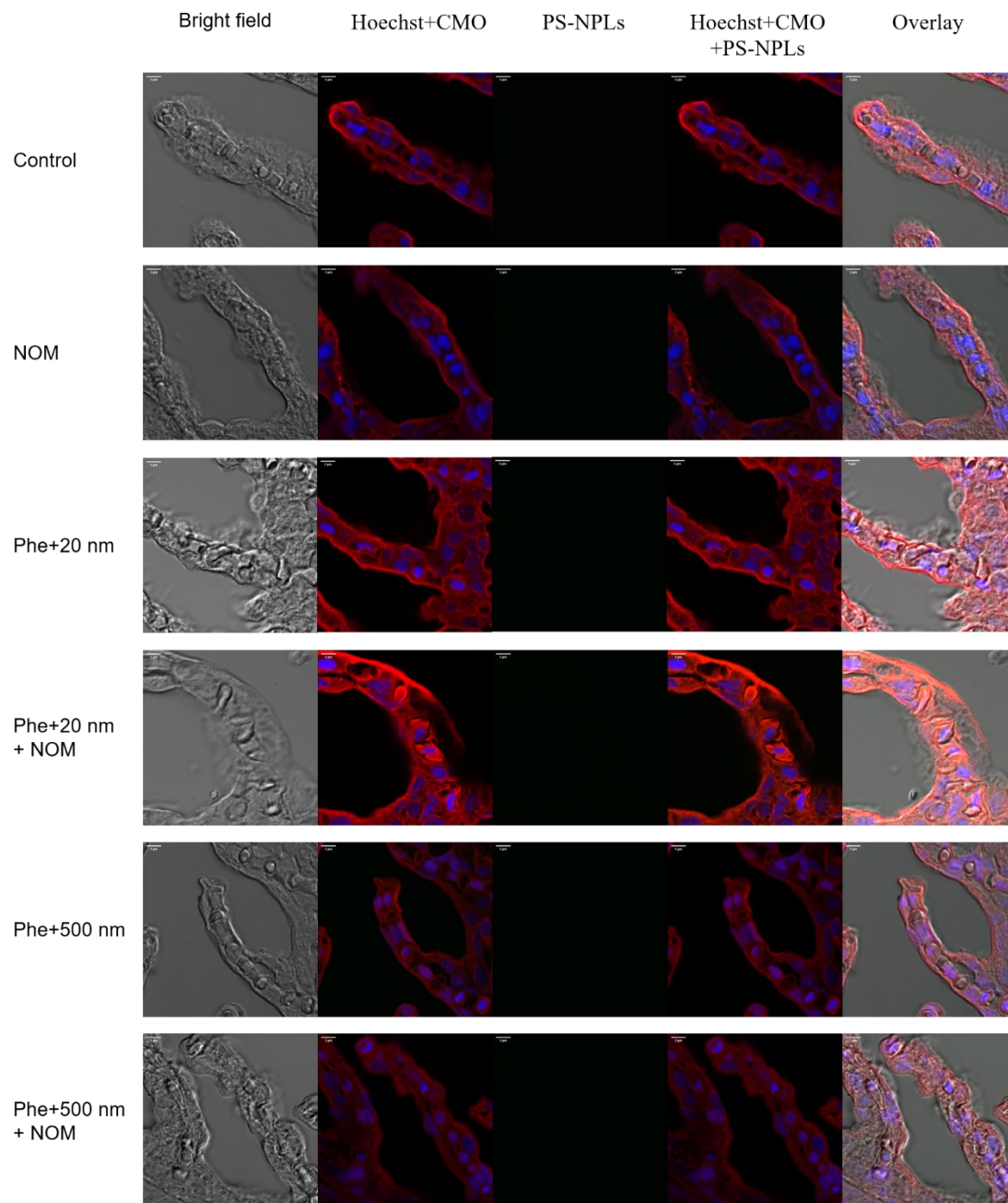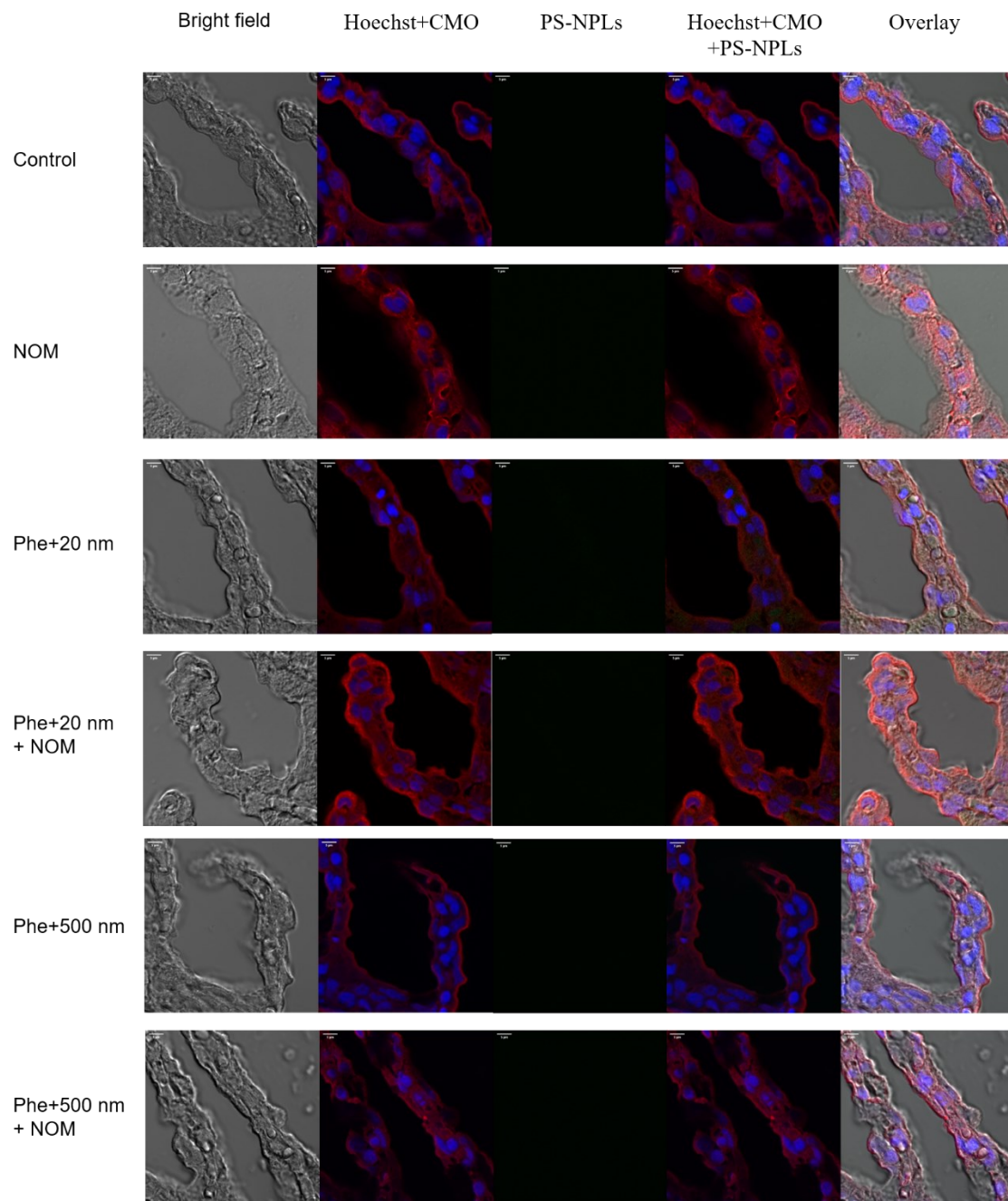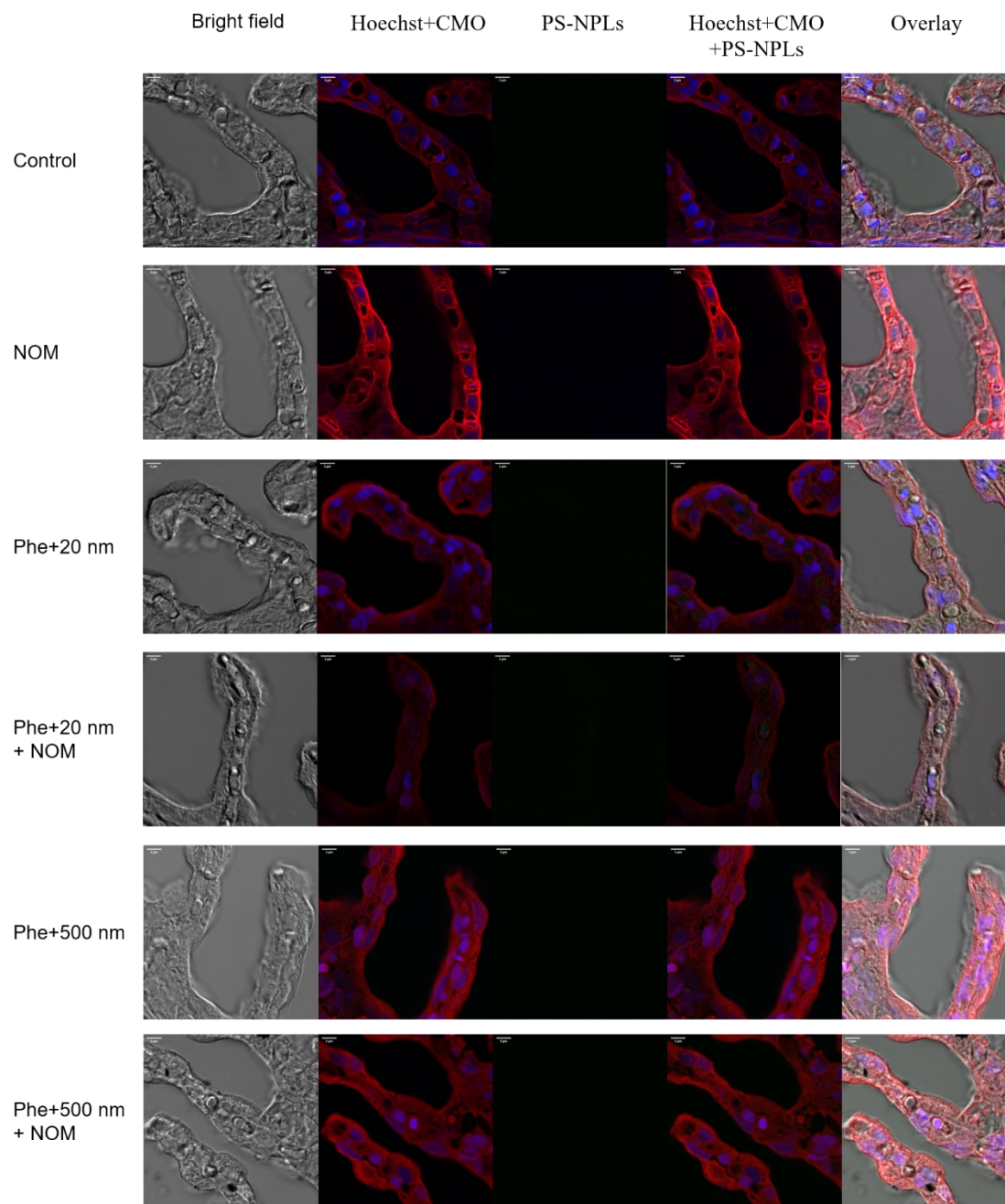
Figure S5-7. Confocal images (bright field, Hoechst+CMO, PS-NPL fluorescence, Hoechst+CMO+PS-NPLs fluorescence and overplay) of livers of rainbow trout fingerlings exposed to control, NOM, phenanthrene in the presence of 20 nm PS-NPLs with or without NOM and phenanthrene in the presence of 500 nm PS-NPLs with or without NOM at 24 h after recovery (C). Scale bars are 5 μm.

Supplemental Text

Appendix 2-1. X-ray photoelectron spectroscopy

The power of CeO_2 NPs was deposited on a double-sided tape. The base and operating chamber pressure were set at 10^{-7} Pa. The samples were irradiated by a monochromatic Al Kα source ($\lambda = 8.34$ Å). The spectra were obtained with an electron take-off angle of 90°. The charge neutralizer filament was used to reduce sample charging. Survey spectra were collected using an elliptical spot with major and minor axis lengths of 2 and 1 mm, respectively, and 160 eV pass energy with a step of 0.33 eV. CasaXPS software (VAMAS) was used to analyze the cerium oxide composition. All spectra were internally calibrated to the C 1s emission (284.8 eV). The Ce3d peak was deconvoluted using CasaXPS software with doublet area ratio constrained 3:2 and doublet separation fixed at 18.1 eV. The integrated area under the curve of each deconvoluted peak was used to calculate the concentration of Ce^{3+} and Ce^{4+}.

Appendix 2-2. Dissolution

Polypropylene beakers (250 mL) were soaked in 1% HNO_3 overnight and rinsed with ddH$_2$O to remove trace metal. Slide-A-Lyzer dialysis cassettes (~1 nm; 2000 molecular weight cut-off; Pierce) were injected with 1 mL of either NP suspensions at a concentration of 5 mg L^{-1} in ddH$_2$O or Rio Negro Amazon water. Cassettes injected with ddH$_2$O or Rio Negro Amazon water without NPs were used as controls. The cassettes were placed in beakers containing 300 mL ddH$_2$O on stir plates with constant slow rotation for 30 min then cassettes were transferred to a new beaker with fresh ddH$_2$O for 96 h to determine the concentration of free metal ions in test NP suspensions. The beakers were covered with

tinfoil to avoid light exposure, and reduce evaporation and production of reactive oxygen species. Water samples were collected in duplicate from each beaker at 0, 0.5, 12, 24, 36, 48, 72 and 96 h. The metal ion concentrations were measured by inductively coupled plasma mass spectroscopy (ICP-MS; Perkin Elmer, Elan 6000).

Appendix 2-3. Concentration and composition of NOM

A Shimadzu TOC –L CPH/CPN analyzer (Shimadzu Corporation Kyoto, Japan) was used to determine dissolved organic carbon concentrations. Standards were prepared from potassium hydrogen phthalate (Mandel Scientific, Guelph, ON) at 5, 10 and 15 mg of C/L. All the samples were filtered and acidified by adding a few drops of concentrated HCl to convert dissolved inorganic carbon into volatile CO_2, and then ddH_2O rinses were made after every sample. Fluorescence excitation-emission matrices (FEEM) was used to determine the molecular and structural composition of the samples. A Varian Cary Eclipse Fluorescence spectrophotometer (Varian, Mississauga, ON, Canada) scanned the emission of wavelengths at 250 to 600 nm in 1 nm increments for intervals of 10 nm excitation wavelengths between 200 and 450 nm to create FEEM plots. The photomultiplier tube was at high detection (800V) and the scan speed was set at 400 nm minute^{-1}.

Appendix 2-4. Inductively Coupled Plasma-Mass Spectroscopy

Water samples from the exposure experiments and dialysis were treated with 12 µL per 10 mL of 15.7 M trace metal nitric acid right after the collections. Analysis for cerium (140Ce) was performed using an Agilent 8800 Triple Quadrupole ICP-MS (ICP-MS/MS) with RF power of 1550 W and an RF reflected power of 18 W. The ICP-MS/MS was operated with a microMist nebulizer and nickel/copper cones. An inline internal standard

system was employed with a solution of 0.5 ppm to correct for instrumental drift. Samples passed through dialysis tubing were analyzed using standards covering a range of 0.0002 ppm to 10 ppm. For particle samples two sets of standards were prepared: 1) from diluting purchased 1,000 Ce standard stock solution (Alfa Aesar), 2) through suspending 300 ppm of CeO_2 particles in 18 MΩ water to cover a range of 0.4-9 ppm of particles. To reduce particle aggregation and sample heterogeneity, samples containing particle samples were sonicated for 1 minute before analysis and throughout the sample uptake using a Fisher 505 Sonic Dismembrator.

Appendix 2-5. Hematoxylin and eosin staining

The fixed gills were rinsed and immersed in 50% ethanol for 4 hours and then processed by Leica tp1020 tissue processor (Leica Biosystems) for 12 hours. After the 12 hour period, gills were embedded in paraffin wax. Tissue blocks were cut at 5μm in the orientation of the lamellar sagittal section by microtome (Leica Biosystems). Tissue slides were processed for histology examination following the standard techniques with hematoxylin and eosin staining. Briefly, slides were immersed with toluene for 5 minutes twice and then 100% ethanol for 2 minutes twice. After that, slides were immersed in 90%, 70%, 50% and distilled water for 2 minutes once and then rinsed with cold distilled water for 15 minutes. After rinsing, slides were immersed in 70% ethanol for 2 minutes once, eosin for 30 seconds once, and 100% ethanol for 2 minutes twice and toluene for 2 minutes twice. Slides were kept in toluene until they were coverslipped with DPX. Slides were kept in an oven at 37 °C overnight for the DPC to solidify.

Appendix 3-1. GC/MS/MS analysis

Water samples were filtered through glass wool, acidified with concentrated H_2SO_4 (pH 2) and extracted by liquid-liquid partitioning using CH_2Cl_2. After phase separation, CH_2Cl_2 extracts were dried with acidified Na_2SO_4, reduced on a Roto-evaporator, and then added to 40 mL hexane. The final volume was reduced to 10 mL for analysis. An Agilent 7000C Pesticide Analyzer Triple Quad GC/MS/MS operating in MRM mode was used to analyze the extracts (2-μL injections). The column was HP-5MS-UI, PN 19091S-433UI 30 m ' 0.25 mm ' 0.25 mm with the temperature at 70°C for 2 min, a ramp of 25°C min^{-1} to 150°C, followed by a ramp of 3°C min^{-1} to 200°C and ramp of 8°C min^{-1} to 280°C (total run time of 38.9 min). One target ion and at least two qualifier ions were monitored to identify compounds at expected retention times. The lower limit of quantification was 25 ng L^{-1} for most compounds and detections below this limit were considered no detects. The water samples of nAz and Az stock solutions prepared for sub-lethal experiments were analyzed through the same method.

Appendix 3-2. Dynamic light scattering

Dynamic light scattering (DLS; Zetasizer Nano Series, Malvern Instruments Ltd.) was used to characterize hydrodynamic diameter and polydispersity index (PDI) and zeta-potential of nAz at nominal concentrations of 20 and 100 μg L^{-1} test suspensions at 28.5 °C at 0, 2, 4, 8, 12, 24, 48, 72 and 96 h in 173° backscatter mode (Zetasizer software, v. 7.01). The cell (ZEN 1002) was inserted into the cuvette and the remaining air bubbles were removed by gently flicking the cuvette to avoid interference with the measurements of zeta potential. Samples were covered by parafilm and kept static between measurements.

Appendix 3-3. Zebrafish larvae images

Larvae at 120 hpf after sub-lethal exposure were transferred into 200 μL micropipette tips and then placed under dissecting microscope (Olympus SZ61) linked to a microscope digital camera (ScopeTek MDC-320, 3.2 Megapixels) that was connected to a computer. The tips containing larvae were rotated and two photos were taken, one was the side view and the other one was the ventral view of zebrafish larvae, the images were processed by ScopeTek Scope Photo version 3.0, and the lengths of three axes of the yolk sac were measured (Figure S3-1).

Appendix 3-4. Oxygen consumption and heart rate

Two embryos/larvae (pooled together as n=1) were placed into a single 250 μl well on a 24-well microplate filled with fresh RO water. The microplate was sealed by a silicone pad in the chamber and placed on a sensor reading dish on a mixing table and incubated at 27 °C. Continuous O_2 measurements were conducted over a period of 20 min, with all recordings being made above 70% air O_2 saturation limits. Final MO_2 measurements were recorded as mg $O_2^{-1}g^{-1}hr^{-1}$. Embryos were disposed of after the measurement. The heart rate of zebrafish larvae was measured at 120 hpf. Briefly, the heart rate of each larva was counted for the 20s under dissecting microscope at 3 times magnification and heartbeats per minute were deduced. This process was repeated three times on each larva and the average was used as the final value.

Appendix 3-5. Enzyme activity assays

Frozen 120 hpf zebrafish (20 larvae per sample) were first left to thaw on ice for 5 min and subsequently sonicated on ice (pulse sonication 1s on/1s off for 8 times, two rounds) by Virtis Virsonic 100 ultrasonic cell disrupter (115 v, 1 amp, 60 Hz) in the appropriate buffer

for the assay. For catalase activity assays, sonicated samples were centrifuged at 10,000 x g

for 15 min at 4°C. For superoxide dismutase (sod) assays, samples were centrifuge at 1,500 x

g for 5 min at 4°C. The supernatant was transferred to an Eppendorf tube on ice. Catalase

activity was measured using Cayman Catalase Assay Kit (Cayman Chemical; Item No.

707002) following the manufacturer's manual. Sod activity was determined by Cayman

Superoxide Dismutase Assay Kit (Cayman Chemical; Item No. 706002) according to the

manufacturer's specifications. All samples were normalized to total protein content which

was pre-determined by the Pierce BCA Protein Assay Kit (Thermo Scientific; 23225) based

on the manufacturer's recommendations.

Appendix 3-6. RNA isolation and cDNA synthesis

Total RNA was isolated from ten 120 hpf larvae of each treatment and control group

mentioned in the sub-lethal experiment using the NucleoSpin RNA Plus (Macherey-Nagel;

740984) following the manufacturer's instructions. RNA quality, including 260/280 and

260/230 ratios and RNA concentration were determined right after RNA isolation using a

NanoDrop spectrophotometer (ND-1000, v.3.8.1). Samples with both ratios between 1.8 and

2.2 and RNA concentration higher than 100 ng mL^{-1} were then subsampled to perform cDNA

synthesis. The first-strand cDNA synthesis was accomplished by using SuperScript^{TM} IV

First-Strand Synthesis System (Thermo Fisher Scientific; 18091050) according to the

manufacturer's instructions.

Appendix 3-7. Western blotting and image processing

Briefly, 10 larvae at 120 hpf (pooled together as n=1) were sonicated in 1% NP-40 cell

lysis buffer (Thermo Fisher Scientific; FNN0021) on ice (pulse sonication 1s on/1s off for 8

times, two rounds) by Virtis Virsonic 100 ultrasonic cell disrupter. Samples were placed on a rotator at 4°C for 20 min to get complete lysis and then centrifuged at 14,000 x g at 4°C for 10 min. The supernatant was transferred to a new tube on ice. Ten μL supernatant was diluted to 40 μL and then used to determine protein concentration by the Pierce BCA Protein Assay Kit. All the original samples were sub-sampled and diluted to the same concentration based on the BCA assay results. Subsamples were diluted in equal volume (1:1) by reducing buffer (10 mL 2x Laemmli sample buffer (Bio-Rad; 1610737) plus 500μL 2-Mercaptoethanol (Sigma-Aldrich; M6250) and then boiled at 95 °C for 10 min. A 20 μg sample was added to each well of 8% gel and then followed Western blotting protocol with anti-4-HNE antibody (67 kDa; StressMarq Biosciences, SMC-511) as the primary antibody (1:1000) and Goat Anti-Mouse IgG (H+L) HRP (ThermoFisher, G-21040) as the secondary antibody (1:1000). 4-HNE was normalized to beta-actin using an anti-beta-actin antibody (42 kDa; ThermoFisher, MA5-15739) as the primary antibody (1:1000) and Goat Anti-Rabbit IgG (H+L) HRP (ThermoFisher, G-21234) as the secondary antibody (1:2000). The membranes were exposed and imagines were captured by ChemiDoc™ Touch Gel Imaging System (Bio-Rad; 1708370). The images were processed and analyzed by Image Lab™ Software (v.6.0.1, Bio-Rad).

Appendix 3-8. Modified thiobarbituric acid reactive substances assay

Briefly, 53.6 mg 2-DR powder (Sigma; 31170) was added into RO water to make a 400 mM 2-deoxy-D-ribose (2-DR) stock solution. The 2-DR stock solution was sonicated in a water bath for 5 min and then 50 μL of 2-DR stock solution was added into each well of polystyrene 12-well plates containing 4.95 mL of either nAz at a nominal concentration of 1 or 10 mg L^{-1}, Az at a nominal concentration of 1 or 10 mg L^{-1}, input polymer at a nominal

concentration of 10 mg L^{-1} or Allosperse at a nominal concentration of 10 mg L^{-1}, RO water or 0.01% methanol. One 12-well plate was incubated 5 cm below UV lamp UVA: 3.0 ± 0.14 W m^{-2}, UVB: 1.5 ± 0.11 W m^{-2}) for 30 min while the other one was incubated under laboratory light. The spectral irradiance from UV lamp with UVA (UVX-36; calibrated at 365 nm) or UVB (UVX-31; calibrated at 310 nm) sensor (Ultra-Violet Products Ltd., CA, USA) was measured by UVX digital radiometer. After incubation, the amount of •OH produced in the presence or absence of UV light was determined by thiobarbituric acid reactive substances (TBARS) assay.

Appendix 5-1. EROD activity in Gill

Gill arches were dissected from the gill and placed in 1 mL of tissue buffer containing ice-cold 1x Hanks' Balanced Salt Solution with calcium, magnesium and glucose (HBSS; ThermoFisher, 14025092) and 1.43 g L^{-1} HEPES (Fisher BioReagents, BP310-1) at pH 7.7 in wells of a 12-well plate. Duplicate groups of ten 2 mm-long filament tips were cut from gill arches and transferred into 1 mL fresh tissue buffer in wells of a 24-well plate. The tissue buffer was replaced with 1 mL of reaction buffer consisting of tissue buffer, 0.603 mg L^{-1} 7-ethoxyresorufin (7-ER) and 3.363 mg L^{-1} dicumarol. Gill filament tips were incubated at room temperature on a shaking plate in the dark for 30 min. After incubation, a triplicate of 0.2 mL aliquots from each well was transferred to a black-walled 96-well plate (Greiner Cellstar, Frickenhausen, Germany) and triplicate 0.2 mL aliquots of resorufin standards (0-1000 pM) were transferred to the same plate to generate a standard curve. The fluorescence was measured by a microplate reader (1420 Multilabel Counter, VICTOR 3V, PerkinElmer, MA, USA) at an excitation wavelength of 353 nm and an emission wavelength of 595 nm. EROD activity was calculated and expressed as a relative fold change to the control group.

Appendix 5-2. EROD activity in liver

Approximately 0.15 g liver was dissected and placed in 2 mL microfuge tubes with 0.5 mL ice-cold KCl-HEPES homogenization buffer (11.18 g L-1 KCl, 4.77 g L-1 HEPES, pH 7.4). Liver tissue was homogenized on ice using a hand-held tissue pestle homogenizer on ice for 15 s and then centrifuged at 10,000g at 4 °C for 20 min. Fifty µL ice-cold supernatant was transferred into a 96-well and then 200 µL ice-cold EROD buffer consisting of 11.12 g L^{-1} Tris-HCl, 0.292 g L^{-1} EDTA and 0.603 mg L^{-1} 7-ER at pH 7.4 and resorufin standards (0-1000 pM) were added into each well. Ten µL of 3.72 g L^{-1} NADPH solution was added into each well to start the reaction. The reaction was incubated at room temperature on a shaking plate in the dark for 20 min. After the incubation, fluorescence was measured at 535/595 (excitation/emission) by the microplate reader. Protein concentration in each liver sample was determined by the Pierce BCA protein assay kit (Thermo Scientific, 23227). EROD activity was normalized based on the protein concentration and expressed as relative fold change to control.

Appendix 5-3. Confocal slides preparation

Tissues were fixed in 4% paraformaldehyde (pH 7.4, diluted from 32% paraformaldehyde, Electron Microscopy Sciences, 15714-S) at 4 °C overnight. The paraformaldehyde was removed and cold 70% ethanol was added to cover the tissues at 4 °C. After 30 min, ethanol was replaced by fresh, cold 70% ethanol. The samples were serially dehydrated in a graded ethanol series followed by being embed into paraffin wax. Tissue blocks were sectioned at 7 µm by microtome (Leica Biosystems) and placed on Superfrost Plus microscope slides (Fisher Scientific, 12-550-15). Slides were deparaffinized by toluene

for 10 mins thrice and immersed in 100%, 95% and 70% ethanol for 10 min once and then washed with phosphate-buffered saline (PBS) for 10 min thrice. Tissues were incubated in 1:1000 diluted (in PBS) Hoechst 33342 nuclear stain (ThermoFisher Scientific, H3570, Excitation/Emission maxima: 352 nm/461 nm) for 10 mins and then slides were washed with PBS for 10 mins trice. Tissues were incubated in 1:1000 diluted (in PBS) CellMask™ Orange Plasma membrane Stain (ThermoFisher Scientific, C10045, Excitation/Emission maxima: 554 nm/567 nm) for 10 mins and then slides were washed with PBS for 10 mins trice. Coverslips were mounted with Fluoro-Gel mounting medium (Fisher Scientific, 50-247-04) and slides were stored at 4 °C.